Final Report - Phase 2 Ext.

Prepared for:

The National Institute for Coastal and Marine Management (RIKZ) and the Directorate North Sea (DNZ) of the Directorate-General for Public Works and Water Management (RWS)

Morphology of Pits, Channels and Trenches

Part II: Model Verification of Delft3D with PUTMOR dataset

D.J.R. Walstra, L.C. van Rijn and M.A.G. van Helvert

October 2002

WL | delft hydraulics

CLIENT: DG Rijkswaterstaat
Rijks-Instituut voor Kust en Zee | RIKZ

TITLE: Morphology of Pits, Channels and Trenches
Part II: Verification of Delft3d with PUTMOR dataset

ABSTRACT:

For several years the large-scale mining of sand from the Dutch Sector of the North sea is in discussion related to the need of sand for shoreface, beach and dune nourishment and large-scale engineering works at sea (Maasvlakte extension, airport at sea). The mining methods considered, basically fall into two categories: wide, shallow or small, deep mining pits. Presently, most sand mining pits with a limited depth, not deeper than about 2 m, are excavated beyond the 20 m depth contour. Deep mining pits have not yet been made extensively. As morphological models are primarily used to assess the impact of sand mining pits it is essential to have a good insight in the quality of the predictions made with these models. In the present study the Delft3D model is evaluated with measurements from a sand mining pit located some 10 km offshore of the Rotterdam harbour entrance. The evaluation involves a comparison with measured water levels and current velocities in the pit and the surrounding area.

The evaluation study has shown that the Delft3D-model is capable of reproducing the measurements with reasonable to good accuracy. However, the agreement did vary in the two periods that were considered. In the first period, around neap tide with relatively high waves and wind, occasionally large deviations between the predictions and measurements were observed. The second period, around spring tide with low waves and wind, was reproduced accurately. In the 2DH-simulations the effect of waves, wind and salinity was limited. The tidal forcing appeared to be dominant at the investigated pit. Comparison with the velocity profiles over the vertical showed that the 3D-model was able to represent the 3D-structure of the currents with good accuracy.

The morphodynamic evaluation, based on a 2DH simulation with representative tidal, wind and wave forcing, showed a reasonable agreement with the sedimentation-erosion patterns derived from the bathymetric surveys. As the measured morphological development has considerable uncertainties an unambiguous conclusion regarding the morphological predictive capabilities of the Delft3D could not be drawn. The morphodynamic sensitivity analysis revealed some differences between the results obtained in 2DH and 3D-mode. In general the morphological changes were larger in 3D. At this time we can not assess the quality of these predictions due to the lack of a reliable measured morphological development. The differences between the 2DH and 3D morphodynamic simulations on the considered time scale of one year are limited. However, more research is required to investigate 3D effects, especially on longer time scales.

REFERENCES: Contract No. RKZ-1079
K2005*ZEEBODEM
Generiek Kustonderzoek VOP Project 2

VER.	ORIGINATOR		DATE	REMARKS	REVIEW		APPROVED BY	
0	D.J.R. Walstra		25 April 2002	Draft	L.C. van Rijn		A. Roelfzema	
1	D.J.R. Walstra		3-6-2002	Final	L.C. van Rijn		A. Roelfzema	
2	D.J.R. Walstra		12-9-02	Draft Ext.	L.C. van Rijn		A. Roelfzema	
3	D.J.R. Walstra		23-10-02	Final Ext.	L.C. van Rijn		A. Roelfzema	

PROJECT IDENTIFICATION:		Z3223						
KEYWORDS:		Morphology of sand mining pits						
CONTENTS:	TEXT PAGES	60	TABLES	15	FIGURES	105	APPENDICES	0

CONFIDENTIAL: ☐ YES, until (date) ☒ NO

STATUS: ☐ PRELIMINARY ☐ DRAFT ☒ FINAL

Contents

Figures

*) indicates figures located at the end of the report, after the text.

Tables

1 Introduction

1.1 General

For several years the large-scale mining of sand from the Dutch Sector of the North sea is in discussion related to the need of sand for shoreface, beach and dune nourishment and large-scale engineering works at sea (Maasvlakte extension, airport at sea). The mining methods considered, basically fall into two categories: wide, shallow or small, deep mining pits. Presently, most sand mining pits with a limited depth, not deeper than about 2 m, are excavated beyond the 20 m depth contour. Deep mining pits have not yet been made extensively.

The morphology is affected in the sense that locally the bed level is lowered substantially in the form of a borrow pit (or channel), which may influence the local flow and wave fields and hence the sand transport rates due to modification of shoaling, refraction and reflection patterns. The pit area (slopes) may migrate towards the shore over time and/or may act as a sink (trapping) for sediments from the nearshore system. On long term (100 years) the area of influence may extend over tens of km's outside the original mining area. Furthermore, the small-scale and large-scale bed forms (from megaripples to sand waves) may be destroyed locally, which may also have an effect on the hydrodynamic system (less friction and turbulence). Various studies of the morphological consequences of sea sand mining have been performed, but most of these consequences can not yet be fully overseen and further studies are required to line up the positive and negative effects of sea sand mining, so that a rational decision with respect to location and quantity of future sea sand mining can be made.

As morphological models are primarily used to assess the impact of sand mining pits it is essential to have a good insight in the quality of the predictions made with these models. In the present study the Delft3D model is evaluated with measurements from a sand mining pit located some 10 km offshore of the Rotterdam harbour entrance. The evaluation involves a comparison with measured water levels, current velocities and morphology in the pit and the surrounding area.

1.2 Assignment

In this context WL | Delft Hydraulics was assigned by Rijkswaterstaat/RIKZ (22 October 2001, Overeenkomst RKZ - 1079) to investigate the effect of deep sand mining pits. To that end, the study was sub-divided into three phases:

1. A literature review in which an overview and inventory of the most relevant studies performed up to now, see Van Rijn and Walstra (2002). This review discusses: a) regulations on sea sand mining, b) morphodynamics of offshore mining areas, c) sediment transport and ecological processes in marine conditions, mathematical

description of sediment transport and available models, data sets and hindcast studies, mathematical studies related to pits in the North Sea.
2. A model study in which field data obtained from the PUTMOR field campaign is used for the verification of Delft3D. In this phase, the quality of hindcasts made with the Delft3D model are assessed via comparison with measured data from the PUTMOR field campaign. The verification consists of comparison of water level, velocities (depth-averaged, 2DH, and 3 dimensional, 3D) and salinity. Furthermore, morphological predictions made with the hydrodynamically verified Delft3D model are compared with the measured bathymetric changes. In addition, a limited morphological sensitivity analysis is carried out in which the predictions made in 2DH and 3D-mode are investigated. Also, the effects of waves on the predicted morphology are investigated. The verification is a first step in the assessment of the quality of predictions made with the Delft3D-model regarding of the possible negative effects of sand mining pits (e.g. morphological stability, water quality, deposition of mud).
3. An assessment of the effects various pit designs may have. With the Delft3D model and the 2DV Sutrench model.

This report constitutes phase 2 of the project.

The study has been done within the Co-operation Framework of Rijkswaterstaat/RIKZ and WL | Delft Hydraulics for Coastal Research (VOP Project 2).

This study was carried out by ir. D.J.R. Walstra (project leader) and ing. M.A.G. van Helvert (model runs). Prof.dr.ir. L.C. van Rijn was the quality coordinator. From R.I.K.Z. the project leaders were ir. M. Boers, ir. J.G. de Ronde and dr. J.P.M. Mulder.

1.3 Reading guide

The set-up of this report is as follows:

First the measured data that is used for the model verification is described in Chapter 2. This chapter contains a general description of the data set (referred to as PUTMOR data set). Furthermore, the selection and processing of data is discussed, based on which some general conclusions are drawn on the quality of the data set.

In Chapter 3, the model schematisations are discussed. It gives account of the quality of the overall model (referred to as HCZ-model) which was used to obtain the boundary conditions of the detailed model (referred to as PIT-model) applied in the actual verification. The description includes the computational grids for the wave and flow modules and the associated boundary conditions for tide, wind, waves and bathymetry.

In Chapter 4 the Delft3D model is verified with the selected PUTMOR measurements. First a quality check is described to assure that the detailed model is capable of reproducing the overall model. Furthermore, an overview is given of the applied statistical parameters to objectively assess the model performance. Next, the model verification is discussed in which the quality of the predictions of the tidal motion is determined. Furthermore, hindcast simulations have been performed in which the observed wind and waves are used as forcing

conditions. An intrinsic part of the evaluation is to assess the influence of wind, waves and salinity have on the predicted water levels and currents. Finally, a morphological evaluation is presented in combination with a sensitivity analysis in which the Delft3D-model is applied in both 2DH as 3D-mode. Furthermore, the effects of waves on the resulting morphology are investigated.

The report is completed with conclusions and recommendations in Chapter 5. The conclusions are focussed on the assessed overall model performance and on the ability of the model to represent the effects the sand mining pit has on the local hydrodynamics. Furthermore, an overview is given of some general research questions related to the impact of sand mining pits. Based on the results of the verification study an attempt was made to answer these research questions, or otherwise indicate with what confidence and how they can be investigated in the next phase of this study.

2 The PUTMOR data set

2.1 Introduction

This chapter describes which data was used from the PUTMOR data set for the evaluation of the Delft3D-model in Chapter 4. First a general description is given of the PUTMOR data set in Section 2.2. Next, the selected measurements and data processing (e.g. derivation of depth averaged velocities) are discussed in Section 2.3. This section also gives a brief interpretation of the 3D structure of the observed velocities (Sub-section 2.3.3).

2.2 General description of PUTMOR data set

Below a description is given of the PUTMOR data set which is largely based on the data analysis reports (Svašek, 2001a, 2001b, 2001c).

Between October 1999 and March 2000 an extensive measuring campaign was held to collect data concerning water movement, water quality and morphology in and around a large sand pit at the North Sea some 10 km off the Dutch coast near Hoek van Holland. The dimensions of the pit are 1300 m x 500 m x 10 m (relative to the seabed at an approximate depth of 24 m water depth, which gives a total volume of circa 6.5 Mm^3). The measurements comprise bathymetry, flow velocities, water levels, temperature, conductivity, turbidity, oxygen content and sampling and analysis of seabed material. The monitoring activities took place after dredging of the pit and before dumping of dredged material.

The preparation and execution of the measuring campaign as well as the processing and analysing of the measurements, are part of the PUTMOR project ('pit morphology'), initialised by Directorate North Sea (DNZ) in co-operation with the National Institute for Coastal and Marine Management (RIKZ). The programme was initiated in view of large dredging and reclamation activities that may occur in the North Sea in the future, like for instance 'Maasvlakte 2' or for the extraction of concrete sand. The aim of the measurements was to assess the impact of a large-scale sand pit on water movement, water quality and morphology.

The data available from the PUTMOR-project can roughly be divided into 3 types. The majority is so called 'PUTMOR' data, measurements that were carried out specifically for this project by Directorate North Sea (DNZ). Besides these PUTMOR data use is made of meteorological and hydrological data that is continuously collected independent of the PUTMOR project by other authorities.

The purpose of the pit (named Lowered Dump Site or LDS) is on the one hand sand mining, and on the other the storage of dredged material from the port of Rotterdam.

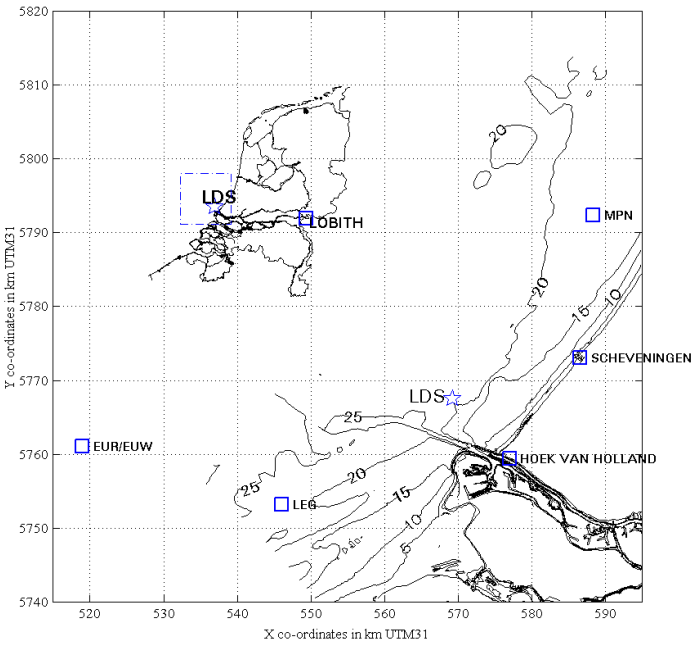

Figure 2.1 Overview of pit location (Svašek, 2001a).

The main measurement locations are location M near the centre of the sand pit, and location A, outside the sand pit. Both at location M and A current velocities (in x, y and z direction) were continuously measured with an ADCP (Acoustic Doppler Current Profiler) throughout the vertical. Twice, flow track measurements were carried out along tracks, of which the first series were rejected because of directional inaccuracies. The position of the locations as well as the tracks sailed with towed ADCP are shown in Figure 2.2.

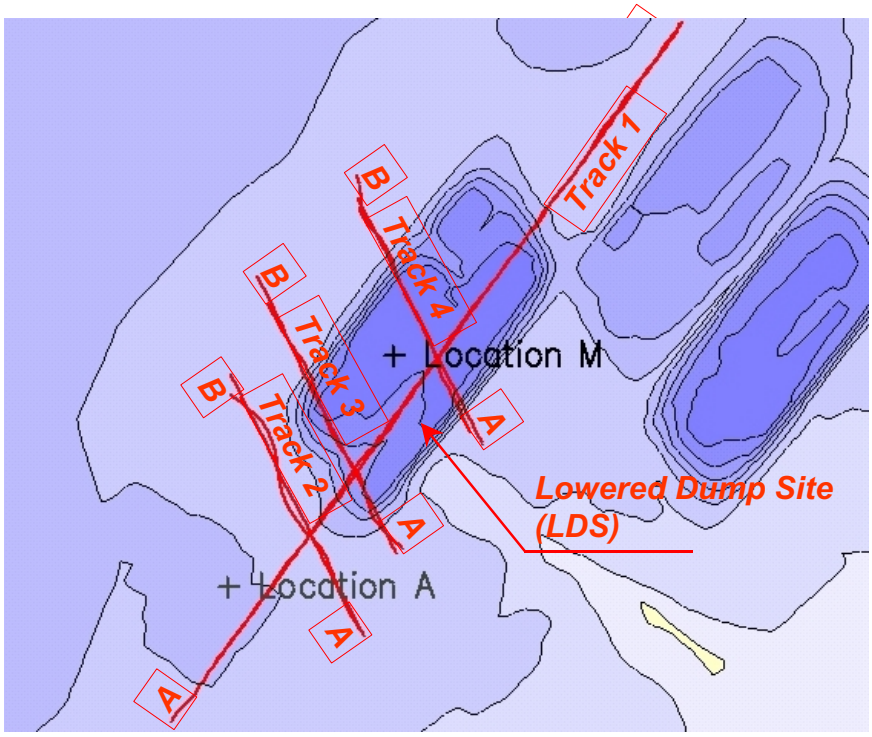

Figure 2.2 Plan view of LDS, measurement locations and measured tracks.

Two Hydrolab instruments were available, one in the LDS at location M and one outside, at location A, measuring the near seabed water temperature, conductivity, turbidity and depth. The Aanderaa string measured the temperature and conductivity at 5 different depths at location M. The Mors was mainly used for its pressure sensor, but also temperature near the seabed was measured. The Mors was located at 'B'. The Seabird observations, consisting of water temperature, conductivity, turbidity, salinity, oxygen content and oxygen saturation percentage, were taken from a ship about once or twice a week at locations A and M, and comprise (almost) the entire vertical.

- location M: approximately (569174, 5767420 m UTM31 or 60456, 452348 m in Paris Coordinates) near the centre of the sand pit, depth approximately 34 m below Mean Sea Level (MSL),
- location A: approximately (568551, 5766480 m UTM31 or 59802, 451428 m in Paris Coordinates) outside the LDS, approximately 1200 m SW from location M, depth approximately 24 m below MSL,
- location B: approximately (570080, 5768732 m UTM31 or 61405, 453631 m in Paris Coordinates) outside the LDS, approximately 1500 m NE from location M, depth approximately 24 m below MSL.

In addition to these PUTMOR data, use is made of prolonged meteorological and hydrological data like water levels at nearby stations, waves, wind, air temperature and river discharge. Details on these data can be found in Svašek (2001a).

Since October 1999 (considered as the reference situation), six bathymetric surveys were carried out in the area of the LDS, to study the morphological development of the sand pit. Also seabed samples were taken. Details on the surveys and the samples can be found in (Svašek, 2001a).

The measuring campaign was divided in four measuring periods, being:

• Period 1:	October 14th, 1999	-	November 24th, 1999
• Period 2:	December 14th, 1999	-	January 14th, 2000
• Period 3:	January 20th, 2000	-	February 21st, 2000
• Period 4:	February 22nd, 2000	-	March 27th, 2000

2.3 Selection and processing of PUTMOR-data for modelling

2.3.1 Selection of PUTMOR data

This study is primarily aimed at evaluating the Delft3D model on its predictive capabilities regarding hydrodynamics (water levels, wind and tidal driven velocities) and morphology (morphological impact of sand mining pits).

Hydrodynamic data

The hydrodynamic evaluation is performed as a hindcast in which all (measured) forcing conditions are imposed as accurate as possible on the model. As a hindcast of the complete

duration of the PUTMOR experiment would involve an unprecedented modelling effort, it was therefore decided to focus on a limited number of representative periods. The selected periods should cover the variation of the tidal motion, wind and waves observed during the PUTMOR experiment.

In Summary, the selection criteria for the model verification regarding the considered period are:

- primarily the occurring wind and wave conditions (calm and storm conditions),
- comparison with the flow track measurement data (one measurement available: 20 March 2000),
- availability of measurement data,
- different tidal conditions (e.g. neap tide and spring tide).

To optimise the modelling efforts it was decided to focus on Period 4 (22 February to 27 March 2000) because of the availability of the flow track measurement data. Within this period two sub-periods were selected for the hindcast, based on the occurring wave and tidal conditions (see Figure 2.3 and Figure 2.5):

- Period I: 26 February 2000 00:00 to 5 March 2000 00:00
  During this period the waves gradually increase from 1m to about 3.5m. This period is around neap tide (smallest tidal range in this period is 1.3m). The average wind speed is 10m/s and the wind direction varies between 240 and 340 ºN (Southwestwest and Northnorthwest).

- Period II: 20 March 2000 00:00 to 26 March 2000 00:00
  This is a calm period with waves of about 0.5 m and low winds. On 20 March the flow tracks were taken which was a main reason for selecting this period. This period is around spring tide (maximum tidal range in this period is 2.1m). The average wind speed is 5m/s and the wind direction is predominantly 240 ºN.

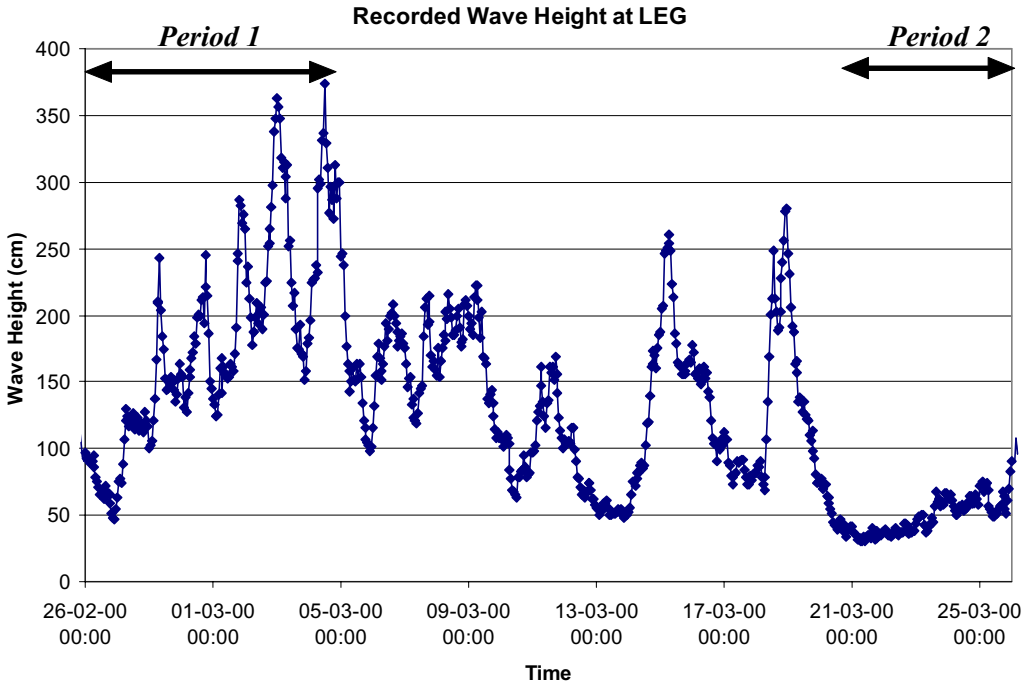

Figure 2.3 Measured wave conditions at Licht Eiland Goeree (LEG).

For the model verification a selection was made from the available data which is summarised in Table 2.1 below.

Instrument	Location	Parameter	Time series	Vert.profiles
Fixed ADCP	A & M	V, U	yes	yes, bin size 0,5 m
Towed ADCP	Tracks 1-4	V, U	-	yes, bin size 0,5 m
Hydrolab	A & M	S, D	yes	-
Aanderaa	M	S	yes	-

Table 2.1 Overview available measured data.

Explanation of the parameter symbols is as follow:

- U longshore component current* [m/s]
- V cross-shore component current* [m/s]
- S Salinity [ppt]
- D Water Depth [m]

*) The velocity data has been converted from true North and South components to components parallel and perpendicular to the length axis of the pit (approximately 35°N, directed parallel to the main tidal direction and local coast orientation). The longshore velocities, *u*, are defined positive in the north-east direction , the cross-shore velocities, *v*, are defined positive in the south-east direction. See also the definition sketch below.

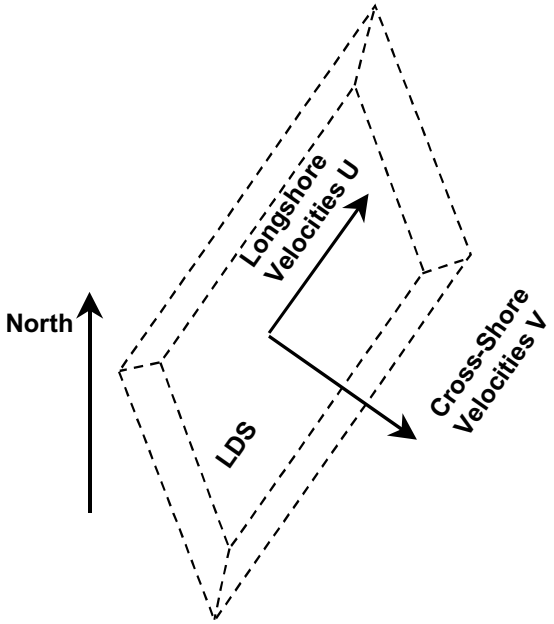

Figure 2.4 Definition of longshore and cross-shore velocity components.

Considering the used instruments, the following remarks can be made:

- Hydrolab instrument: the instrument height above the sea bed is 0.60 m. The time series exist of momentary observations with a 10 minute time step. Note that the depth includes the 0.60 m instrument height, and is considered from seabed to water surface. The depth has been corrected for air pressure fluctuations.
- Aanderaa instrument: five sensors were positioned along the Aanderaa string, on the following heights above the seabed: 2m, 7m, 12 m, 22 m, 28 m. The time series exist of momentary observations with 10 minute time step.
- The measured water depths were transformed into water levels relative to MSL. For Location A and M the water depth was assumed at the zero level obtained from the harmonic analysis carried out by Svašek (Table 4.1 in Svašek, 2001b) being 23.971m and 33.337m respectively. The water levels are compared in Figure 2.5 for both Periods.

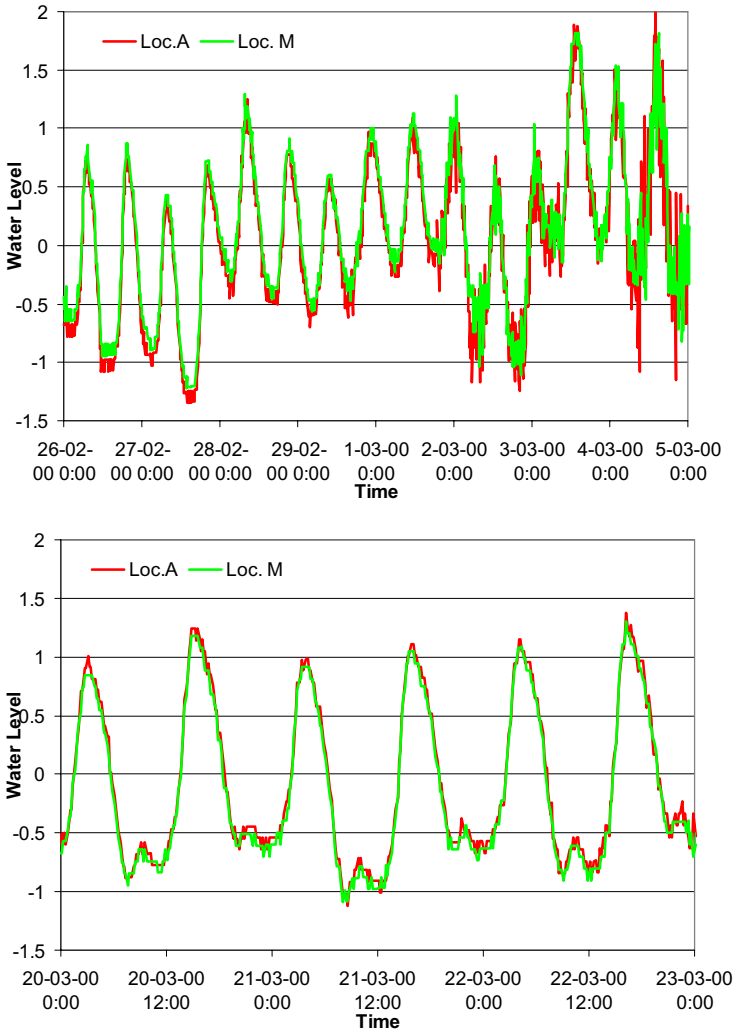

Figure 2.5 Measured water levels at Locations A and M for Period I (top) and Period II (bottom).

Due to the relative small distance between Locations A and M, a large agreement between both water levels is to expected. Although the general trends at both locations is similar, locally relative large deviations are present. Part of the difference may be explained by the fact the Hydrolab instrument recorded instantaneously. Although Svašek (2001b) discusses the possible errors, no accuracy ranges were given for the Hydrolab measurements. However, based on the comparison shown above it seems to be reasonable to assume an error range in the order of 1% of the water depth. This implies an error of about 25 to 30 cm inaccuracy at both locations.

During the measuring campaign a number of bathymetric surveys was carried out in order to study the morphological development of the LDS. The survey conducted after construction of the pit (surveyed October 1999) was used to construct the model bathymetry.

More details regarding the data can be found in the Svašek reports (Svašek, 2001a - 2001c).

Morphology data

The six bathymetric surveys that were carried during the PUTMOR experiment could not directly be used for comparison as the accuracy of the individual surveys was smaller then the observed morphological development. However, based on a statistical analysis of the six bathymetric surveys RIKZ was able to construct a map of sedimentation-erosion patterns which was scaled to one year. This plot is shown in Figure 2.6 below, blue is erosion and red is sedimentation. The measured changes are limited, the maximum changes are present on the slopes of the LDS. An indication of the accuracy of the bottom changes is shown in Figure 2.7, where the squared correlation factors between the six bathymetric surveys are plotted. For large areas there is a relatively low correlation (less then 0.4) which implies that in those regions the measured bottom changes were close to, or smaller then, the accuracy of the measurements. The bottom changes at the northern and southern pit slopes can be considered inaccurate. The measurements at the western (seaward) and eastern (landward) slopes can be used for comparison. Furthermore in the regions North, South and landward of the LDS where erosion occurs there is a relative high correlation. This implies that in these regions primarily erosion occurs.

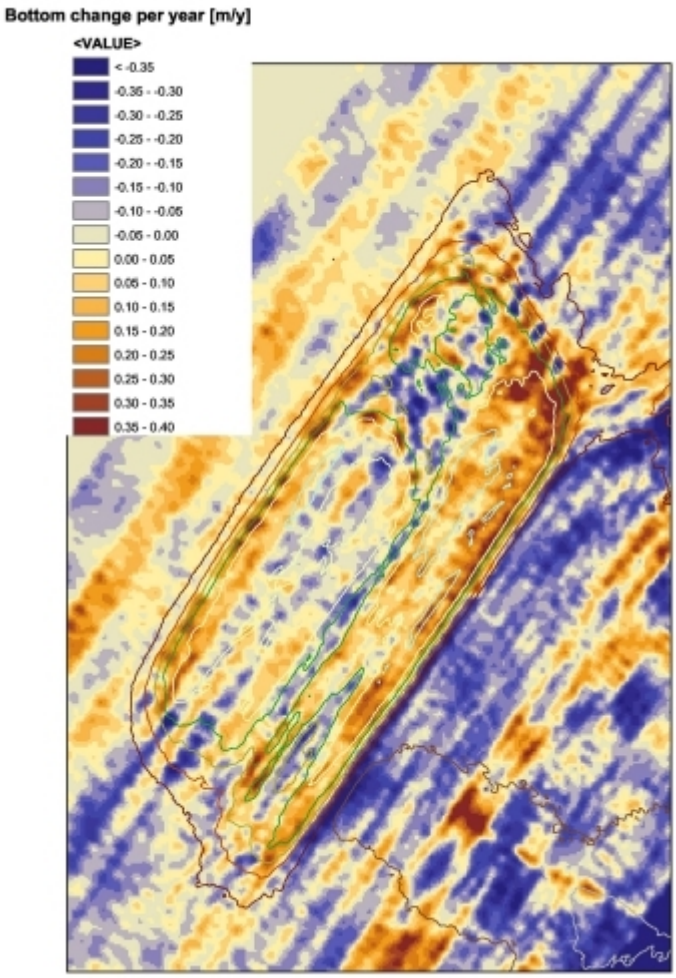

Figure 2.6 Sedimentation-erosion patterns scaled to one year, derived from six bathymetric surveys during the Putmor project.

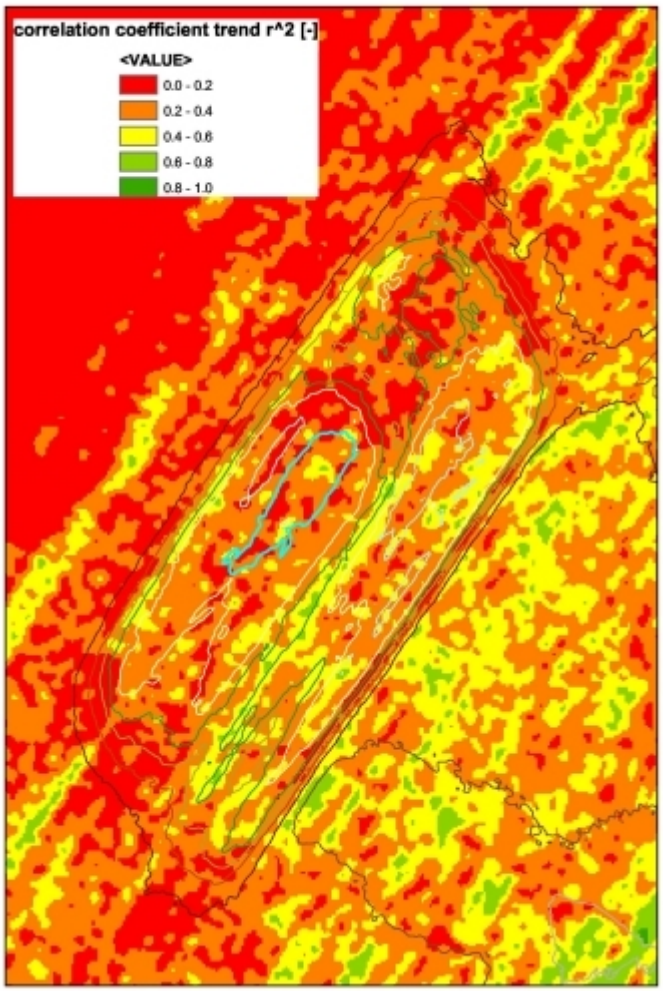

Figure 2.7 Map of squared correlation factor of the six bathymetric surveys during the Putmor project.

2.3.2 Derivation of depth averaged velocities

The Delft3D model will be run in 2DH-mode and in 3D-mode. To evaluate the model performance in 2DH-mode, depth averaged velocities are required for both Locations A and M and the track measurements. Although Svašek (2001b) describes a procedure to derive depth averaged velocities from the vertical velocity profile, this data is not available in the PUTMOR data set.

Following Svašek (2001b), the depth averaged velocities are derived from the measured velocity profiles by excluding the top 9.5 m of the water column due to inaccuracies (or lack of data) in the measurements in this upper part of the water column, for a definition of the bins is referred to Figure 2.8.

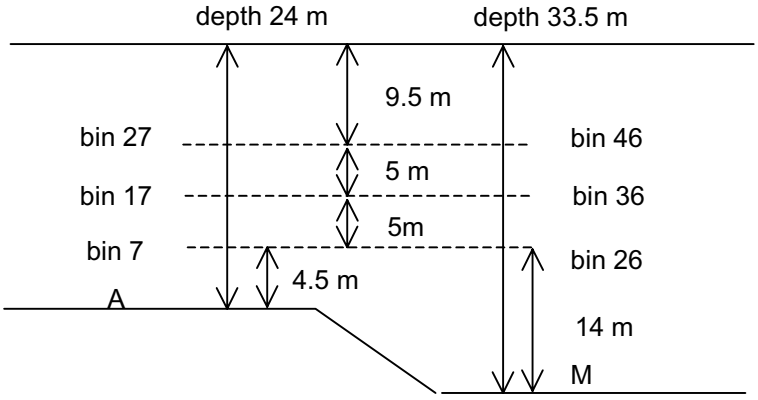

Figure 2.8 Overview of bins at Locations A and M (Svašek, 2001b).

The depth averaged velocities have been calculated by integration of the vertical velocity profile from Bin 1 to Bin 27 for Location A and from Bin 1 to Bin 46 for Location M (see Figure 2.8). For the extrapolation from Bin 1 to the sea bed an average velocity has been assumed in this area of 75 % of the velocity at Bin 1, as suggested by Svašek (2001b).

By definition the calculated velocities in a 2DH-run are based on a logarithmic profile assumption. To investigate the effect of excluding the top 9.5m of the water column on the depth averaged velocities, calculated 2DH-velocities where used to construct a logarithmic profiles according to Eq. (2.1) which were subsequently integrated from the bottom to 9.5m below the water level to obtain corrected depth averaged velocities. In Figures 2.9 and 2.10 time series at Locations A and M are compared in which the red lines indicate the original 2DH-velocities from Delft3D and the black lines the corrected depth averaged velocities excluding the top 9.5 m of the water column. It can be seen that the maximum difference of the velocities is 0.05 to 0.10 m/s for Location A and 0.05 m/s for Location M. The difference in agreement at both stations is due to the larger water depth at Location M. It is thought that this difference between the actual and corrected depth averaged velocities can not be ignored in this evaluation study. Therefore all 2DH modelled velocities are adapted according to the method outlined above in this evaluation study (i.e. both in the visual comparisons and statistical analyses the adapted depth averaged velocities are used).

$$u(z) = \left(\frac{\overline{u}}{\frac{z_0}{h} - 1 + \ln\left(\frac{h}{z_0}\right)} \right) \ln\left(\frac{z}{z_0}\right) \tag{2.1}$$

where z is the vertical coordinate (zero at the bed, positive upwards), $\overline{u}$ is the depth averaged, z_0 is the roughness height which is set to 0.005 m (i.e. k_s = 0.15 m) and h is the total water depth.

2.3.3 Investigation of vertical velocity profiles

This sub-section contains an analysis of the measured velocity profiles. First a comparison for the track measurements is made in which the measured data is converted to depth-averaged velocities according to the method proposed in Svašek (2001b). This especially

provides insight into the vertical distribution of the velocities inside and outside the pit. Furthermore, some velocity profiles are shown over a tidal cycle for the fixed Locations A and M.

In Figures 2.11 and 2.12 the measured velocities during flood and ebb are shown for Track 1 (along the length axis of the pit, see Figure 2.2) and in Figures 2.13 and 2.14 for Track 4 (perpendicular to the length axis of the pit, see Figure 2.2). In these figures the measurements (crosses) and logarithmic velocity profiles (lines) derived from the measured vertical velocity profiles, see Eq. (2.1), are shown. Note that both tracks are presented along the sailed tracks from south-west (left, A) to north-east (right, B) for Track 1 and from south-east (left, A) to north-west (right, B) for Track 4. For the longshore velocities (top plots) there is a fair agreement between the measured vertical velocities and the derived logarithmic profiles, especially in the lower half of the water column. However, the upper half of the water column shows a consistent velocity increase, especially during flood. As wind and wave are almost negligible during this period, this is most likely caused by the fresh water discharge from the Nieuwe Waterweg. This could also explain the more uniform vertical velocity profiles during ebb because the water column is less stratified. The cross-shore velocities are significantly smaller and show less agreement with a logarithmic velocity distribution as in many cases there is a reversal of direction. For both velocity components no significant velocity reduction is visible in the pit, but this will be investigated further in Chapter 4. As the track measurements were carried out under specific circumstances (spring tide, small waves and maximum horizontal tide) the findings have a limited validity. To investigate the temporal variation during a tidal cycle, vertical velocity profiles are analysed next.

To investigate the 3D character of the flow during a tidal cycle velocity data is used from the fixed locations A and M. In Figures 2.15 and 2.16 measured velocity profiles are shown over a tidal cycle with a hourly time step (numbers in legend indicate the time: “1” is at 26-02-2000 11:05 and “12” is at 26-02-2000 22:05). For Location A (Figure 2.15) only measured data is available for the lower half of the water column. It can be seen that about 50% of the presented profiles have an approximate logarithmic distribution, but that the remaining profiles deviate considerably. For Location M, the measured data extends to -5 m below the water surface. For the lower half of the water column the same conclusion can be drawn as for Location A. The upper half of the water column shows significant influences of wind and salinity (density). Especially during around flood and ebb the profiles are relatively uniform, which cannot be said for the remaining periods.

Based on the presented results it is clear that the flow has a 3-dimensional character, especially if the upper layers are considered. This is consistent with the analysis presented in Svašek (2001c). Where, based on a harmonic analysis of the measured velocities, it was found that residual currents in the upper layer and lower layers are in opposite directions. In Chapter 4 measured and modelled residual currents will be compared for both locations.

3 DELFT3D model schematisations

3.1 Introduction

The basis for the model verification using the PUTMOR data is a Delft3D model of the Dutch coast developed in the Flyland project (WL | Delft Hydraulics, 2001) called the Holland Coastal Zone model, abbreviated as HCZ-model. The HCZ-model obtains its boundary conditions from a well calibrated model called the large scale fine grid model covering the entire North-Sea (see WL | Delft Hydraulics, 2001, for details). In the Flyland study it was shown that both models showed excellent agreement with available field data. To enable an efficient modelling of the LDS area a more detailed model was constructed with a high resolution at the investigated pit and the surrounding area. This so-called PIT-model was nested in the HCZ-model.

In the following sections model schematisations for the HCZ-model and PIT-model are described. Section 3.2 contains a general description of the HCZ-model which is largely taken from WL Delft | Hydraulics (2001). Section 3.3 describes the PIT-model, which involves a flow model (Sub-Section 3.3.1) and a wave model (Sub-Section 3.3.3).

3.2 The HCZ overall model

The present section is largely taken from WL Delft | Hydraulics (2001).

The model grid of the HCZ-model was derived from the fine grid large scale model of the entire North Sea. A coastal stretch, reaching from “Schouwen Duiveland” to “Terschelling”, with an off-shore extent of 70 km was taken from the large scale model. In the vicinity of the “Marsdiep” the orientation of the grid lines was modified to allow for a better representation of the “Texelstroom”.

By refinement of the grid mesh the required resolution, especially in the near shore zone, was obtained. This results in grid distances in cross-shore direction varying between 50 m at the beach to 5 km at open sea. Alongshore grid distances equal approximately 1 km. In total the computational grid contains approximately 20,000 computational elements.

The model computations aim at predicting the morphological development of the shoreline. To allow for a retrieving coastline, the computational grid also covers some 200 m of the beach/dune area.

The resulting computational grid is shown in Figure 3.1.

Bathymetry
To represent the present situation, an initial bathymetry was generated using depth data originating from the “Kuststrook” model bathymetry. This depth data covers the area of

specific interest for the present study in greatest detail. However, comparison of the depths generated using the Kuststrook data with the model bathymetry of the fine grid large scale model set-up previously (Roelvink et al., 2001) revealed large depth differences, up to 5 m, most pronounced near the open sea boundary of the HCZ model. Therefore, depths in the deeper areas, outside the areas covered by JARKUS and 'vaklodingen', were regenerated using recent Dutch Continental Shelf Data supplied by TNO-NITG. This data also served to generate, a part of, the bathymetry of the fine grid large scale model set-up previously. Figure 3.2 shows the present situation model bathymetry.

Open boundary conditions
The open boundary conditions of the HCZ-model were derived from 3-dimensional computations with the large scale fine grid model covering the entire North-Sea. Since the HCZ model was set-up to represent average conditions, the model computation of the fine grid large scale model used for the generation of boundary conditions also represents the average conditions, i.e. a south-westerly wind of 7 m/s and long term average river discharges.

At the cross-shore open sea boundary near "Schouwen Duiveland" a velocity boundary is defined. All of the other open boundaries are defined as water level boundaries. The reason for this type of boundary definition is that water level boundaries provides more freedom to simulate other wind conditions than the long term average wind conditions used for the generation of boundary conditions.

The boundary conditions as generated by the fine grid large scale model are specified as time series of water levels or velocities. Hence, they are related to the simulation period of the fine grid large scale model. To allow for the simulation of any calendar period in time, the original time-series boundary conditions were converted into astronomical boundary conditions by means of a tidal analysis on the time series.

In the present study the constant discharge values for the Haringvliet and the Nieuwe Waterweg were replaced with the measured values (obtained from http://www.waterbase.nl). In the table below an overview is given of the applied discharge rates.

Location	Discharge rate:
Haringvliet	Time series (see Figure 3.4)
Nieuwe Waterweg	Time series (see Figure 3.3)
Sluices of IJmuiden	80 m^3/s
Sluices of Den Oever	250 m^3/s
Sluices of Kornwerderzand	200 m^3/s

Table 3.1 Overview of applied discharges in HCZ model.

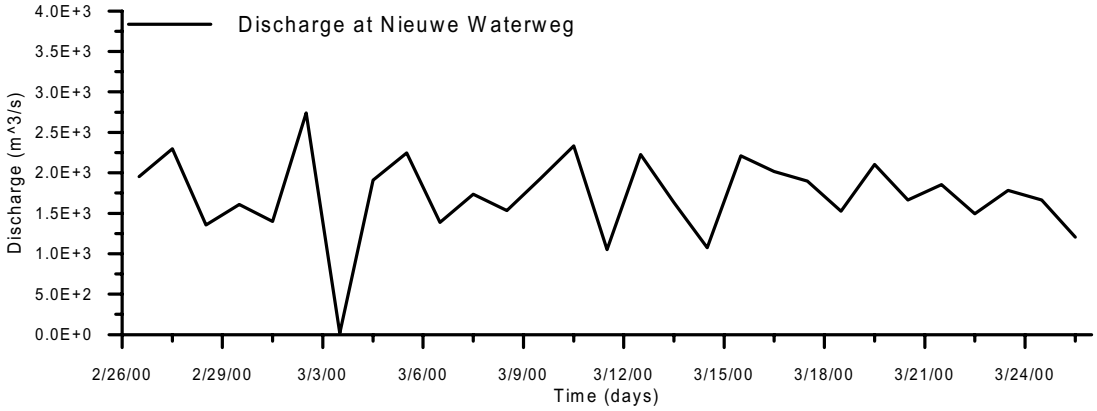

Figure 3.3 Discharge at Nieuwe Waterweg.

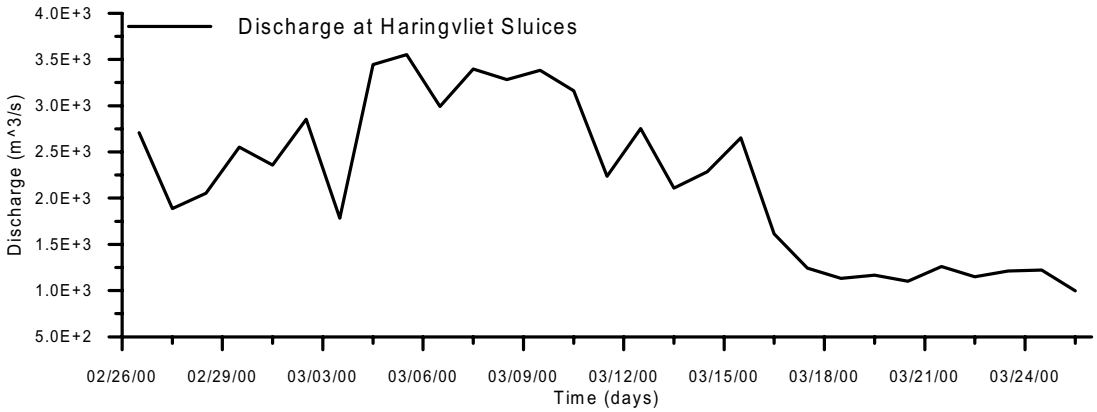

Figure 3.4 Discharge at Haringvliet sluices.

Other model parameters

- Computational time step
  Previous modelling exercises with the fine model revealed that the flow rates through the "Marsdiep" appeared to determine the maximum computational time step allowed. From this analysis it was found that a time step of 5 minutes is allowed for the HCZ-model.
- Bed roughness distribution
  The bed roughness is prescribed by a Manning coefficient. The spatial distribution of bed roughness is taken from the large scale fine grid model set-up previously. For the shallow areas, depths less than 30 m, a Manning value of 0.028 is used. In the deeper areas a Manning value of 0.026 is applied.

HCZ-model performance (assessed in Flyland)

The HCZ model is a nested model itself. Hence, computational results are, too a large extent, determined by the boundary conditions applied. The best that might be expected of this type of model is that it reproduces, on a global scale, the computational results of the overall model used for the generation of boundary conditions. Therefore, the validation of the HCZ model was aimed at reproducing the results of the fine grid large scale model (in which the HCZ model was nested). Computational results of this overall model were already shown to be in excellent agreement with measurements in Roelvink et al. (2001). In

the validation conducted in WL | Delft Hydraulics (2001) it was found that the HCZ-model reproduces the overall large scale fine grid model. Both models were in good agreement with measured water levels. In the referred study, a comparison was made with velocity measurements from the "Noordwijk raai" experiment. A summary of the validation results for the HCZ-model is given below (modified from WL | Delft Hydraulics, 2001):

Validation of tidal water levels
Computed HCZ water levels are compared with previous modelling results and with the measurements in terms of amplitudes and phases of the most important tidal constituents. From the comparison it followed that:

- The nested, detailed, HCZ model reproduces the water levels as computed with the large scale fine grid model accurately.
- Both for the overall and the HCZ-model it holds that computed amplitudes and phases of the most important semi-diurnal constituent, i.e. the M_2 constituent, are in good agreement with the measured values: within 10 % throughout the model area and below 5 % in the area of interest (offshore at IJmuiden).
- The computed amplitudes of the other important semi diurnal constituents, i.e. S_2 and N_2, are slightly overestimated (2 - 4 cm) by both models when comparing with measured amplitudes. Phases of these constituents are reproduced accurately.
- Amplitude of the most important diurnal constituent, i.e. the O_1 constituent, are slightly overestimated (2 cm) by both the overall and the HCZ-model. Phases of this constituent are reproduced accurately.
- Amplitudes and phases of the K_1 constituent are reproduced accurately by both the overall and the HCZ-model.
- For the most important quarterly diurnal constituent, i.e. the M_4 constituent which accounts for tidal asymmetry, it holds that the amplitudes are reproduced within 2 cm error by both the overall and the HCZ-model. Computed phases differ some 10 - 25^o from measured phases. This corresponds with approximately 15 - 30 minutes.

In conclusion, the HCZ-model reproduces the overall large scale fine grid model. Both models are in good agreement with measured water levels.

Validation of tidal velocities
During the "Noordwijk raai" experiment, velocities were measured at various positions and at various depths in front of Noordwijk. Tidal velocities vary over the water depth with relatively small velocities near the sea bed and relatively large velocities near the water surface. At 1/3 of the local water depth the velocity approximately equals the depth averaged velocity.

Measured alongshore velocities were compared with computed velocities for measurement station "Noordwijk 10", located 10 km offshore, the measurement was taken at 5 m above the bed whereas the local water depth is 20 m. These measured velocities are therefore expected to correspond with depth-averaged velocities. For measurement station "Noordwijk 30", located 30 km offshore, measurements were taken at 4 m above the bed whereas the local water depth is 22.5 m.

To allow for a fair comparison between the measurements and the computational results, the computed depth-averaged velocities were adjusted, assuming a logarithmic velocity profile, such that they represent the velocities at the height of the measurements.

In general, the velocity measurements were reasonably reproduced by the HCZ-model. However, the difference between spring and neap tidal velocities was underestimated by the model by some 10 cm/s. The best agreement is found during tides with somewhat above average amplitude.

Validation of flow rate through the Marsdiep
The "Marsdiep" is the tidal inlet to the Dutch Wadden Sea in between "Texel" and "Den Helder". Over the years, extensive ADCP current measurements were executed by ferries crossing the inlet. From these measurements, flow rates through the inlet were determined. From the comparison it followed that the computed flow rates of the HCZ-model are comparable to flow rates computed by the overall model.

3.3 The detailed PIT-model

3.3.1 FLOW schematisations (2DH)

The PIT-model was nested in the HCZ-model to enable an increased resolution in the LDS area without having an unacceptable increase of CPU-time. With an automatic nesting procedure an optimal transition is guaranteed between the overall HCZ and PIT model. The PIT computational grid was constructed by taking a selection of the HCZ-model which was locally refined in the LDS area to have an accurate representation. The design criteria of the detailed grid were:

- a minimum of 20 computational grid points should cover the longshore axis of the pit, whereas for the cross-shore axis a minimum of 10 was used,
- the minimal distance of a boundary to the location of the pit 10 km to avoid boundary related disturbances,
- the fresh water discharge and tidal motion of the Nieuwe Waterweg may not be influenced by the boundaries.
- the boundaries of the PIT model should coincide as much as possible with the overall HCZ grid to avoid interpolation errors.

In Figure 3.5 the computational flow grid of the PIT model is shown.

The associated bathymetry was obtained from the PUTMOR survey after construction of the pit. The remaining bathymetry was obtained from the HCZ model bathymetry. In Figure 3.6 the overall bathymetry is shown. In Figure 3.7 a detail of grid and bathymetry are shown for the LDS area, it can be seen that the resolution is high enough in both longshore and cross-shore direction to meet the standards listed above.

Boundary conditions were obtained from the HCZ-model. Both lateral boundaries were velocity boundaries whereas the coast parallel seaward boundary was largely a water level boundary.

Two discharges were included in the model. The discharge from the Nieuwe Waterweg was obtained from the HCZ-model (in which the measured values were used). The measured discharges at the Haringvliet sluices were directly imposed on the PIT model.

A short overview of the of the PIT-model characteristics is given in the table below.

Unit	Quality
Grid	Curvilinear, originates from HCZ-model. Refined to get better resolution in the LSD vicinity (approx. 50 × 50m). Number of grid points: 16000
Bathymetry	Originates from HCZ-model and PUTMOR data.
Time frame	According to period 4, computational time step 0.25 min
Boundaries	Generated by the HCZ-model, mainly current except SW-corner water level.
Roughness	From HCZ-model, Manning
Wind	Observed wind speed and direction from Licht Eiland Goeree (see Figure 3.11)
Discharges	Haringvliet and Nieuwe Waterweg daily data (measured, see Figure 3.3 and Figure 3.4).

Table 3.2 Characteristics of PIT-model.

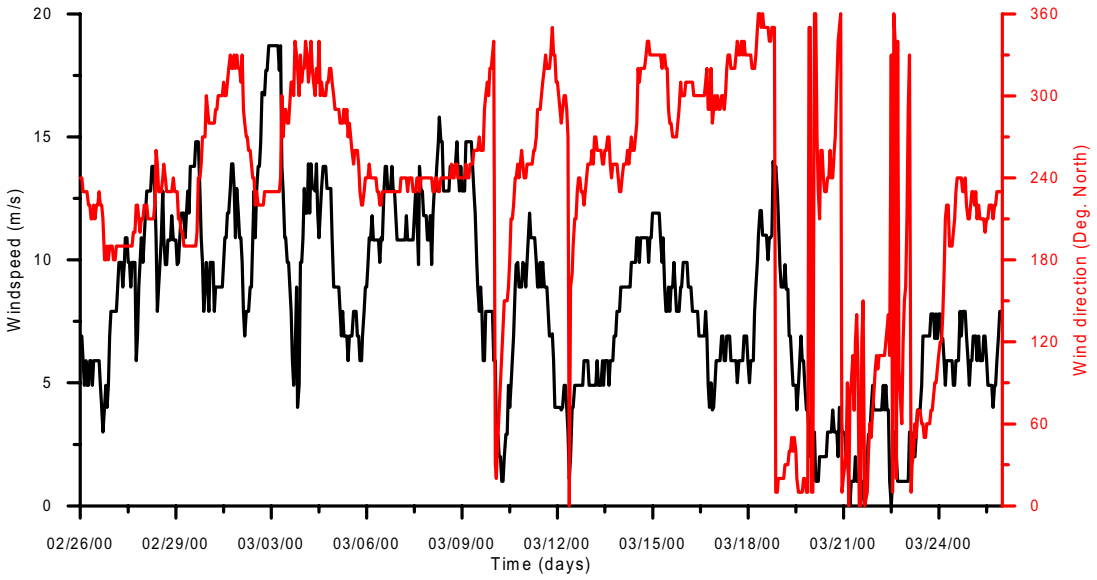

Figure 3.11 Observed wind speed (black) and direction (red) at LEG.

3.3.2 FLOW schematisations (3D)

The 3D-model applied in this study is based on the model described in the previous sub-section. The same bathymetry, horizontal grid and boundary conditions are used. The extensions necessary for the 3D-model are described below.

As the Delft3D model uses a sigma-coordinate system for the vertical grid, only the number of layers and relative thickness of each layer has to be specified. The vertical grid in the 3D-simulations used in the hydrodynamic verification consisted of ten vertical layers with an equidistant spacing over the vertical (Note that in the 3D-morphodynamic simulations a non-equidistant spacing of the vertical grid is used as a relative high resolution is required near the bed).

The boundary conditions for water levels, velocities and salinity are identical to the 2DH boundary conditions under the assumption of a logarithmic distribution across the vertical for velocities, and a uniform distribution for salinity.

A k-ε turbulence model is used to determine the vertical viscosity.

To reduce simulation time, initial conditions for salinity, water levels and velocities obtained from a 2DH-run were used to 'hot start' the 3D-run. The salinity and velocities from the 2DH-run were prescribed on all 10 layers.

3.3.3 WAVE schematisations

In order to simulate the wave propagation and transformation from deep water towards the shore, the wave module of the Delft3D model suite has been used. Two wave models are available within the wave module, i.e. the second generation HISWA wave model and its successor the third generation SWAN wave model. In this study the SWAN model has been used since it allows for a direct coupling with the FLOW (and MOR) grid due to the availability of curvilinear grids. The most recent version of the SWAN model, available at the start of the project, was used which is Version 40.11. This version was upgraded at Delft Hydraulics with the bug fixes (A,B,C,D,E,F) as provided by Delft University of Technology.

In the Flyland study (WL | Delft Hydraulics, 2001) it was found that "in view of the overall uncertainties in morphological modelling it was concluded that the influence of second- or third-generation wave modelling on the resulting transports was very limited. Therefore the SWAN model was run in second generation mode to reduce the overall computing time of the simulations". Following these conclusions in the present study, the SWAN model was also applied in 2nd generation mode. The following physics were taken into account: wave propagation in space, shoaling, refraction, wind growth, white capping, and depth-induced breaking.

The SWAN model uses the same computational curvilinear grid and bathymetry as used by the flow model (see Figure 3.5). This avoids inaccuracies in the interpolation of data between the various Delft3D modules. The harbour moles of Rotterdam were represented in the SWAN model by obstacles with zero transmission (fully blockage of wave energy).

The wave data recorded at Licht Eiland Goeree (LEG) could directly be used as boundary conditions for the SWAN model as the seaward extent of the computational is in approximately the same water depth (see Figure 2.1 for LEG location). For the considered period SWAN was run with the recorded wave height, period and direction with a time step

of 6 hours (see Figure 2.3 for details). Wave boundary conditions were applied at the seaward boundary of the SWAN model as well as on both lateral boundaries. The wind conditions were prescribed as uniform wind fields over the model area with a time step identical to the wave forcing (i.e. 6 hours).

A selection of the simulated significant wave height and wave period patterns are presented in Figures 3.9 and 3.10. From these figures it can be seen that, especially for oblique incident waves, some disturbances are present at the lateral model boundaries. These disturbances are caused by the uniform boundary conditions applied at the lateral boundaries. Here the uniform wave heights are not in accordance with the local depths, thereby introducing additional wave breaking which results in the wave patterns shown in the figures. As the lateral boundary are located sufficiently far from the area of interest (i.e. LDS) these disturbances have negligible influence on the hydrodynamic computations.

4 Model verification

4.1 Introduction

In this chapter the Delft3D model is compared with the PUTMOR data set. The evaluation is based on a selection of measurements described in Chapter 2. As the model schematisation that is used for the actual evaluation (referred to as PIT-model) obtains its boundary conditions from a larger model (referred to as the HCZ-model), the first step is to verify if the PIT-model reproduces the HCZ-model accurately. This verification is presented in Section 4.2. The next section briefly describes the applied error statistics that are used to objectively assess the model performance. The hydrodynamic verification using the PUTMOR data is presented in Section 4.4. The evaluation in Section 4.4 is sub-divided in establishing the model performance for purely tidal driven flows in Sub-Section 4.4.1, for a period around a neap tide with high waves and wind in Sub-Section 4.4.2 and for a period around a spring tide with low waves and wind in Sub-Section 4.4.3. In these three sections the model is applied in 2DH-mode. In Sub-Sections 4.4.4 and 4.4.5 the model is run in 3D-mode and is verified for the same periods. In Sub-Section 4.4.6 an intercomparison between the 2DH and 3D-mode is made. In Sub-Section 4.4.7 the current velocities in and outside the pit are compared to investigate the effects of the pit on these velocities. Finally, in Section 4.5 a morphological verification is described for which both 2DH and 3D morphodynamic simulations were made. The effects of waves were also investigated (in 2DH-mode).

4.2 Intercomparison HCZ-model and PIT-model

The PIT-model is a nested model. Hence, computational results are, to a large extent, determined by the applied boundary conditions. As a first quality check, it is investigated if the PIT-model reproduces, on a global scale, the computational results of the overall HCZ-model used for the generation of boundary conditions. The intercomparison is focussed on the measurement locations A and M of the PUTMOR data set. Both models were run with the boundary conditions described in the previous chapter (i.e. measured wind forcing, measured discharges at Haringvliet and Nieuwe Waterweg, salinity included).

In Figures 4.1 to 4.3 it can be seen that the water levels and velocity-components (in true North and East) of both models show good agreement. The small deviation in the velocity components at Location M is caused by the fact that the LDS pit is not included in the HCZ-model due to its low resolution in this area, whereas the LDS pit is included in the PIT-model. From the comparison it can be concluded that the PIT-model gives a good representation of the water levels and flow velocities in the area of interest compared with the HCZ-model.

4.3 Overview of statistical parameters

For an objective evaluation of the model performance a number of statistical parameters are used. This section gives a brief overview of the applied statistics in combination with an interpretation. Notice that the errors in the measurements are not taken into account.

The linear correlation coefficient can be to determine the relationship between modelled and measured parameters (e.g. water level, velocity components), and is written as:

$$r = \frac{\mathrm{cov}(x, y)}{\sigma_x \sigma_y} \tag{4.1}$$

Where x is the measured parameter and y is the modelled parameter, cov is the covariance and σ_x and σ_y are the standard deviations. By definition r lies between -1 (i.e. perfect negative correlation) and 1 (i.e. perfect positive correlation). A value of 0 indicates no correlation. In a model comparison there should be a strong positive correlation, which implies values close to 1.

Furthermore, the slope m of the best-fit line (forced though the origin) between x and y is used:

$$m = \frac{\sum_{i=1}^{N} x_i y_i}{\sum_{i=1}^{N} x_i^2} \tag{4.2}$$

The slope m predicts the change in y per unit increase in x, in other words, m should be close to 1, a larger value indicates an over-prediction by the model (and vice versa).

To give an indication of the actual error, the root mean square error ε_{rms} is also used:

$$\varepsilon_{rms} = \left\langle (x - y)^2 \right\rangle \tag{4.3}$$

The ε_{rms} has the unit of the considered parameter and should obviously be close to zero.

The above described parameters can only operate on scalar values (here water levels, U- and V-velocity components). For the evaluation of the flow velocity vector the Relative Error Vector (*REV*) is used, see Eq.(4.4), this parameter is illustrated in Figure 4.4:

$$REV = \frac{\left\langle \sqrt{\left(u_{meas} - u_{calc}\right)^2 + \left(v_{meas} - v_{calc}\right)^2} \right\rangle}{\left\langle \sqrt{\left(u_{meas} + v_{meas}\right)^2} \right\rangle} \tag{4.4}$$

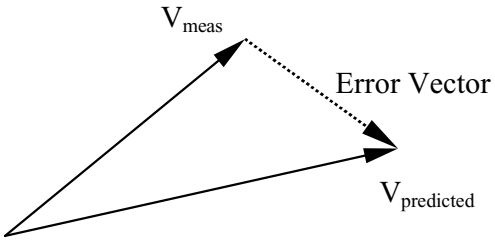

Figure 4.4 Definition of the Error Vector.

This parameter was developed in the Coast3D project (Van Rijn et al., 2002). Because experience with the parameter is limited only a preliminary indication was given of the interpretation of this statistic, which is summarised in Table 4.1.

In the statistical analysis the error ranges in the measurements were not included eventhough these may have a considerable positive effect on the outcome of the statistical parameters.

Qualification	REV
Excellent	<0.2
Good	0.2-0.4
Reasonable/Fair	0.4 - 0.7
Poor	0.7 - 1.0
Bad	>1.0

Table 4.1 Qualification of the Relative Error Vector (Van Rijn et al., 2002).

4.4 Model verification with hydrodynamic PUTMOR data

4.4.1 Tidal predictive capabilities of the PIT-model

In Svašek (2001b) a harmonic analysis was made of the measured tidal signals at Locations A and M. The resulting 7 astronomical components can be used to obtain a reasonable estimate of a pure tidal driven signal. As the HCZ-model is forced by astronomical components (and as a consequence also the PIT-model). A comparison of the model with astronomic time series gives a good indication of the tidal predictive capability of the PIT-model.

In Figures 4.5 and 4.6 a comparison of water levels is shown between the model and the astronomic time series for Location A (top panel) and M (bottom panel). It can be seen that for Period I the phase of the tide is accurately reproduced, but the modelled water level amplitude is considerably larger then the tidal prediction. For Period II both the phase and amplitude show reasonable agreement. However, during falling tide a systematic over-prediction of the water levels can be seen which explains the relative large ε_{rms} and lower r-values (see Table 4.2).

Water Levels	Location A			Location M		
Run-ID	*r*	*m*	ε_{rms}	*r*	*m*	ε_{rms}
Period I	0.98	1.19	0.29	0.98	1.18	0.25
Period II	0.95	1.00	0.24	0.94	0.98	0.25

Table 4.2 Summary of errors of model compared with the harmonic time series for Periods I and II.

It is thought that the difference in agreement in both period is likely to be caused by the limited number of astronomic components that was presented in Svašek (2001b). The absence of important semi-diurnal constituents such as the K_2 and N_2 constituents will, especially near neap tides, results in a deviating prediction (e.g. Period I). Near spring tide the most important semi-diurnal constituent, i.e. the M_2-constituent, is dominant which will results in a better prediction.

Based on the comparisons it is concluded that the tidal prediction for Period I, based on the astronomical components, is probably too inaccurate to assess the model performance. For Period II the tidal prediction is fairly accurate and can be used to assess the model performance. A maximum error of about 10 cm during flood and ebb is present, whereas the phase is reproduced accurately.

4.4.2 Verification for Period I with Delft3D run in 2DH-mode

The verification using Period I is focussed on the measured water level and velocity time series at Locations A and M. The PIT-model has not been calibrated in any way to optimise agreement with the measurements. The model has been nested into the HCZ-model and all relevant parameters (e.g. roughness, viscosity) were obtained from this model as well.

Simulations were made to investigate the effect of the presence of waves and wind on the resulting water levels and current velocities at Locations A and M. In Table 4.3 below an overview is given of the executed simulations.

Run-ID	Waves	Salinity	Wind
PT2	-	+	+
PT4	-	+	-
PT2-Waves	+	+	+

Table 4.3 Overview of executed 2DH simulations for Period I

The effect of wind is investigated in Figures 4.7 to 4.9. In Figure 4.7 the water levels the predicted water levels are compared for Locations A and M. It can be seen that the effect of wind is almost negligible. The model gives an accurate representation of the tidal phase but the amplitude of the water levels shows relative large deviations in this period. Deviations at high and low water are in the order of 0.2 to 0.4 m, but occasional larger deviations are also present. With an *r*-value of 0.76 and an ε_{rms} of 0.4 m the quality of the water level prediction can at best be categorised as “reasonable” (see Table 4.4 and Table 4.5 for an overview of the error statistics). It is thought that the relative large errors are caused by the fact that large scale meteorological variations can not be included in the model due to the

relative small size of the HCZ-model. In order to include these effects the complete North Sea should be modelled in which moving pressure fields and time and space varying wind fields are included. However, this was outside the scope of this project. As stated in Chapter 2, the errors of the measurements have not been taken into account in the statistical analysis. If for the water levels an error range of 0.25 m is assumed (about 1% of the water depth), the ε_{rms} would decrease by approximately 0.20 m for this parameter.

In Figure 4.8 the velocities are compared for Location A. As with the water levels, the phase is reproduced accurately. The maximum ebb velocities are reproduced relatively well for both velocity components. The error in maximum ebb-tidal velocities is in the order of 0.05 to 0.10 m/s, but occasionally deviations of up to 0.5 m/s are present (see e.g. the longshore velocities at 29 February 12:00). The maximum flood velocities are systematically over-predicted in the order of 0.10 m/s for the longshore velocities and 0.05 m/s for the cross-shore velocities. At location M, shown in Figure 4.9, agreement is somewhat better, but shows the same over-predictions of the maximum flood, but the maximum ebb velocities are reproduced accurately.

The errors in the velocity predictions are smaller than of the water levels (see Table 4.4 and Table 4.5). The *r* -values for the longshore tidal velocities are about 0.9 compared to *r*-values of 0.75 to 0.78 for the water levels. The Relative Error Vector has values range from 0.44 to 0.51 which can be categorised as a “reasonable” prediction according to Table 4.1.

The wind effect on the water levels and current velocities is limited, the on average south-westerly wind results in slightly larger northward longshore velocities and reduced southern velocities, whereas the cross-shore velocities are hardly affected. As stated earlier, the wind effect is probably under-estimated in the model as large scale meteorological effects can not be included. Furthermore, the boundary conditions of the HCZ-model are based on average wind conditions. As the PIT-model is located relatively close to the southern boundary of the HCZ-model (which is a velocity boundary) the effect of (strong southerly) winds is under-estimated in the HCZ-model and as a consequence also in the PIT-model. A more accurate prediction could be made by using the actual wind forcing in the fine grid large scale model in which the HCZ-model is nested. However this lies outside the scope of the report as this would involve simulations of the fine grid large scale model with the measured conditions for discharge and wind included to generate boundary conditions for HCZ-model.

In Figures 4.10 to 4.12 the inclusion of waves is investigated. As expected the wave effect on the water levels and current velocities is small at the considered water depths. As can be seen in Table 4.4 and Table 4.5 the effect of waves and wind is limited: most statistics show only small changes.

The effect of the pit on the flow velocities (at location M) is reproduced accurately by the model. The correlation coefficient *r*, the best-fit slope *m* and ε_{rms} have comparable values.

Location A	*Water Levels*			*Longshore Component*			*Cross-Shore Component*			*Vector*
Run-ID	*r*	*m*	ε_{rms}	*r*	*m*	ε_{rms}	*r*	*m*	ε_{rms}	*REV*
PT2	0.76	0.68	0.44	0.89	1.01	0.18	0.75	0.70	0.09	0.50
PT4	0.75	0.67	0.45	0.88	0.98	0.19	0.74	0.71	0.09	0.50
PT2-Waves	0.76	0.67	0.42	0.89	0.99	0.18	0.73	0.66	0.09	0.51

Table 4.4 Period I: Statistics for Location A.

Location M	*Water Levels*			*Longshore Component*			*Cross-Shore Component*			*Vector*
Run-ID	*r*	*m*	ε_{rms}	*r*	*m*	ε_{rms}	*r*	*m*	ε_{rms}	*REV*
PT2	0.78	0.71	0.41	0.91	1.01	0.15	0.73	1.07	0.06	0.44
PT4	0.77	0.70	0.42	0.91	0.99	0.16	0.73	1.08	0.06	0.45
PT2-Waves	0.77	0.73	0.39	0.91	1.01	0.16	0.71	1.06	0.06	0.46

Table 4.5 Period I: Statistics for Location M.

In Figure 4.13 the predicted and measured salinity values are compared. The measured salinity at Location A is obtained from the Hydrolab instrument at 0.60 m above the bed which is expected to be somewhat higher then the computed depth averaged salinity. At Location M there where, apart for the Hydrolab measurement, also salinity data available from the Aanderaa instrument at 5 locations in the vertical (2 m, 7 m, 12 m, 22 m and 28 m above the bed). It can be seen that this instrument shows a much larger variable salinity signal, but on average the approximately the same salinity value was found as with the Hydrolab instrument, which indicates a fairly well mixed lower water column. It has to be noted that no data was available for the top layer which is likely to have significantly lower salinity values. Note that the model uses a salinity of 31 ppt, therefore the model can never exceed this salinity value. To obtain a better overall agreement, this salinity boundary conditions should probably be set to about 33 ppt.

4.4.3 Verification for Period II with Delft3D run in 2DH-mode

Comparison of time series

Due to the calm wave (and wind) conditions during this period the model was used to investigate the effect of salinity on the water levels and current velocities at Locations A and M. In Table 4.6 below an overview is given of the executed simulations.

Run-ID	Salinity	Wind
PT5	+	+
PT6	-	+

Table 4.6 Overview of executed 2DH simulations for Period II.

In Figures 4.14 to 4.16 the model results are compared. In Figure 4.14 it can be seen that the water levels are reproduced with much greater accuracy in Period II compared with Period I. The maximum errors are in general less then 0.10 m during high water, but during ebb the error is somewhat larger and in the order of 0.15 to 0.20 m (ε_{rms} is approximately 50% lower at 0.25 to 0.28 m, see Table 4.7 and Table 4.8). The phase is reproduced accurately. The current velocities for Location A are shown in Figure 4.15. It can be seen that the depth averaged velocities could not be derived from the measured velocity profiles during large portions of Period II due to lack of data at Location A. Despite this lack of data it can be seen that the amplitude and phase of the longshore velocities are reproduced with reasonable accuracy, but there seems to be a systematic over-prediction. The cross-shore velocities are reproduced with more accuracy. The offshore velocity peaks (negative sign) show good agreement, whereas the onshore peaks (positive sign) are under-estimated. In Figure 4.16 the velocity components for Location M are compared. It can be seen that on average the maximum ebb and flood longshore velocities are over-predicted by 0.05 to 0.10 m/s. The cross-shore velocities are reproduced remarkably well. The resulting statistics confirm the accurate predictions for Period II (*r*-values of 0.98-0.99 for the longshore velocities), but that the velocities are systematically over-predicted (*m*-values 1.12 to 1.15). The REV-values indicate that the quality of the predictions at both locations can be characterised as "good".

Comparison of the model runs reveals that the density effects due salinity are very small in the 2DH-runs for both the water level and current velocity predictions.

Location A	*Water Levels*			*Longshore Component*			*Cross-Shore Component*			*Vector*
Run-ID	*r*	*m*	ε_{rms}	*r*	*m*	ε_{rms}	*r*	*m*	ε_{rms}	*REV*
PT5	0.97	0.99	0.28	0.98	1.15	0.13	0.90	0.79	0.07	0.32
PT6	0.97	1.01	0.25	0.98	1.15	0.13	0.91	0.73	0.07	0.31

Table 4.7 Period II: Statistics for Location A.

Location M	*Water Levels*			*Longshore Component*			*Cross-Shore Component*			*Vector*
Run-ID	*r*	*m*	ε_{rms}	*r*	*m*	ε_{rms}	*r*	*m*	ε_{rms}	*REV*
PT5	0.97	0.96	0.31	0.98	1.12	0.11	0.89	1.15	0.06	0.26
PT6	0.97	0.98	0.29	0.99	1.14	0.11	0.89	1.08	0.05	0.24

Table 4.8 Period II: Statistics for Location M.

In Figure 4.17 the salinity is compared for Locations A and M. It seems that the model gives a more accurate for the salinity then Period I. The observed decreasing trend is not found in the predicted salinities. This is probably caused by the fact that the model simulations do not cover a long enough time period. If accurate salinity distributions are required it will be necessary to perform simulations over longer periods to take the fluctuating discharges from especially the Nieuwe Waterweg and Haringvliet sluices into account. However, the tidal variation observed in the measurements is reproduced reasonably well.

Comparison for towed measurements

In this sub-section the flow track measurements are compared. In total 4 track were measured, each track during approximately maximum ebb and maximum flood velocities (see also Section 2.3.3 and Figure 2.2. The measured vertical velocity profiles were again depth averaged to enable comparison with the predicted depth averaged velocities. As it takes between 20 and 40 minutes to sail each track. The model results have been interpolated in space and time (velocity maps were saved with a 10 minute interval) according to the available *(x, y, t)* tables. As a reference, the bottom profile is also shown in the figures. Note that is was not necessary to correct for the depth averaged velocities as the measured profiles cover the upper levels as well (the ADCP was mounted on the survey ship at approximately 2 m below the actual water level, the first measurement location is 3 m below the water level). The velocities are compared for longshore (positive in north-east direction) and cross-shore components (positive in south-east direction). For the sailed tracks is referred to Figure 2.2 or Figure 4.22.

In Figure 4.18 the comparison is made for Track 1 which course is along the length axis, parallel to the dominant tidal motion. The flood velocities (two upper plots in Figure 4.18) are reproduced reasonably well. The measured velocity decrease in the pit is somewhat under-estimated but qualitatively reproduced by the model. During ebb (two lower plots in Figure 4.18) the longshore velocities show a more pronounced decrease compared to flood which is predicted as well. However, south of the pit the longshore velocities are over-estimated. The cross-shore ebb velocities show good agreement.

In Figure 4.19 the comparison is made for Track 2, located south of the pit. Its course is parallel to the short axis of the pit, perpendicular to the dominant tidal motion. For both the ebb and flood tracks the model compares reasonably well with the measurement, although the longshore flood velocities are over-predicted somewhat. In both the measurement and the prediction no effect of the pit can be distinguished as the flow is fairly uniform along the track.

In Figure 4.20 the comparison is made for Track 3, located on southern slope of the pit. Its course is parallel to the short axis of the pit, perpendicular to the dominant tidal motion. The longshore flood velocities (top plot) are over-predicted consistently by some 0.10 m/s, as are the cross-shore flood velocities. The measured longshore ebb velocities show a distinct deceleration of the flow on the slope of the pit which is absent in the flood velocities. The model is not able to reproduce this velocity decrease.

At Track 4 located in the centre of the pit, parallel to the short axis of the pit (see Figure 4.21), there is a small but consistent decrease in longshore flow velocities during both ebb and flood. The modelled longshore velocities do not show such a decrease. The pit does not induce a significant decrease in the cross-shore flow velocities which is also predicted.

Although the flow velocities in the pit have reduced slightly, the reduction should be in the order of 25% if the discharge rates would stay constant in the pit (velocity decrease is approximately proportional to the relative water depth increase). This implies the volume of water travelling over the pit is increasing. In fact, already at Track 3 during flood (Track 3 is then the upstream slope) the flow already has almost adjusted itself: there is only a slight

decrease of the longshore flood velocities. Whereas during ebb (Track 3 is then located on the downstream slope) the longshore velocities do show a significant deceleration on the slope. This is not represented accurately by the model. The transition between the velocities inside and outside the pit do not show the measured deceleration. This could be caused by the fact that the prescribed roughness in the pit is too low or that the viscosity may be set too high which causes an over-prediction of lateral mixing of momentum across the pit. The latter can especially important on the slopes perpendicular to the main tidal currents (i.e. northern and southern pit-slopes). Furthermore 3D-effects may play a role, this will be investigated in Section 4.4.3 where model results from 3D-simulations are compared with the track measurements.

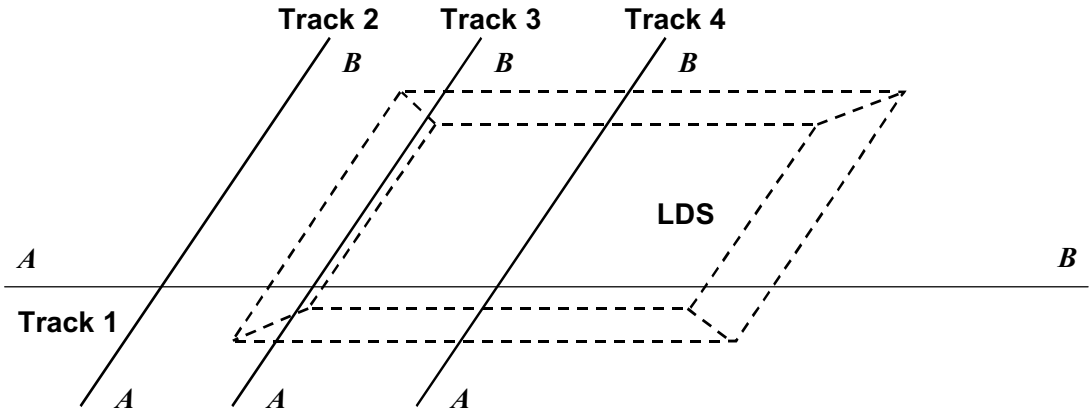

Figure 4.22 Schematic map of the sailed tracks.

4.4.4 Verification for Period I with Delft3D used in 3D-mode

The verification of the 3D-model for Period I is focussed on the velocity time series for Locations A and M at various vertical positions. Furthermore, velocity profiles are compared. As stated in Chapter 3, the 3D-model is based on the 2DH-model, e.g. roughness values and boundary conditions are similar. The vertical grid consists of 10 equidistant layers.

In the 3D-run, the effects of salinity and wind were included, waves were not included.

Comparison of velocity profiles

In Figures 4.23 and 4.24 vertical velocity profiles are compared for Locations A and M during the beginning of Period I when the wind speed is relatively low. The displayed profiles have an hourly time step starting at 26-02-2000 11:05 (indicated by “1” in legend) to 26-02-2000 22:05 (indicated by “12” in legend). The solid lines show the calculated results and the dashed lines the measured results, the lines in blue indicate the longshore velocities and the lines in red the cross-shore velocities. For both locations it is evident that both the calculated longshore and cross-shore velocity profiles regularly deviate from a logarithmic shape in the upper part of the water column. As wind speed is relatively low during this period, this is probably mainly caused by the fresh water discharge from the Nieuwe Waterweg. Although there are no measurements in the upper part of the water

column to verify predictions at Location A, the agreement in the velocities in the lower part of the water column are reproduced fairly well. At Location M the measurements extend to 5 m below the water surface, it can be seen that the model is capable of reproducing the velocities with reasonable accuracy at this depth.

In Figures 4.25 and 4.26 a comparison is made near the end of Period I (04-03-2000 11:05 to 23:05) when high waves and wind are present. Layout of the figures is similar to Figures 4.23 and 4.24 described above. Also for this period the flow often has a 3-dimensional character with opposite flow velocities in the upper and lower parts of the water column. The predictions at Location A show that at 4 March the model shows larger errors compared to 26 February (compare Figures 4.23 and 4.25). However for Location M errors during both tides are comparable. However, it is interesting to see that the model over-predict the longshore velocities during flood for the second period, but not for the first period. Whereas the longshore ebb velocities over-predicted in the first period, but not in the second period. At both locations the cross-shore velocities are reproduced remarkably well for both tides.

Comparison of velocity time series

In Figures 4.27 and 4.28 time series of the longshore and cross-shore velocity components at various depths are shown for Location A, respectively. In Figure 4.29 and 4.30, the longshore and cross-shore velocity components at various depths are compared for Location M. The levels considered for Location A are: 1.5 m, 4 m, 9.5 m and 14.5 m relative to the local bed (or approximately 22.5 m, 20 m, 14.m and 9.5 m below MWL). For Location M the considered levels are: 2 m, 4 m, 18 m and 28 m relative to the local bed (or approximately 31.3 m, 29.3 m, 15.3 m and 5.3 m below MWL). The modelled velocities were interpolated to the vertical measurement coordinates. For both locations the longshore velocities are reproduced accurately, especially at the lower levels. At the highest levels the longshore peak flood velocities are reproduced accurately, but the peak ebb velocities are systematically over-predicted at both locations. The cross-shore velocities are reproduced remarkably well at both locations across the vertical. The largest errors are at the same times as the maximum errors which occurred in the 2DH-runs (e.g. compare Figure 4.12 with Figures 4.29/4.30 for 29-02-2000 12:00 to 24:00). Although storm conditions were present during this time, these do not differ significantly from the surrounding periods. This implies that the southern velocity boundary (which is derived from simulations with the HCZ-model with averaged wind conditions imposed) is not the main source of error. As stated earlier, moving pressure fields may have had a significant influence. The high fresh water discharges from the Nieuwe Waterweg and the Haringvliet may have had a local effect which was not reproduced by the model can be another source of error.

Comparison of residual velocities

In Figure 4.31 the residual velocity profiles are compared for Locations A and M, derived for Period I. In general the model predicts lower longshore residuals, but the vertical distribution agrees qualitatively well with the measurements. For both locations the longshore residual velocities have the highest agreement close to the bed which is important for morphological modelling. The increasing deviations higher in the water column are

mainly caused by the over-predictions of the ebb velocities. The cross-shore residual velocities slightly over-predict the positive velocities near the bed and the negative velocities near the surface. However, the measured vertical distribution of the cross-shore velocities is reproduced remarkably well.

These findings are in accordance with the conclusions drawn in Svašek (2001c). In this report the residual velocities were investigated for Location M at 1.5 m above the bed (Bin 1) and 28 m above the bed (Bin 54). Note that these residual velocities were based on a harmonic analysis of the complete measured velocity time series. In Figure 4.32 it can be seen that the residual velocities at both levels agree in direction with the predicted values. This applies to both the longshore and cross-shore residual velocity components.

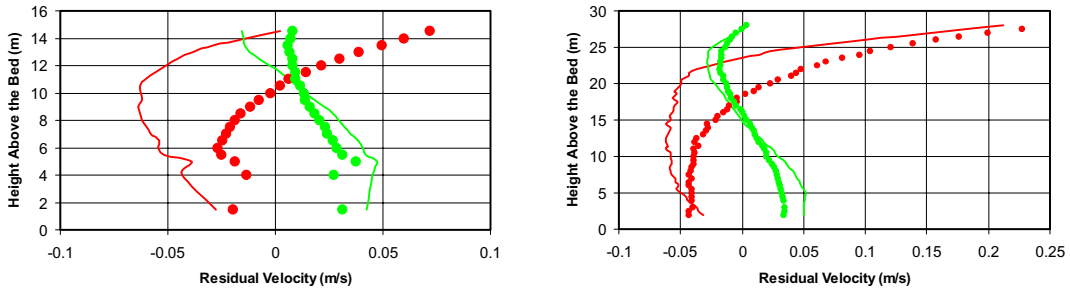

Figure 4.31 Comparison of residual velocities at Locations A (left) and M (right) for Period I. Red: Longshore and Green: Cross-Shore; Solid: Model and Circles: Measurements.

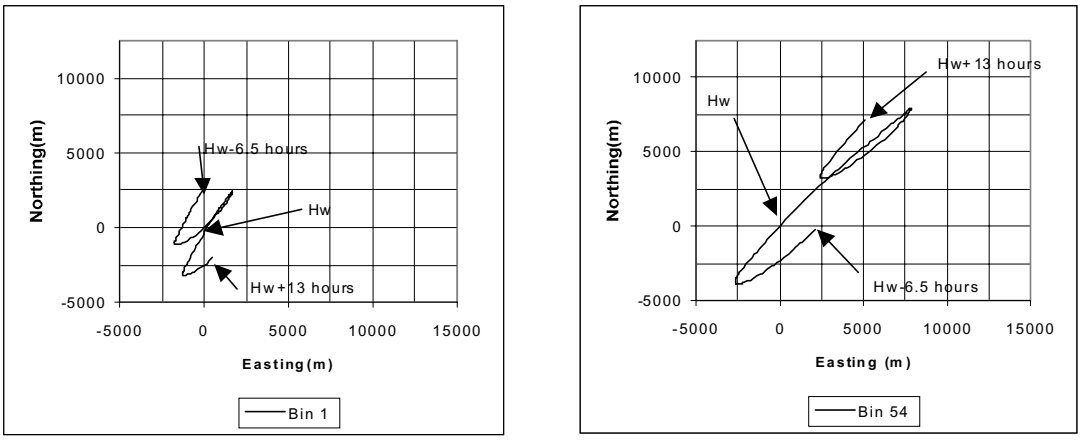

Figure 4.32 Tidal excursion at Location M at 1.5 m above the bed (left: Bin 1) and 28 m above the bed (right: Bin 54), after Svašek (2001c).

Statistical evaluation

Apart from the visual inspection at a limited number of heights presented above, a statistical analysis was performed for all vertical measurement coordinates (22 and 53 levels for Locations A and M, respectively with about 1100 data points per level). The resulting statistics are summarised in Figure 4.33 below. The resulting statistics are shown with respect to the vertical coordinate. The left column represents Location A and the right column Location M. The line colours indicate the longshore (red) or cross-shore (green)

velocity components. The correlation (top row of plots) for the longshore velocities is almost constant along the vertical, but in the cross-shore a decreasing correlation occurs higher in the water column which is most pronounced for Location M. The lower correlation of the cross-shore velocities compared to the longshore correlation is mainly due to the significantly lower cross-shore velocities. This is confirmed by the ε_{rms} (second row of plots) which is significantly lower for the cross-shore velocities. The ε_{rms} values for both locations are comparable and show a gradual increase higher in the water column which is mainly due to the larger velocities. The best fit slope, *m*, is more or less constant for the longshore velocities. However, it decreases significantly, higher in the water column for the cross-shore velocities. This seems to give a somewhat negative impression of the cross-shore velocity predictions which is not confirmed by the time series comparisons. The decreased *m*-values are probably caused by outliers which have large effect on the resulting best fit slope. The relative error vector is also approximately constant across the vertical with values in the range of 0.5 to 0.6 which results in a 'reasonable to fair' qualification according to Table 4.1.

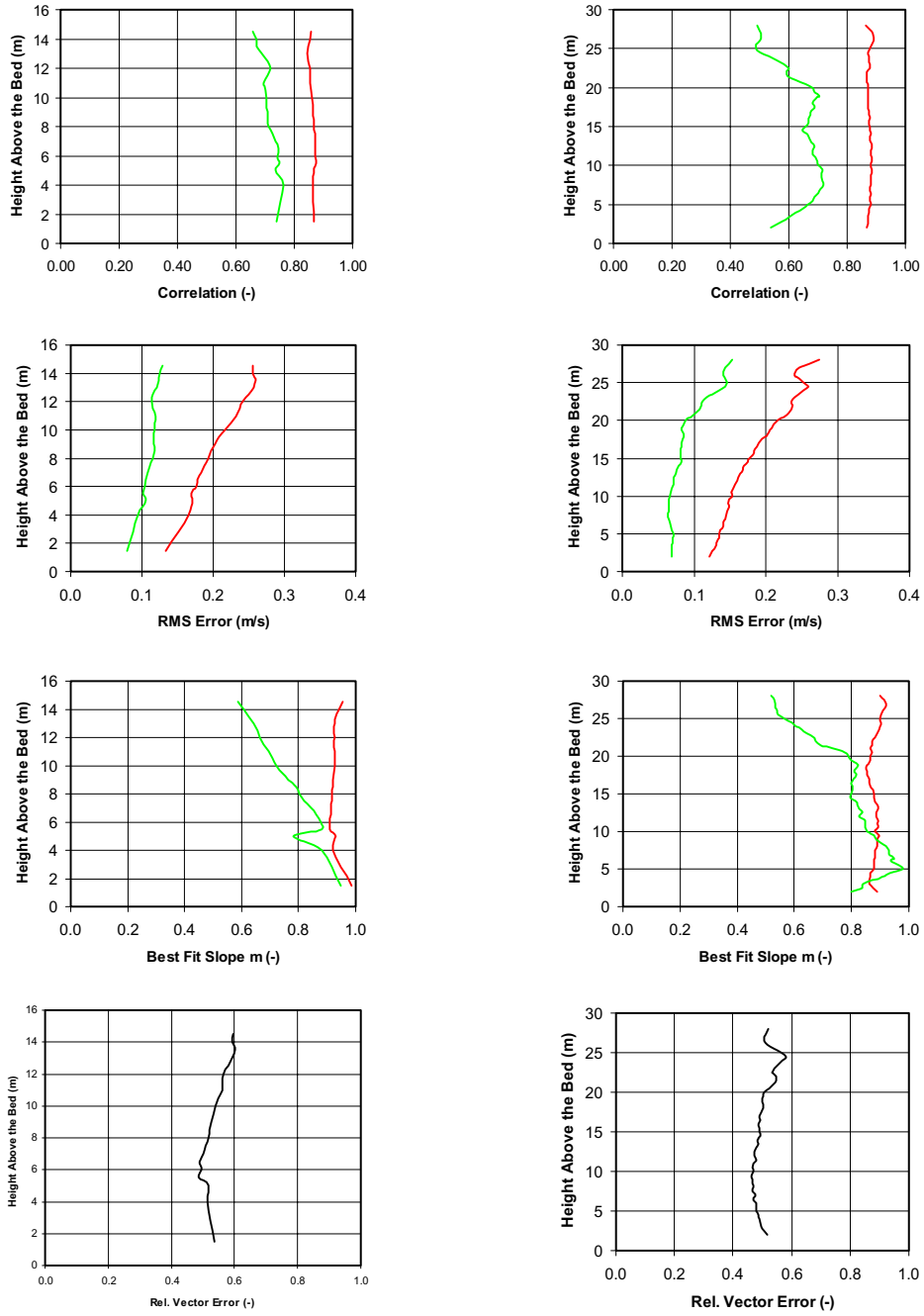

Figure 4.33 Statistic results for Period I at Locations A (left column) and M (right column), longshore and cross-shore components indicated by red and green lines respectively (top row: correlation, second row: ε_{rms}-values, third row: best fit slope - forced through the origin - and bottom row: relative error vector).

4.4.5 Verification for Period II with Delft3D used in 3D-mode

The 3D-simulations were primarily aimed at a comparison with the towed measurements, but also a comparison was made with measured velocity time series at Location A and M for 19 March 2000 00:00 hr to 21 March 00:00 hr (approximately 4 tides). The comparison of the time series is first discussed followed by an evaluation of the towed measurements.

Comparison of velocity time series

In Figures 4.34 and 4.35 the longshore and cross-shore velocities are compared for Location A. In Figures 4.36 and 4.37, the longshore and cross-shore velocities are compared for Location M. The levels considered for Location A are: 1.5 m, 4 m, 9.5 m and 14.5 m relative to the local bed (or approximately 22.5 m, 20 m, 14.m and 9.5 m below MWL). For Location M the considered levels are: 2 m, 4 m, 18 m and 28 m relative to the local bed (or approximately 31.3 m, 29.3 m, 15.3 m and 5.3 m below MWL). The modelled velocities were interpolated to the vertical measurement coordinates. Although relatively large gaps are present in the measured data, it is clear that the model gives a very accurate representation of the measured velocities at all displayed levels in both longshore and cross-shore direction.

Comparison of residual velocities

In Figure 4.38 the residual velocities are compared for both locations for the subset of Period II used in the comparison of the time series above. Compared to residual velocities for Period I, the longshore residual velocities show a different vertical distribution. This is primarily caused by the small but systematic under-prediction of the ebb velocities higher in the water column. In the lower regions good agreement is found. The cross-shore residual velocities are reproduced with reasonable accuracy. The measured onshore directed residual velocities are also predicted by the model. It has to be noted that the reliability of the residuals for such a short period is not representative. Moreover, the relative large gaps in the measured data hamper an accurate derivation of the residual velocities.

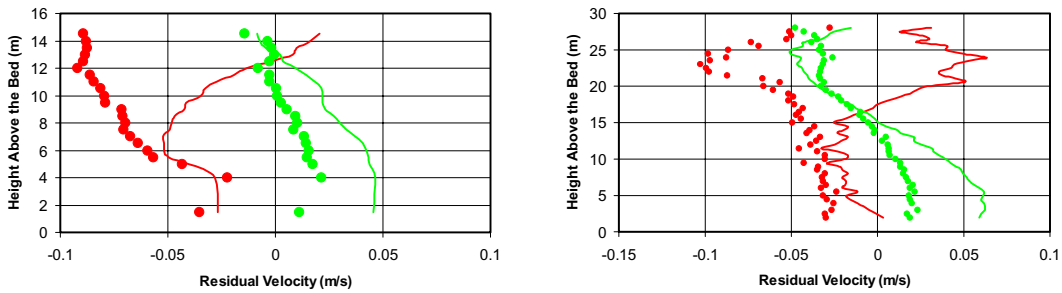

Figure 4.38 Comparison of residual velocities at Locations A (left) and M (right) for subset of Period II. Red: Longshore and Green: Cross-Shore; Solid: Model and Circles: Measurements.

Statistical evaluation

As for Period I, a statistical analysis was performed for all vertical measurement coordinates (22 and 53 levels for Locations A and M, respectively). The resulting statistics are summarised in Figure 4.39 below. The resulting statistics are shown with respect to the vertical coordinate. The left column represents Location A and the right column Location M. The line colours indicates the longshore (red) or cross-shore (green) velocity components. Because the considered period was significantly shorter compared to Period I and more data gaps were present the number of data points was much lower: between 166 and 175 per level for Location A and between 256 and 285 per level for Location M.

Compared to Period I, the model has a higher correlation for the longshore (≈0.98 for Period II against ≈0.88 for Period I) and cross-shore velocities (≈0.84 for Period II against ≈0.6-0.7 for Period I) at both locations. It is interesting to see that the correlation for the cross-shore velocities has a similar vertical distribution at Location M for both periods with relatively low correlation (0.55 and 0.65 for Period I and II) near the bed which increases to values of 0.7 and 0.9 for Period I and II at about 7.5 m above the bed. For the longshore velocities the best fit slope, *m*, shows a significant improvement for both locations, but the cross-shore *m*-values have not improved significantly. The longshore ε_{rms}-values have reduced significantly, but for the cross-shore velocities approximately the same values were found. Because the longshore velocities are dominant this also results in significantly reduced relative error vector values of between 0.2 and 0.4 which qualifies these model results as 'good' according to Table 4.1. The vertical distribution of the relative error vector is very similar for both periods.

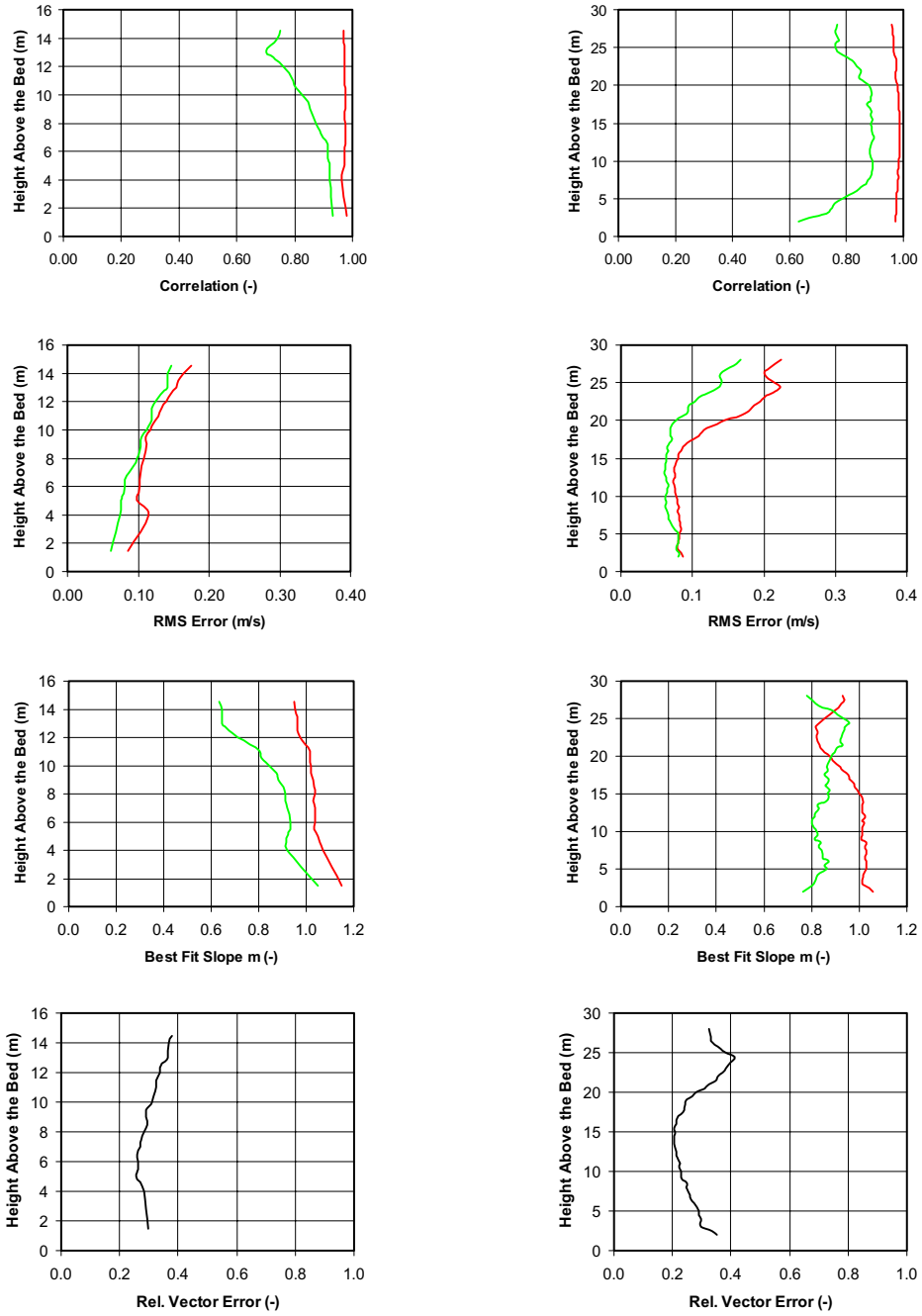

Figure 4.39 Statistic results for Period II at Locations A (left column) and M (right column), longshore and cross-shore components indicated by red and green lines respectively (top row: correlation, second row: ε_{rms}-values, third row: best fit slope - forced through the origin - and bottom row: relative error vector).

Comparison for towed measurements

In this sub-section the flow track measurements are compared with the results from the 3D simulations. As with the 2DH comparison (see Section 4.4.3), the 3D model results have again been interpolated in space and time (velocity maps were saved with a 5 minute interval for the complete 3D-grid) according to the available (*x, y, t*) tables of the sailed tracks. The Figures 4.40 to 4.47 show a comparison of measured and modelled velocities

along the four tracks (see also Figure 2.2 and Figure 4.22 for maps of the sailed tracks). In these figures the top plot always shows the longshore velocities (positive north) and the bottom plot the cross-shore velocities (positive onshore). The comparison shows that the model is able to give a good representation of the measured velocity profiles, even the complex cross-shore velocity profile in which often the direction reverses, is modelled well. In general, the model over-estimates the longshore flood velocities in the upper 10 m of the water column, but near the bed there is usually good agreement. The longshore ebb velocities are usually predicted with a higher accuracy. The over-prediction of the flood velocities higher in the water column is caused by a small phase difference during rising tide at this level (see e.g. Figure 4.36, where the longshore velocities are compared). From Figure 4.36 it is clear that during all four rising tides that were considered this small phase difference is present. Lower in the water column agreement this phase shift is not present, but an over-estimation of the longshore peak flood velocities does occur. During ebb, the deviations are usually less during the considered period. This implies that the comparison of the towed tracks can be regarded as a representative indication for spring tides (and low waves and wind).

In general the model performs exceptional well considering the course resolution of only 10 vertical layers which is used in the 3D model simulation.

In Figures 4.40 to 4.47 a selection of the available velocity profiles had to be made. To investigate the model performance in more detail, relevant statistical parameters were determined for each available vertical velocity profile. To that end, the model data was interpolated to the vertical measurement levels. Although the number of data points per velocity profile is somewhat low (between approximately 35 and 60 levels) to determine reliable statistics, the spatial distribution along the tracks should be able to give an indication on the model performance in the pit and on the slopes of the pit. In Figures 4.48 to 4.51 the statistical results are plotted against the local horizontal track coordinates and the bottom profile is again included as a reference. It is evident that the longshore velocities are generally reproduced accurately with correlation and *m*-values close to 1. The cross-shore performance often shows a irregular pattern, which is mainly caused by the relative small velocities and the more complex vertical distributions. If the cross-shore statistics during flood and ebb are compared it is revealed that during ebb, the cross-shore velocities show better agreement. However, the inspection of the velocity profiles does not support these qualifications. The lower correlation and *m*-values during flood are mainly caused by the deviations in the upper levels, near the bed the accuracy during flood and ebb is comparable. As for the correlations, the ε_{rms}-values (second and bottom plots in figures) do not give any indication of increasing errors in the pit or on the pit slopes. Although occasionally exceeding 0.10 m/s, the ε_{rms} in general stays well below 0.05 m/s. The Relative Error Vector, *REV*, distributions (black lines in first and third plot) also do not vary significantly along the tracks and has values in the range of 0.10 to 0.50, but mostly has values of about 0.20-0.25. Based on the classification of Table 4.1 the qualification of the model performance is ‘Excellent’ to ‘Good’.

4.4.6 Comparison between 2DH and 3D

The limited comparison discussed here is based on the velocity time series for Period I and the towed measurements. In both cases the 3D-model results were depth averaged to enable a comparison between the depth-averaged simulations and the 3D simulations.

In Figures 4.52 and 4.53 the depth-averaged velocities derived from the 3D-simulation are compared with measurements and the 2DH-results. Note that the approximate upper 9 m of the water column were excluded from the depth averaging procedure of the 3D-velocities. It can be seen that for both locations there is a significant difference between the 2DH and 3D runs. Especially in the first half of Period I (26-02-2000 to 01-03-2000) the 3D run gives better agreement, whereas for the second half of Period I agreement is more or less similar.

In Figures 4.54 to 4.57 the towed measurements are compared, the two upper plots for the flood track and the two bottom plots for the ebb track. In general the differences between the 2DH and 3D runs is small. At tracks 1 and 2 the 3D model over-estimates the longshore flood velocities which is mainly caused by the over-estimation of the velocities in the upper layer of the water column (see Figures 4.40 and 4.42). However, the 3D runs are capable to predict the lower longshore flow velocities in the pit (e.g. for the ebb velocities at Tracks 3 and 4, Figures 4.56 and 4.57). This mixed picture is confirmed by the statistics presented in Figure 4.58 and Figure 4.59 below. The relative large variation of the resulting correlations is mainly due to the limited number of data points. The 3D-simulations has resulted in a slightly higher overall correlation for longshore as well as cross-shore velocities. Interestingly, the cross-shore velocities correlations have, on average, approximately the same value as the longshore correlation. In general the Relative Error Vector lies below 0.2 which is classifies these model results as ‘Excellent’ according to the qualifications of Table 4.1.

From this intercomparison between the 2DH and 3D runs, it could be concluded that the former is producing reasonable results against low computational effort and that the latter only results in a limited improvement of the predictions against a very high computational effort. However, it has to be stressed that the presented intercomparison has a limited validity. Especially for morphological models the lower part of the water column is important as most sediment is transported in this region. The vertical velocity profiles have revealed that they often are complex especially in the cross-shore direction. For an accurate morphological prediction it may therefore still be necessary to make use of a 3D-model. This is investigated in the next section where a limited morphological sensitivity analysis is carried out.

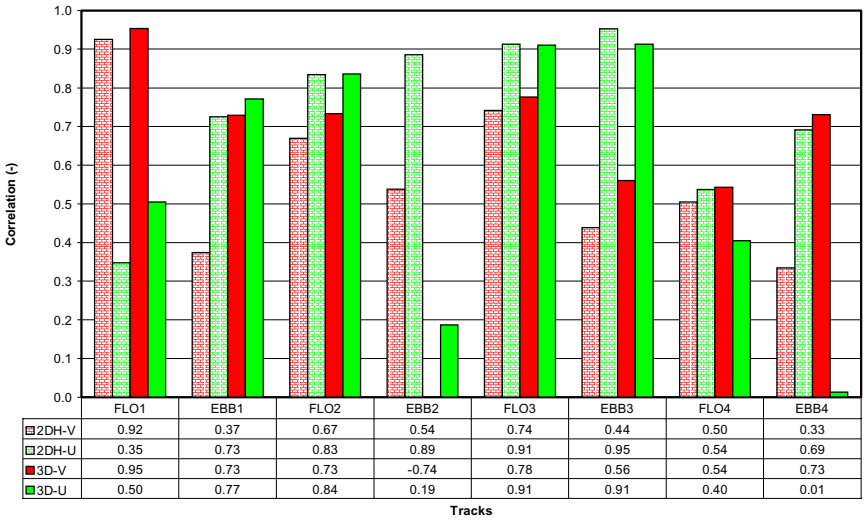

	FLO1	EBB1	FLO2	EBB2	FLO3	EBB3	FLO4	EBB4
2DH-V	0.92	0.37	0.67	0.54	0.74	0.44	0.50	0.33
2DH-U	0.35	0.73	0.83	0.89	0.91	0.95	0.54	0.69
3D-V	0.95	0.73	0.73	-0.74	0.78	0.56	0.54	0.73
3D-U	0.50	0.77	0.84	0.19	0.91	0.91	0.40	0.01

Figure 4.58 Comparison of correlations for depth-averaged velocities derived from the 2DH and 3D simulations.

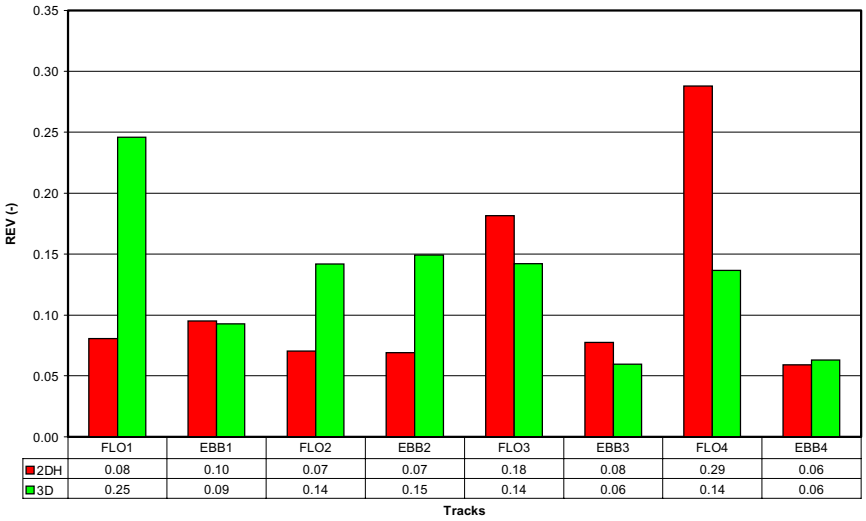

	FLO1	EBB1	FLO2	EBB2	FLO3	EBB3	FLO4	EBB4
2DH	0.08	0.10	0.07	0.07	0.18	0.08	0.29	0.06
3D	0.25	0.09	0.14	0.15	0.14	0.06	0.14	0.06

Figure 4.59 Comparison of Relative Error Vectors (REV) for the depth-averaged velocities derived from the 2DH and 3D simulations.

4.4.7 Intercomparison of measurements at Location A and M

Based on the data analysis in the Svašek reports, a hypothesis regarding flow contraction in the LDS was formulated:

"During flood the velocities in the LDS (Location M) appeared to be larger then the velocities upstream of the LDS (Location A), whereas during ebb no significant differences could be found of the velocities inside the LDS (Location M) and downstream of the LDS (Location A). Because no measurements were available north of the LDS, the model could provide insight if this effect also occurs downstream of the LDS during flood and upstream of the LDS during ebb".

The measured and modelled velocities inside and South the LDS are compared to investigate the first part of the hypothesis: larger longshore flood velocities inside the LDS

compared to the measured velocities upstream (i.e. South) of the LDS and no significant differences during ebb downstream of the LDS. Next, the modelled time series in the LDS and just South and North of the LDS are compared to investigate if the model can represent the observed influence of the LDS and to investigate the second part of the hypothesis: are the downstream and upstream effects also present North of the LDS.

In Figure 4.60 the measured longshore velocities are compared for Locations A and M at three levels in the water column (top plot: 14.5 m above the bed, middle plot: 9.5 m above the bed and bottom plot: 4 m above the bed). The flood velocities at 14.5 m above the bed South of the LDS are consistently higher then inside the LDS, which is not observed during the peak ebb velocities. This marked influence of the LDS is not present in the plotted lower levels. At 9.5 m above the bed almost the opposite is present: at this level the peak flood velocities are approximately similar, but the peak ebb velocities show a larger reduction in the pit compared to the ebb velocities at 14.5 above the bed. At 4 m above the bed the no significant differences were observed.

In Figure 4.61 the modelled longshore velocities inside the LDS (Location M), just South (Location A) and just North (Location B) of the LDS are compared. The velocities South (Location A) and North of the LDS (Location B) show a fairly consistent agreement at all three investigated levels, whereas the peak velocities inside the LDS are consistently lower. The increasing agreement lower in the water column is consistent with the observations.

The small velocity differences imply that the discharge per unit width has increased in the pit (the water depth has increased with about 30% in the pit which, in case of a constant discharge per unit width, would result in an equal reduction of the velocities in the pit).

The first part, concerning the peak flood velocities, of the hypothesis is rejected. Moreover, the opposite effect is present higher in the water column (i.e. a reduction of the peak flood velocities in the pit compared to the velocities outside the pit). The ebb velocities do show higher level of agreement which supports the hypothesis, concerning the ebb velocities. To answer the second part of the hypothesis, the modelled velocities North and South of the LDS are considered. Because the modelled velocities North and South of the LDS show a high level of agreement it is concluded that the upstream and downstream influence North and South of the LDS is comparable during ebb.

4.5 Morphological Verification

In this section the Delft3D is used to perform morphodynamic simulations. First the model is applied with representative boundary conditions to enable a comparison with the measured morphological development in Sub-section 4.5.1. In addition, a limited sensitivity analysis was conducted with the verified model using the forcing conditions of the two periods used in the hydrodynamic verification described in the previous section. The model was applied in 2DH and 3D-mode for both periods. For Period I (26-02-2000 00:00 to 05-03-2000 00:00) 2DH and 3D simulations were carried out with waves included. To investigate the effects waves may have on the morphology, also a 2DH-simulation was made without waves for this period. For Period II (20-03-2000 00:00 to 26-03-2000 00:00) a 2DH and a 3D simulation were made without waves. The sensitivity runs for Period I and

II can be found in Sub-sections 4.5.2 and 4.5.3, respectively. In Table 4.9 the morphological sensitivity simulations are summarised. Note that salinity and wind were included in all morphodynamic simulations.

In the morphodynamic simulations the new 'sediment on line' version was used. This has recently been introduced in the Flow module, so that the transport components can be calculated during the flow simulation. In this 'on-line' mode the transport rates can be computed using:

- a multi-layer model approach (3D) based on the numerical solution of the 3D advection-diffusion equation (Lesser, 2000);
- a one layer model approach (2DH) based on sand transport capacity formulations for bed-load and suspended load transport excluding or including the Galapatti method to account for the lag effects of the suspended load transport (van Rijn et al., 2001).

Period	RUN-ID	2DH	3D	Waves
I	PT2	+	-	+
I	PT2-NW	+	-	-
I	PT2-3D	-	+	+
II	PT5	+	-	-
II	PT5-3D	-	+	-

Table 4.9 Overview of morphodynamic simulations.

All the morphodynamic simulations were scaled to one year to enable comparison with the measured bathymetries. Additional input parameters are summarised in the table below. Note that in contrast to the 3D hydrodynamic runs, where a equidistant vertical grid of 10 layers was applied, the flow-model uses a non-equidistant vertical grid of 10 layers in the 3D morphodynamic simulations, as a relative high resolution is required near the bed. The layer distribution was set to (in % of the water depth from surface to bottom): 10.00, 10.00, 15.00, 22.50, 15.75, 10.50, 6.75, 4.50, 3.00, and 2.00.

Input Parameter	Value
Sediment Density	2650 (kg/m^3)
Median Sediment Diameter, D50	240 (μm)
Dry Bed Density	1600 (kg/m^3)

Table 4.10 Additional model input parameters for morphodynamic simulations.

4.5.1 Morphological verification with representative boundary conditions

The measured morphological development of the LDS has been derived from six bathymetric surveys and was scaled to one year. To make a direct comparison with the measurements, representative boundary conditions for waves, wind and tide are required. To that end, representative conditions derived in earlier studies are used here. A representative morphological tide derived by Walstra et al. (1997) is used in this study. The morphological tide runs from 3hr20 min 18 July 1988 to 15h40m 18 July 1988. This tide is used in the HCZ-model to obtain tidal boundary conditions for the detailed PIT-model.

Furthermore, one single representative wave condition from Walstra et al. (1998, 1999) is used. This climate consists of a single wave condition from 315 ° N with a height of 2.25 m, a period of 6.6 s occurring 84 % of the time. A representative constant wind of 7 m/s from the southwest was also included.

In Figure 4.62 the measured (left) and simulated sedimentation-erosion patterns (right) after 1 year are compared. The model result also shows the yearly averaged total transport vectors. The green line indicates the transect which was used by the Sutrench model for the comparison with Delft3D (see Walstra et al. 2002). The measured morphological development had to be derived from a statistical analysis of the available bathymetric surveys as the individual surveys had an accuracy which was smaller then the observed morphological changes. Therefore, the presented sedimentation-erosion is only reliable on the pit slopes (excluding the southwestern pit slope) and the areas just southeast and northwest of the pit. The outer regions and the landward side of the pit are considered to be too inaccurate for a comparison with the model.

Taking these limitations into account, the following conclusions were drawn from the measured bottom changes:

- Northeast and Southwest of the pit mainly erosions occurs, whereas the pit slopes experience sedimentation.
- Apart from the erosion of the ridge in the north part of the pit, the pit itself does not show any significant changes although it does seem to experience an overall small sedimentation.
- The southwest pit slope does not show any significant changes, but this is thought to be due to inaccuracies in the measurements.

The modelled bottom changes predict that most changes occur on the pit slopes and just southwest and northeast of the pit which agrees with the trends derived from measured bottom changes. In the pit no significant changes are predicted. However, the ridge in the northern region of the pit is eroded, this sediment is mainly deposited northeast and southwest of this ridge. This erosion was also found in the measurements, although evidence of deposition in the surrounding regions could not found. Apart from the expected upstream and downstream erosion of the areas just northeast and southwest of the pit, the model also predicts a surprisingly large erosion of the upper areas of the landward pit slope. This seems to be confirmed by the measurements where the landward region just east of the pit is eroded, however this conclusion can not be firm due to the unreliable measurements in this area. For the seaward region, just west of the pit, the model also predicts a limited erosion. The sedimentation of the pit slopes parallel to the dominant tidal motion (i.e. the eastern and western pit slopes) is surprisingly large. This is primarily caused by flow contraction in the pit. As the verification study, carried out in the previous phase of this project (Walstra et al., 2002), showed that the flow contraction is under-predicted in 2DH it is thought that the sedimentation of these parallel pit slopes is under-estimated. Considering the relative small time scale of the morphodynamic simulation it is concluded that cross-shore transports due to flow contraction can not be ignored in long term morphodynamic simulations.

A detailed inspection of the results is shown in Figure 4.63 where the profile changes, residual longshore transports and residual cross-shore transports are shown along the transect indicated by the green line in Figure 4.62. The longshore transports (3rd graph in Figure 4.63) inside the trench are of the same order as outside the trench, but on the slopes the transports show a significant variation. The eastern and western slopes both experience sedimentation. The top of the western slope also shows some erosion which is mainly caused by compensating flows resulting in shoreward transports, this phenomenon is not found at the eastern slope. On the southwestern pit slope the residual transports show an increase of about 100% compared to the transports south of the pit. The same effect is present at the northeastern pit slope. As mentioned earlier this is caused by flow contraction on these pit slopes which cause an additional erosion just southwest of the pit and a sedimentation just northeast of the pit. The cross-shore transports also show a significant influence of the pit, although the magnitude is of a smaller order then the longshore transports. Especially, on the southwestern pit slope a significant increased cross-shore transport is predicted which is probably caused by the flow contraction which attracts water offshore from the pit. However the fact that the main tidal motion is not exactly parallel to the orientation of the long axis of the pit can also not be ignored. This could explain the reduction of the cross-shore transports at the northeastern pit slope.

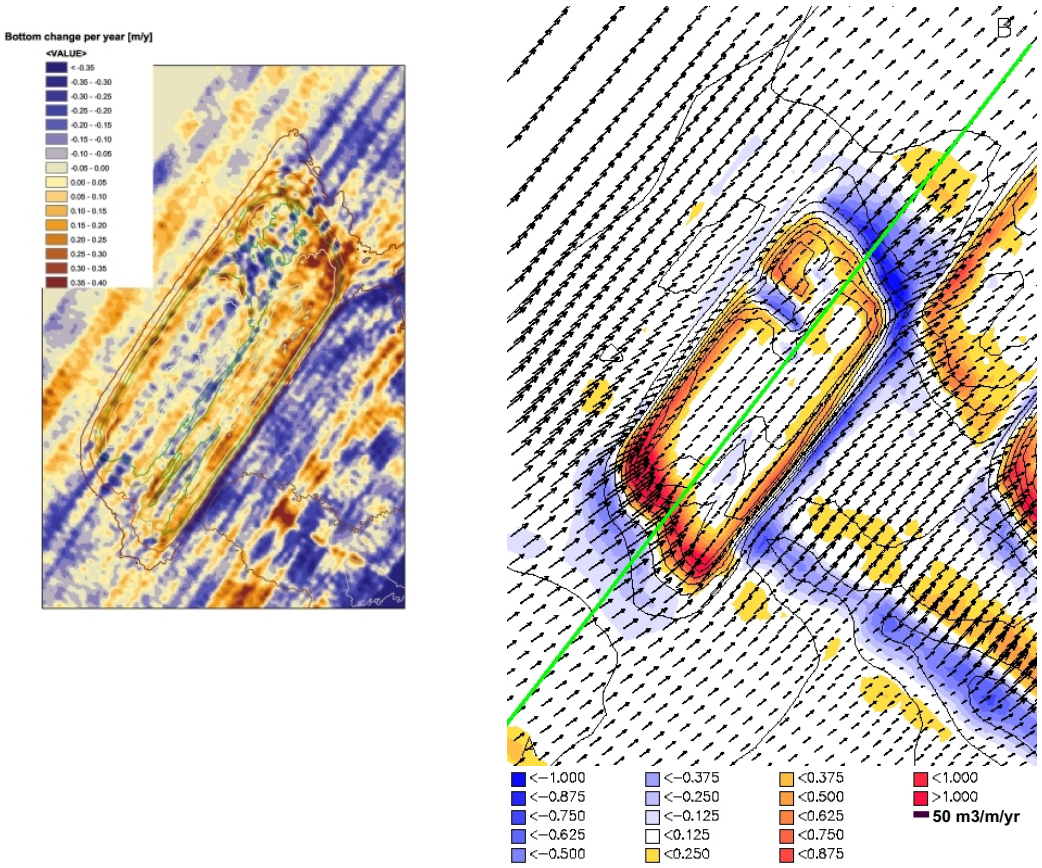

Figure 4.62 Comparison of measured and simulated sedimentation-erosion patterns after one year (left: derived from surveys carried in Putmor project, right: Delft3D model result). The green line indicates the Sutrench transect.

4.5.2 Morphological Sensitivity Simulations for Period I

In Figure 4.64 the predicted sediment-erosion patterns and the residual total depth averaged transports are shown for the 2DH and 3D simulation (both with waves included). The 3D simulation has resulted in somewhat larger changes in the morphology, but in both simulations most changes have occurred in the direct vicinity of the pit: erosion just outside the pit and mainly sedimentation on the pit slopes. In both simulations the largest changes are present on and just outside the northeastern and southwestern slopes of the LDS. The sedimentation on the landward and seaward slopes of the LDS is more pronounced in the 3D simulation. This is mainly caused by secondary cross-shore flows caused by the presence of the LDS. In the hydrodynamic verification it was shown that this was modelled well in 3D but not in 2DH.

To inspect the results in more detail, bottom profiles, sediment-erosion and the residual transports were interpolated along the tracks which were also used in the hydrodynamic verification (see Figure 2.2 and Figure 4.22). Track 2 is omitted as it lies outside the pit where little changes have occurred. In Figures 4.65 to 4.67 the results are shown for the 3D simulation and in Figures 4.68 to 4.70 for the 2DH simulation. The top plots shows the bottom profile at the start and after one year, the second plot shows the sedimentation-erosion along the track and the two bottom plots show the longshore and cross-shore residual transports. In each plot the initial bottom profile is again shown as a reference. Although the morphology along Track 1 only shows marginal differences, the longshore and cross-shore residual transports show marked differences. South and inside the LDS the 3D model predicts higher transports whereas on the northern slope negative transports are predicted (compare Figures 4.65 and 4.68).

For Track 3, located along the southern slope, the sedimentation is comparable for the 2DH and 3D simulations (compare Figures 4.66 and 4.69). The 3D longshore transports show a gradual increase of about 100% on the slope whereas in 2DH the pit does not have a significant influence on the longshore transports. The cross-shore transports have a comparable distribution over Track 3, but the pit slopes induce a stronger influence in the 3D model. The results along Track 4 (compare Figures 4.67 and 4.70), located in the centre of the pit are similar to the results of Track 3. From these results it can be concluded that in 3D mode the effects of the pit are significantly larger then when modelled in depth averaged mode.

The effects of waves was investigated by performing an additional 2DH simulation without waves. The resulting sedimentation-erosion patterns are shown in Figure 4.71 for the simulation with waves (top plot) and without waves (bottom plot). It can be seen that the waves have a limited effect on the morphological development. As could be expected the sedimentation-erosion with waves is somewhat higher, but the patterns are very similar for both runs.

4.5.3 Morphological Sensitivity Simulations for Period II

In Figure 4.72 the sedimentation-erosion and the residual total depth averaged transports for the 2DH and 3D simulations are shown. The spring tide occurring in this period is resulting

in significantly larger bottom changes compared to Period I. Consistently with the findings for Period I, the 3D simulation has resulted in larger changes compared to the 2DH simulation. However, the overall sedimentation-erosion patterns are comparable. The main differences are the erosion west of the pit in the 3D simulation, which is not present in 2DH. Furthermore, the sedimentation in the northern half of the pit that was found in the 3D simulation is not present in 2DH. The erosion west of the pit is mainly caused by secondary onshore currents which sub-sequently results in an enhanced sedimentation of the western pit slope in the 3D simulation. These onshore directed 3D transports along the western pit slope, which is not predicted in 2DH, is consistent with the findings for Period I.

The morphology and transports are again shown along the tracks in Figures 4.73 to 4.75 for the 3D simulation and in Figures 4.76 to 4.78 for the 2DH simulation. Note that the residual transports during this period are about 3 to 5 times larger then the reported yearly averaged representative longshore transports by Van Rijn et al. (1995). Comparing Figures 4.73 and 4.76 for Track 1 it can be seen that the longshore and cross-shore transports are about 40% higher for the 3D case just South of the pit, whereas North of the pit the 2DH transports are higher. The influence of the pit slopes is comparable for both runs. As a consequence, the sedimentation-erosion distribution along Track 1 is comparable for both simulations, but the absolute changes are larger in the 3D simulation due to the overall higher transports rates. The sedimentation on the southern slope, Track 3 (see Figures 4.74 and 4.77) is comparable for both runs. As for Track 1, the 3D longshore transports are again higher, but the cross-shore transports are comparable. The distribution of both the longshore and cross-shore transports over Track 3 is very similar, which is in accordance with the findings for Period I. At Track 4 the flattening of the seaward slope in the 3D simulation is most obvious difference with the 2DH simulation which is caused by the increased onshore transports on the seaward slope of the pit. The longshore transports have comparable distributions. As was found in Period I, the 3D longshore transports have decreased significantly seaward of the pit which is not the case for the 2DH simulation.

4.5.4 Comparison between 2DH and 3D

If the suspended and bottom transports are compared for both model simulations, it can be seen that in general the suspended transport is approximately the same, but that the bed load is usually higher in the 3D simulations. Especially on the pit slopes and southwest of the pit significant differences are found. As the same bed load formulation is used in both 2DH and 3D-mode, the difference originates from the bed shear stress. In 2DH these are derived from the depth averaged velocities whereas in 3D, the velocity in the bottom layer is used. In Figures 4.79 and 4.80 the time averaged bed shear stress magnitude for the 2DH and 3D simulations are compared. In the top plots the ratio between the 2DH and 3D bottom shear stress magnitude is shown. The middle and bottom plots show the time averaged bed shear stress of respectively the 2DH and 3D simulation.

From the figures it is clear that locally significant differences are present. Especially on the western pit slope and southwest of the pit the time averaged bed shear is 10 times higher for the 3D simulations for both periods. It is interesting to see that for the northeastern pit slope significant differences between the 2DH and 3D simulations are found for Period I while at

the southwestern pit slope the differences are small. For Period II the opposite ratio distribution is found: significant differences on the southwestern slope and minor differences at the northeastern slope.

Considering the good performance of the 3D model in the hydrodynamic verification, it is thought that the 3D results are more reliable. A more detailed comparison is required to obtain a better insight in the differences between 2DH and 3D. Ideally such a comparison should be based on morphodynamic simulations covering a larger time scale then was considered here.

5 Conclusions

5.1 Hydrodynamic Verification

5.1.1 Overall model performance in 2DH-mode

The evaluation study has shown that the Delft3D-model is capable of reproducing the measurements with reasonable to good accuracy. However, the agreement did vary in the two periods that were considered. In the first period, around neap tide with relatively high waves and wind, occasionally large deviations between the predictions and measurements were observed. It is thought however, that these deviations were caused by the fact that the overall HCZ-model, in which the PIT-model was nested, was unable to accurately account for (high) wind speeds. The second period, around spring tide with low waves and wind, was reproduced accurately.

In the 2DH-simulations the effect of waves, wind and salinity was limited. The tidal forcing appeared to be dominant at the investigated pit. It has to be stressed however that especially wind effects are under-estimated in the present model set-up.

The comparison with the flow track measurements showed that the model was capable of reproducing the current velocities with reasonable accuracy. The deceleration of the flow across the long axis of the pit was represented well, especially during the ebb measurements. However, during flood the deceleration was under-estimated in comparison with the flow tracks on the southern slope. This under-estimation is mainly caused by the 2DH approximation as the 3D simulations were able to model this phenomenon. Because the tracks were sailed during maximum flood and ebb, small errors in the phase could also results in deviations, especially during flood which has a characteristic peaked character.

The error statistics, summarised in Table 5.1 below, show that the trends in water level predictions are reasonable with correlation coefficients of 0.76 and 0.97 for Periods I and II respectively. The velocities are reproduced well with correlation coefficients generally exceeding 0.9, whereas the root mean square error for the velocities lies between 0.11 and 0.18 m/s. for the longshore velocities and between 0.06 and 0.09 m/s for the cross-shore velocities.

The relative error vector *REV* indicates a “reasonable” prediction for Period I and a “good” prediction for Period II, according to definitions given in Table 4.1.

Location A	*Water Levels*			*Longshore Velocities*			*Cross-Shore Velocities*			*Vector*
	r	*m*	ε_{rms}	*r*	*m*	ε_{rms}	*r*	*m*	ε_{rms}	*REV*
Period I	0.76	0.67	0.42	0.89	1.01	0.18	0.75	0.70	0.09	0.50
Period II	0.97	0.99	0.28	0.98	1.15	0.13	0.91	1.15	0.07	0.32
Location M	*Water Levels*			*Longshore Velocities*			*Cross-Shore Velocities*			*Vector*
	r	*m*	ε_{rms}	*r*	*m*	ε_{rms}	*r*	*m*	ε_{rms}	*REV*
Period I	0.78	0.71	0.41	0.91	1.01	0.15	0.73	1.07	0.06	0.44
Period II	0.97	0.96	0.31	0.99	1.14	0.11	0.89	1.15	0.06	0.26

Table 5.1 Summary of error statistics for 2DH-model.

5.1.2 Overall model performance in 3D-mode

It was shown that Delft3D running in 3D-mode was capable of reproducing the 3D character of the flow accurately. The vertical distribution of the residual velocities was reproduced well. The northward residual velocities in the upper layers and the southward residual velocity near the bed were also predicted by the model for Period I. For Period II the longshore residual velocities agreed well near the bed, but higher in the water column significant deviations were present. The relative short time period over which the residual were determined is probably the main cause of this deviation. The cross-shore residual velocities agreed well for this period.

Location A	*Longshore Velocities*			*Cross-Shore Velocities*			*Vector*
	r	*m*	ε_{rms}	*r*	*m*	ε_{rms}	*REV*
Period I	0.86	0.93	0.21	0.71	0.75	0.11	0.54
Period II	0.97	1.02	0.12	0.83	0.83	0.11	0.31
Location M	*Longshore Velocities*			*Cross-Shore Velocities*			*Vector*
	r	*m*	ε_{rms}	*r*	*m*	ε_{rms}	*REV*
Period I	0.88	0.88	0.19	0.63	0.78	0.09	0.50
Period II	0.98	0.96	0.12	0.84	0.86	0.09	0.28

Table 5.2 Summary of error statistics for 3D-model (time and vertically averaged statistics).

The statistical analysis showed that the correlation for the longshore velocities was comparable to the results of the 2DH-simulations. As was the case for the 2DH-simulations, the 3D cross-shore velocities had lower correlations and *m*-values compared to the longshore statistics (see also Table 5.2 in which the vertically averaged statistics are summarised. Moreover, the correlation for the cross-shore velocities did show relative large variation across the vertical whereas for the longshore velocities this parameter was approximately constant. The Relative Error Vector also had an approximate constant vertical distribution for both periods with an average value of 0.5 to 0.54 for Period I and

0.28 to 0.31 for Period II. This characterises the model performance as 'reasonable' and 'good' for Periods I and II respectively.

The 3D-model showed good agreement with the flow track measurements. In all cases the vertical distribution of the longshore velocities was represented well. The cross-shore velocities often had a complex character with opposite velocity directions in the upper and lower layers, this was reproduced remarkably well by the 3D-model. For most tracks the Relative Error Vector was in the range of 0.20 to 0.25, which classifies the predictions as 'good'.

5.1.3 Effects of the LDS-pit

The presence of the pit locally influences the flow velocities; especially on the slopes of the pit deceleration or acceleration flows could be observed which could not be modelled accurately in 2DH-mode. Although this was occasionally represented well by the 2DH-model, the general trend was an under-estimation of this phenomenon. However, in 3D-mode the agreement with the measurements increased significantly.

For both periods, the peak longshore velocities outside the pit at Location A exceed the velocities in the pit at Location M. The average difference is usually less than 0.10 m/s during peak flood and ebb, but during the remaining time the differences are less. Furthermore, no significant phase shifts were observed. The small velocity differences are reproduced by the model as well. The small velocity differences imply that the discharge per unit width has increased in the pit (the water depth has increased with about 30% in the pit which, in case of a constant discharge per unit width, would result in an equal reduction of the velocities in the pit).

5.2 Morphological Verification

The morphodynamic evaluation, based on a 2DH simulation with representative tidal, wind and wave forcing, showed a reasonable agreement with the sedimentation-erosion patterns derived from the bathymetric surveys. As the measured morphological development has considerable uncertainties an unambiguous conclusion regarding the morphological predictive capabilities of the Delft3D could not be drawn.

The morphodynamic sensitivity analysis revealed some significant differences between the results obtained in 2DH and 3D-mode. In general the morphological changes were larger in 3D. Especially the flattening of the seaward pit slope was significantly larger in the 3D simulations. This is mainly caused by onshore transports in this region due to secondary onshore currents. Furthermore, the residual longshore transports south of the pit and on the southern slope of the pit were larger in 3D. This is mainly attributed to flow contraction effects.

At this time we can not assess the quality of these predictions due to the lack of a reliable measured morphological development. The differences between the 2DH and 3D morphodynamic simulations on the considered time scale of one year are limited. However, more research is required to investigate 3D effects, especially on longer time scales. This

could be achieved by setting up schematic models which do not take too much CPU-time to run. Although the hydrodynamic verification showed that in 2DH-mode good estimates of the depth-averaged velocities could be obtained, the evaluation of the morphodynamic results revealed that the velocities near the bed are critical for making reliable morphological predictions. Considering the good performance of the 3D model in the hydrodynamic verification for the velocities near the bed it is thought that the 3D results are more realistic.

5.3 Comparison between 2DH and 3D

The choice between 2DH and 3D application of the Delft3D model should always be based on the specific characteristics of the investigated area. These characteristics comprise the effects wind, waves and density currents may have on the vertical velocity distribution. Furthermore, the presence of structures such harbour dams and groynes may require a 3D application. Practical aspects such as the considered time scales and the availability of high speed computers also play a role.

The application of a 3D model will always require a more comprehensive study compared to a 2DH application. The usual approach will be the construction of a 2DH model which, after a verification, is extended to three dimensions. The actual construction of a 3D model, based on a 2DH model, only requires the specification of a vertical grid and prescription of some additional model parameters. A 3D model itself does not require additional data if it is based on a well constructed 2DH model. However, the verification of a 3D model can require a significant increased effort due to the longer simulation time and the increased amount of model data that needs to be processed.

In the present study, the 3D simulations did result in an improved agreement with the measurements based on comparisons of time series at locations both in the pit and outside the pit. The comparison with the flow track measurements showed that the 3D model, in contrast to the 2DH model, was able to predict the decreased velocities in the pit. Furthermore, it was shown that the 3D model was able to give a good representation of the complex vertical velocity profiles in both longshore and cross-shore directions. The morphological verification revealed that the 2DH and 3D morphodynamic simulations in general predicted similar sedimentation-erosion patterns. Local differences were present which mainly related to the more accurate modelling of flow contraction in 3D. However, the predicted bathymetric changes were consistently larger in 3D. It is thought that the 3D morphodynamic simulations gave a more accurate prediction, but this conclusion can not be firm due to the lack of reliable measured bottom changes. Moreover, the relative small time scale of one year that was considered is too short to draw any definite conclusions.

5.4 Research Questions

In the next phase of this project, following the verification study presented in this report, the Delft3D model will be applied to determine the impact of mining pits of various dimensions. It is imperative that in the verification the anticipated research questions are considered, the constructed models should not only be suitable for the verification, but must

be applicable on the anticipated research questions as well. To that end, an overview is given of some general research questions in combination with (preliminary) answers based on the results of the verification study.

Q1 There is a concern that pits will be filled with sand from the coastal zone. Therefore, the models should be able to give indications of the sand transport over e.g. the -20 m and -8 m depth contours on various time scales.

A1 In the morphological verification the Delft3D model gave a reasonable accurate representation of the measured bottom changes for a 10 m deep pit at a water depth of 25 m. The second part of the question can not directly be answered as no verification was carried out for pits at a water depth of 8 m.

Q2 The morphological development of pits should be investigated (migration and deformation) to determine its effect on other functions (e.g. cables and other constructions). The models should be able to indicate what the bathymetric changes will be at various distances from the original pit (50, 100, 200, 500 en 1000 m) on various time scales (1, 2, 5, 10 en 25 years after construction).

A2 The morphological verification has shown that the model was able to reproduce the measured bottom changes after one year. Because no verification on longer time scales was made (due to the lack of long term morphological data) no firm conclusions can be drawn for the longer time scales. However, the good performance of the Delft3D model in the hydrodynamic and morphodynamic verification seems to suggest that the model can be applied on these longer time scales with reasonable confidence. The differences between the 3D and 2DH model morphodynamic simulations have revealed significant differences. At present it is thought that the 3D-model is more reliable, but this can not be confirmed with measurements. There is no practical limitation to apply these models on decadal time scales, even in 3D. However, the morphological performance must be assessed first in order to characterise the quality of the predicted morphological changes on such large time scales.

Q3 Can the morphological development of pits be modelled with 2DH-models or is a full 3D-model required.

A3 The hydrodynamic verification study has shown that with a 3D-model better agreement is obtained then simulations in 2DH-mode for the PUTMOR data. The differences between the morphological predictions in both modes underlines that there is still some uncertainty regarding the quality of the morphological predictions. The results presented in this report seem to suggest that 3D morphological simulations are necessary. However, due to the lack of morphological data with sufficient accuracy and measured over a longer period this is only a preliminary finding.

Q4 Oxygen depletion depends on the extent to which the exchange of water between surface and bottom layer is reduced. The models must be able to predict water refreshment rates in the pits and to determine if there are any areas where there is no exchange of water (stagnant water).

A4 It is thought that the prediction of flow velocities across the vertical is accurate enough to investigate this question. In the LDS the entire water column was refreshed at each tidal cycle (which was both observed and predicted).

Q5 Are there conditions that deposition of mud occurs on time scales larger then the tidal cycle.

A5 This can be investigated by investigating the bottom shear stresses in the pit. As the flow predictions are of sufficient accuracy this question can be investigated in the next phase of the project.

Q6 If mud settles in the pit, will it be removed by the flow and if so how long will it take for the mud to be eroded.

A6 See ***A5.***

Q7 What will the general applicability be of the findings of this study. To what extent can the conclusions drawn in this study be applied on pits at other locations along the Dutch coast.

A7 Delft3D is an advanced process based model in which numerous physical phenomena have been implemented. This implies that the presented verification is appropriate at other locations along the Dutch coast with approximately the same characteristics (e.g. non-breaking waves). The model has performed well, taking the complexity of the modelled area into account (e.g. irregular bathymetry and density effects due to fresh water discharges from the New Waterway). This gives good confidence of the applicability of the model at other locations.

6 References

Lesser, G., Roelvink, J.A. and Van Kester, J., 2000. On-Line sediment transport in Delft3D-FLOW,WL | Delft Hydraulics report, Delft, The Netherlands.

Roelvink, J.A., T. van der Kaaij, B. G. Ruessink, 2001. Calibration and verification of large-scale 2D/3D flow models. Phase 1, Parcel 2, Subproduct 2, ONL FLYLAND report

Svašek, 2001a. PUTMOR, field measurements at a temporary sandpit. Part 1: processing and validation. Svašek Report 01037/1177.

Svašek, 2001b. PUTMOR, field measurements at a temporary sandpit. Part 2: data analysis. Svašek Report 01244/1177.

Svašek, 2001c. PUTMOR, field measurements at a temporary sandpit. Part 3: final report. Svašek Report 01453/1177.

Van Rijn, L.C. and Walstra, D.J.R., 2001. Morphology of Pits, Channels and Trenches; Part I: Literature Review and Study Approach. WL | Delft Hydraulics report Z3223.

Van Rijn, L.C., Walstra, D.J.R., Grasmeijer, B.T., Sutherland, J., Pan, S. and Sierra, J.P., 2002. Simulation of nearshore hydrodynamics and morphodynamics on the time scale of storms and seasons using process-based profile models. In Coast3D - Egmond; The behaviour of a straight sandy coast on the time scale of storms and seasons. Eds. Van Rijn, L.C., Ruessink, B.G. and Mulder, J.P.M.. Aqua Publications, Amsterdam, The Netherlands, ISBN 90-800356-5-3, NUGI 816/831.

Van Rijn, L.C., Reniers, A.J.H.M, Zitman, T. and Ribberink, J.S., 1995. Yearly averaged transports at the -20 m and -8 m NAP depth contours of the JARKUS-profiles 14, 40, 76 and 103. WL | Delft Hydraulics report H1887.

Walstra, D.J.R., Renier, A.J.H.M., Roelvink, J.A., Wang, Z.B., Steetzel, H.J., Aarninkhof, S.G.J., van Holland, G. and Stive, M.J.F., 1997. Morphological impact of large-scle marine sand extraction (in Dutch). Report Z2255, WL | Delft Hydraulics.

Walstra, D.J.R., L.C. van Rijn, S.G.J. Aarninkhof, 1998. Sand transport at the middle and lower shoreface of the Dutch coast. Simulations of SUTRENCH-model and proposal for large-scale laboratory tests.

Walstra, D.J.R., L.C. van Rijn, S.E Hoogewoning, S.G.J. Aarninkhof, 1999. Morphodynamic modelling of dredged trenches and channels. ASCE, Coastal sediments, vol 3 1999 2355-2370. Ed: N.C. Kraus, W.G. McDougal.

Walstra, D.J.R., L.C. van Rijn and de Boer, G., 2002. Morphology of Pits, Channels and Trenches. Part III: Investigation of the longshore and cross-shore impact of various pit designs. WL | Delft Hydraulics report Z3223.30.

WL | Delft Hydraulics, 2001. Reference scenarios and design alternatives, Phase 1. WL | Delft Hydraulics report Z3029.20 (Phase 1, Parcel 2, Subproduct 3, ONL FLYLAND report).

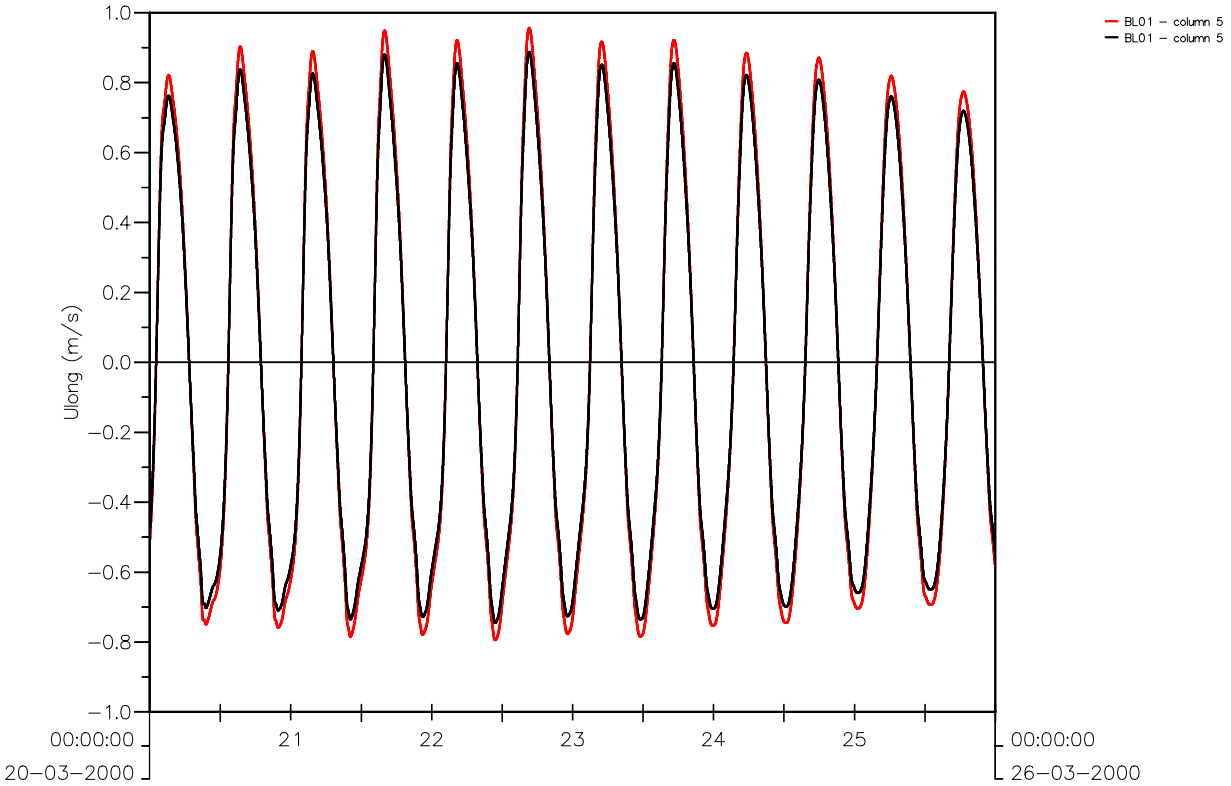

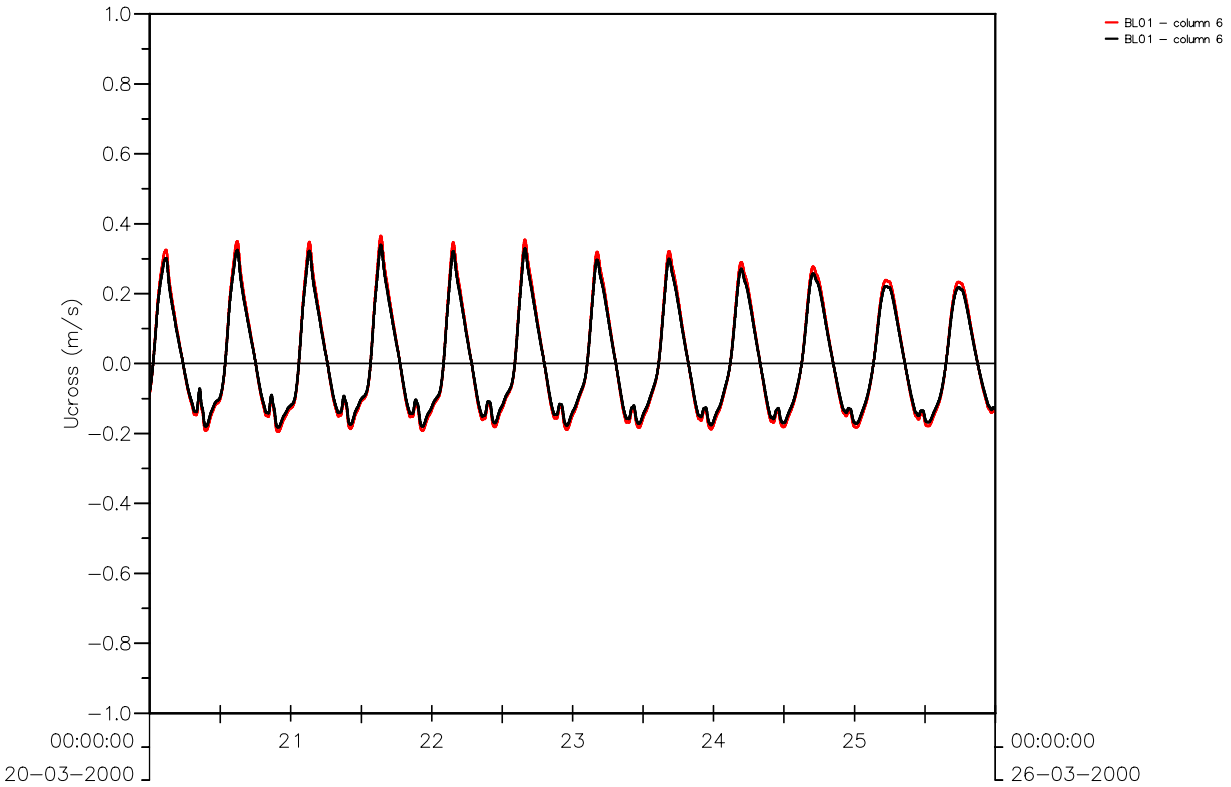

Morphology of pits, channels and trenches Part II: Verification of Delft3D with PUTMOR dataset 2DH Vel. Location A Red: Total Depth, Black: Excluding top 9.5 m		Z3223
		Period 20−03 to 26−03
WL | DELFT HYDRAULICS		Fig. 2.9

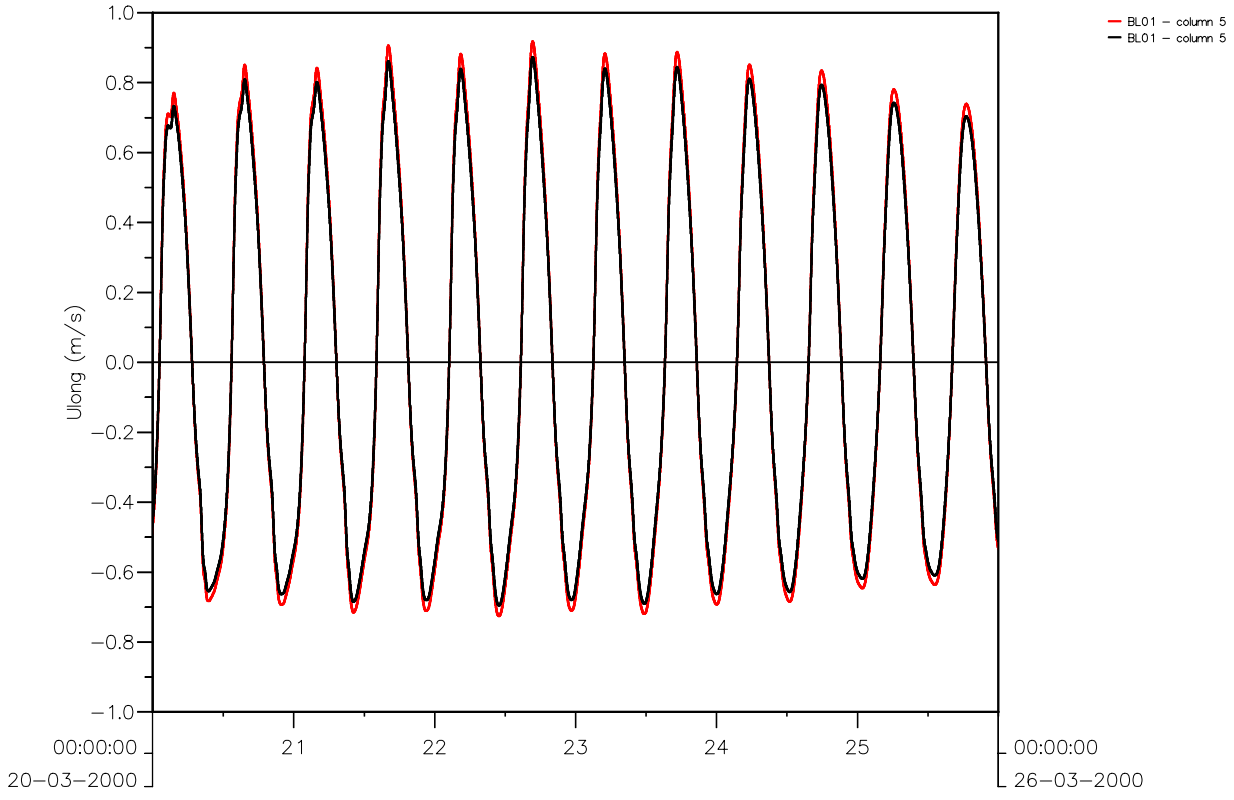

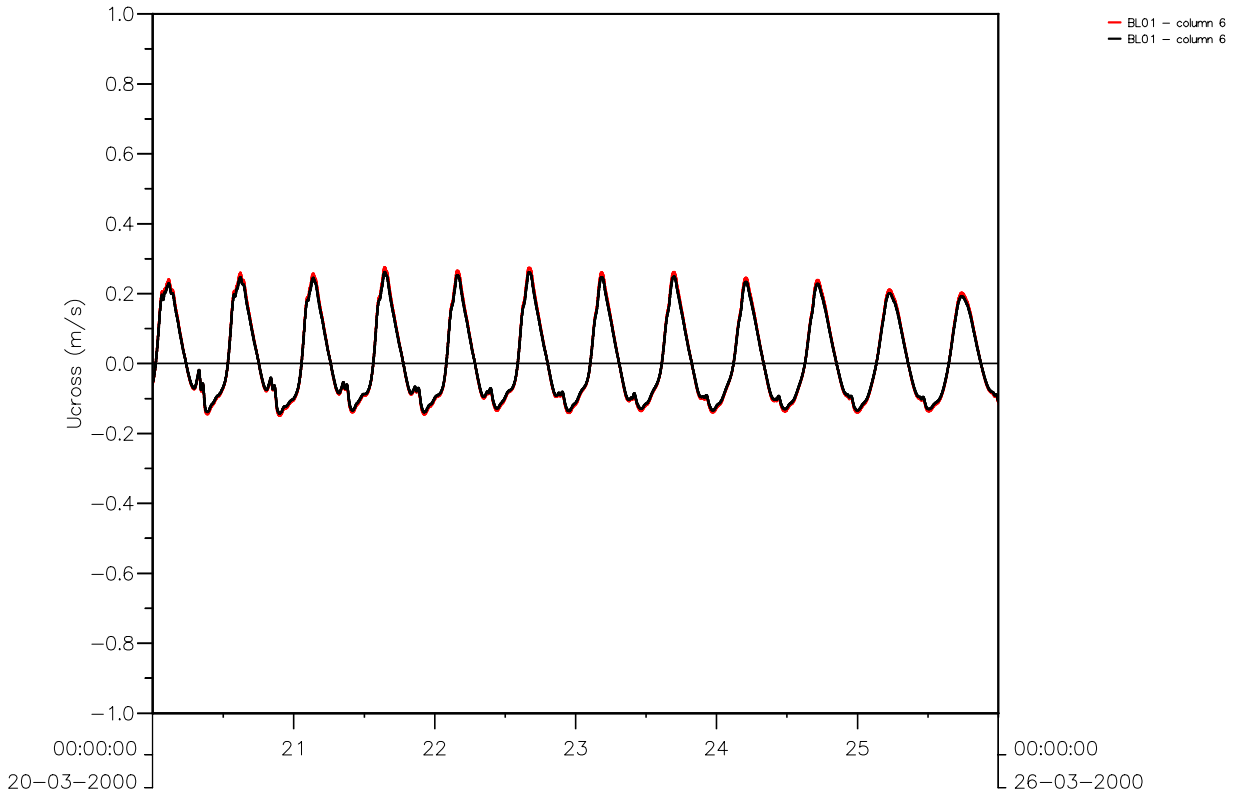

Morphology of pits, channels and trenches
Part II: Verification of Delft3D with PUTMOR dataset
2DH Vel. Location M Red: Total Depth, Black: Excluding top 9.5 m

Z3223

Period 20−03 to 26−03

WL | DELFT HYDRAULICS

Fig. 2.10

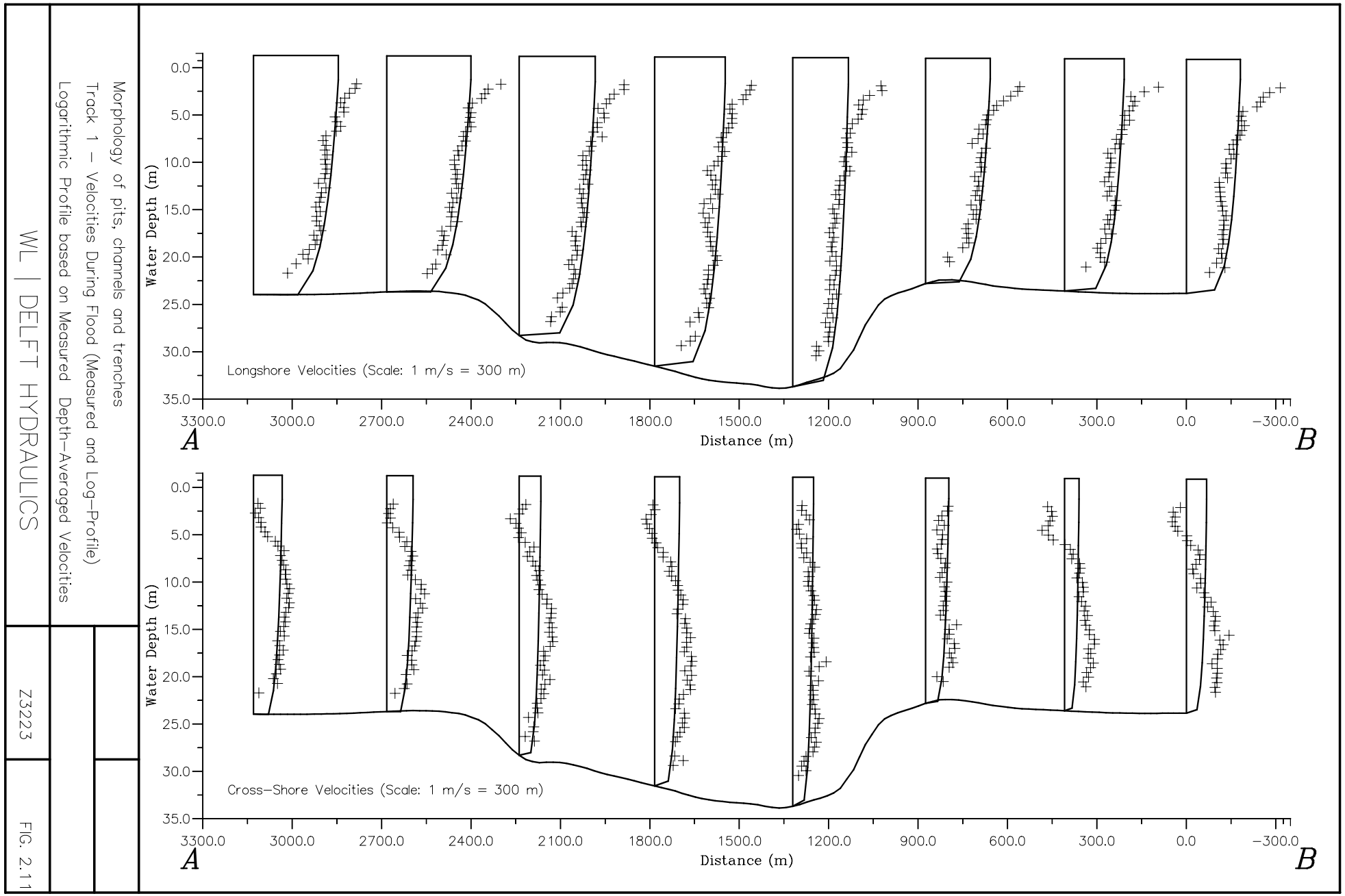

Morphology of pits, channels and trenches

Track 1 – Velocities During Flood (Measured and Log-Profile)

Logarithmic Profile based on Measured Depth-Averaged Velocities

WL | DELFT HYDRAULICS

Z3223

FIG. 2.11

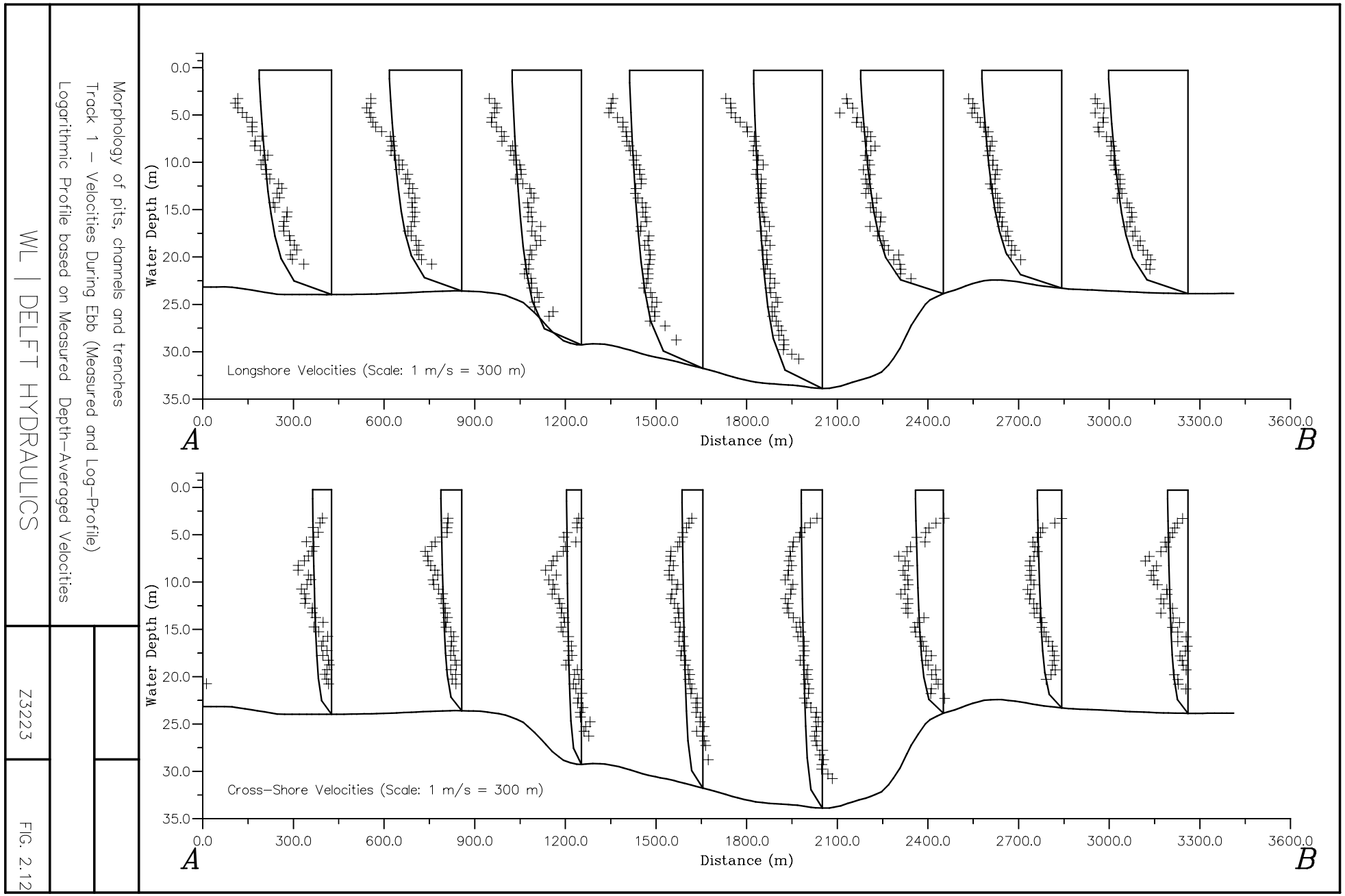

Morphology of pits, channels and trenches

Track 1 – Velocities During Ebb (Measured and Log-Profile)

Logarithmic Profile based on Measured Depth-Averaged Velocities

WL | DELFT HYDRAULICS

Z3223

FIG. 2.12

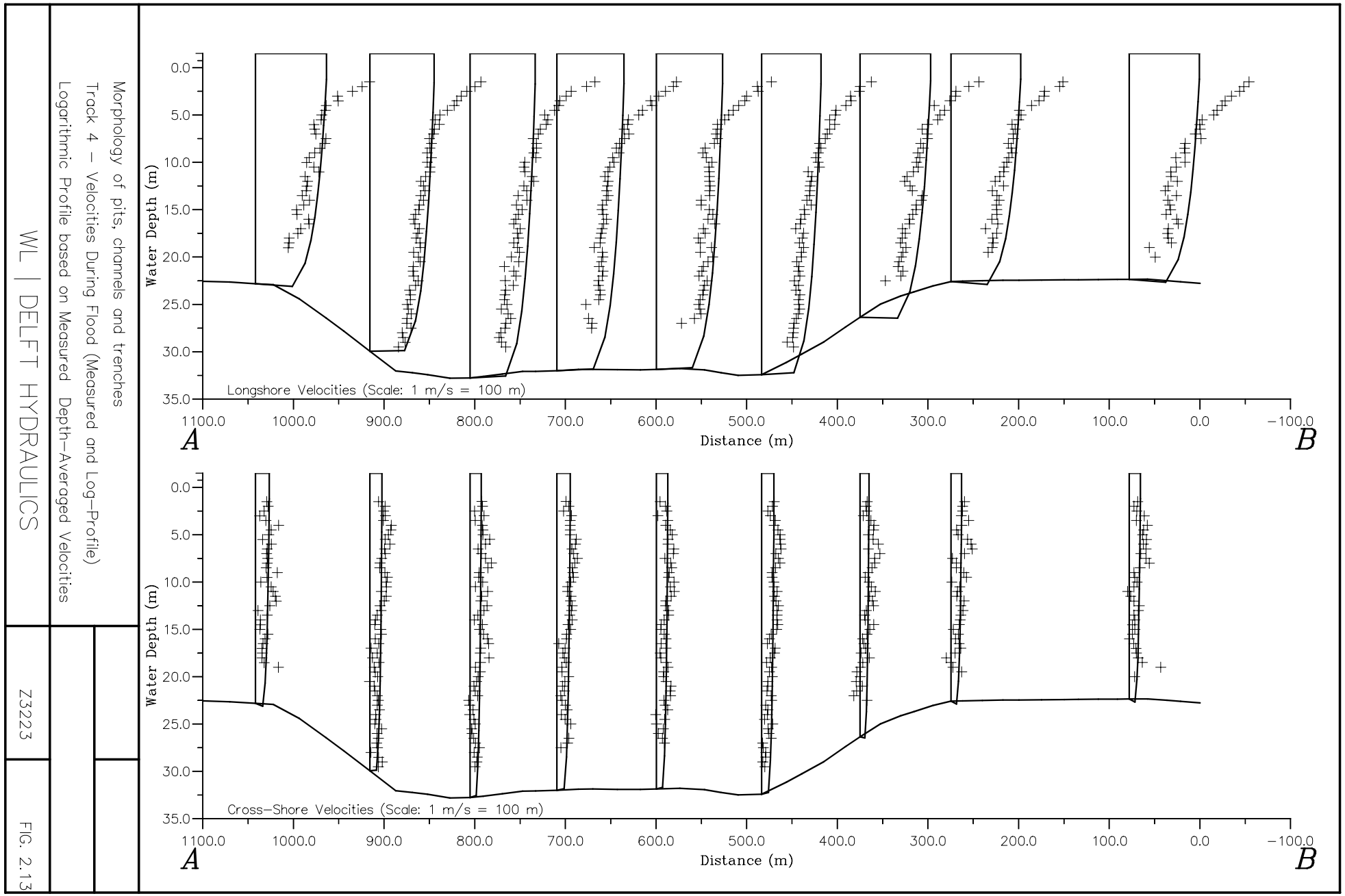

Morphology of pits, channels and trenches

Track 4 – Velocities During Flood (Measured and Log-Profile)

Logarithmic Profile based on Measured Depth-Averaged Velocities

WL | DELFT HYDRAULICS

Z3223

FIG. 2.13

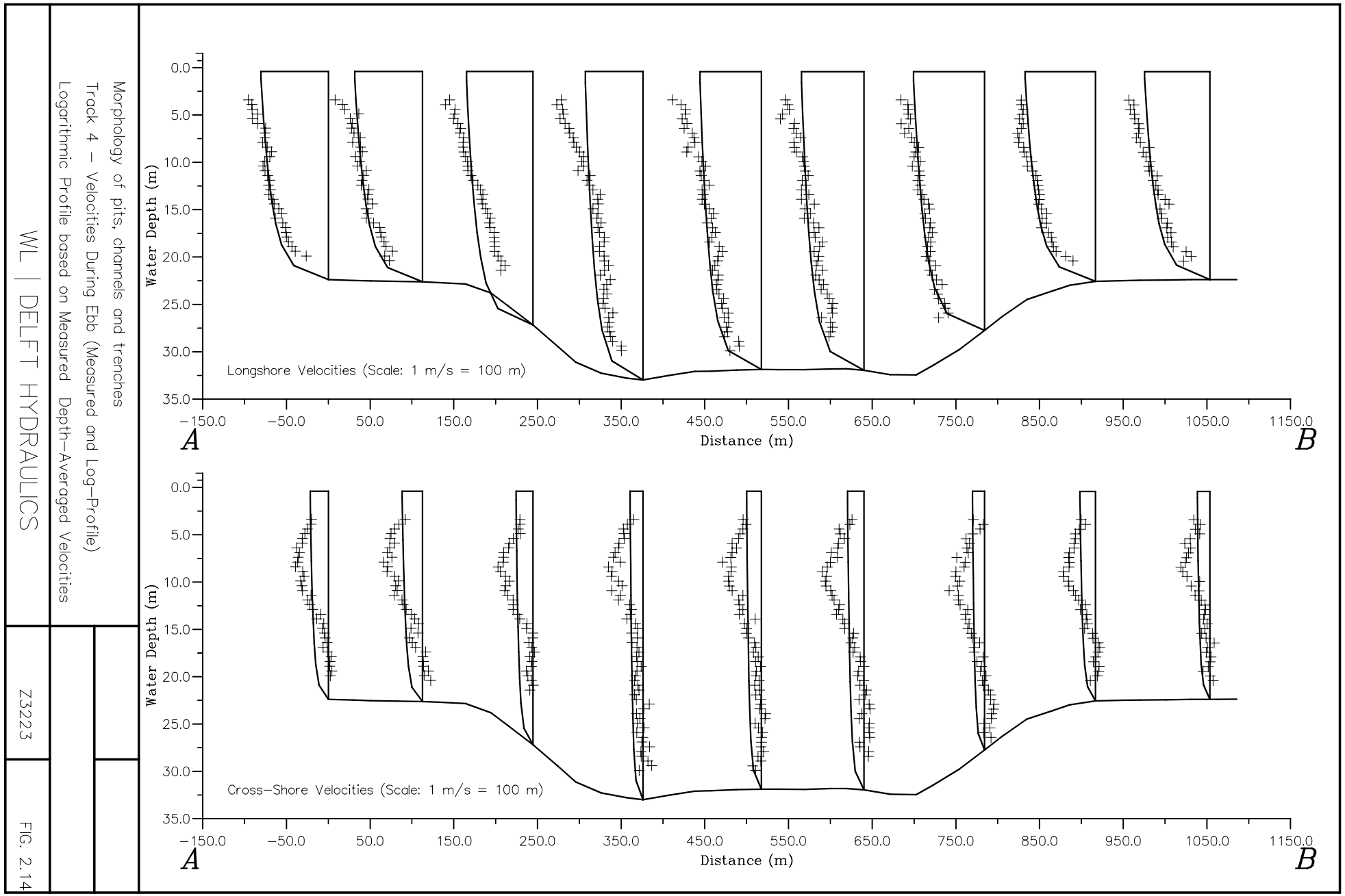

Morphology of pits, channels and trenches

Track 4 – Velocities During Ebb (Measured and Log–Profile)

Logarithmic Profile based on Measured Depth–Averaged Velocities

WL | DELFT HYDRAULICS

Z3223

FIG. 2.14

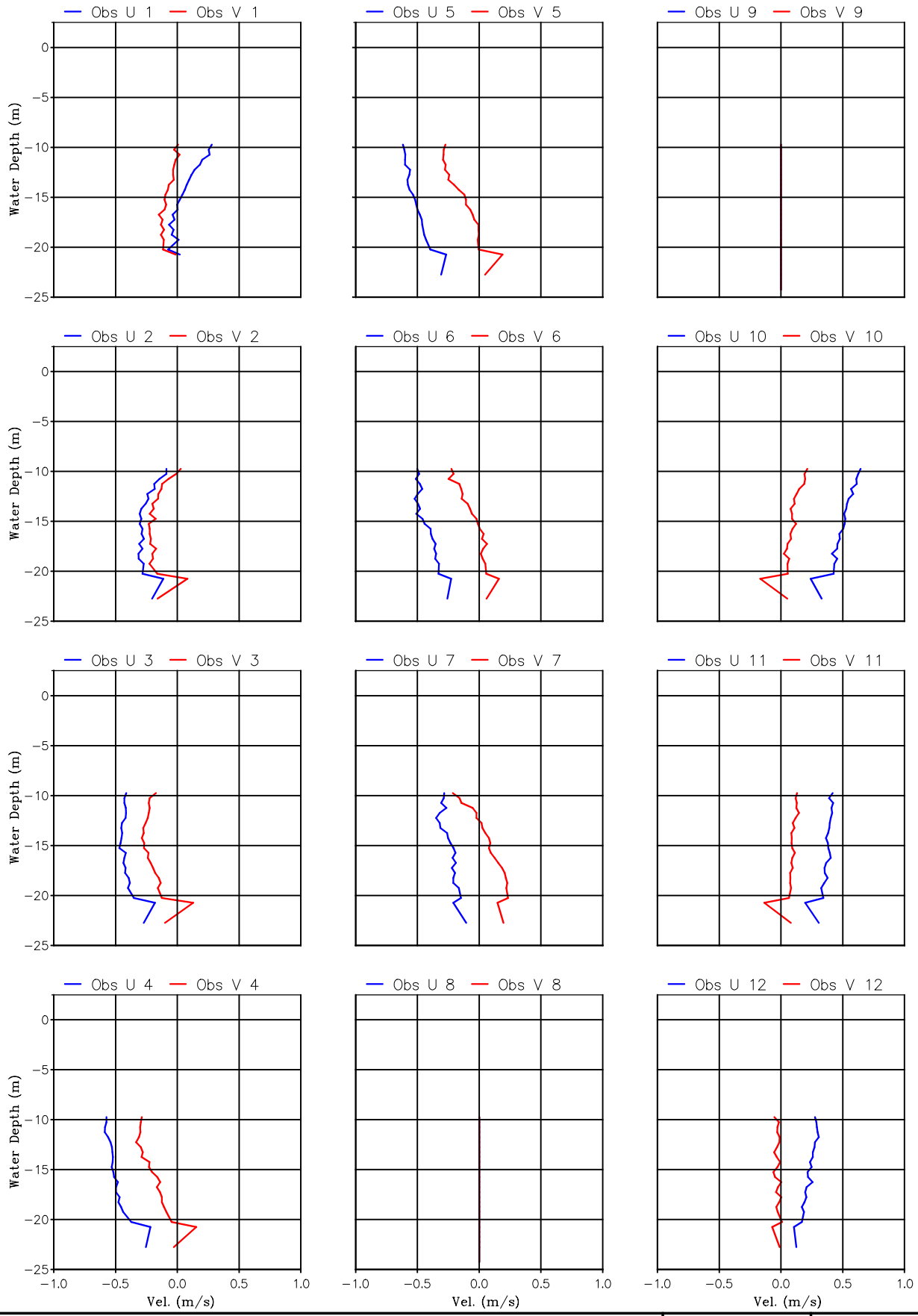

Vertical current profiles (hourly for 1 tidal period)

Location A observed velocity profiles (Blue: Longshore, Red: Cross-shore)

Period 2000-02-26 11:05:00 - 2000-02-26 23:05:00

Z3223

WL | DELFT HYDRAULICS

Fig. 2.15

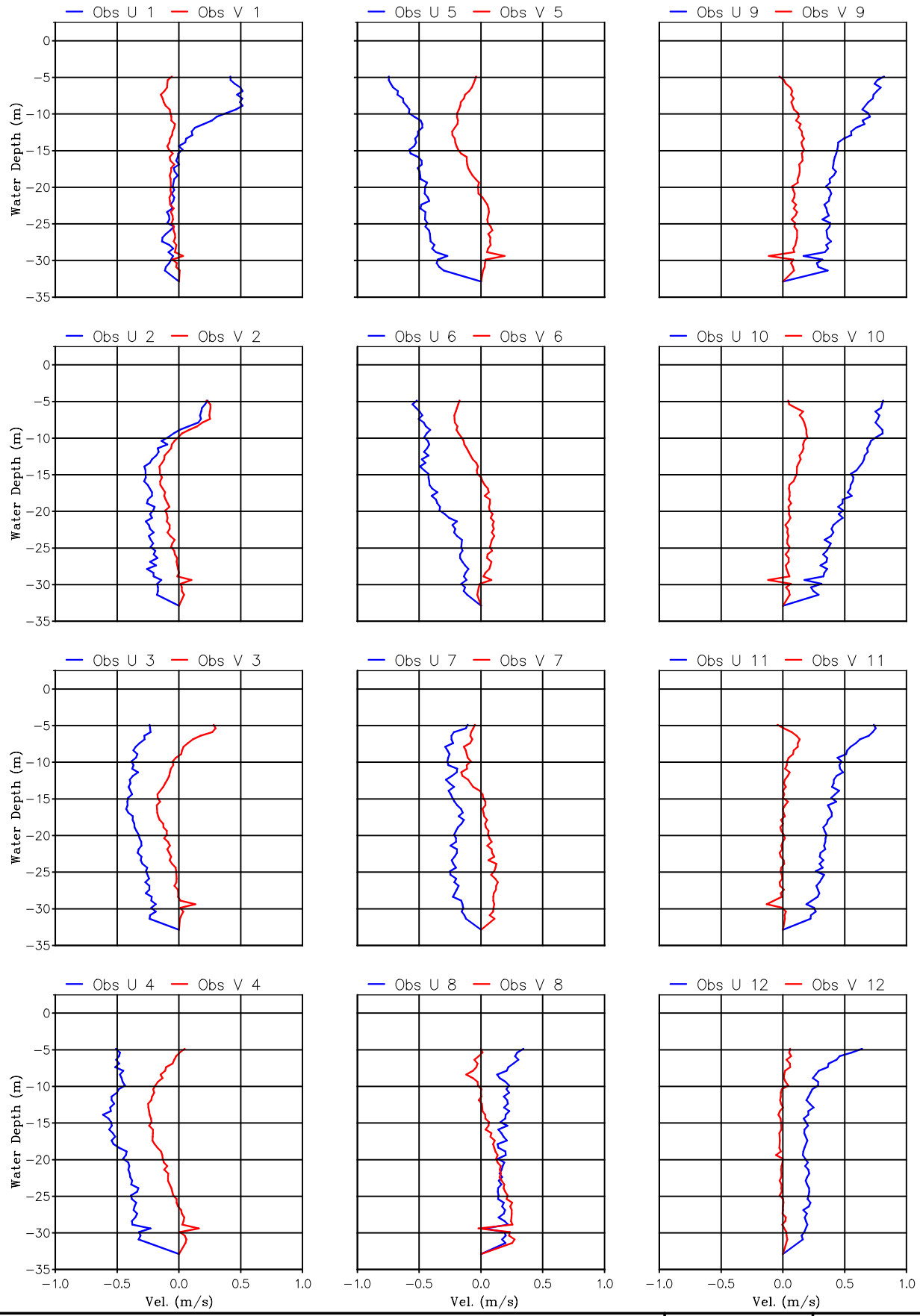

Vertical current profiles (hourly for 1 tidal period)

Location M observed velocity profiles (Blue: Longshore, Red: Cross-Shore)

Period 2000-02-26 11:05:00 - 2000-02-26 23:05:00

Z3223

WL | DELFT HYDRAULICS

Fig. 2.16

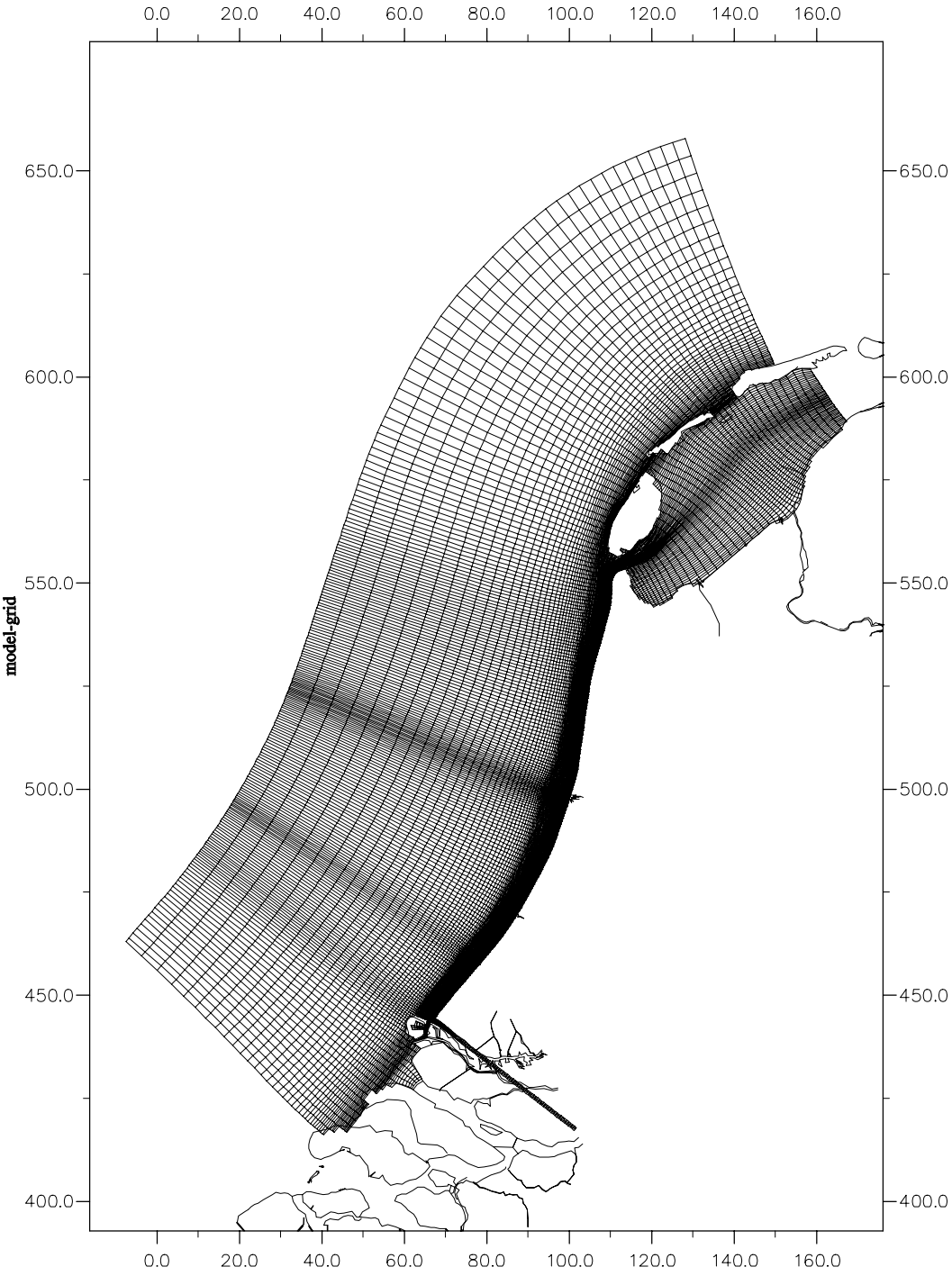

Morphology of pits, channels and trenches Part II: Verification of DELFT3D with PUTMOR dataset Grid HCZ—model		Z3223
WL | DELFT HYDRAULICS		Fig. 3.1

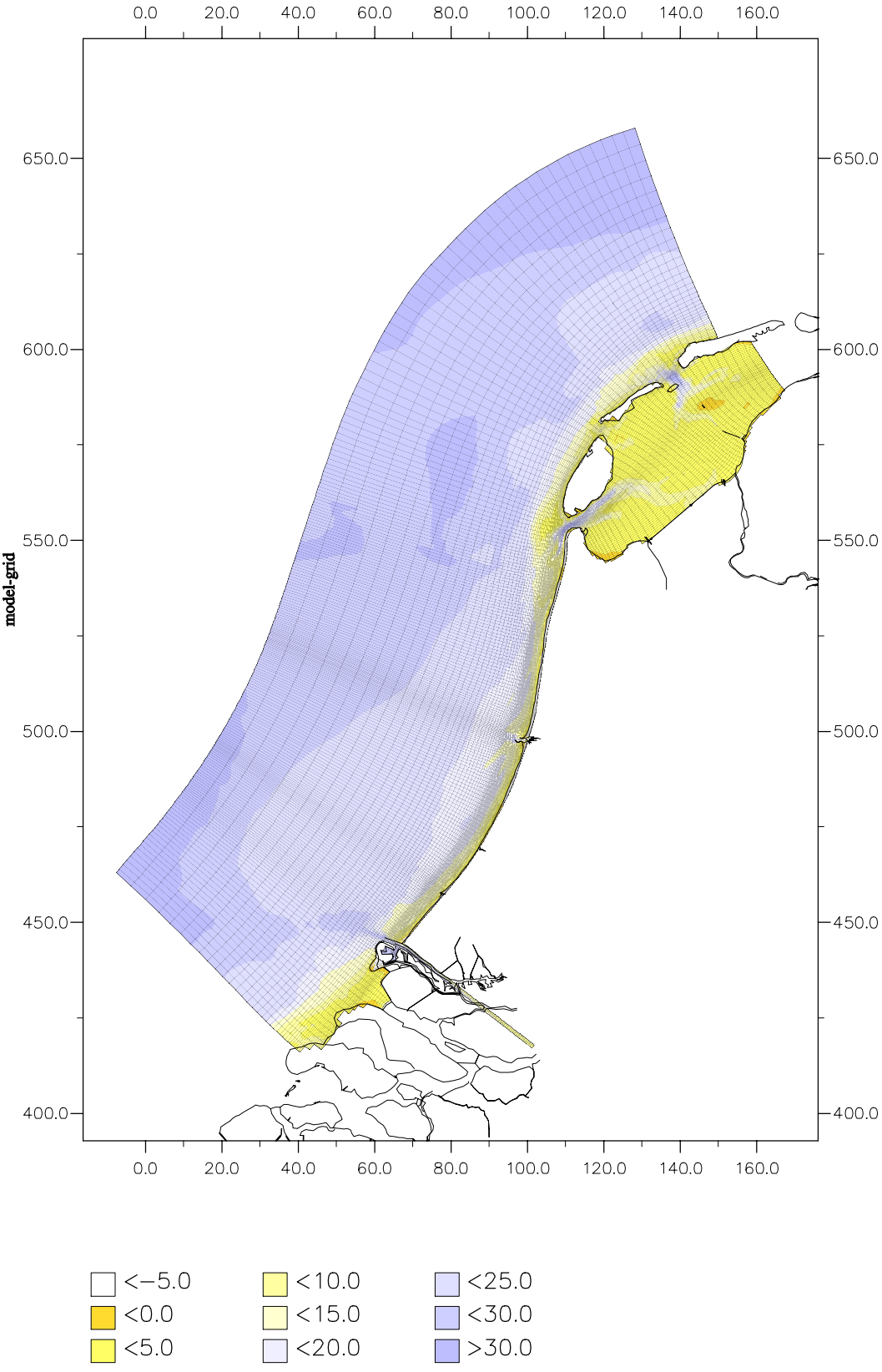

Morphology of pits, channels and trenches
Part II: Verification of DELFT3D with PUTMOR dataset
Bathymetry HCZ–model

Z3223

WL | DELFT HYDRAULICS

Fig. 3.2

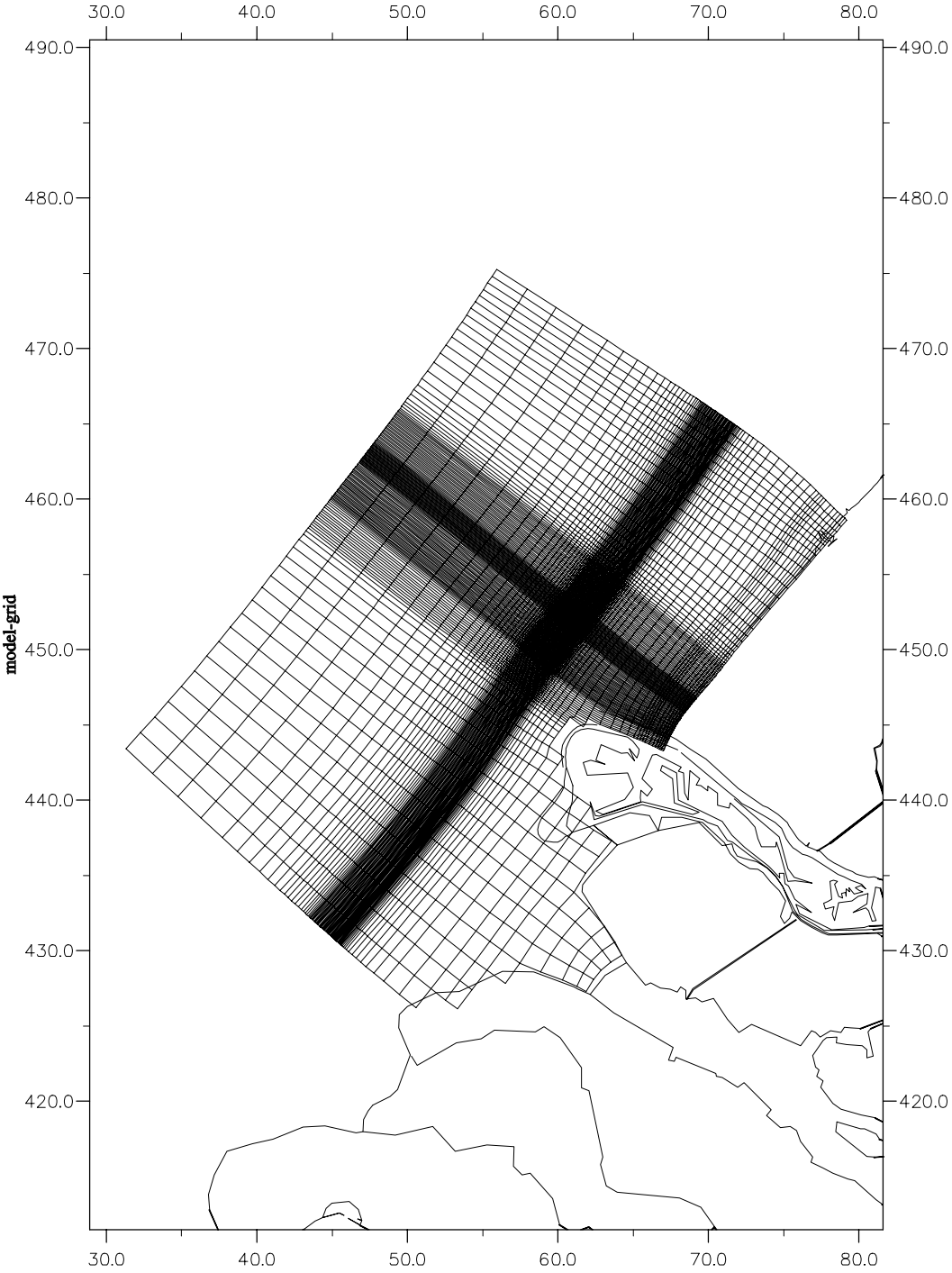

Morphology of pits, channels and trenches Part II: Verification of DELF3D with PUTMOR dataset Grid Pit—model		Z3223
WL | DELFT HYDRAULICS		Fig. 3.5

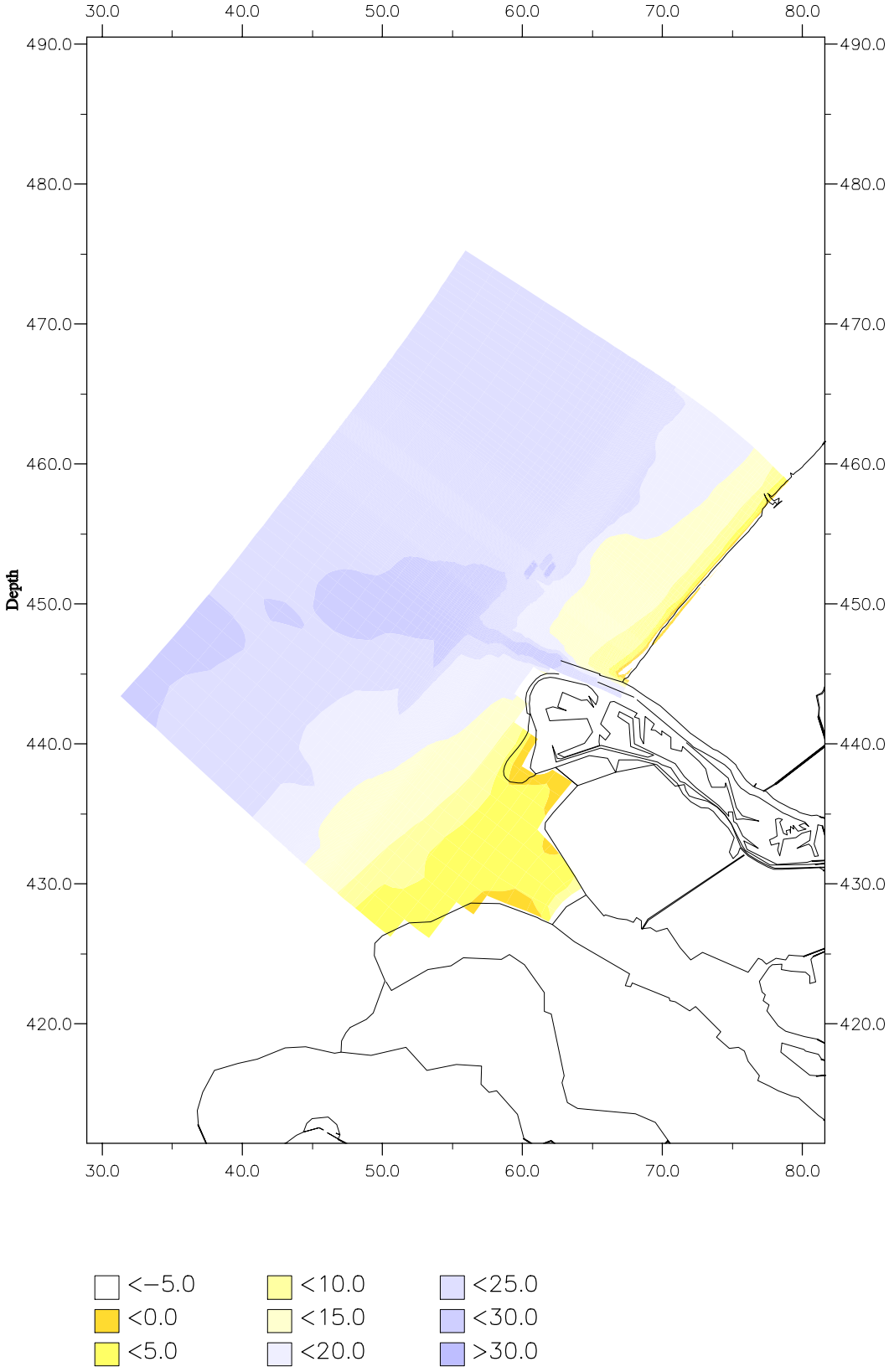

Morphology of pits, channels and trenches Part II: Verification of DELFT3D with PUTMOR dataset Bathymetry Pit–model		Z3223
WL | DELFT HYDRAULICS		Fig. 3.6

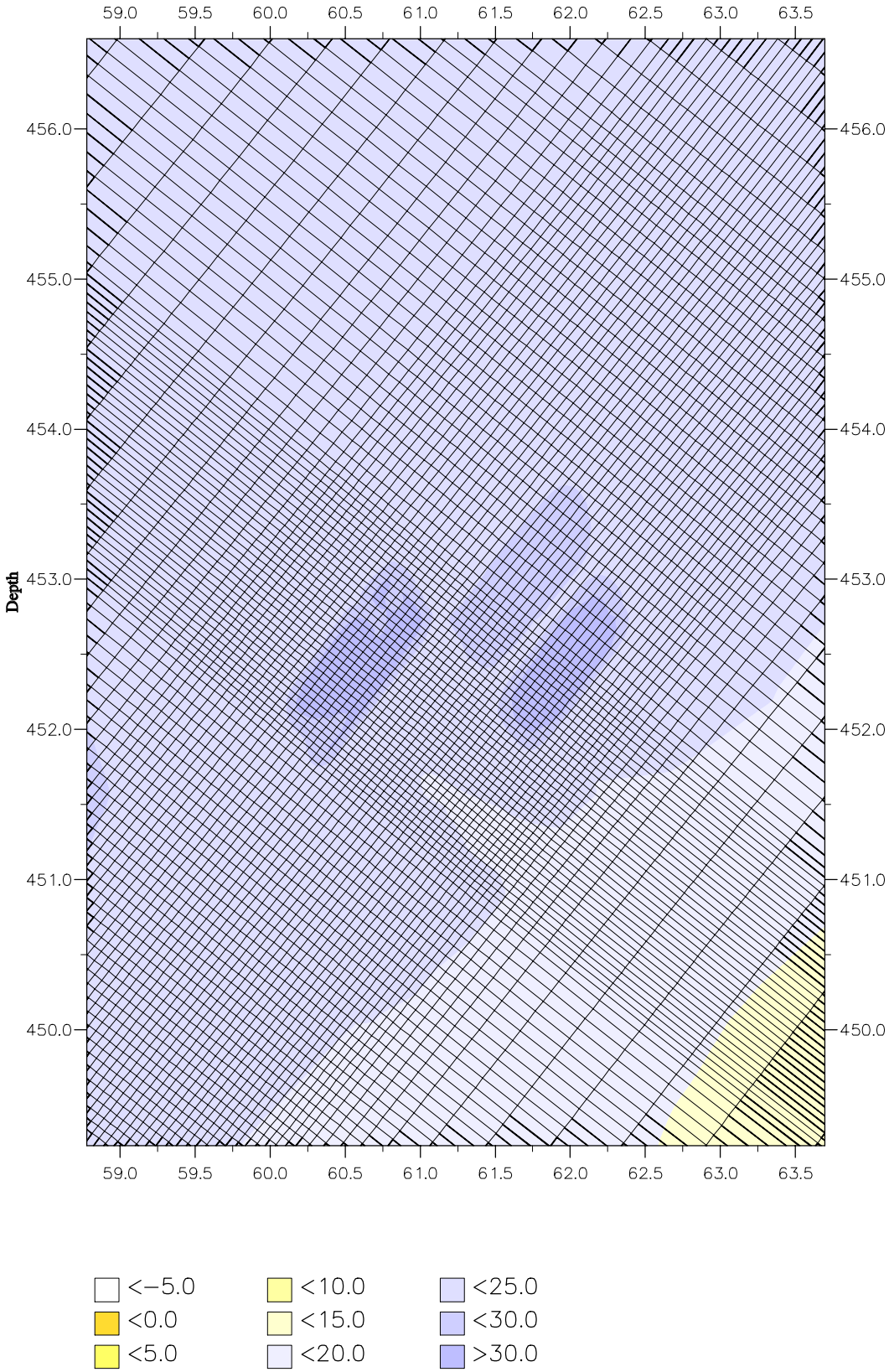

Morphology of pits, channels and trenches
Part II: Verification of DELFT3D with PUTMOR dataset
Detail sandpits bathymetry Pit−model

Z3223

WL | DELFT HYDRAULICS

Fig. 3.7

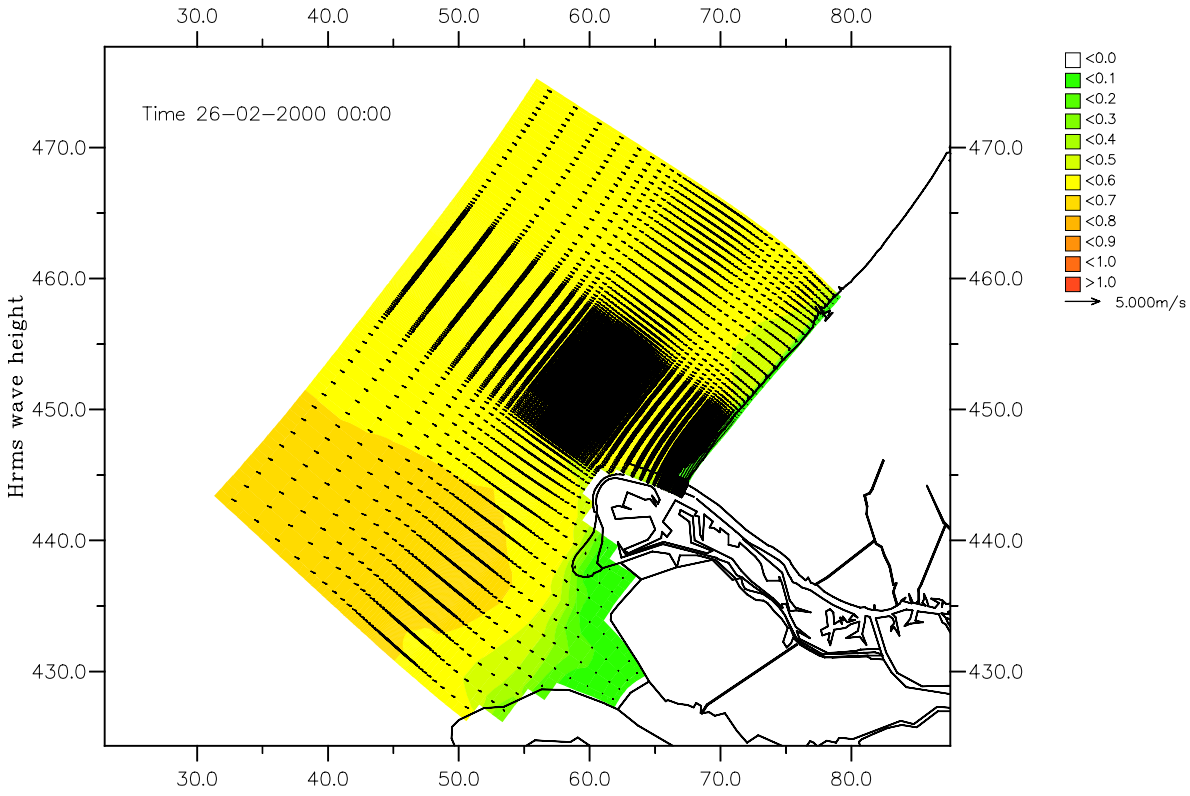

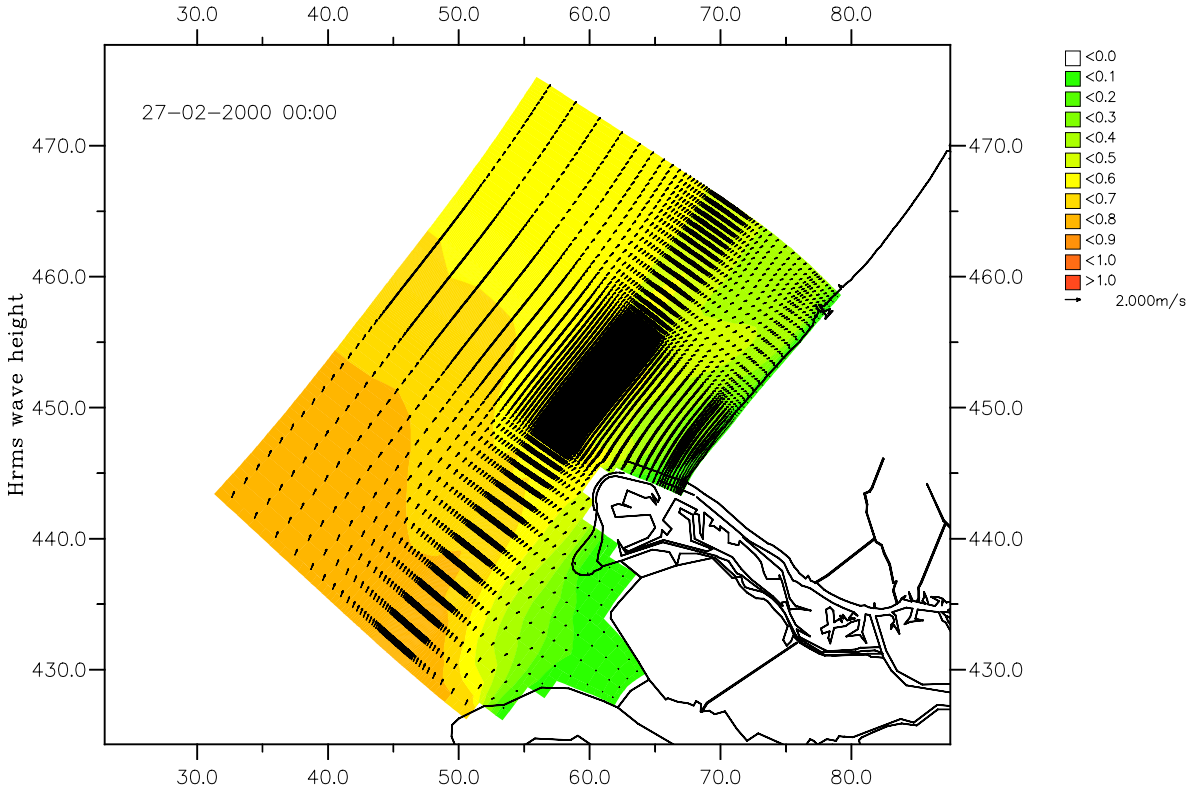

Morphology of pits, channels and trenches Part II: Verification of Delft3D with PUTMOR dataset RMS Wave Height at selected times		PT2WF
	26-02 to 05-03	
WL | DELFT HYDRAULICS	Z3223	Fig. 3.9

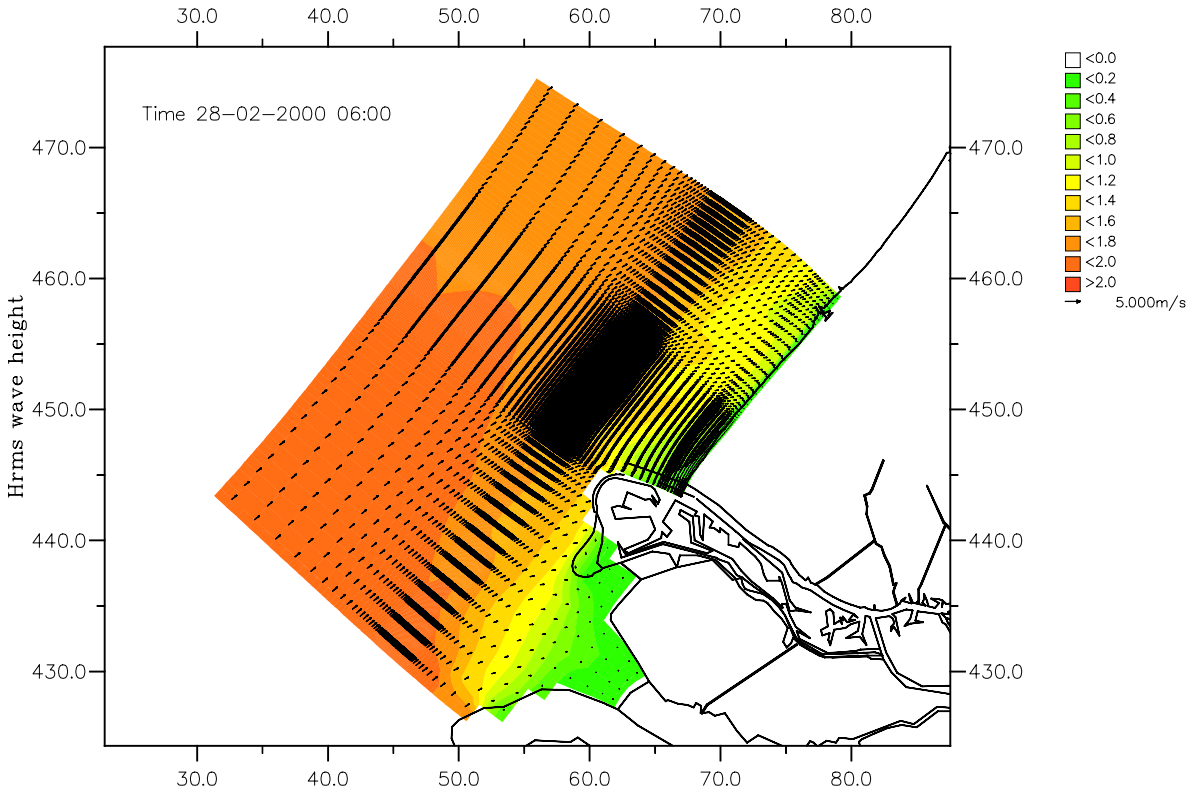

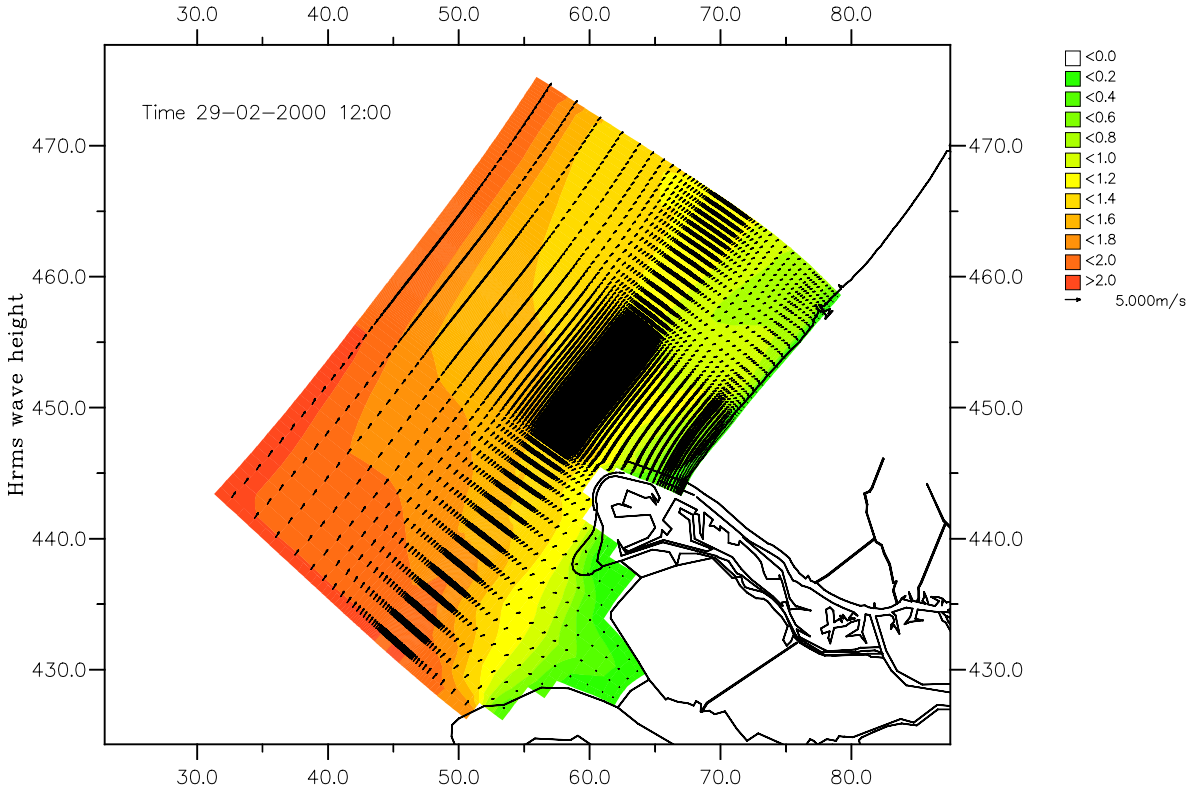

Morphology of pits, channels and trenches Part II: Verification of Delft3D with PUTMOR dataset RMS Wave Height at selected times		PT2WF
	26-02 to 05-03	
WL | DELFT HYDRAULICS	Z3223	Fig. 3.10

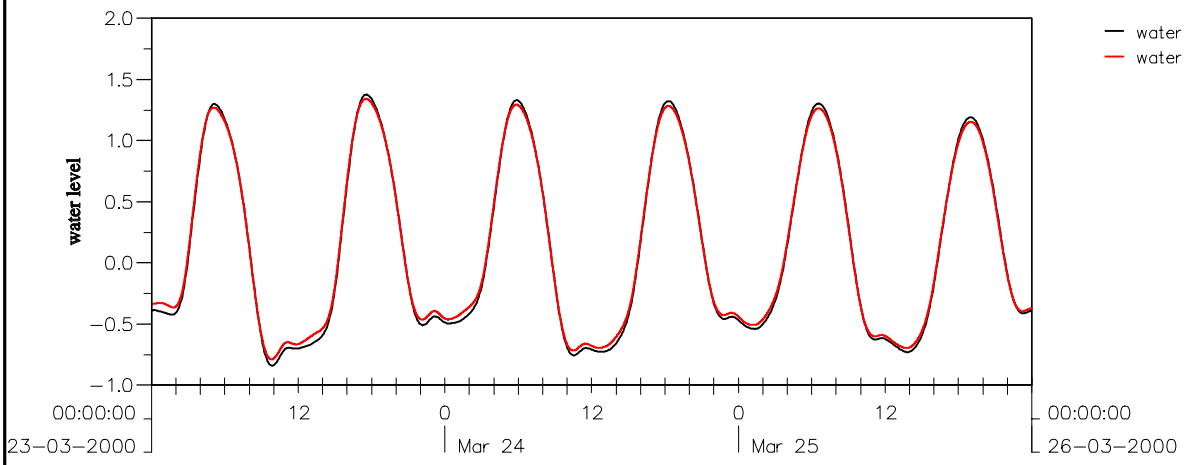

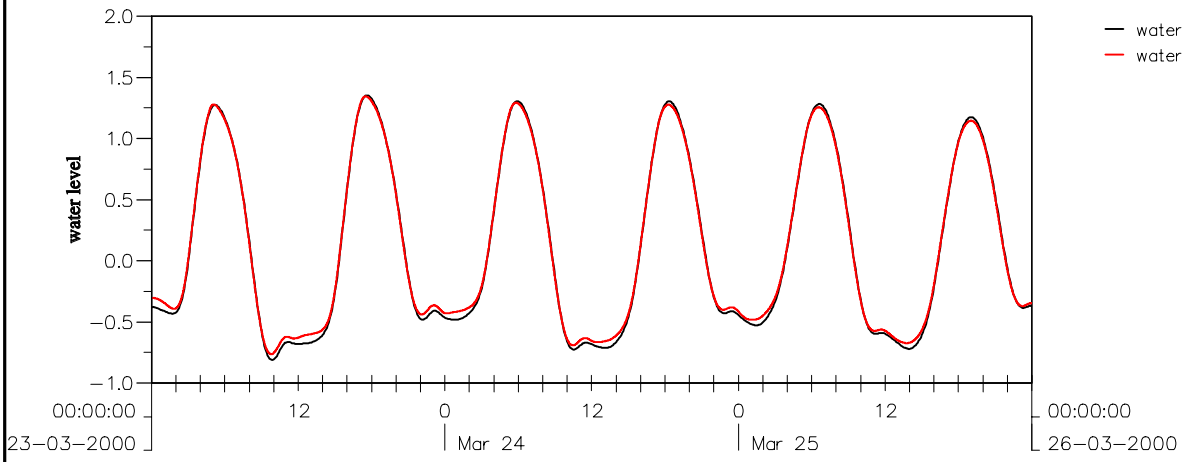

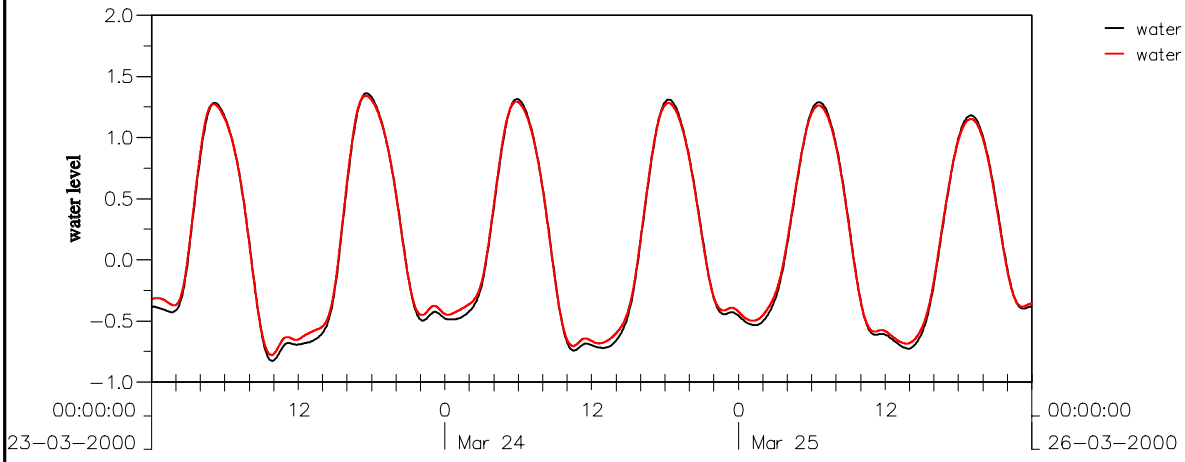

Morphology of pits, channels and trenches
Comparison of waterlevel HCZ – PIT model locations A, B & M
Black HCZ–model, red PIT–model

Z3223

WL | DELFT HYDRAULICS

Fig. 4.1

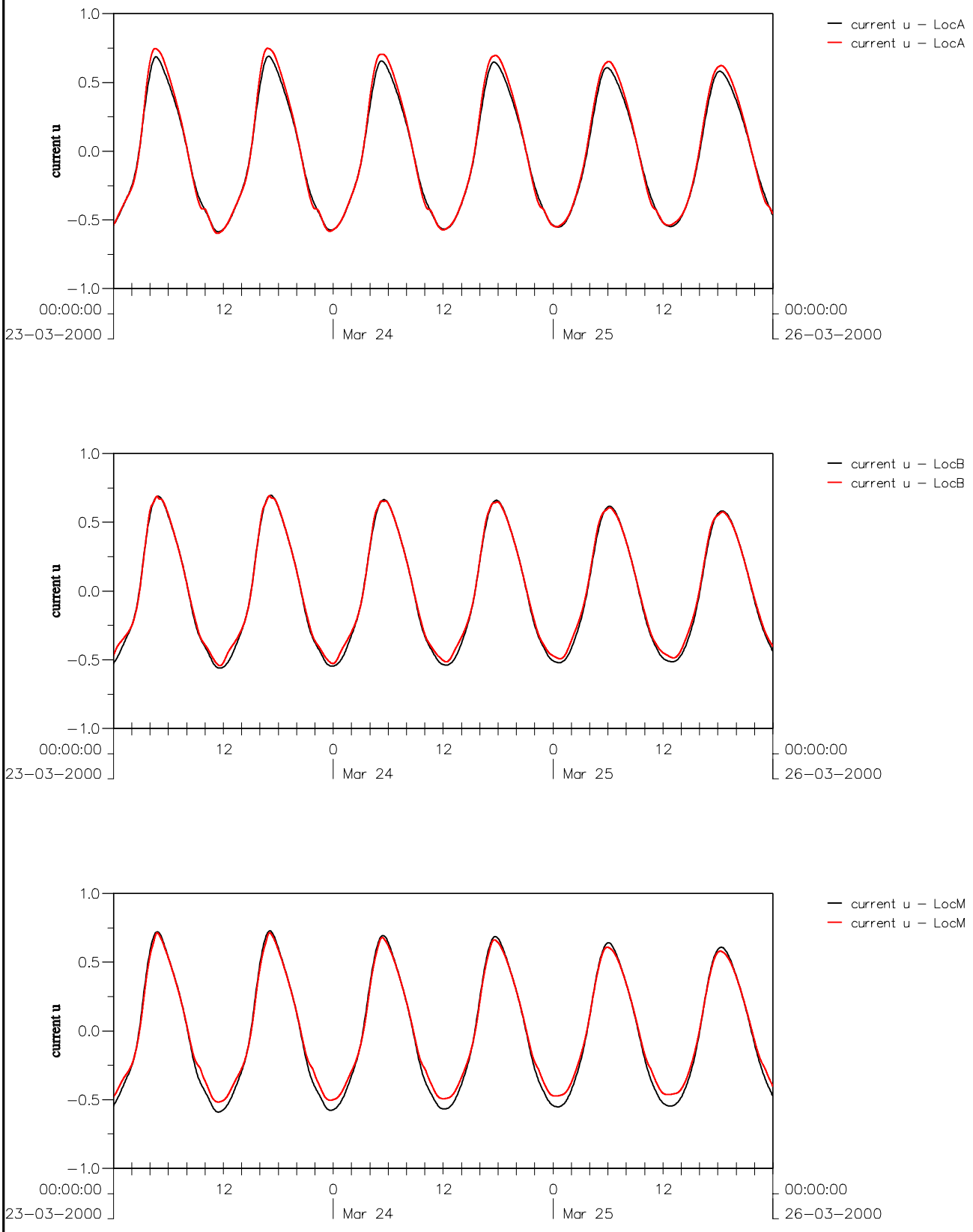

Morphology of pits, channels and trenches

Comparison of current u HCZ – PIT model locations A, B & M

Black HCZ–model, red PIT–model

Z3223

WL | DELFT HYDRAULICS

Fig. 4.2

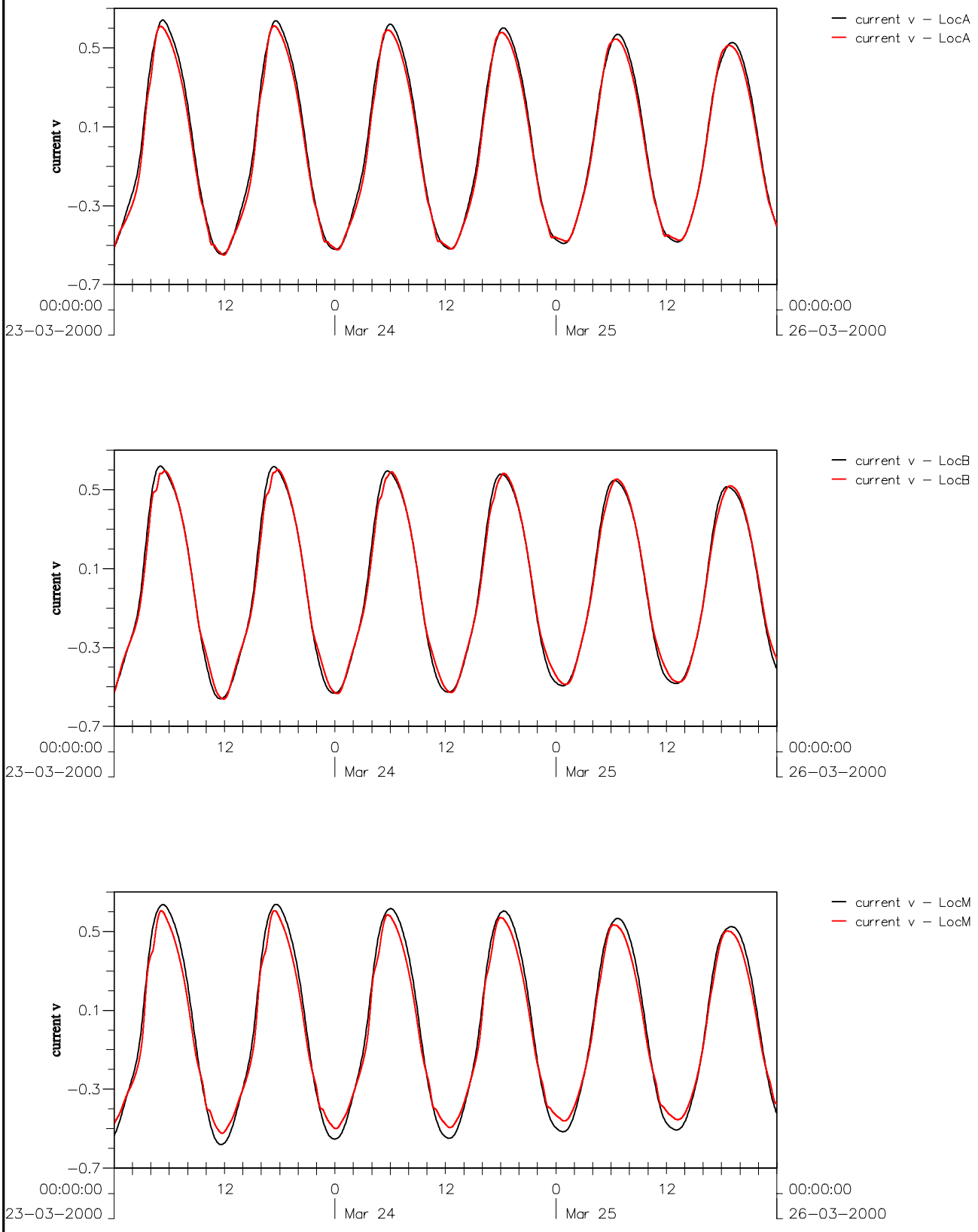

Morphology of pits, channels and trenches

Comparison of current v HCZ – PIT model locations A, B & M

Black HCZ–model, red PIT–model

Z3223

WL | DELFT HYDRAULICS

Fig 4.3

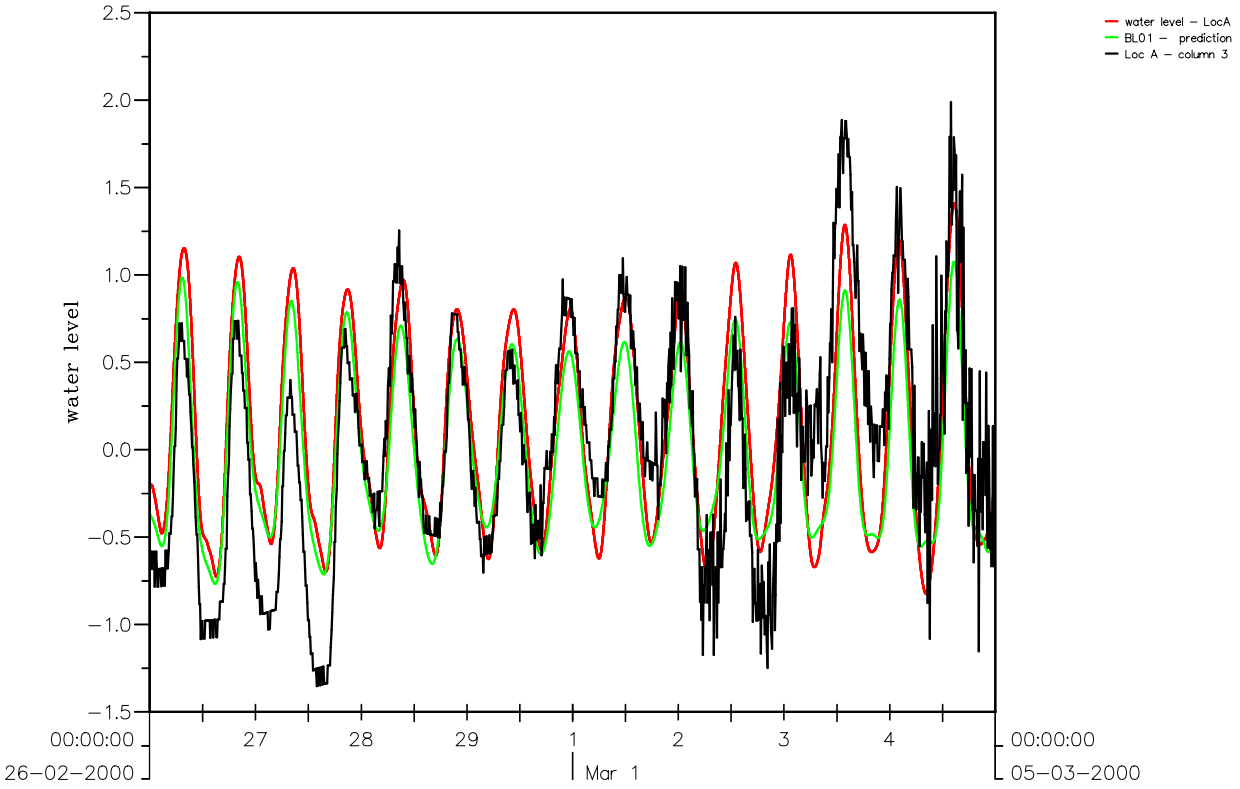

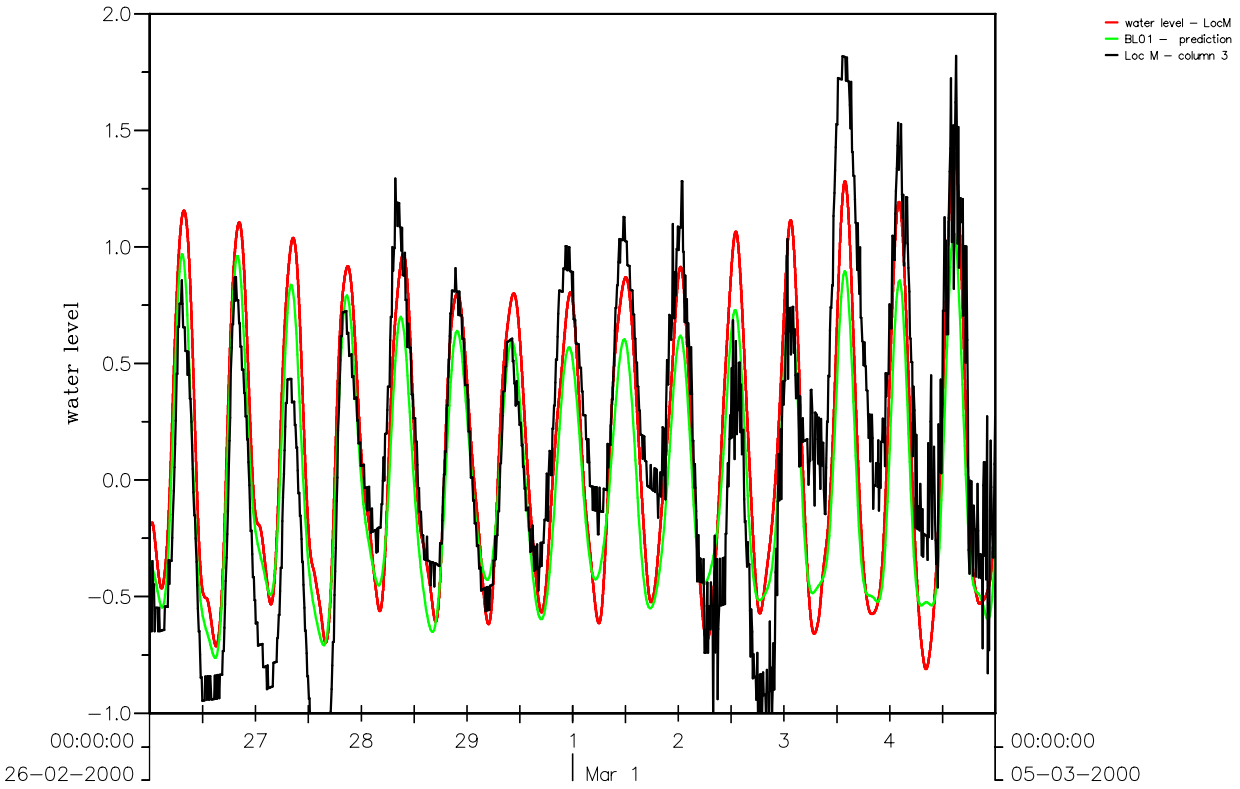

Morphology of pits, channels and trenches Part II: Verification of Delft3D with PUTMOR dataset Water level Comparison (Black: meas., Red: model, Green: harmonic)	PIT−model	Z3223
	Period 26−02−00 − 05−03−00	
WL | DELFT HYDRAULICS	2DH	Fig. 4.5

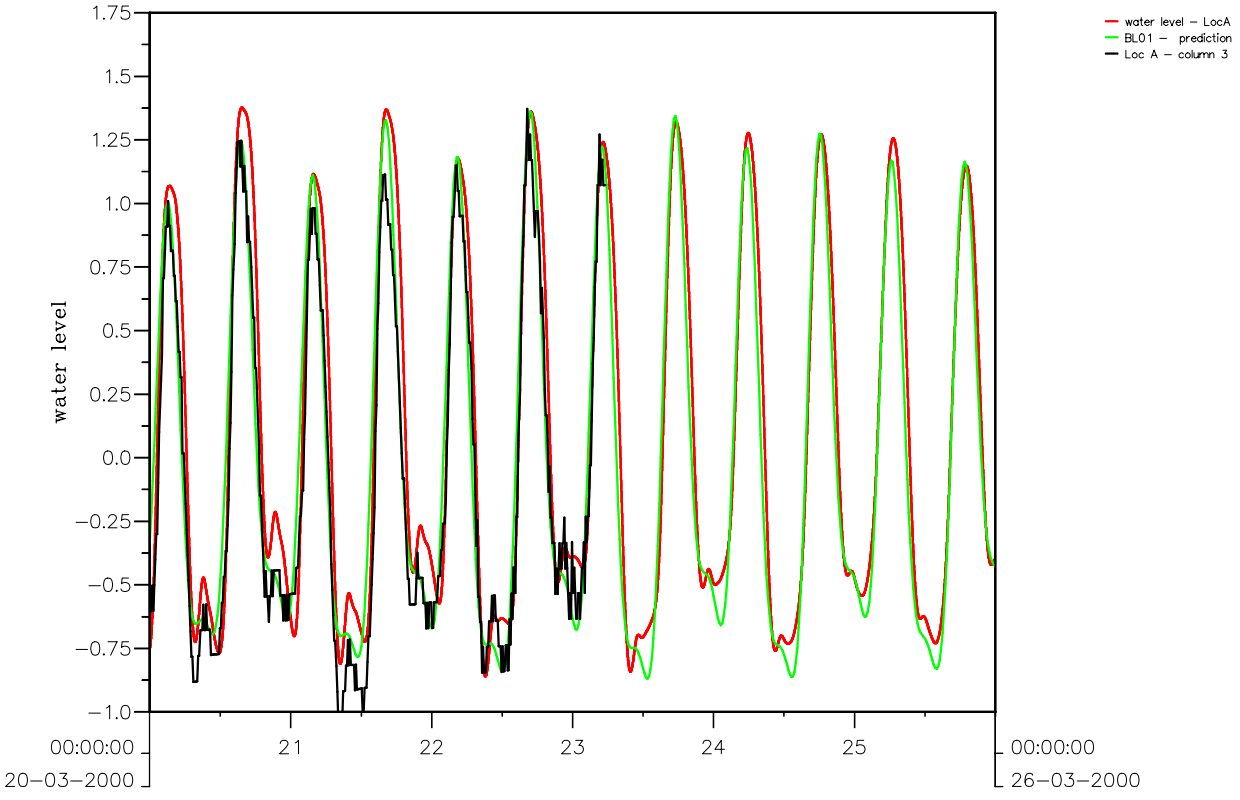

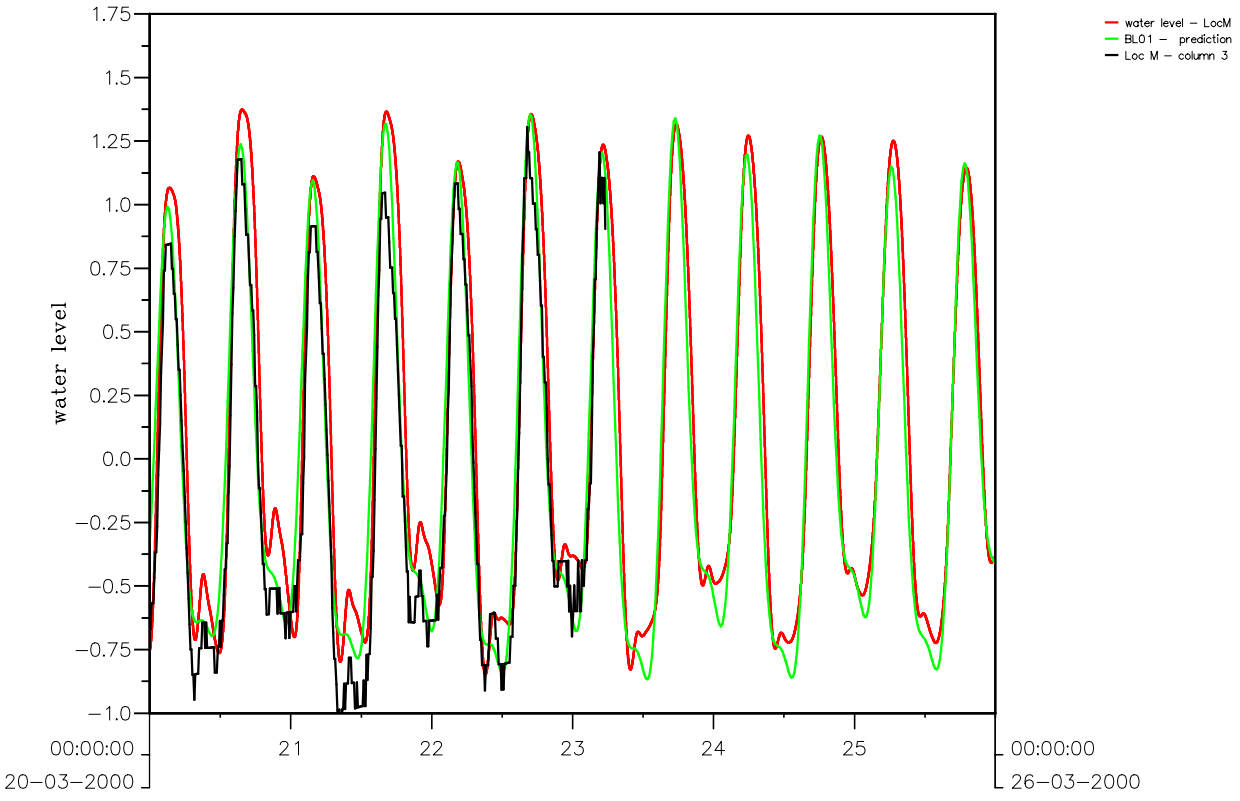

Morphology of pits, channels and trenches Part II: Verification of Delft3D with PUTMOR dataset Water level Comparison (Black: meas., Red: model, Green: harmonic)	PIT–model	Z3223
	Period 20–03–00 – 25–03–00	
WL | DELFT HYDRAULICS	2DH	Fig. 4.6

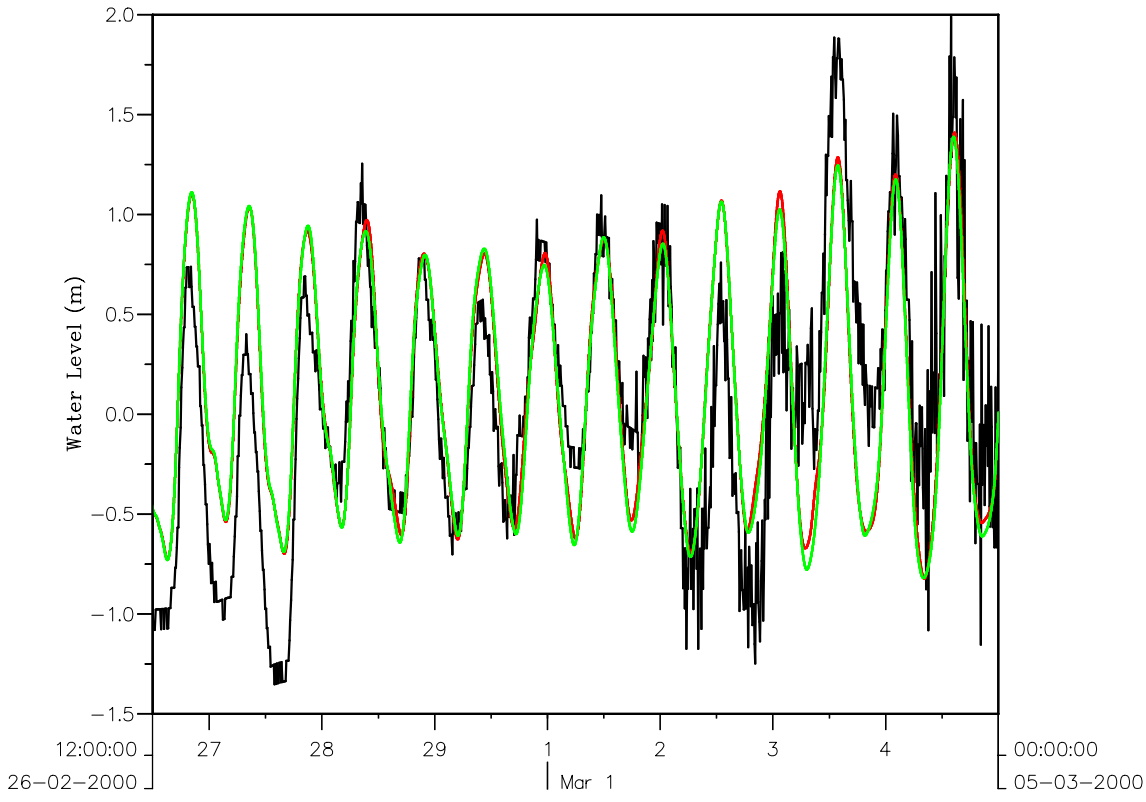

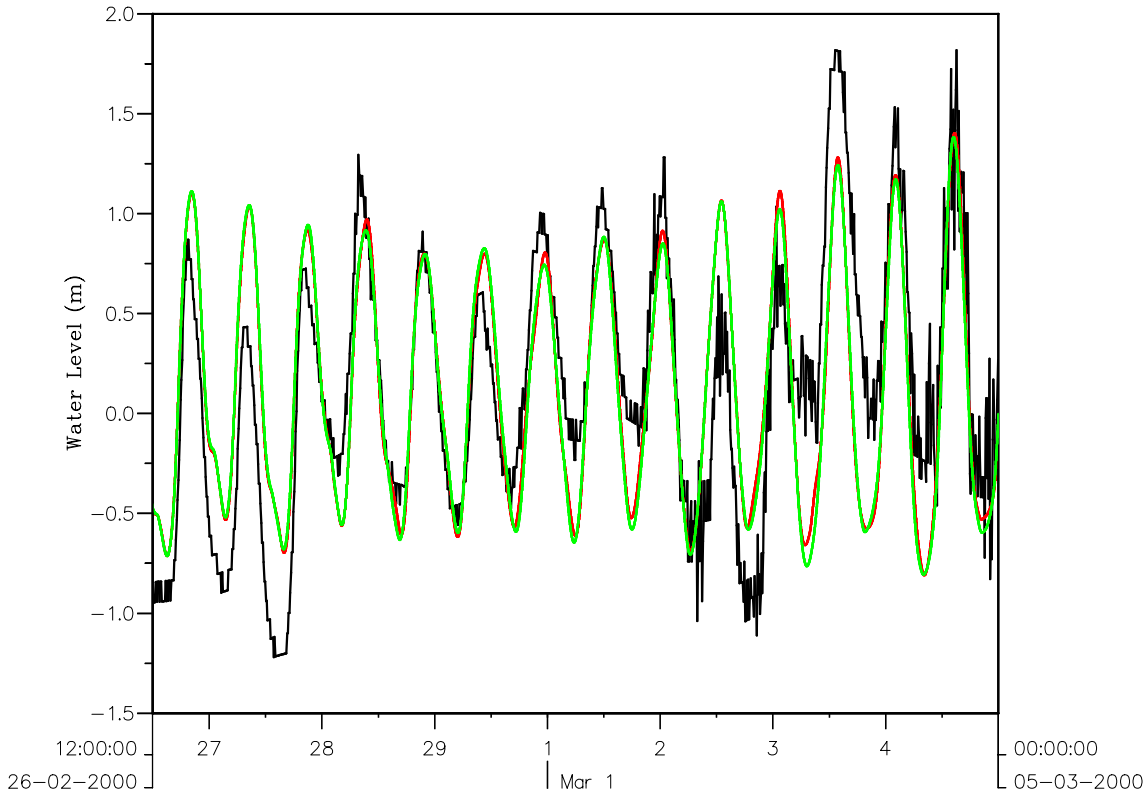

Morphology of pits, channels and trenches Part II: Verification of Delft3D with PUTMOR dataset Water Levels at Locations A & M (Black: meas., Red: Wind, Green: No Wind)	PIT−2DH	PT2 and PT4
	26−02 to 05−03	
WL | DELFT HYDRAULICS	Z3223	Fig. 4.7

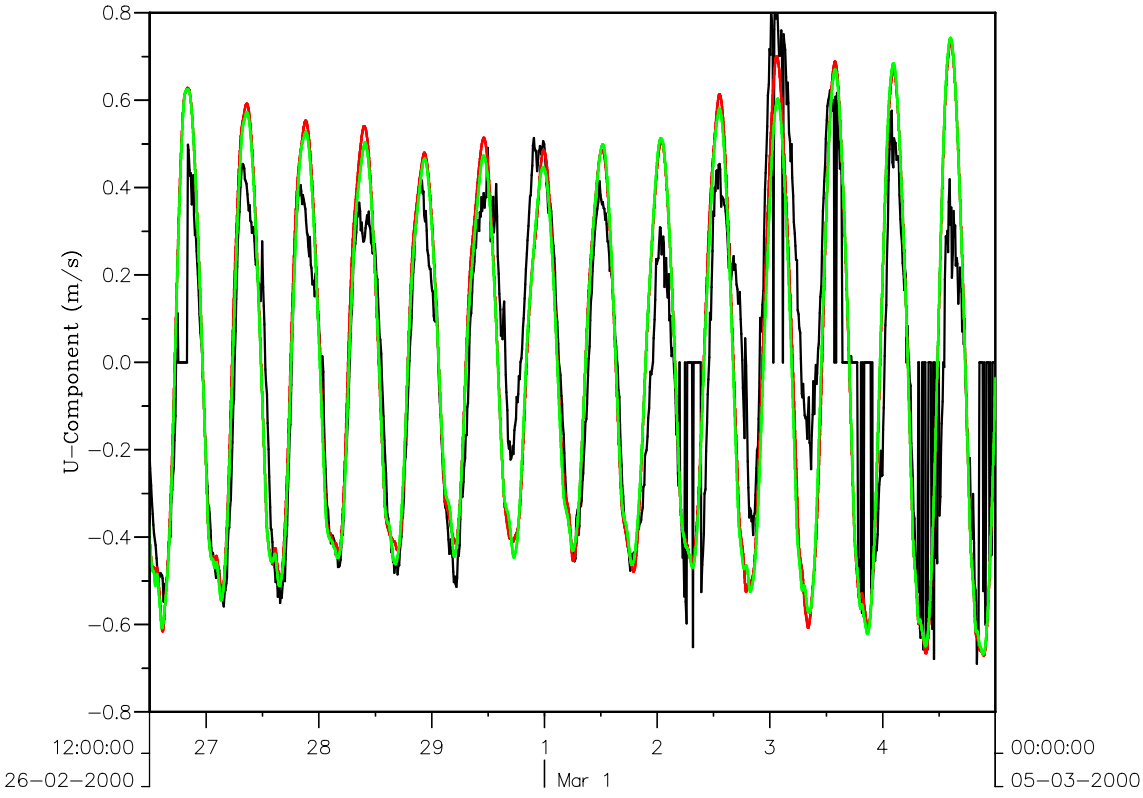

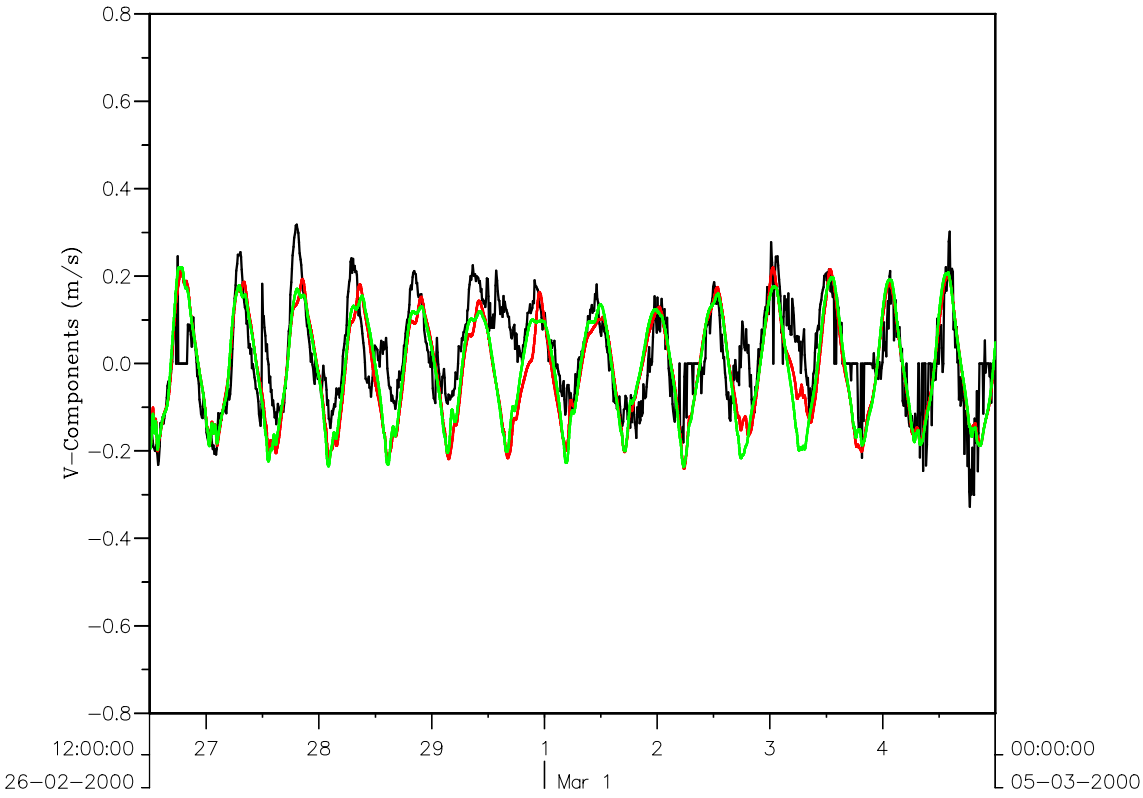

Morphology of pits, channels and trenches Part II: Verification of Delft3D with PUTMOR dataset Locations A Currents (Black: meas., Red: Wind, Green: No Wind	PIT−2DH	PT2 and PT4
	26−02 to 05−03	
WL | DELFT HYDRAULICS	Z3223	Fig. 4.8

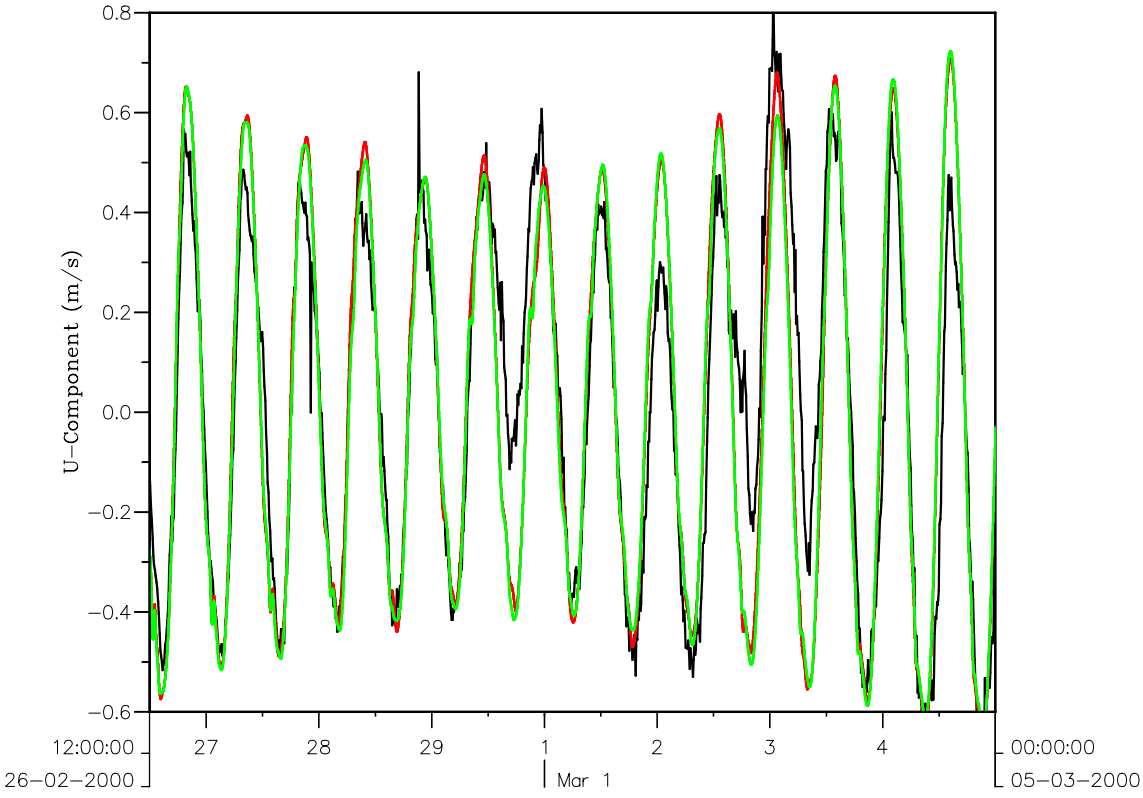

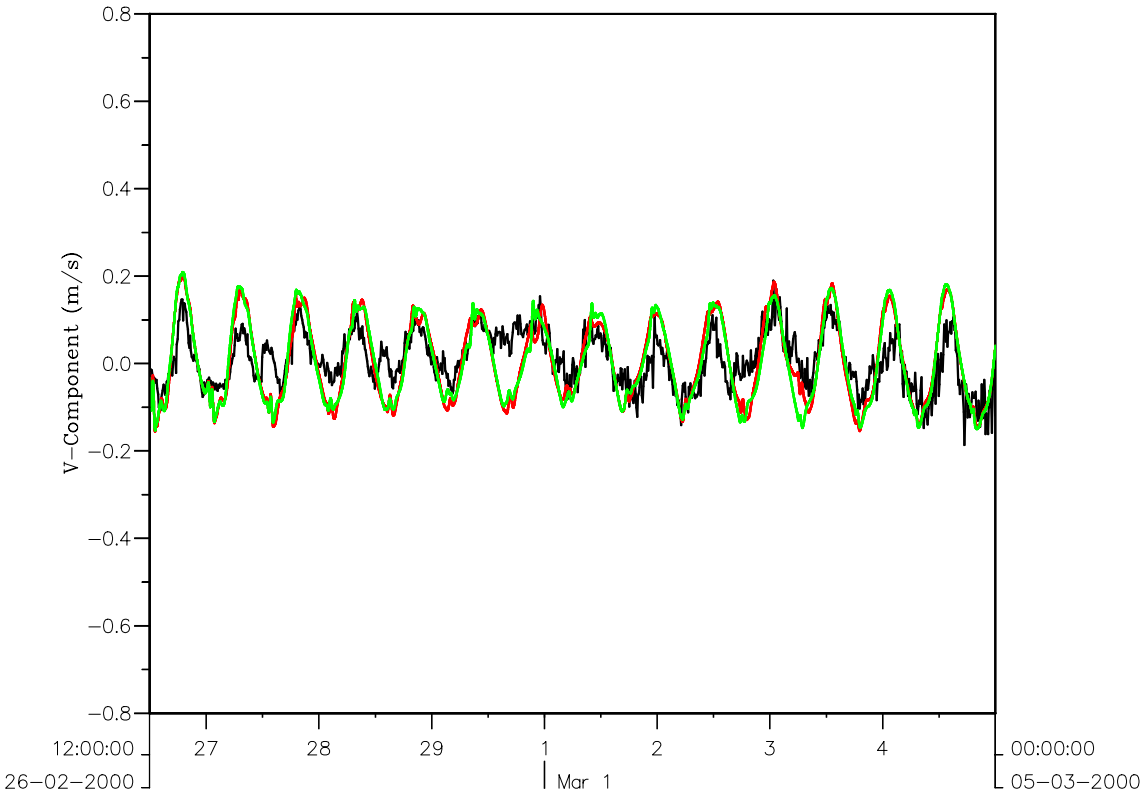

Morphology of pits, channels and trenches Part II: Verification of Delft3D with PUTMOR dataset Locations M Currents (Black: meas., Red: Wind, Green: No Wind	PIT−2DH	PT2 and PT4
	26−02 to 05−03	
WL | DELFT HYDRAULICS	Z3223	Fig. 4.9

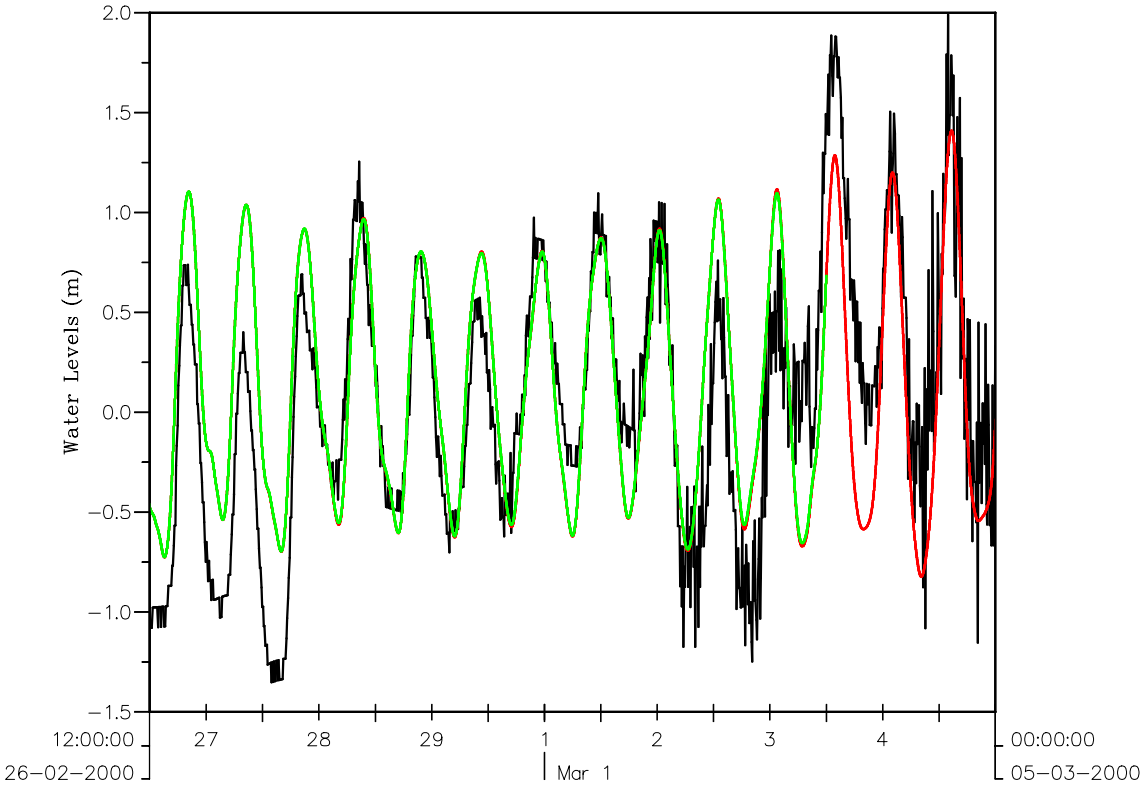

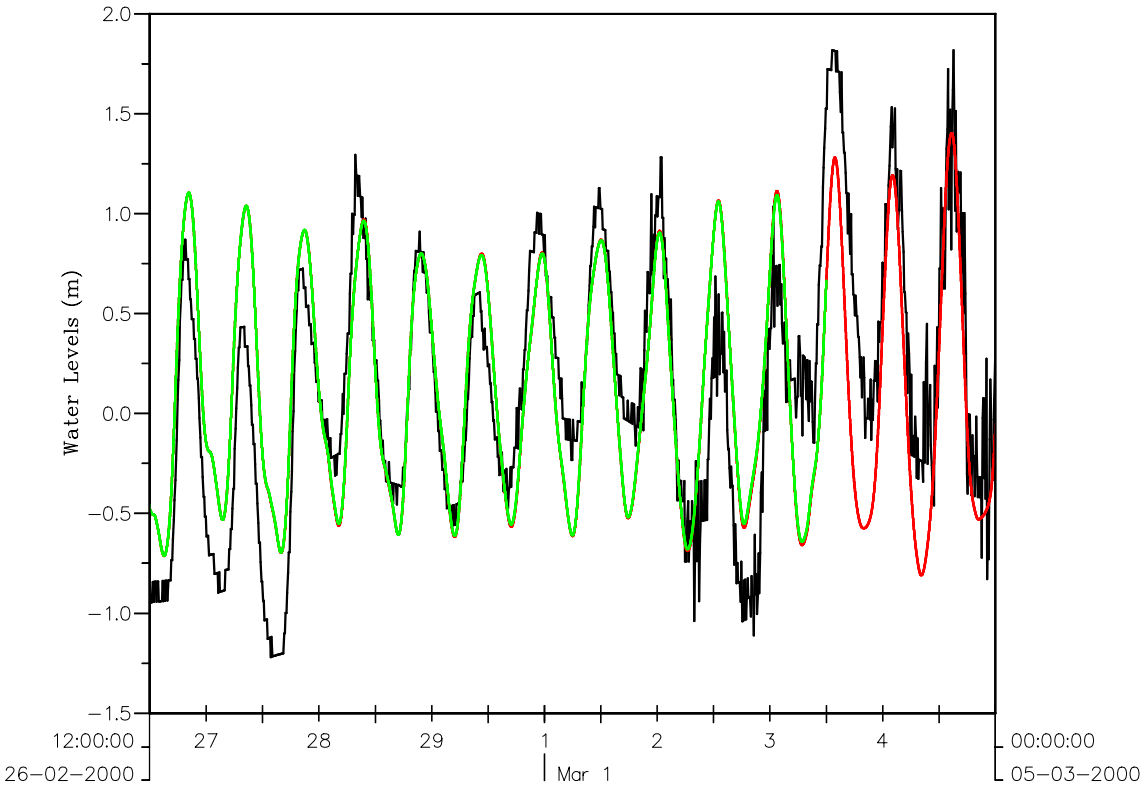

Morphology of pits, channels and trenches Part II: Verification of Delft3D with PUTMOR dataset Water Levels Locations A & M (Black: meas., Red: No Waves, Green: Waves)	PIT−2DH	PT2 and PT4
	26−02 to 05−03	
WL | DELFT HYDRAULICS	Z3223	Fig. 4.10

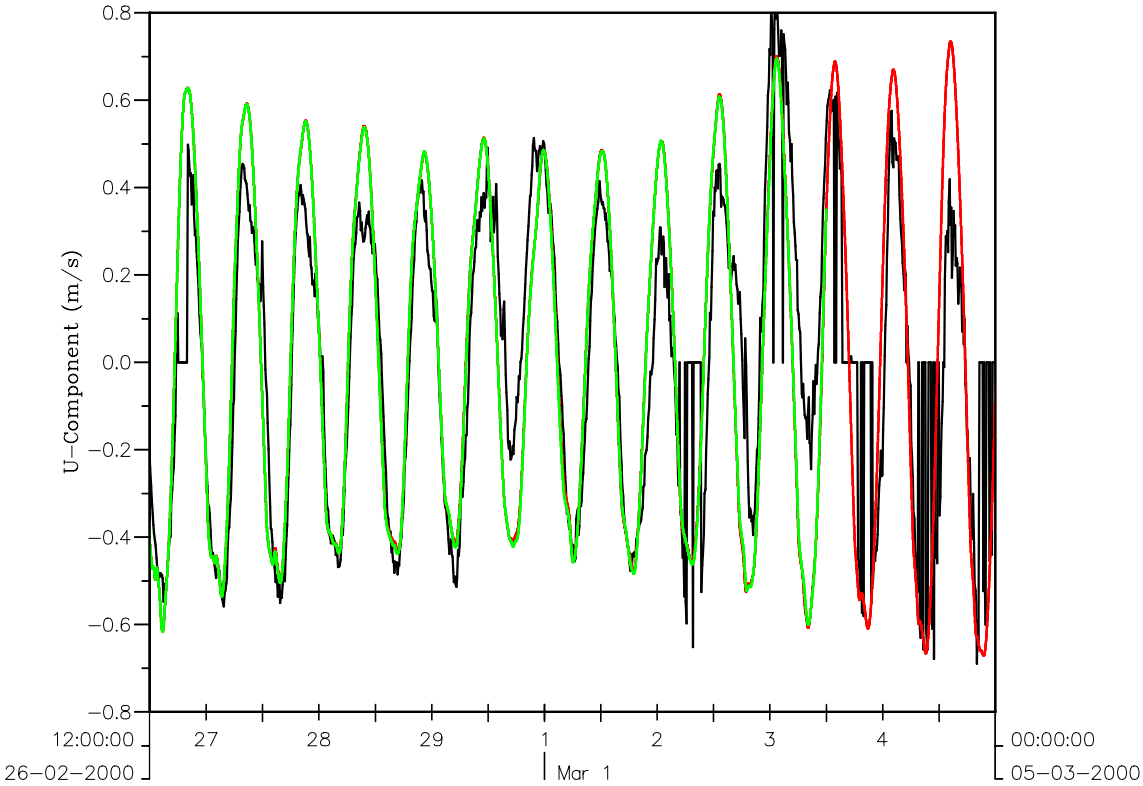

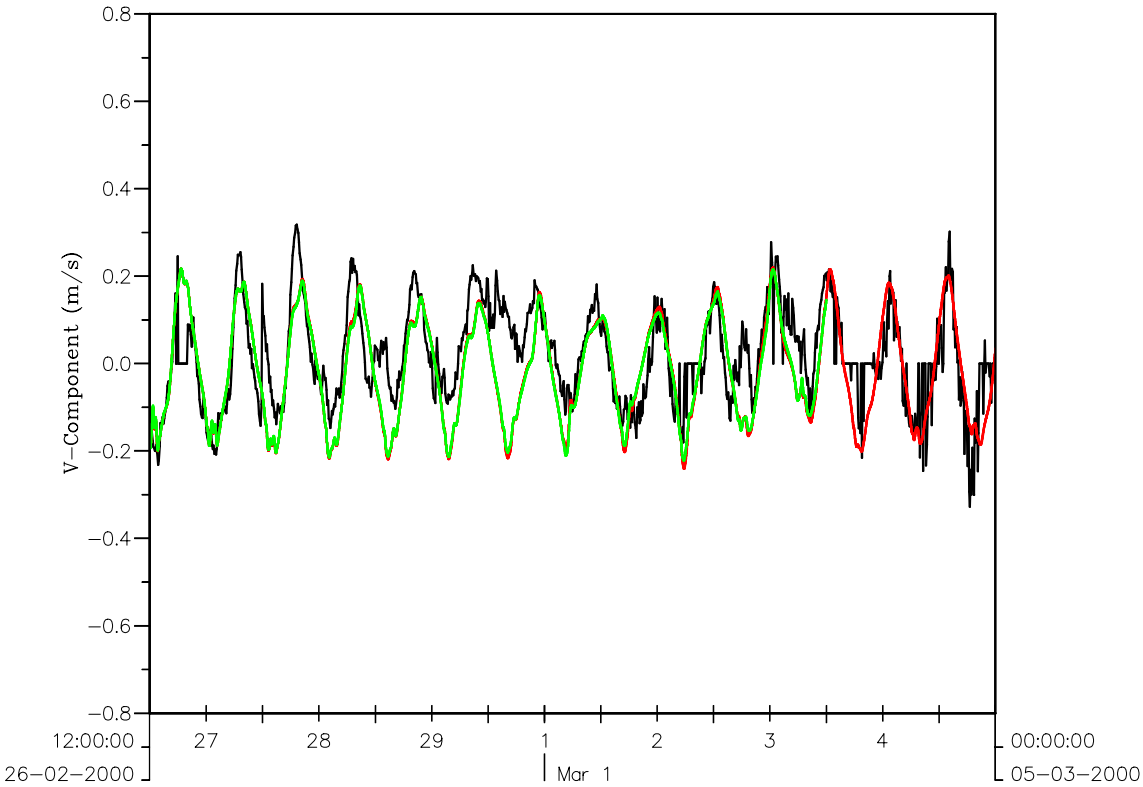

Morphology of pits, channels and trenches Part II: Verification of Delft3D with PUTMOR dataset Locations A Currents (Black: meas., Red: No Waves, Green: Waves	PIT−2DH	PT2 and PT4
	26−02 to 05−03	
WL | DELFT HYDRAULICS	Z3223	Fig. 4.11

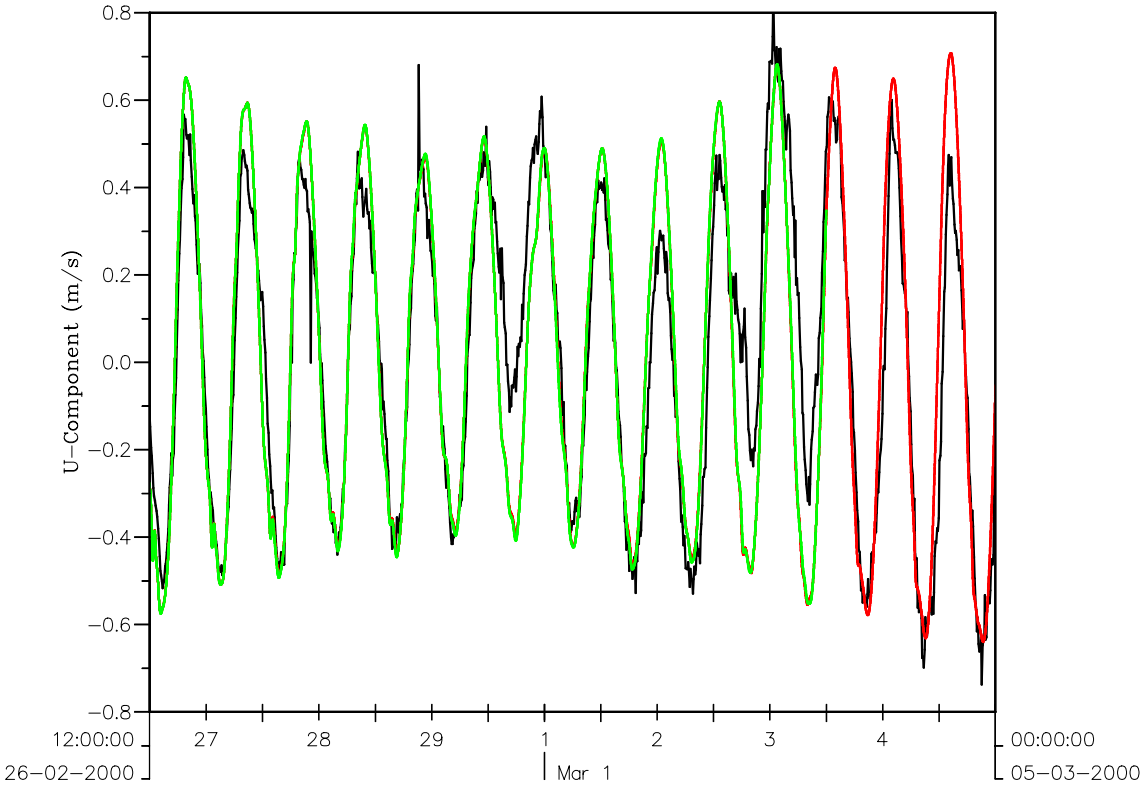

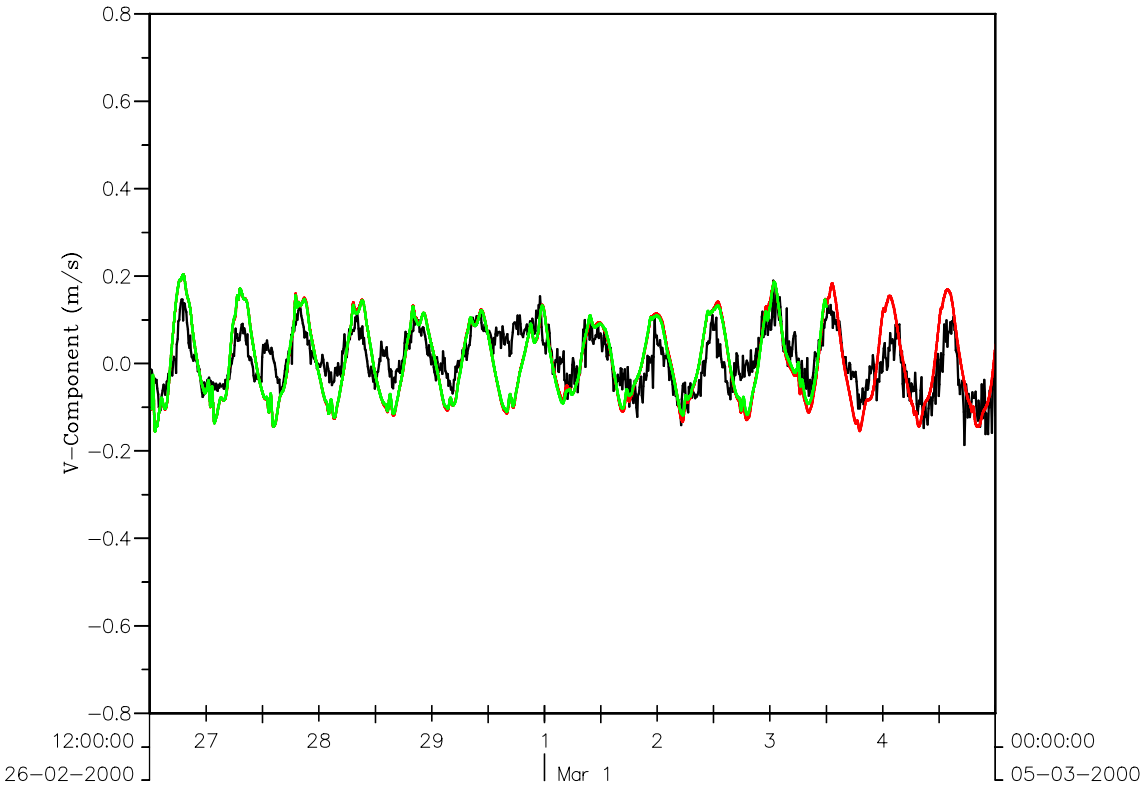

Morphology of pits, channels and trenches Part II: Verification of Delft3D with PUTMOR dataset Locations M Currents (Black: meas., Red: No Waves, Green: Waves	PIT−2DH	PT2 and PT4
	26−02 to 05−03	
WL | DELFT HYDRAULICS	Z3223	Fig. 4.12

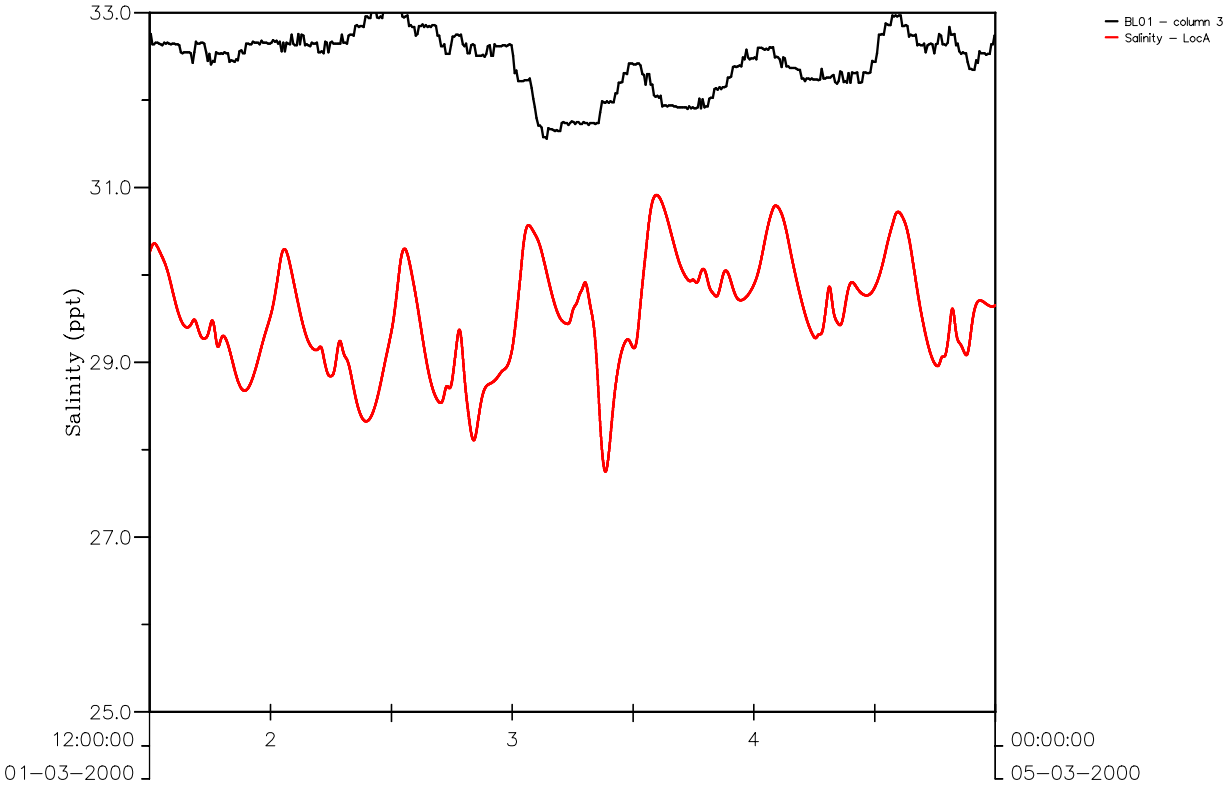

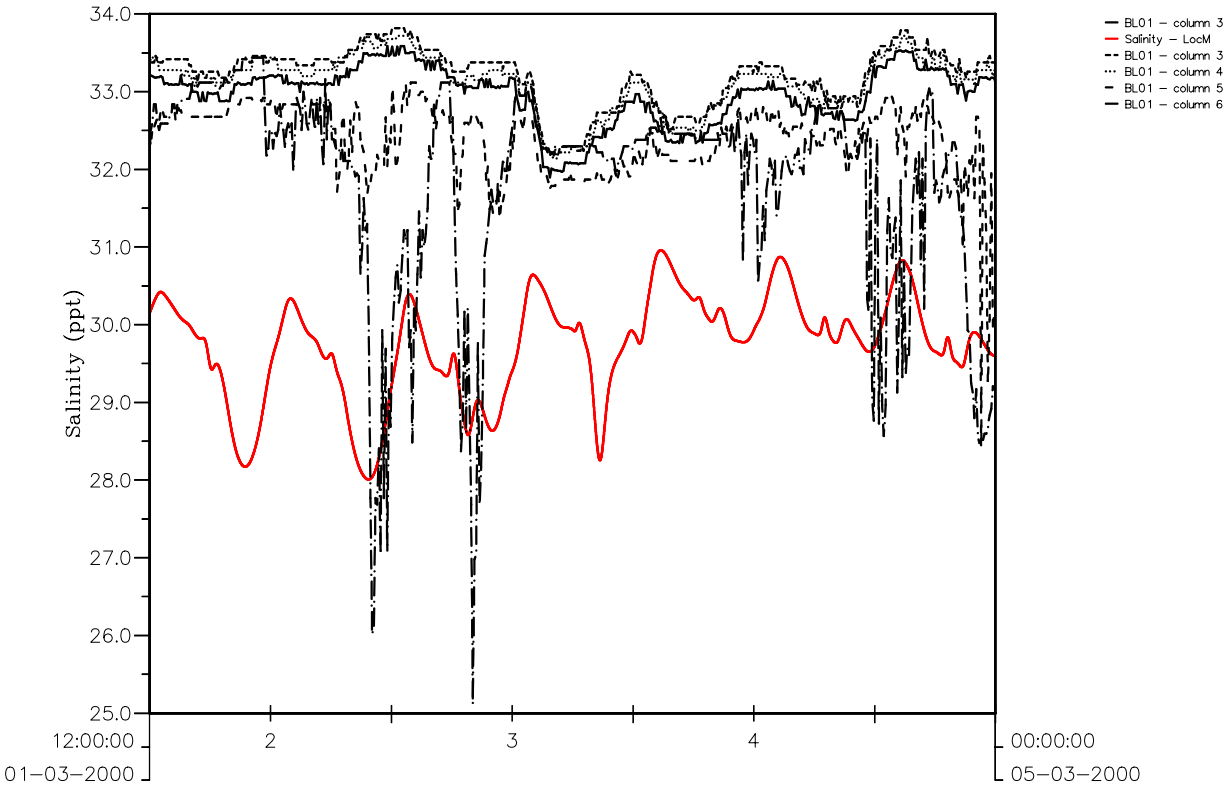

Morphology of pits, channels and channels Part II: Verification of Delft3D with PUTMOR dataset Salinity (ppt) – Black: Measured, Red: Modelled Top: A, Bottom: M	PIT–2DH	Z3223
	Period 1 March to 5 March	
WL | DELFT HYDRAULICS		Fig. 4.13

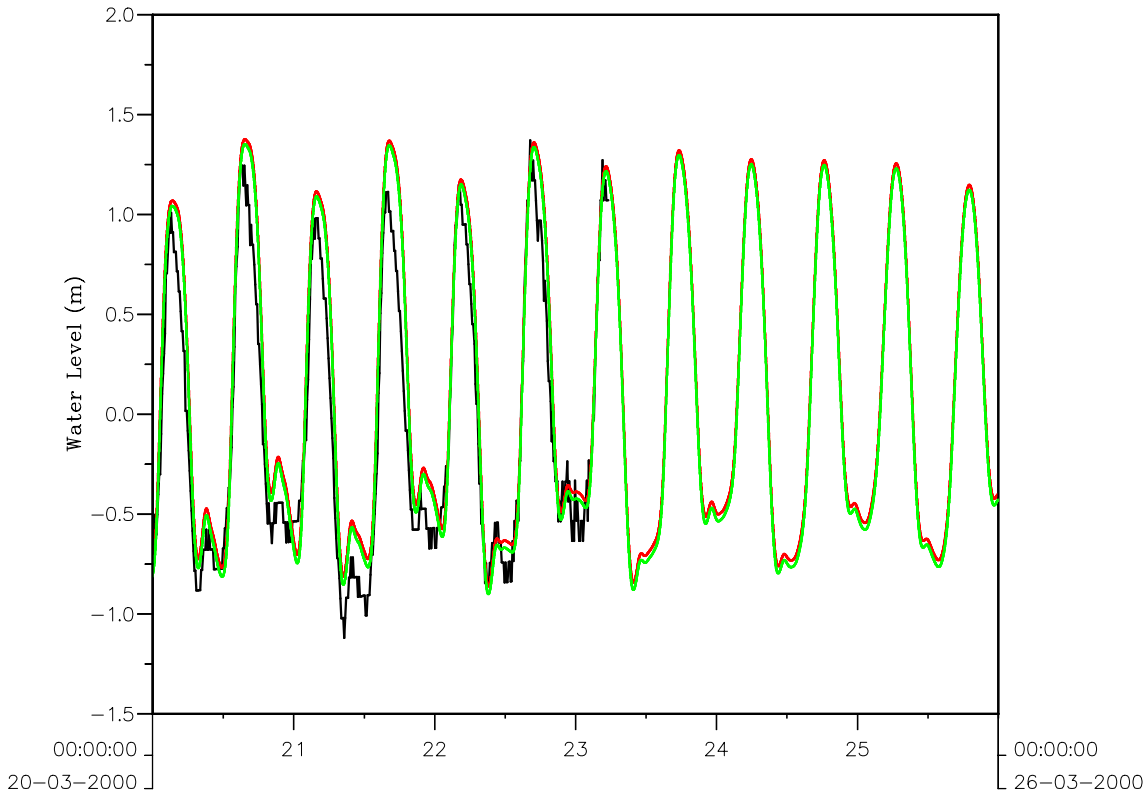

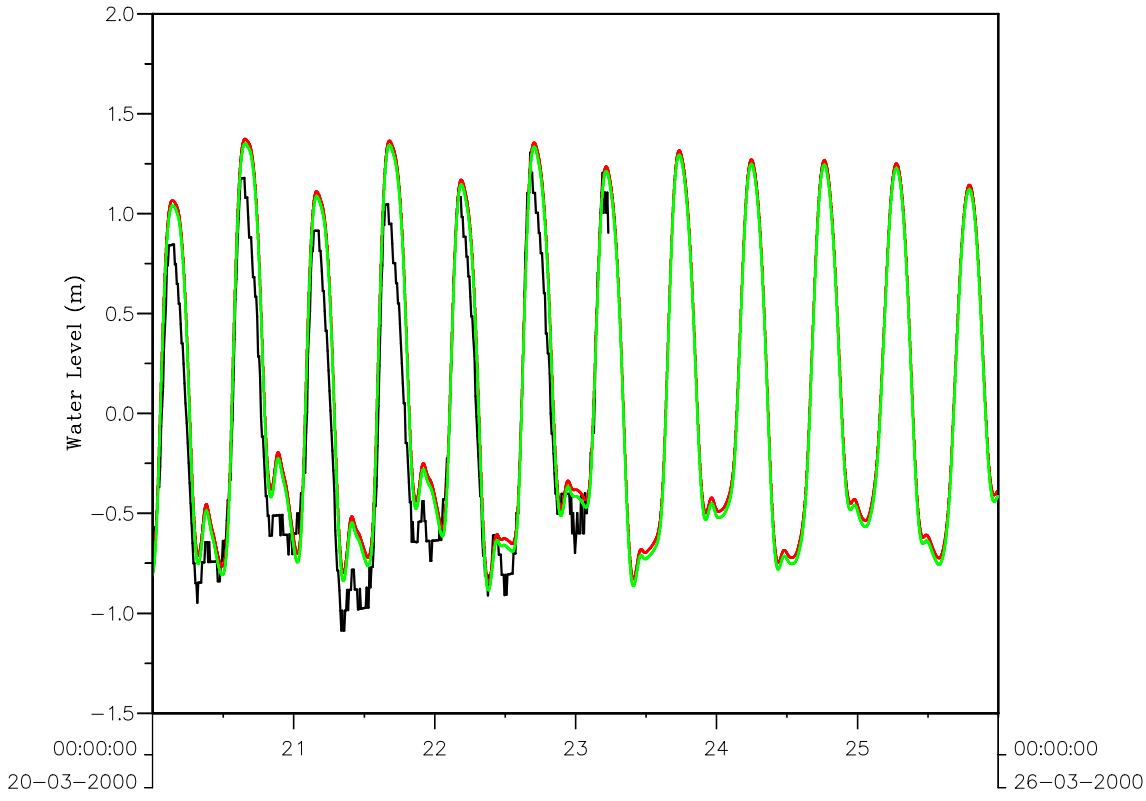

Morphology of pits, channels and trenches Part II: Verification of Delft3D with PUTMOR dataset Water Levels Locations A & M (Black: meas., Red: Salinity, Green: No Salinity)	PIT−2DH	pt5 and pt6
	20−03 to 26−03	
WL | DELFT HYDRAULICS	Z3223	Fig. 4.14

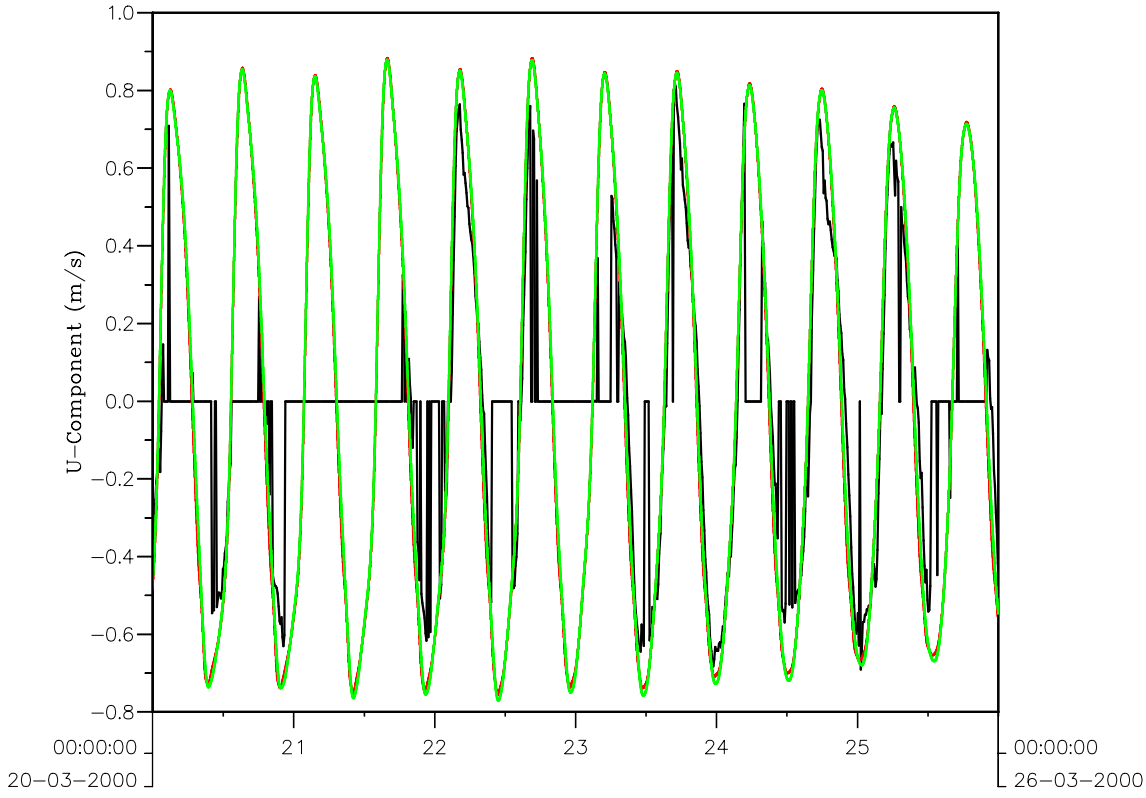

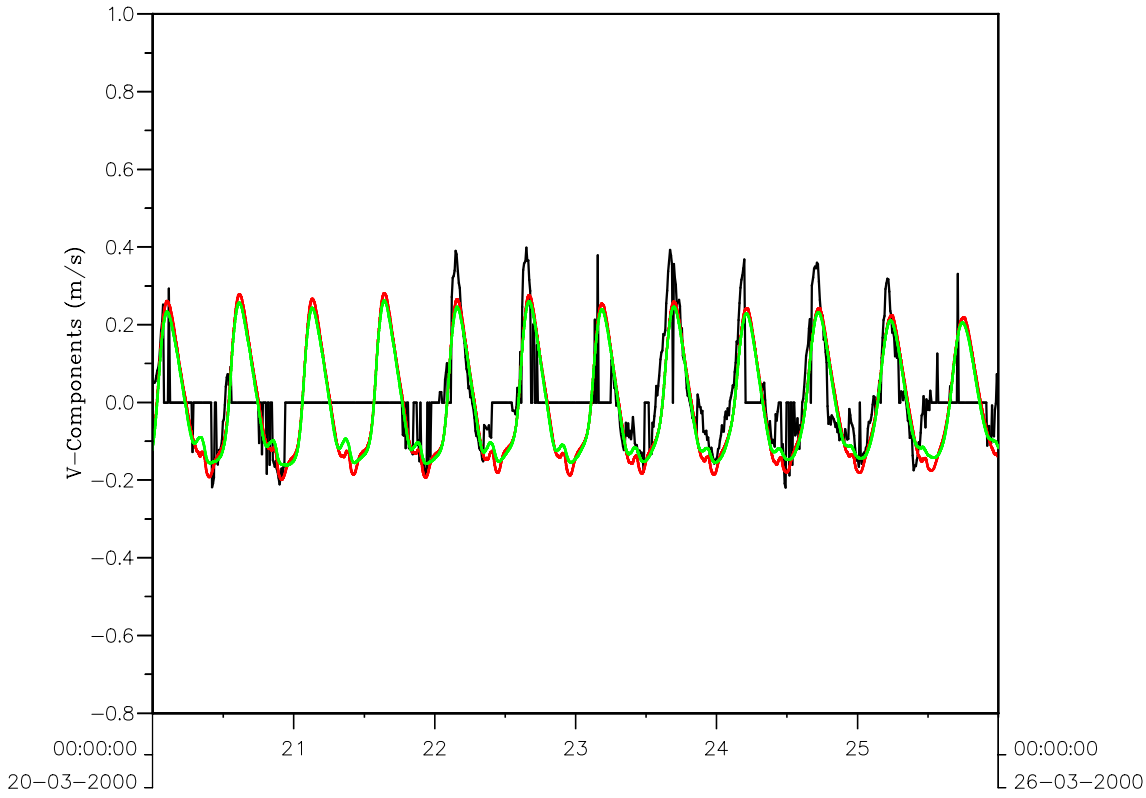

Morphology of pits, channels and trenches Part II: Verification of Delft3D with PUTMOR dataset Location A Currents (Black: meas., Red: Salinity, Green: No Salinity)	PIT-2DH	pt5 and pt6
	20-03 to 26-03	
WL | DELFT HYDRAULICS	Z3223	Fig. 4.15

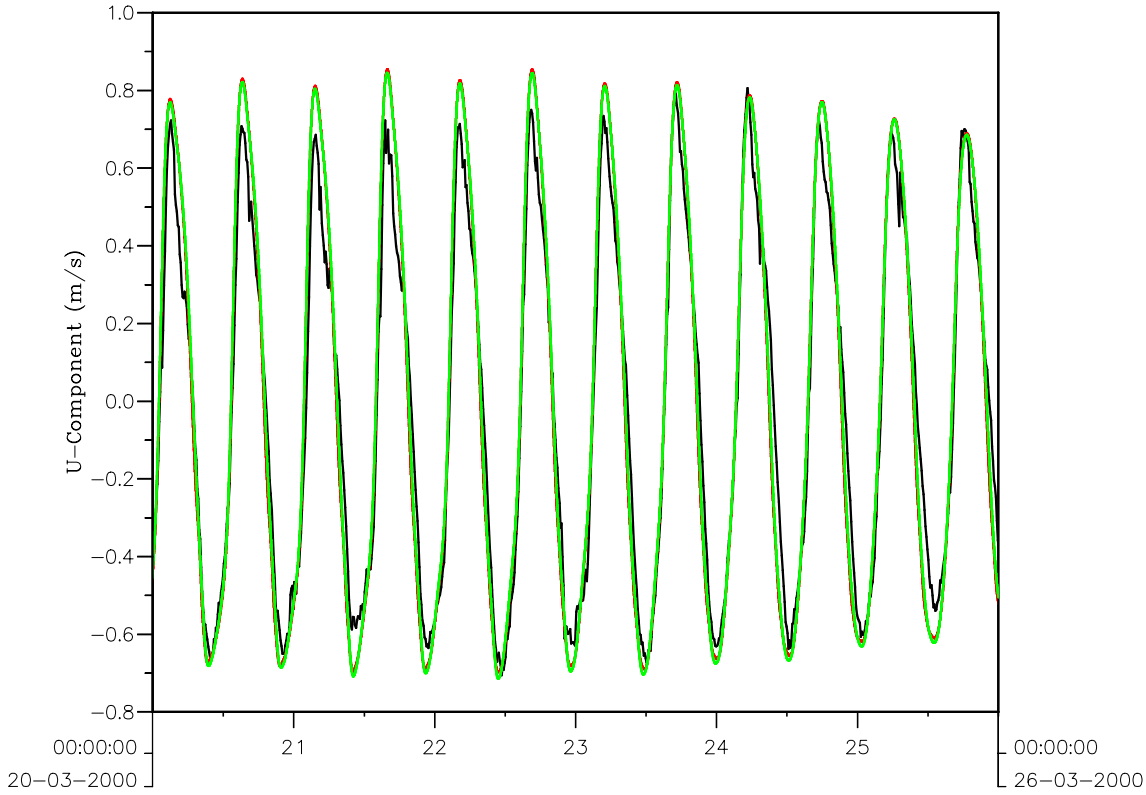

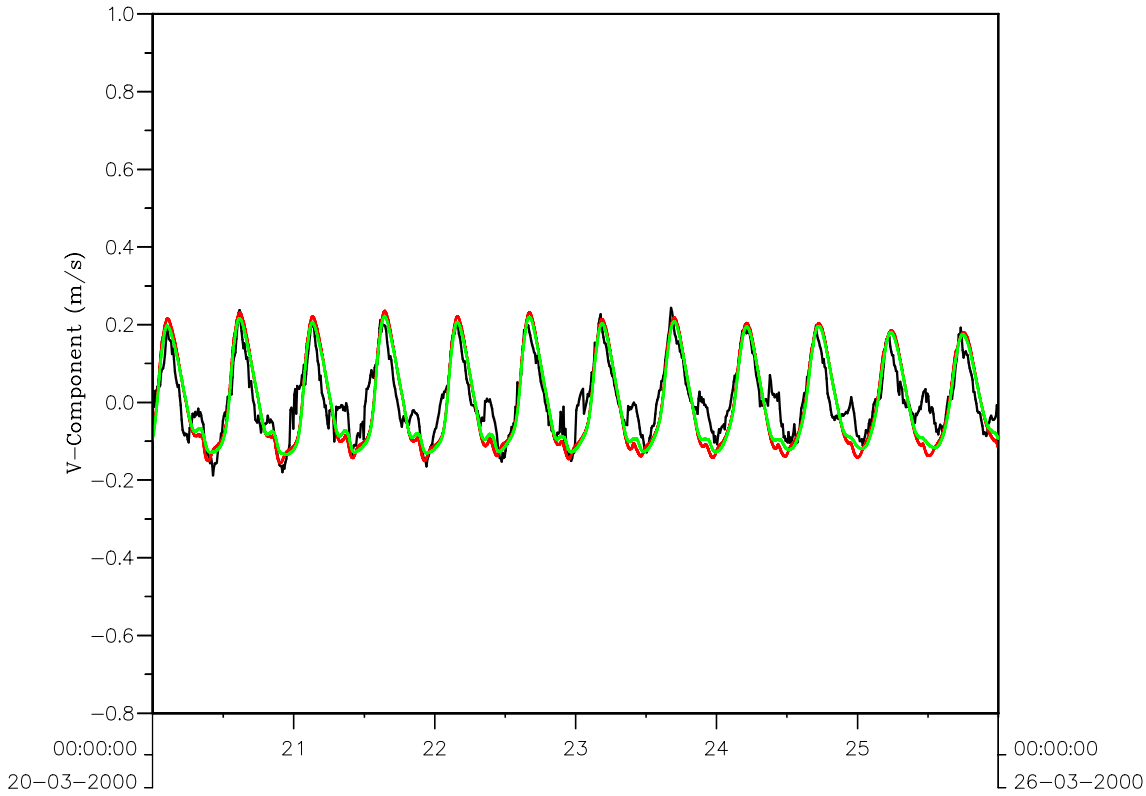

Morphology of pits, channels and trenches Part II: Verification of Delft3D with PUTMOR dataset Location M Currents (Black: meas., Red: Salinity, Green: No Salinity)	PIT−2DH	pt5 and pt6
	20−03 to 26−03	
WL | DELFT HYDRAULICS	Z3223	Fig. 4.16

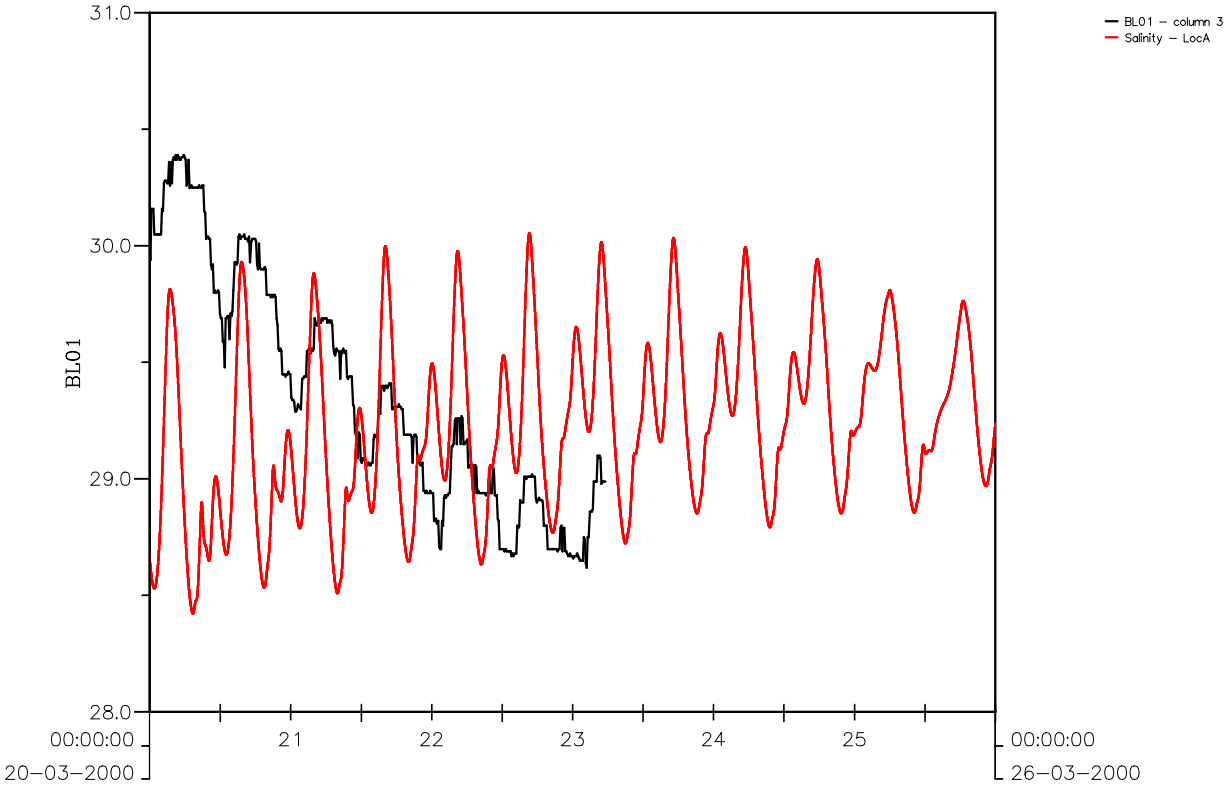

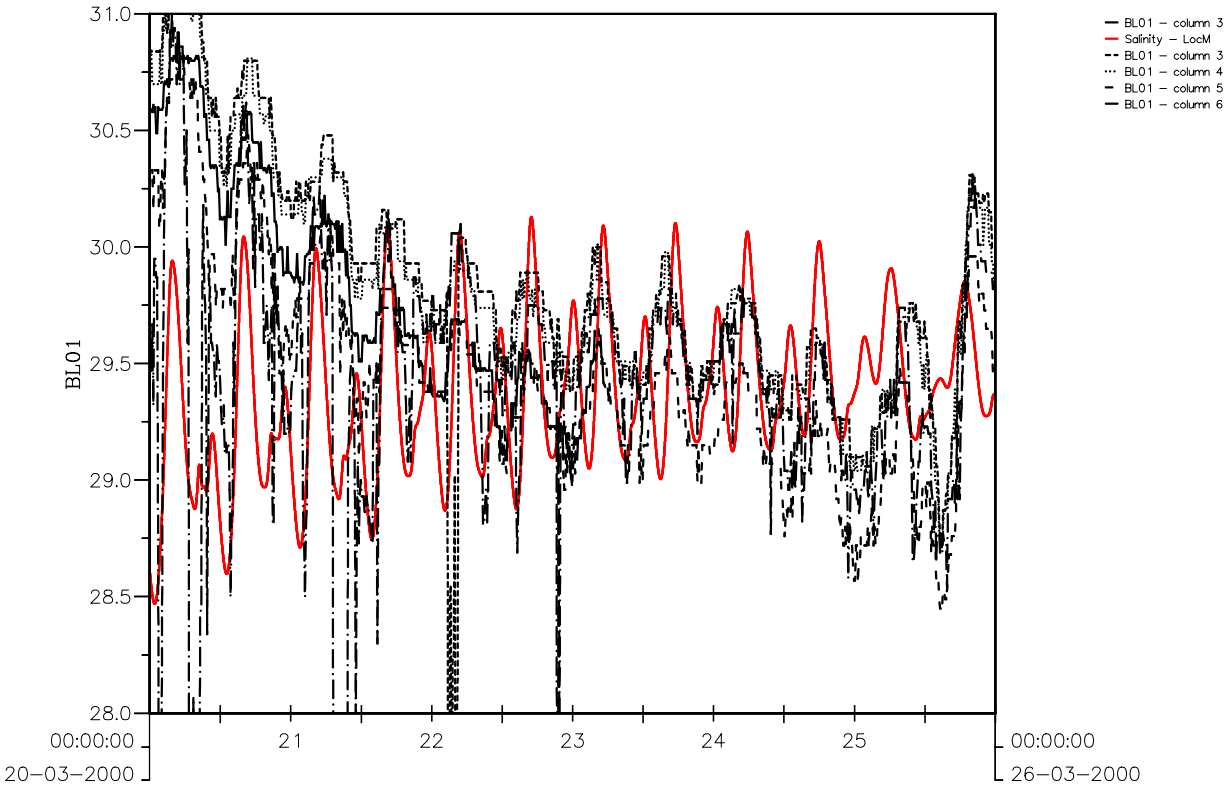

Morphology of pits, channels and trenches Part II: Verification of Delft3D with PUTMOR dataset Salinity (ppt) – Black: Measered, Red: Modelled Top: A, Bottom: M	PIT–2DH	Z3223
	Period 20–03 to 25–03	
WL | DELFT HYDRAULICS		Fig. 4.17

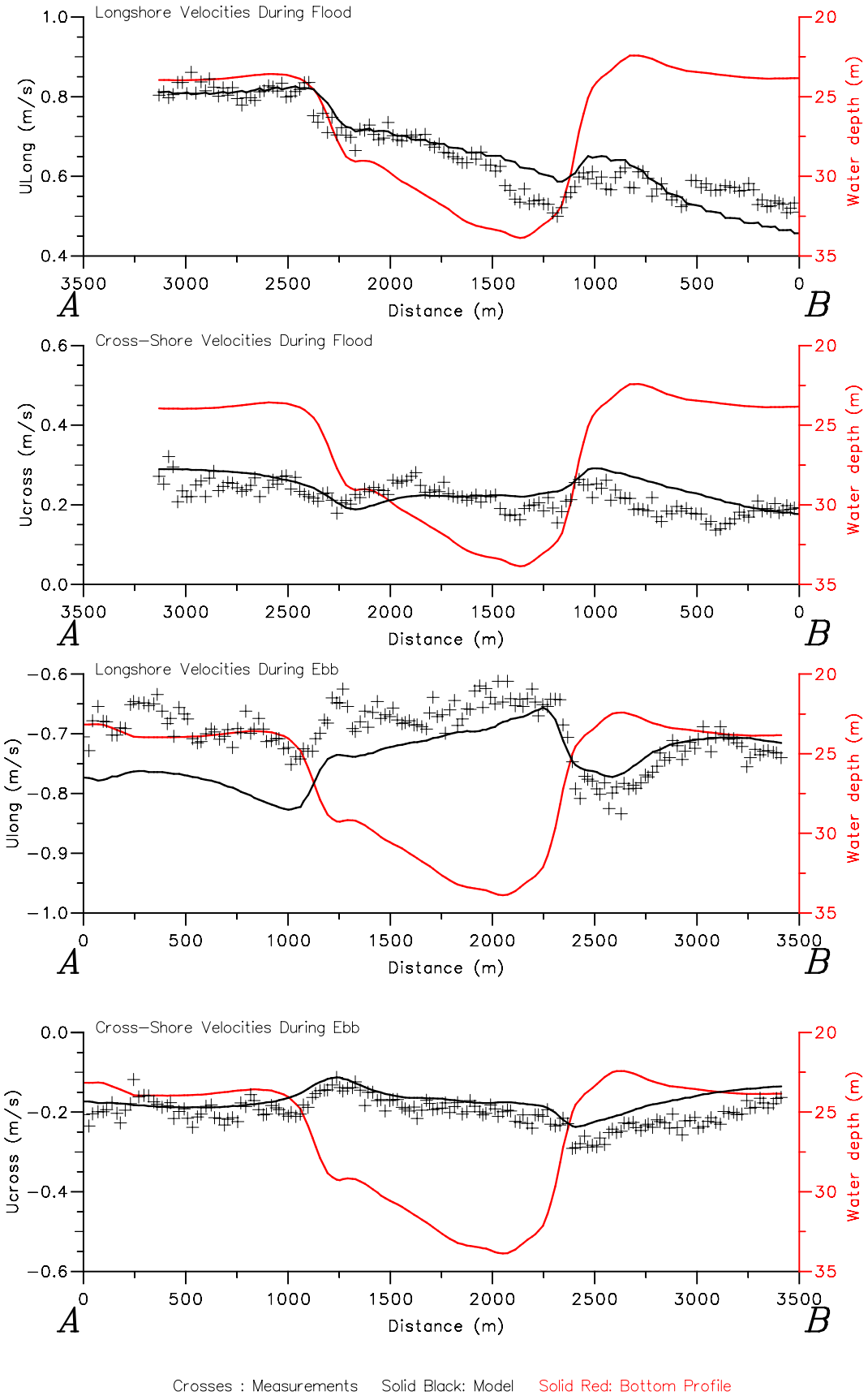

Crosses : Measurements Solid Black: Model Solid Red: Bottom Profile

Morphology of pits, channels and trenches Part II: Verification of Delft3D with PUTMOR dataset Track 1 – Depth Averaged Velocities		PT5–2DH
WL | DELFT HYDRAULICS	Z3223	FIG. 4.18

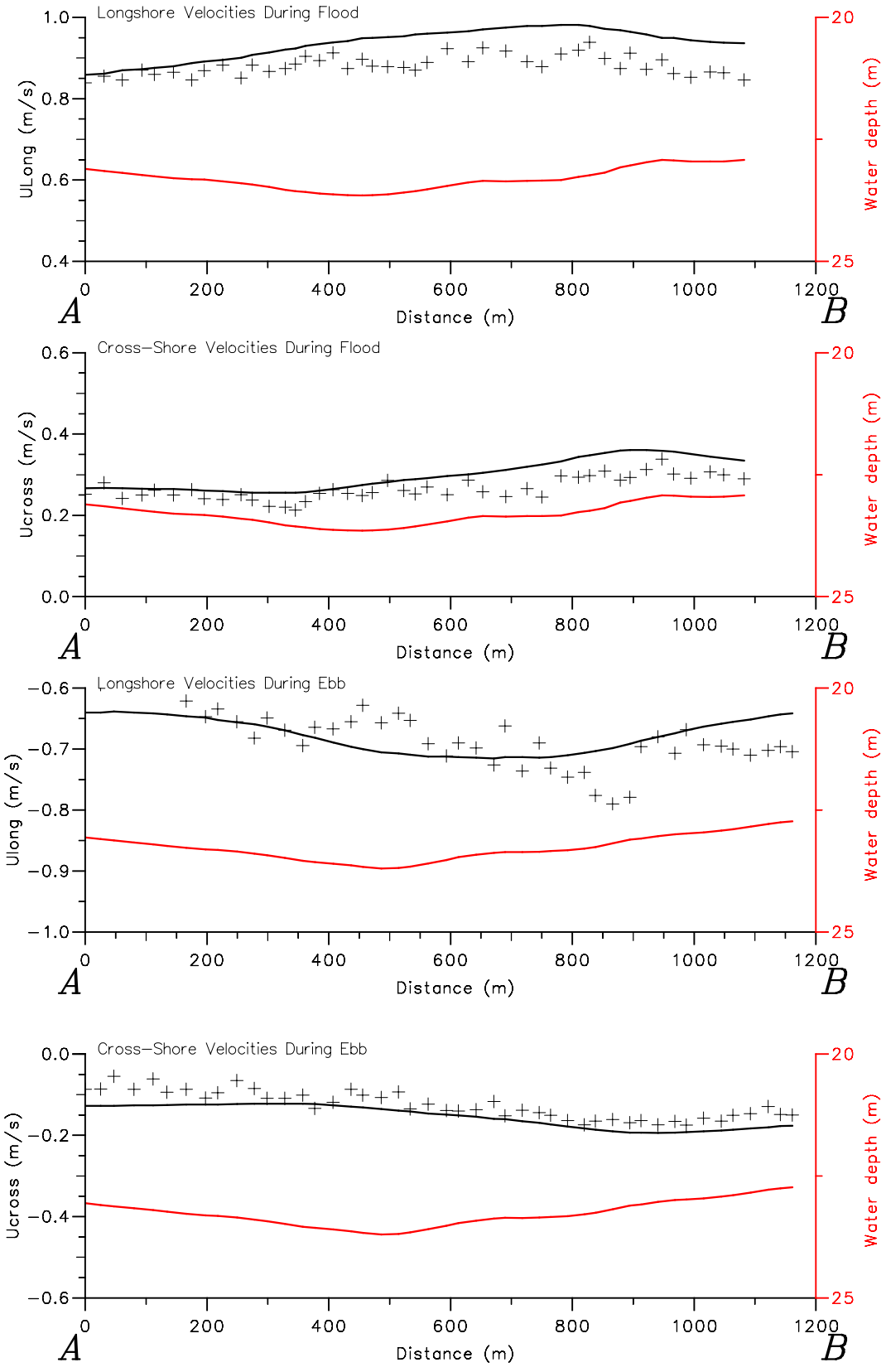

Crosses : Measurements Solid Black: Model Solid Red: Bottom Profile

Morphology of pits, channels and trenches Part II: Verification of Delft3D with PUTMOR dataset Track 2 – Depth Averaged Velocities		PT5–2DH
WL | DELFT HYDRAULICS	Z3223	FIG. 4.19

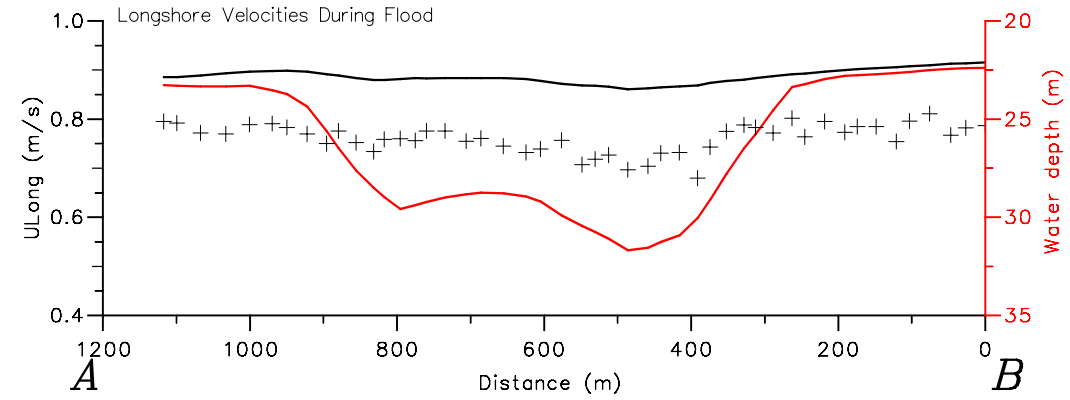

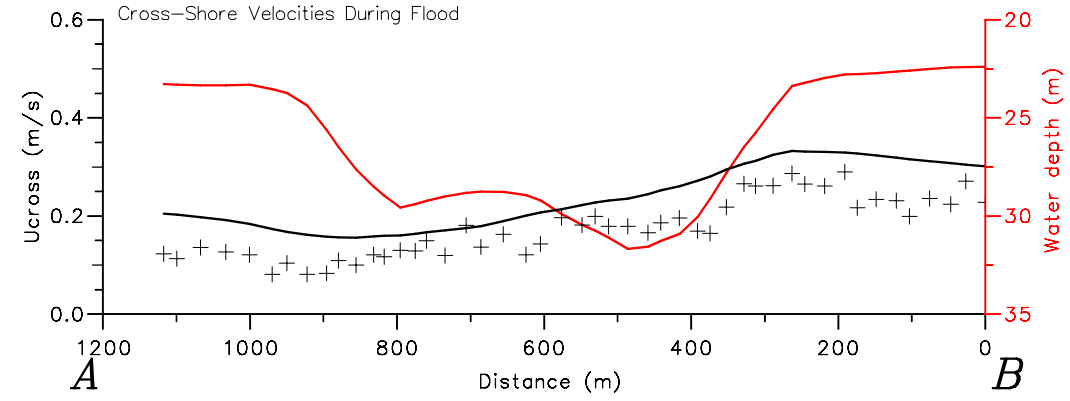

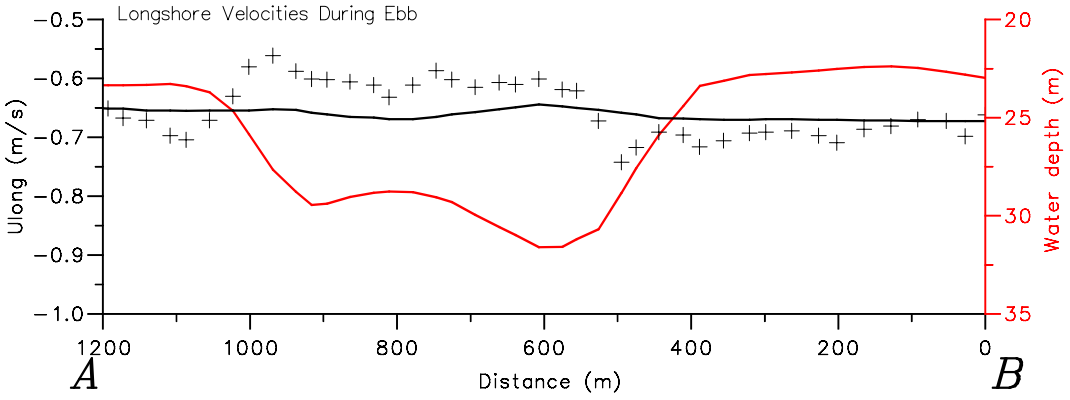

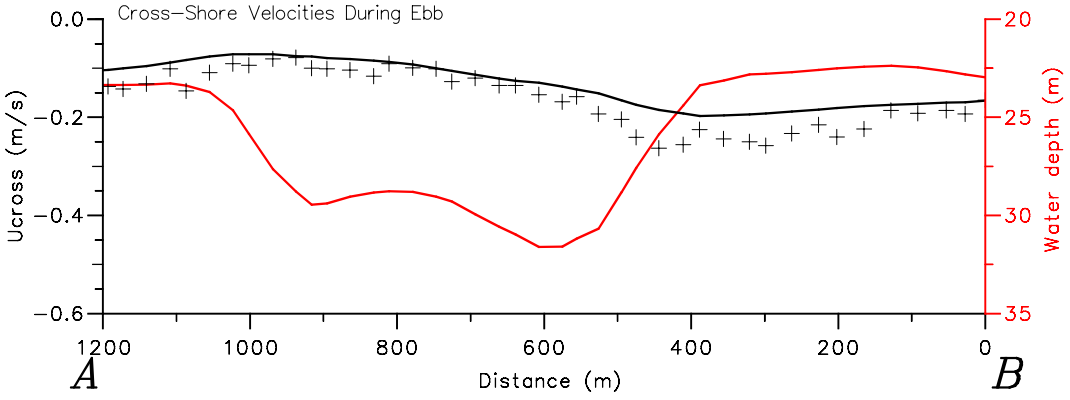

Crosses : Measurements Solid Black: Model Solid Red: Bottom Profile

Morphology of pits, channels and trenches Part II: Verification of Delft3D with PUTMOR dataset Track 3 – Depth Averaged Velocities		PT5–2DH
WL | DELFT HYDRAULICS	Z3223	FIG. 4.20

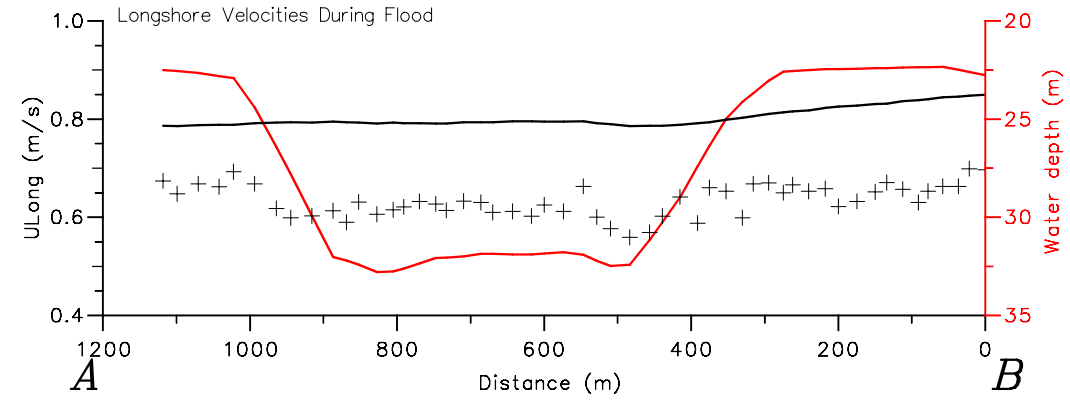

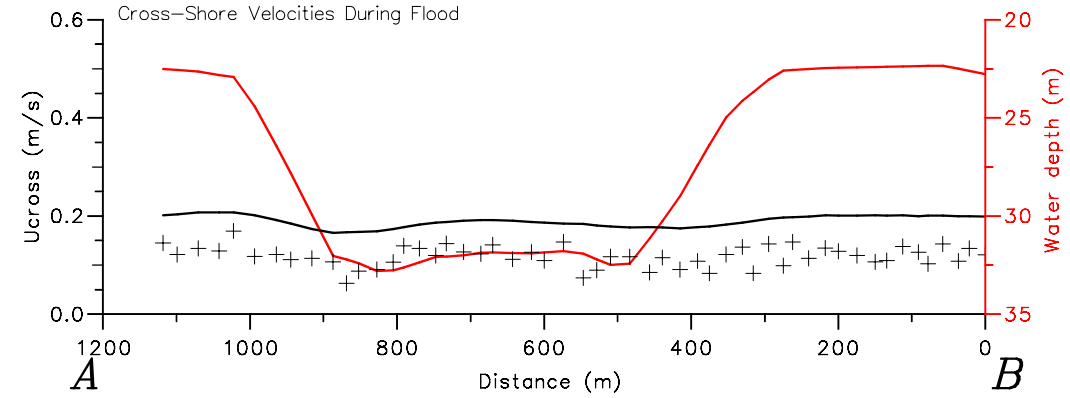

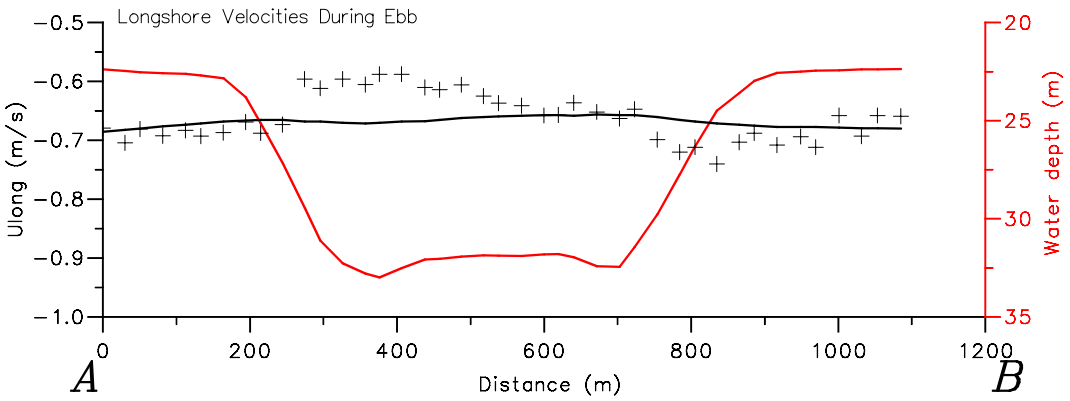

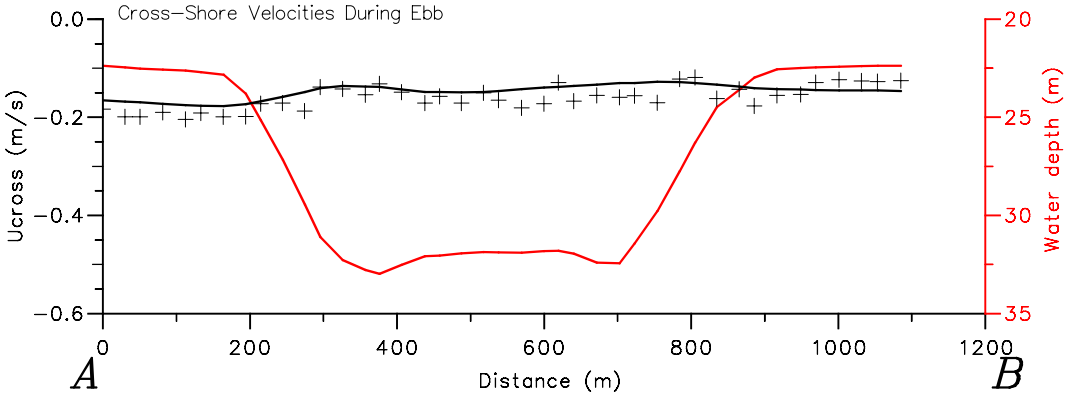

Crosses : Measurements Solid Black: Model Solid Red: Bottom Profile

Morphology of pits, channels and trenches Part II: Verification of Delft3D with PUTMOR dataset Track 4 – Depth Averaged Velocities		PT5–2DH
WL | DELFT HYDRAULICS	Z3223	FIG. 4.21

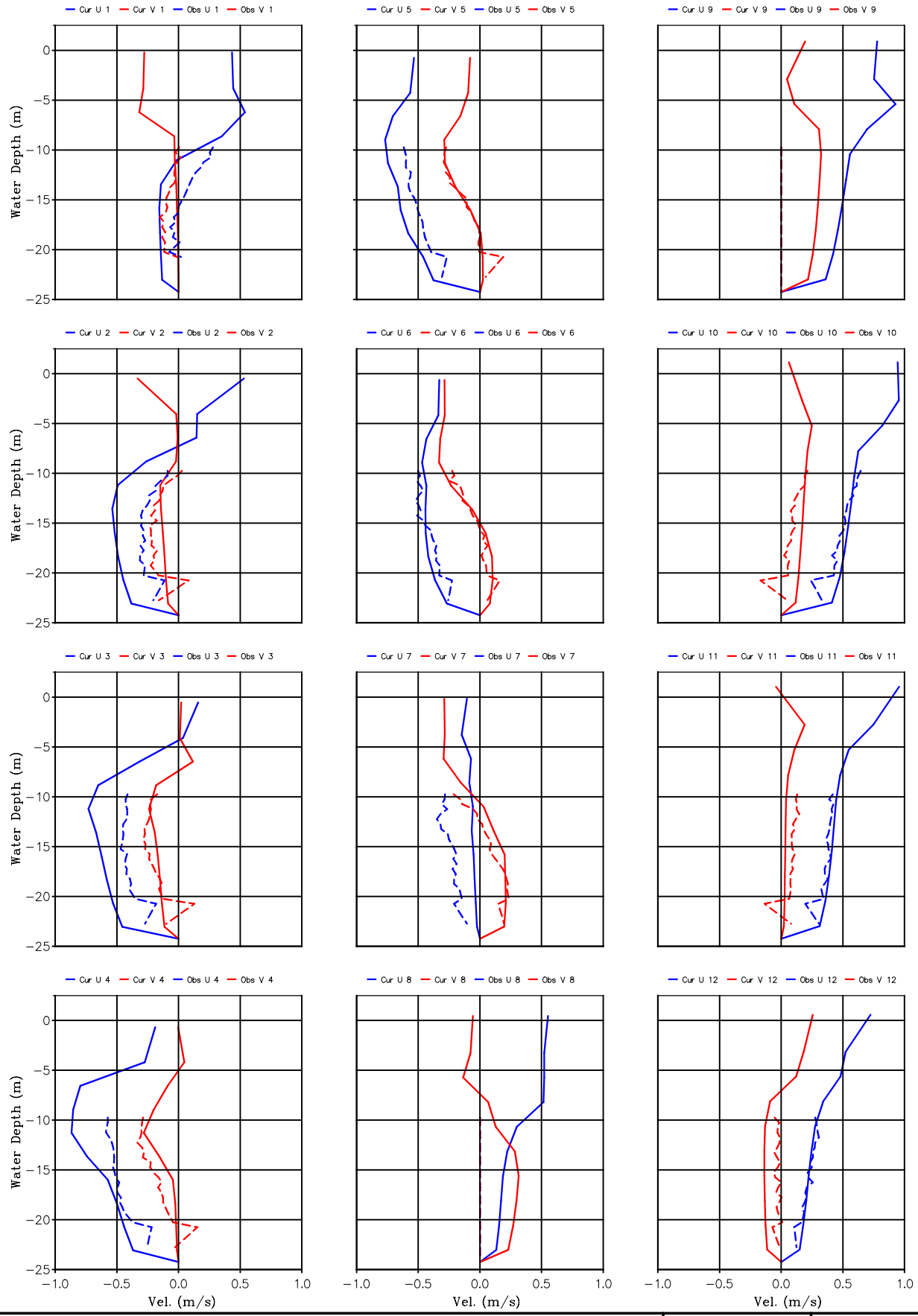

Vertical current profiles (hourly for 1 tidal period)

Location A (Blue: U–Long, Red: V–Cross, Solid: Calculated, Dashed: Measured)

Period 2000–02–26 11:05:00 – 2000–02–26 23:05:00

Z3223

WL | DELFT HYDRAULICS

Fig. 4.23

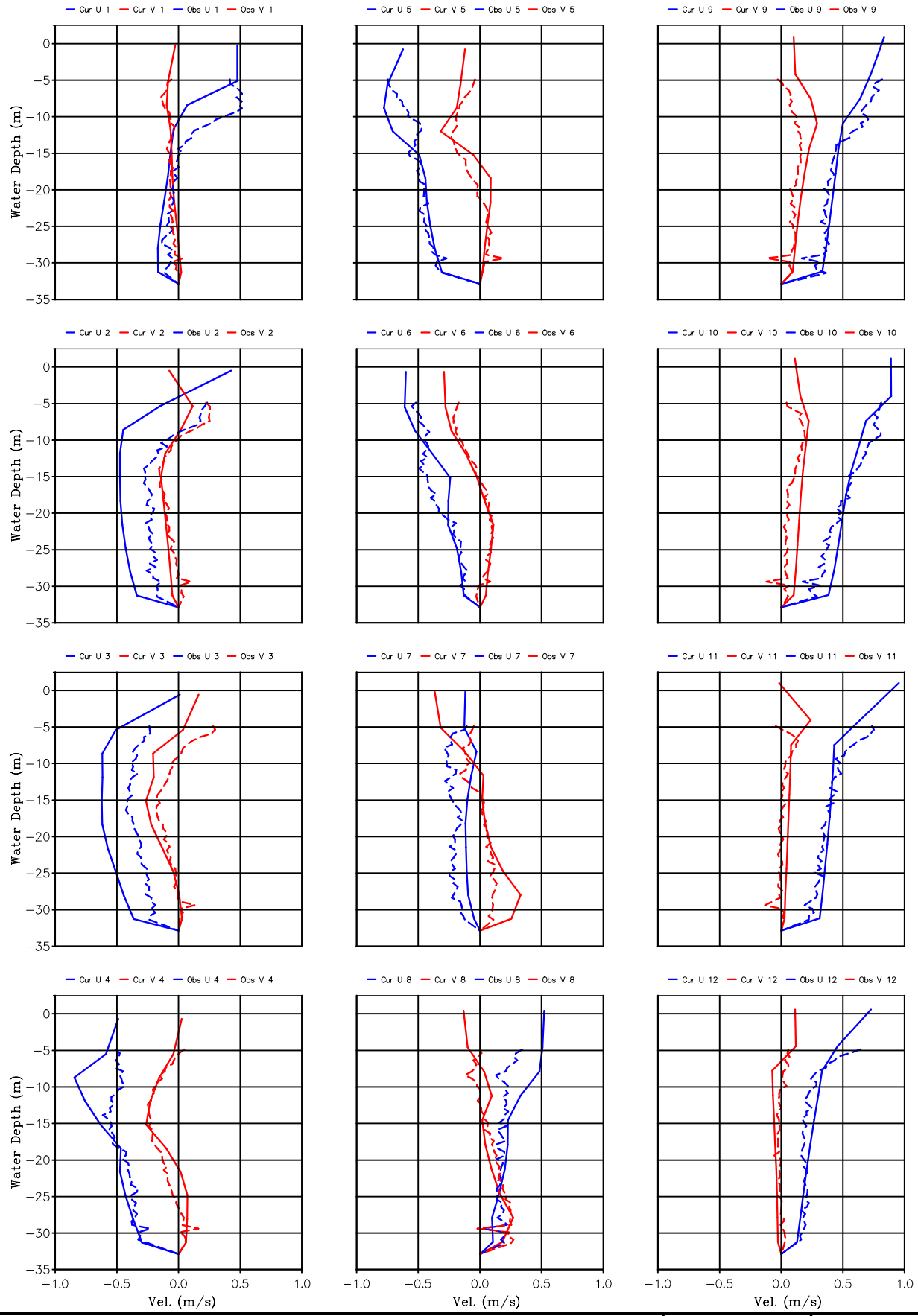

Vertical current profiles (hourly for 1 tidal period)

Location M (Blue: U–long, Red: V–Cross., Solid: Calculated, Dashed: Measured)

Period 2000–02–26 11:05:00 – 2000–02–26 23:05:00

Z3223

WL | DELFT HYDRAULICS

Fig. 4.24

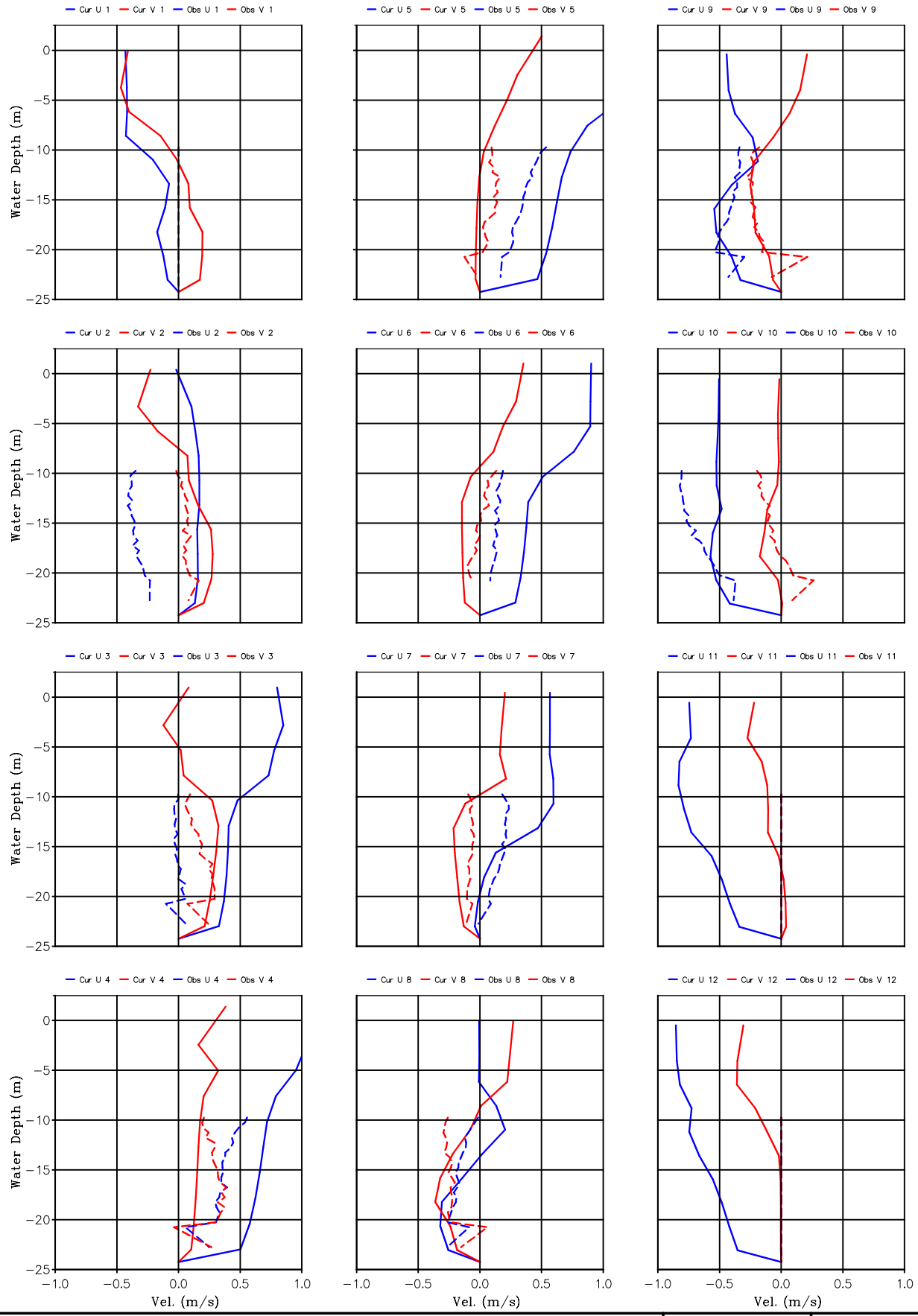

Vertical current profiles (hourly for 1 tidal period)

Location A (Blue: U–Long, Red: V–Cross, Solid: Calculated, Dashed: Measured)

Period 2000–03–04 11:05:00 – 2000–03–04 23:05:00

Z3223

WL | DELFT HYDRAULICS

Fig. 4.25

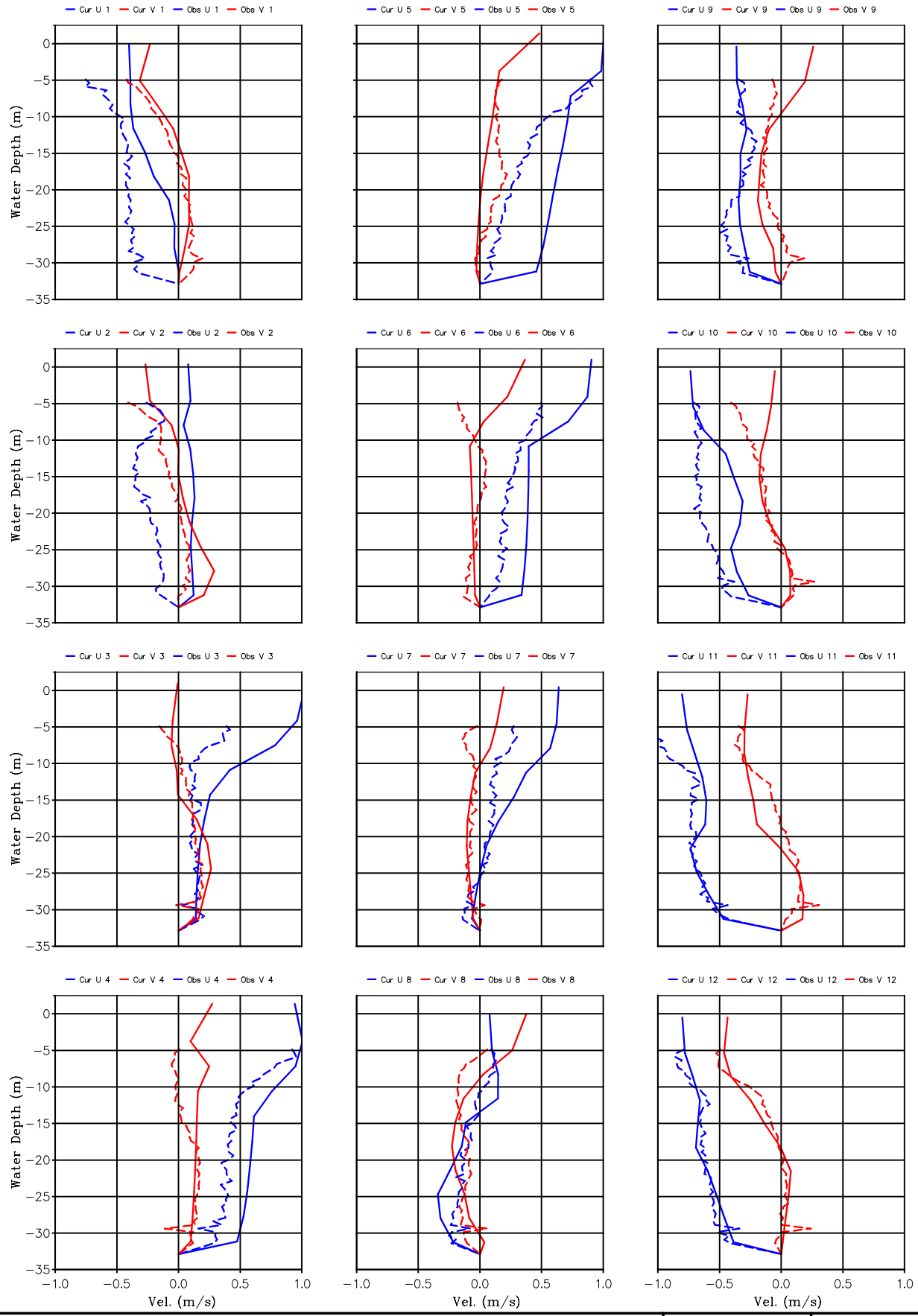

Vertical current profiles (hourly for 1 tidal period)

Location M (Blue: U–long, Red: V–Cross, Solid: Calculated, Dashed: Measured)

Period 2000–03–04 11:05:00 – 2000–03–04 23:05:00

Z3223

WL | DELFT HYDRAULICS

Fig. 4.26

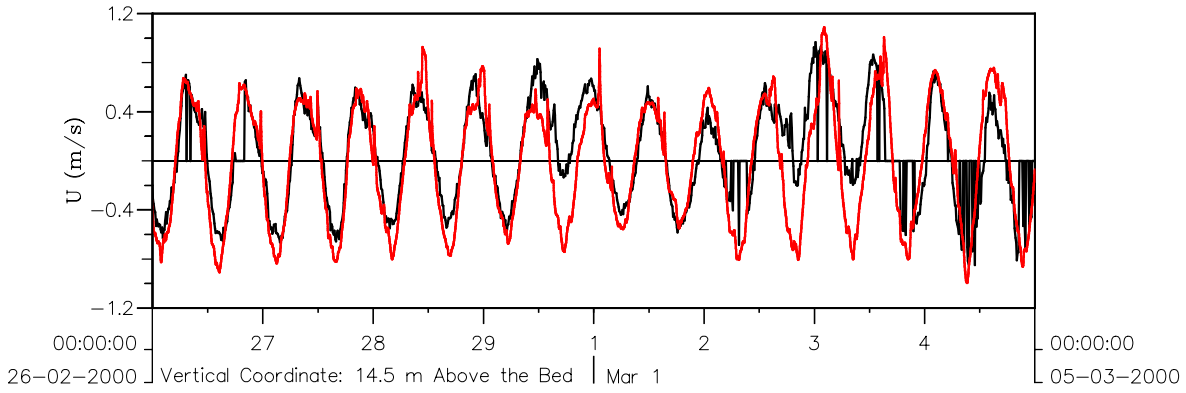

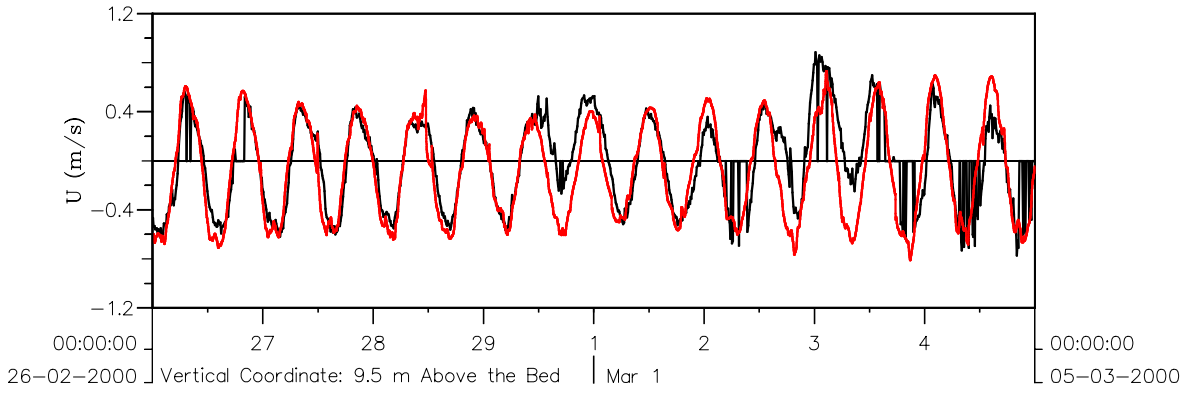

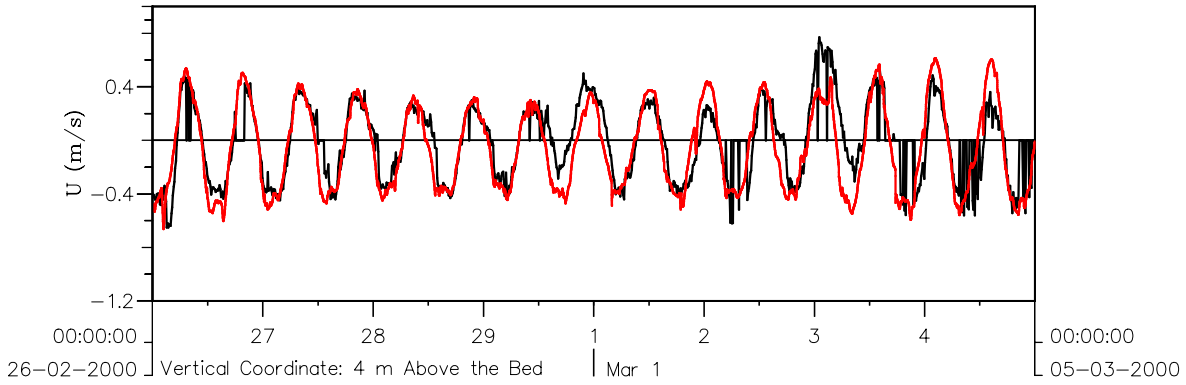

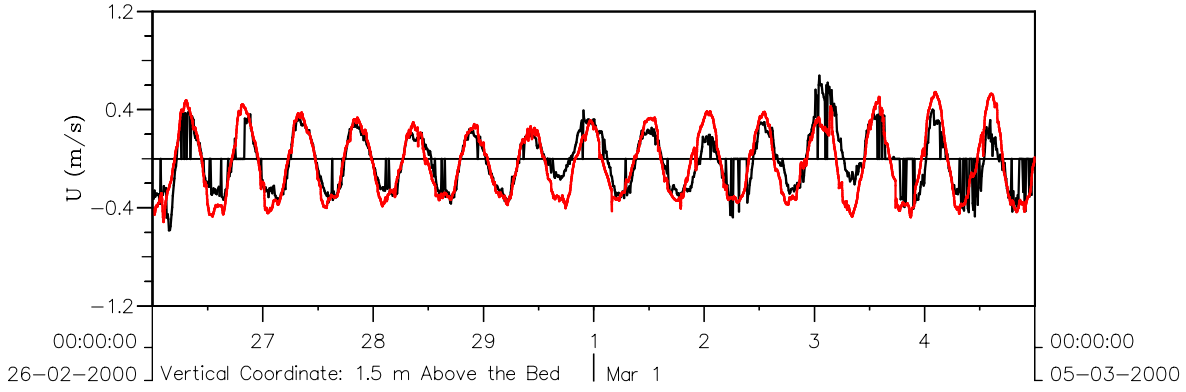

Morphology of pits, channels and trenches Part II: Verification of Delft3D with PUTMOR dataset Location A: Longshore Velocities at Various Water Depths		PT2−3D
	Black Meas., Red Model	
WL | DELFT HYDRAULICS	Z3223	FIG. 4.27

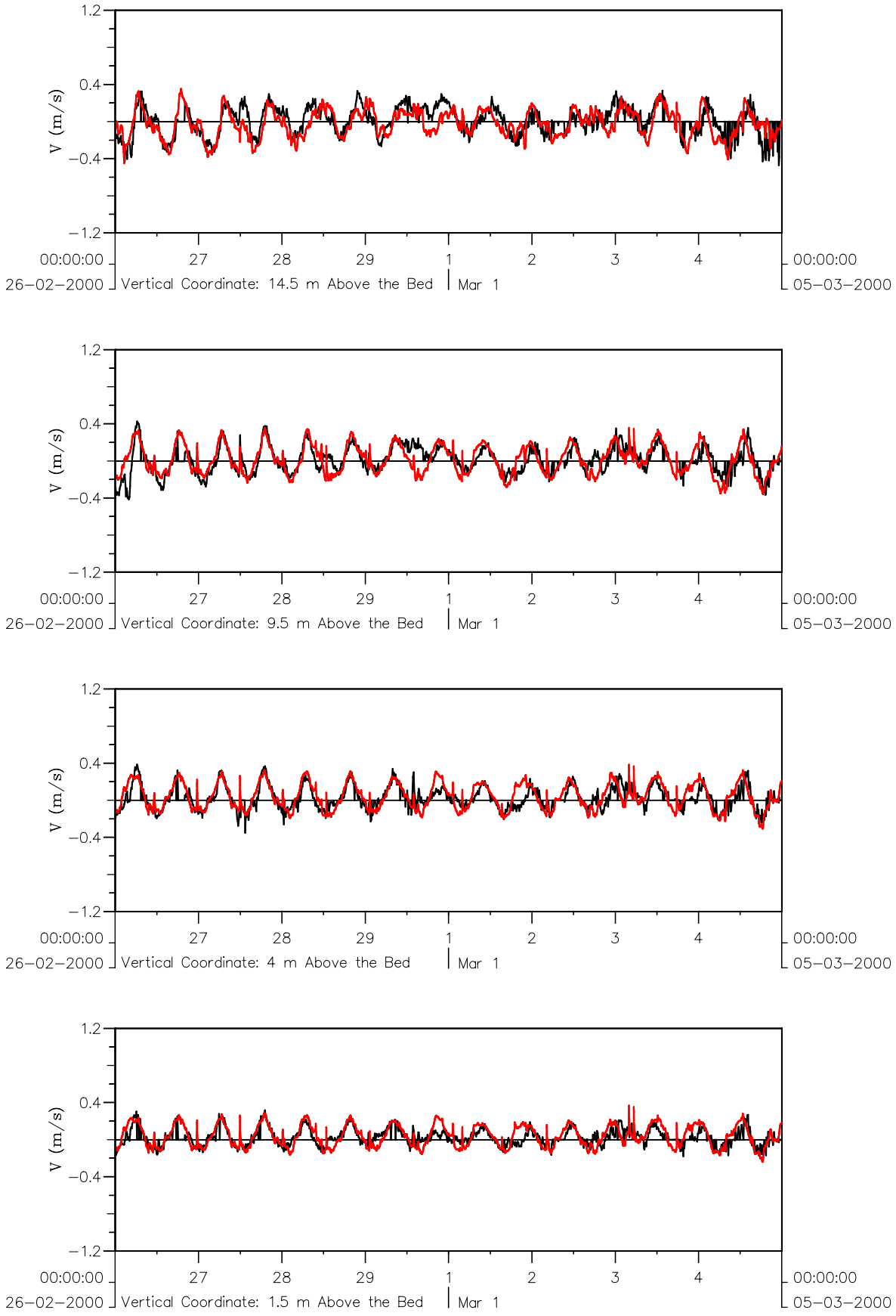

Morphology of pits, channels and trenches Part II: Verification of Delft3D with PUTMOR dataset Location A: Cross−Shore Velocities at Various Water Depths		PT2−3D
	Black Meas., Red Model	
WL | DELFT HYDRAULICS	Z3223	FIG. 4.28

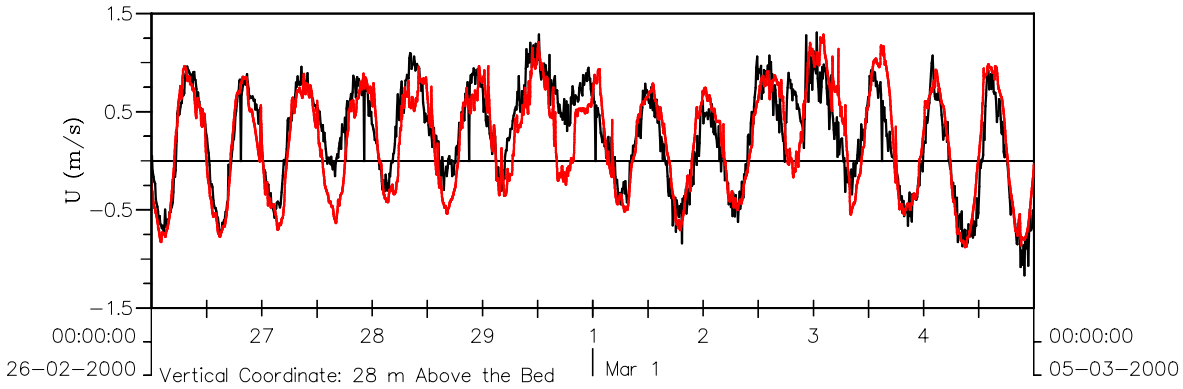

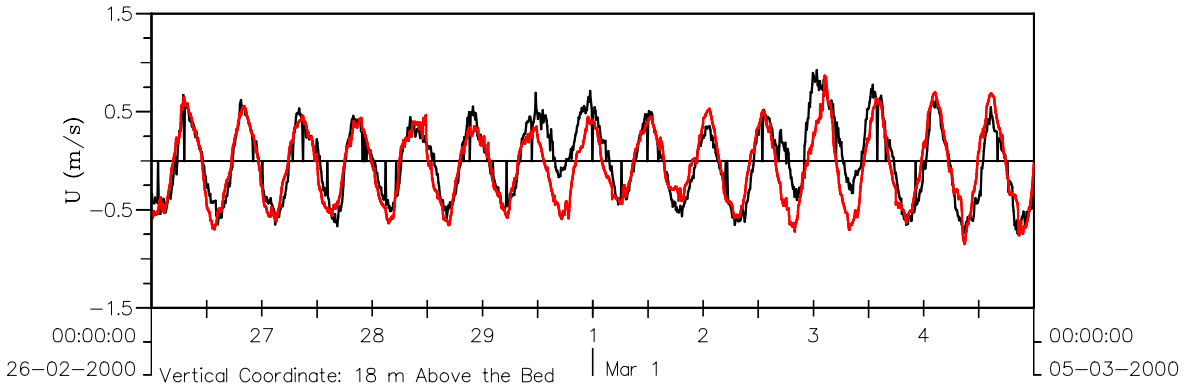

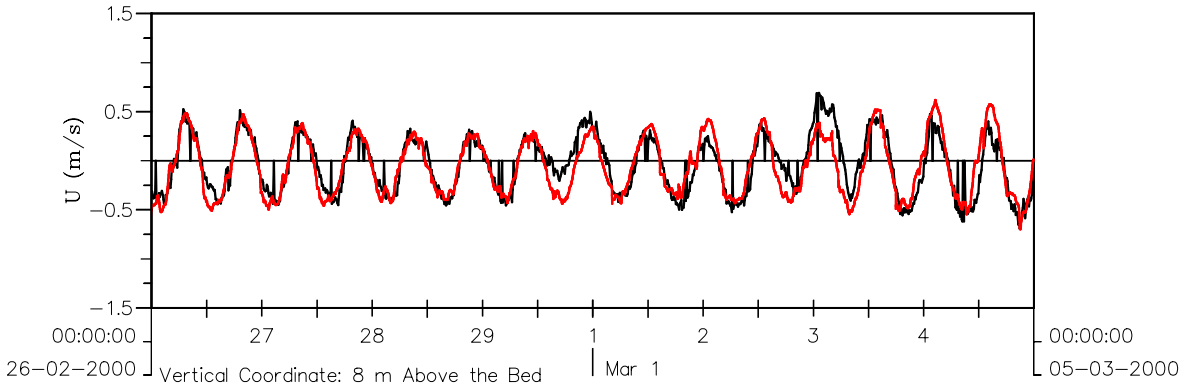

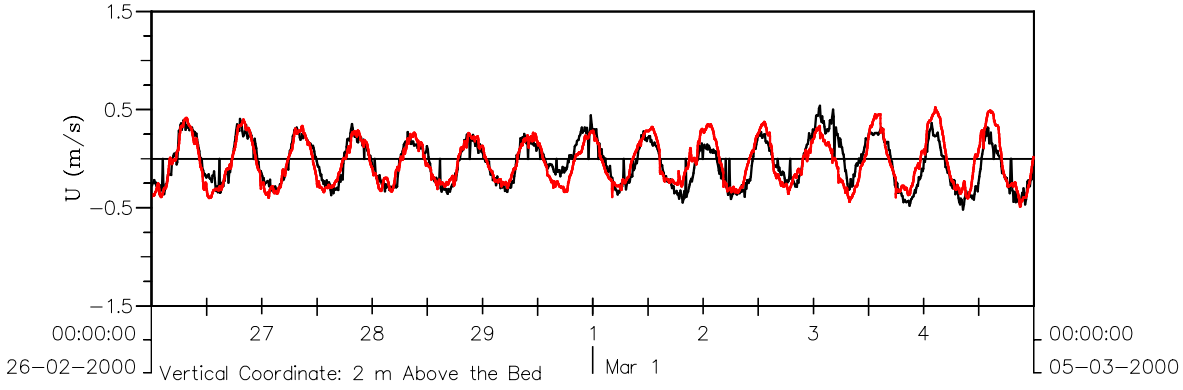

Morphology of pits, channels and trenches Part II: Verification of Delft3D with PUTMOR dataset Location M: Longshore Velocities at Various Water Depths		PT2−3D
		Black Meas., Red Model
WL | DELFT HYDRAULICS	Z3223	FIG. 4.29

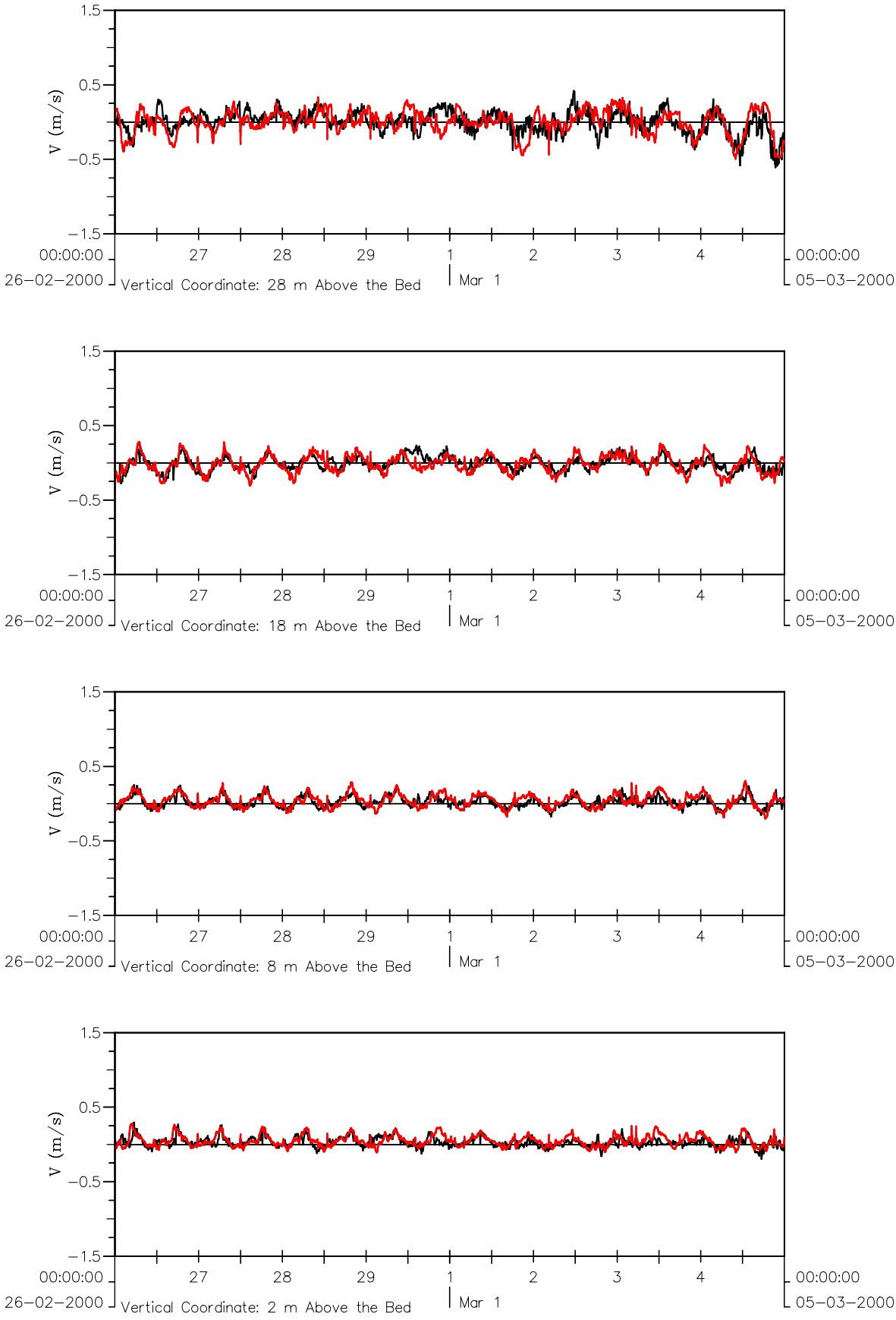

Morphology of pits, channels and trenches Part II: Verification of Delft3D with PUTMOR dataset Location M: Cross−Shore Velocities at Various Water Depths		PT2−3D
	Black Meas., Red Model	
WL | DELFT HYDRAULICS	Z3223	FIG. 4.30

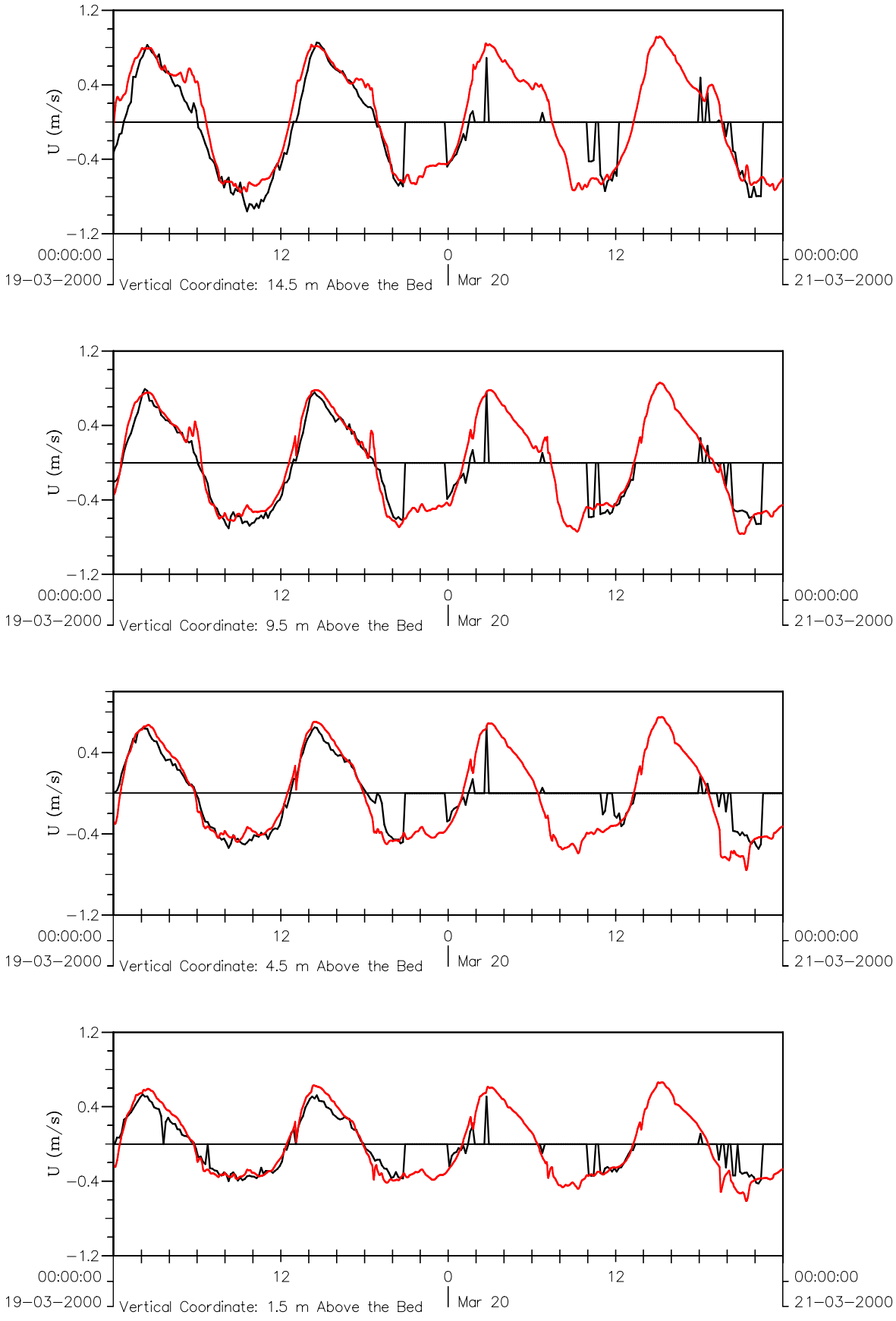

Morphology of pits, channels and trenches Part II: Verification of Delft3D with PUTMOR dataset Location A: Longshore Velocities at Various Water Depths		PT5−3D
	Black Meas., Red Model	
WL | DELFT HYDRAULICS	Z3223	FIG. 4.34

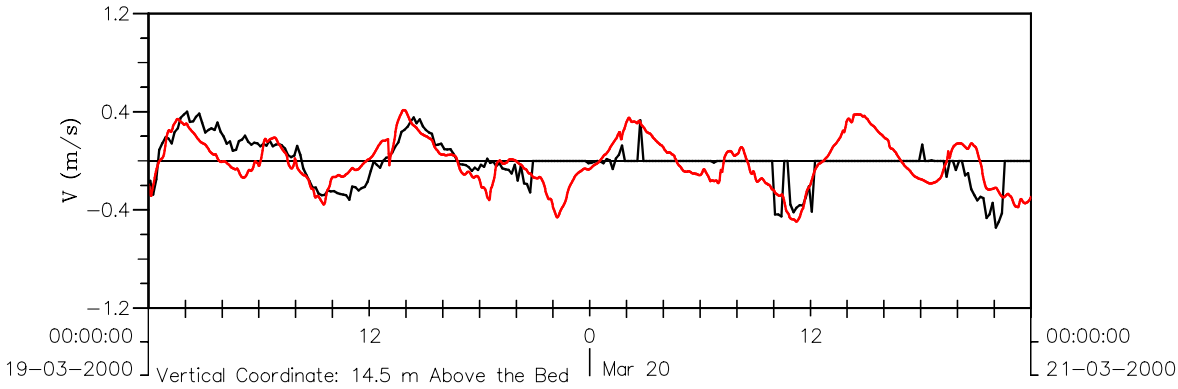

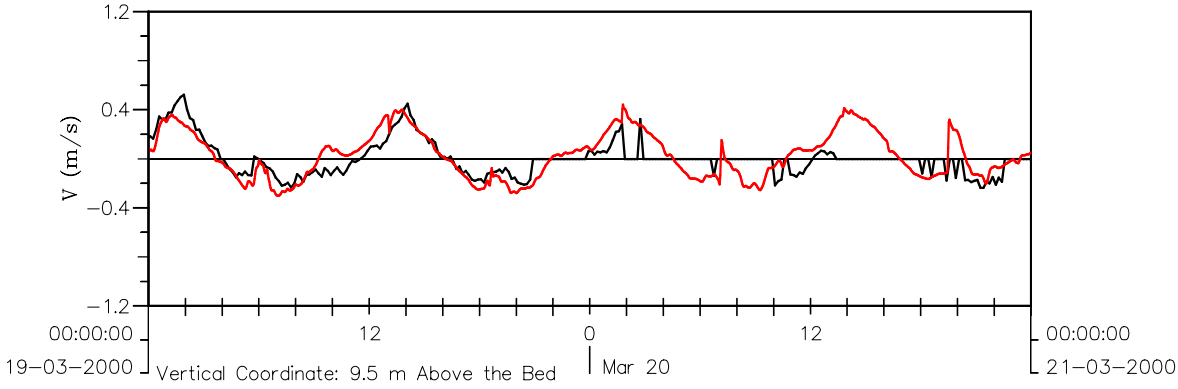

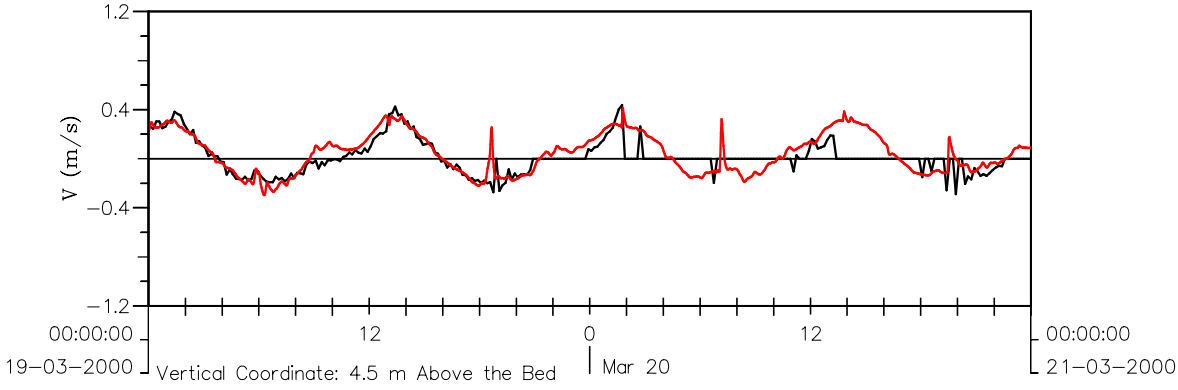

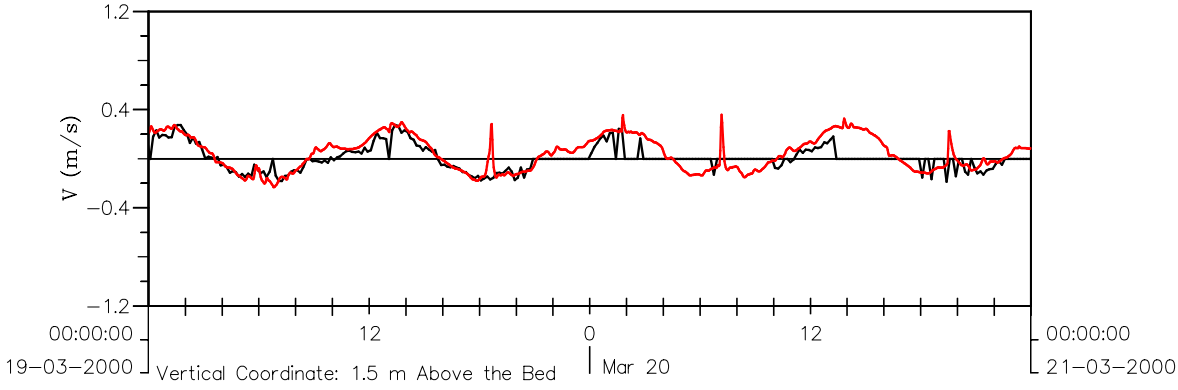

Morphology of pits, channels and trenches Part II: Verification of Delft3D with PUTMOR dataset Location A: Cross−Shore Velocities at Various Water Depths	PT5−3D Black Meas., Red Model
WL | DELFT HYDRAULICS	Z3223 FIG. 4.35

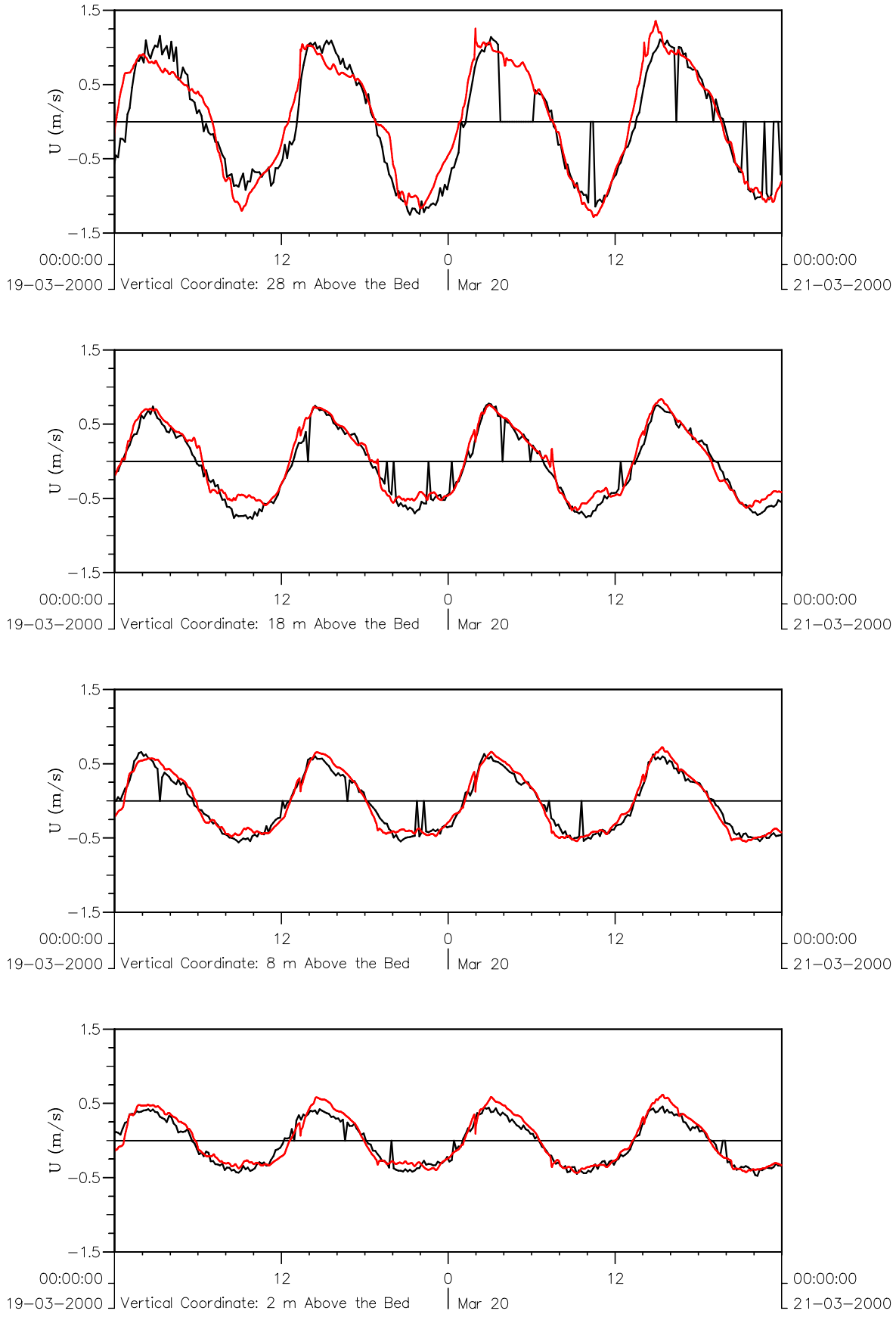

Morphology of pits, channels and trenches Part II: Verification of Delft3D with PUTMOR dataset Location M: Longshore Velocities at Various Water Depths		PT5−3D
	Black Meas., Red Model	
WL | DELFT HYDRAULICS	Z3223	FIG. 4.36

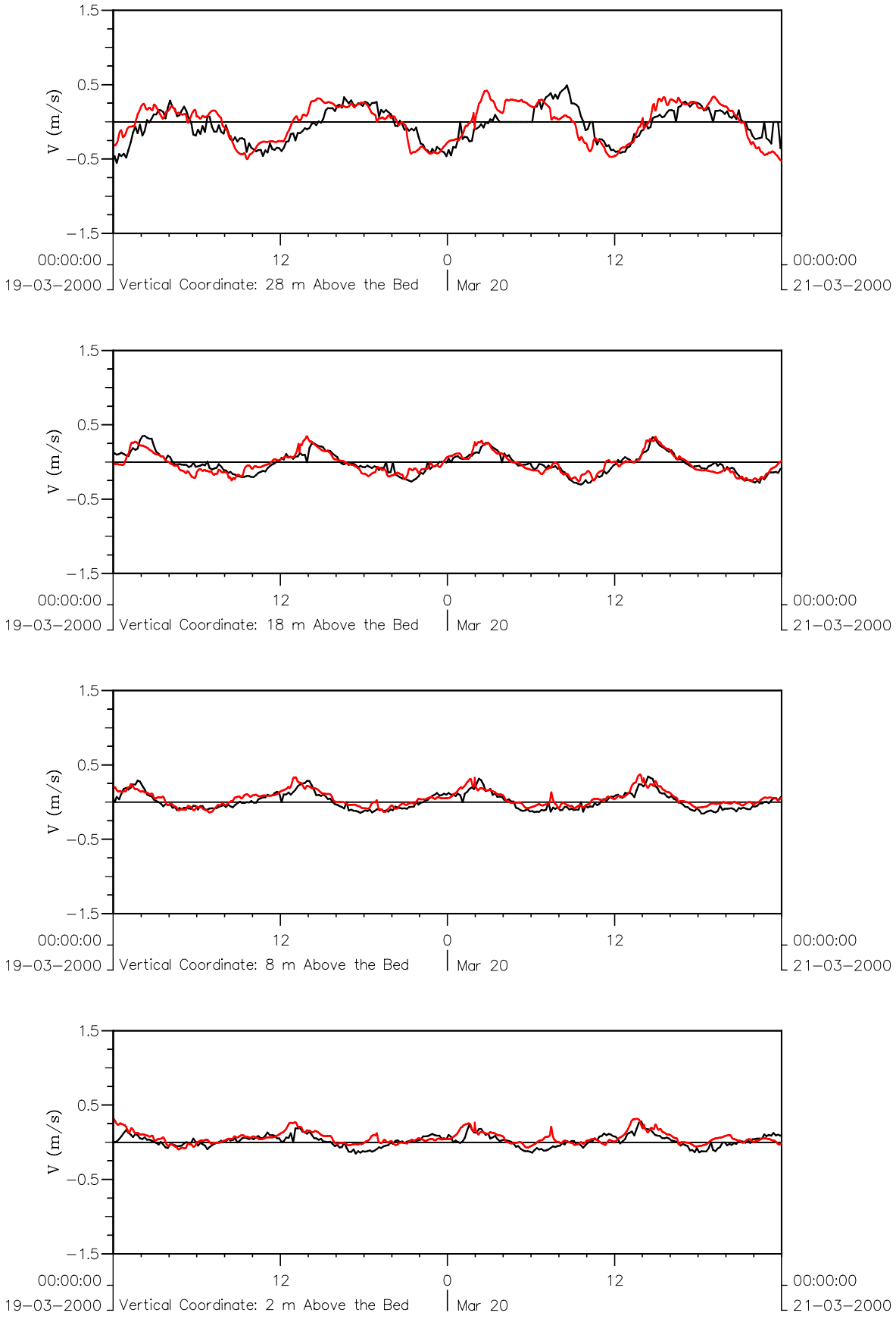

Morphology of pits, channels and trenches Part II: Verification of Delft3D with PUTMOR dataset Location M: Cross−Shore Velocities at Various Water Depths		PT5−3D
	Black Meas., Red Model	
WL | DELFT HYDRAULICS	Z3223	FIG. 4.37

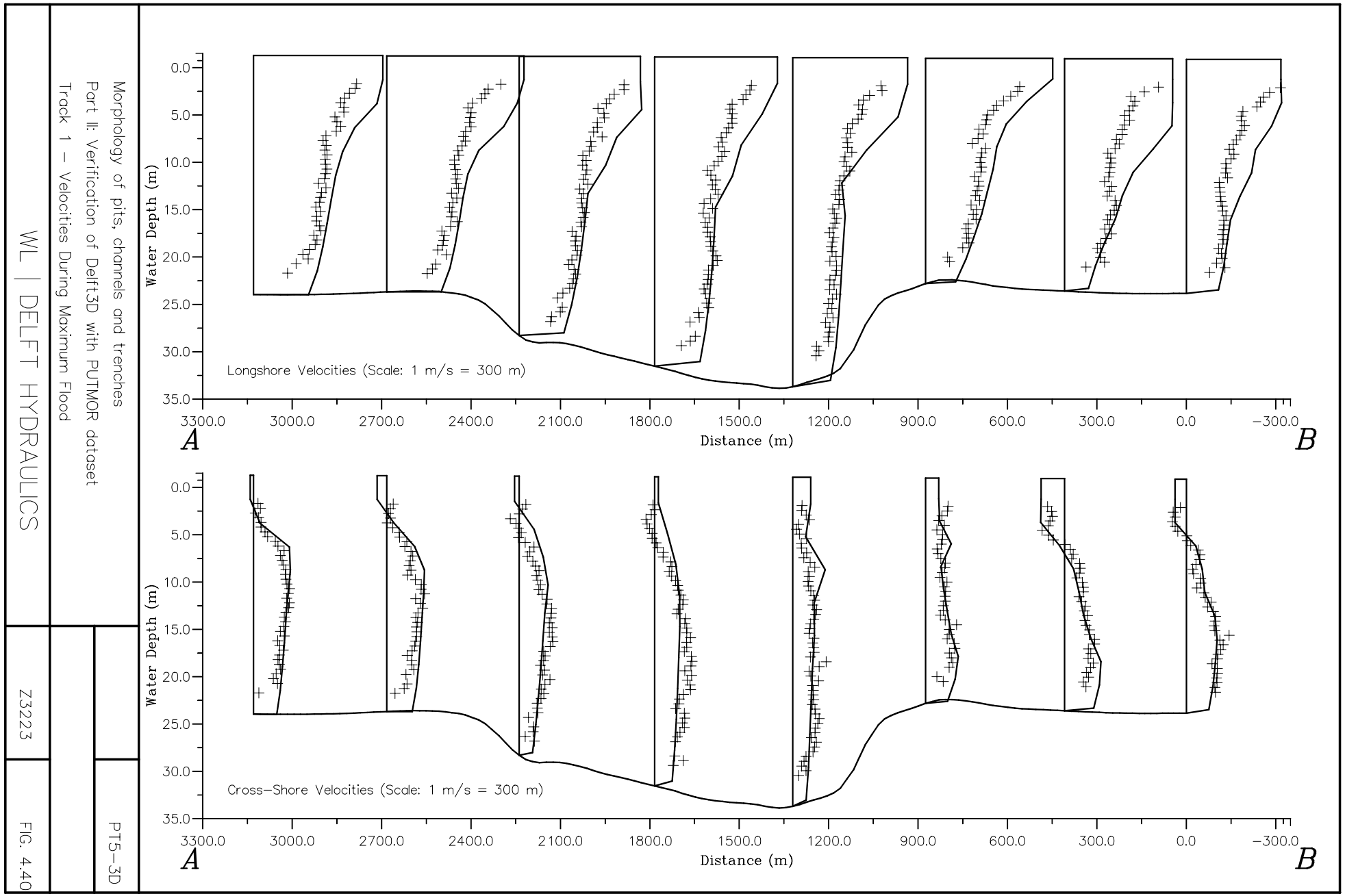

WL | DELFT HYDRAULICS

Morphology of pits, channels and trenches

Part II: Verification of Delft3D with PUTMOR dataset

Track 1 – Velocities During Maximum Flood

Z3223

PT5–3D

FIG. 4.40

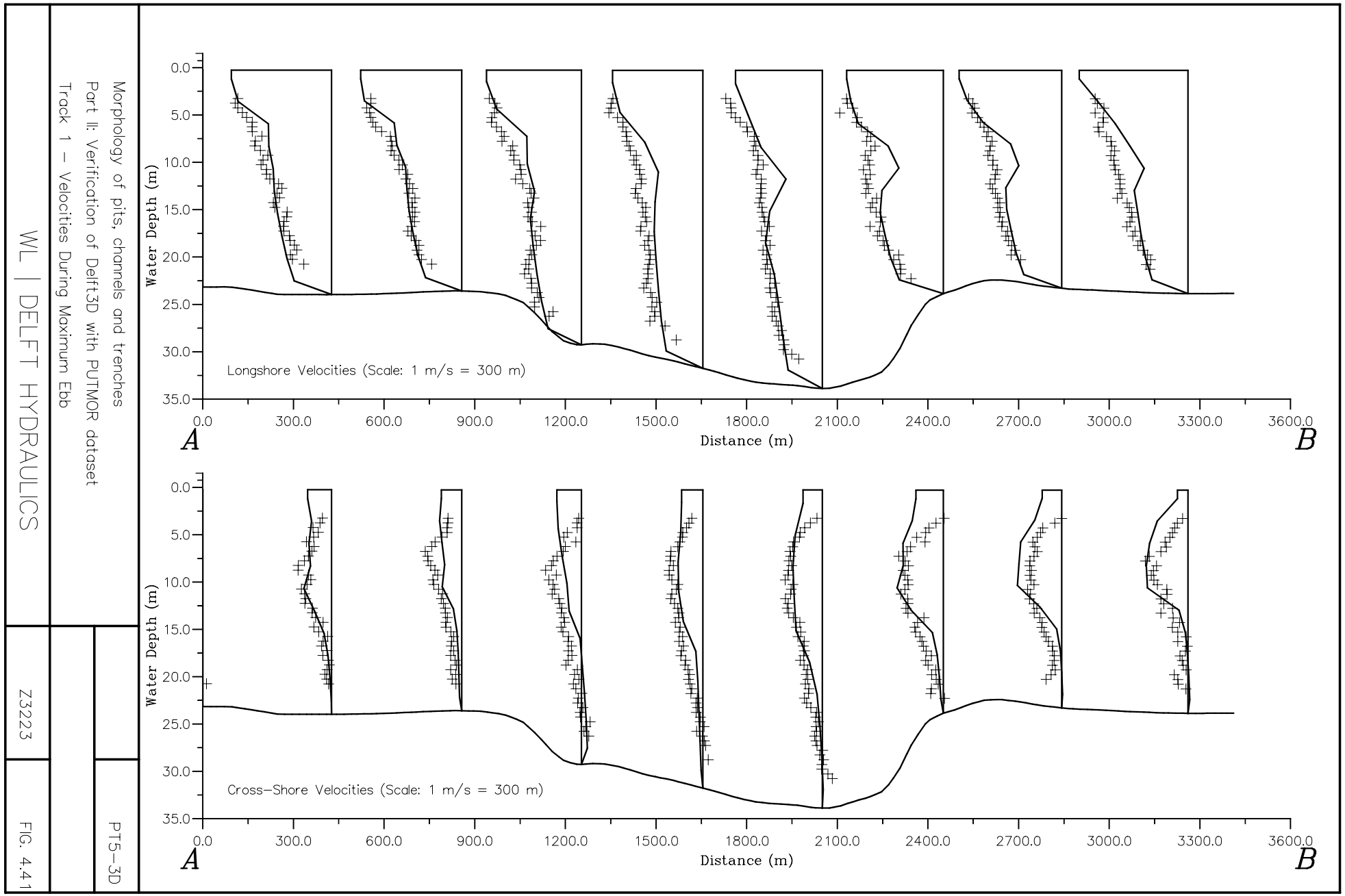

WL | DELFT HYDRAULICS

Morphology of pits, channels and trenches

Part II: Verification of Delft3D with PUTMOR dataset

Track 1 – Velocities During Maximum Ebb

Z3223

PT5–3D

FIG. 4.41

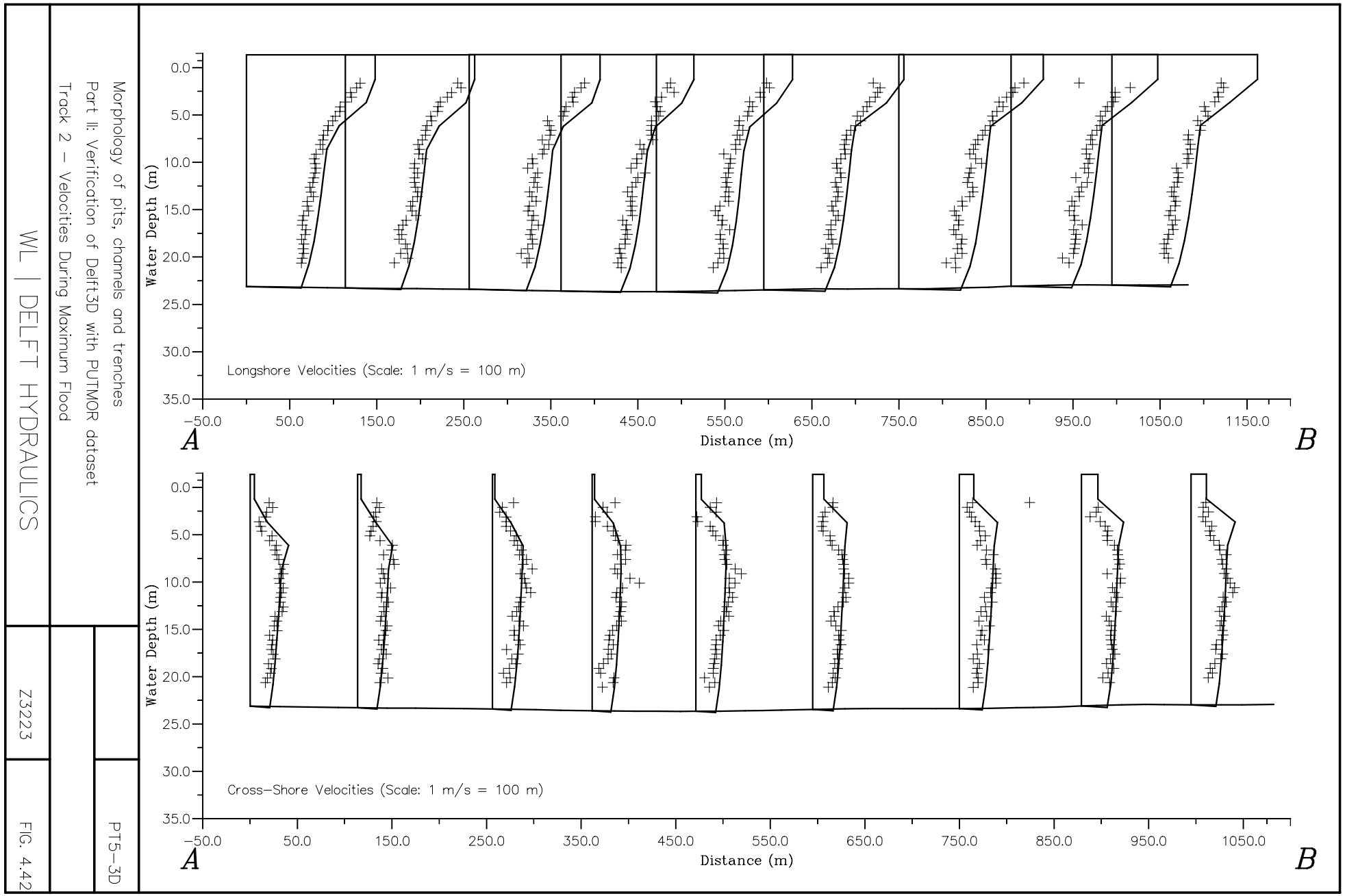

WL | DELFT HYDRAULICS

Morphology of pits, channels and trenches

Part II: Verification of Delft3D with PUTMOR dataset

Track 2 – Velocities During Maximum Flood

Z3223

PT5–3D

FIG. 4.42

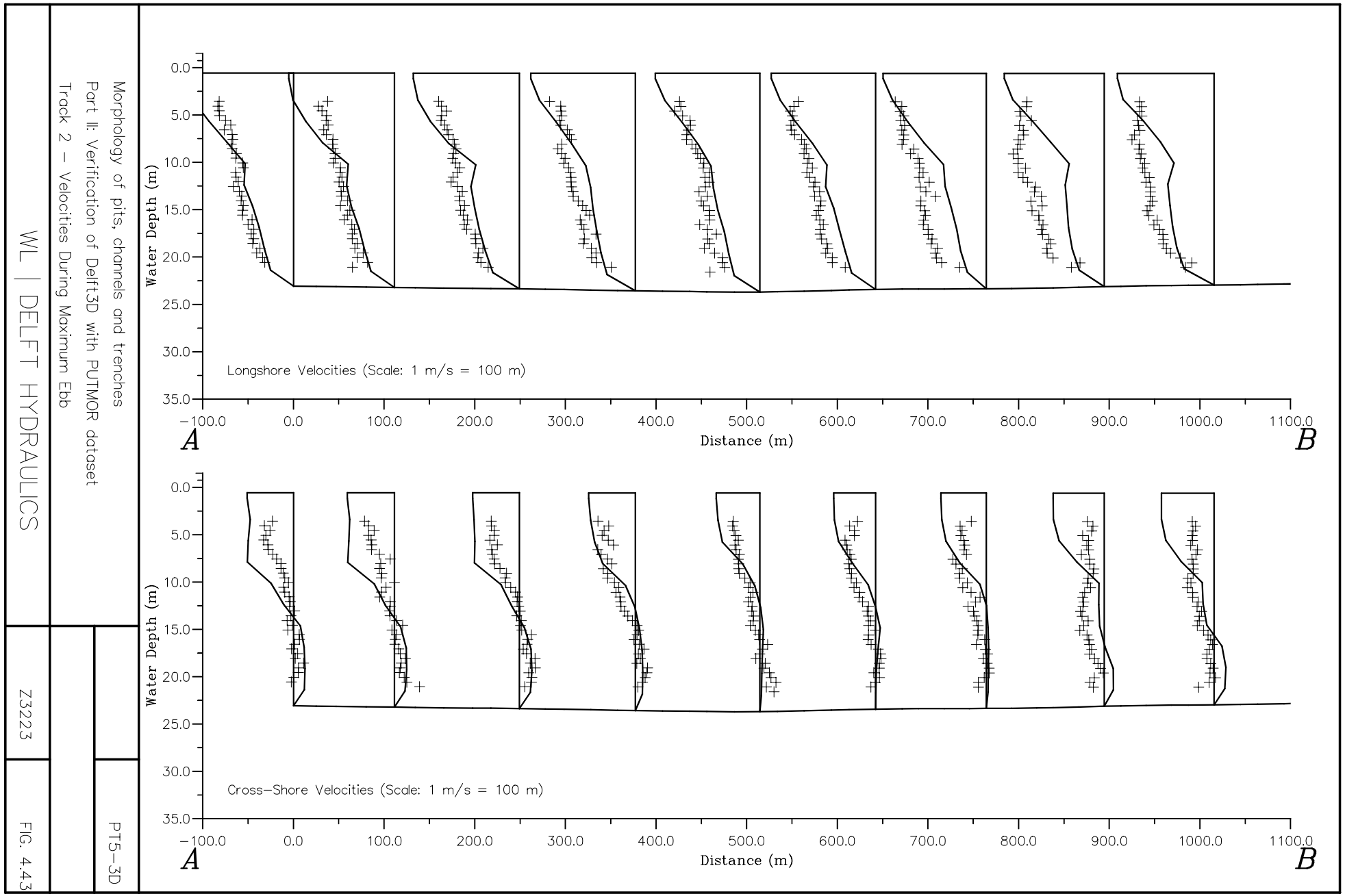

Morphology of pits, channels and trenches

Part II: Verification of Delft3D with PUTMOR dataset

Track 2 – Velocities During Maximum Ebb

WL | DELFT HYDRAULICS

Z3223

PT5–3D

FIG. 4.43

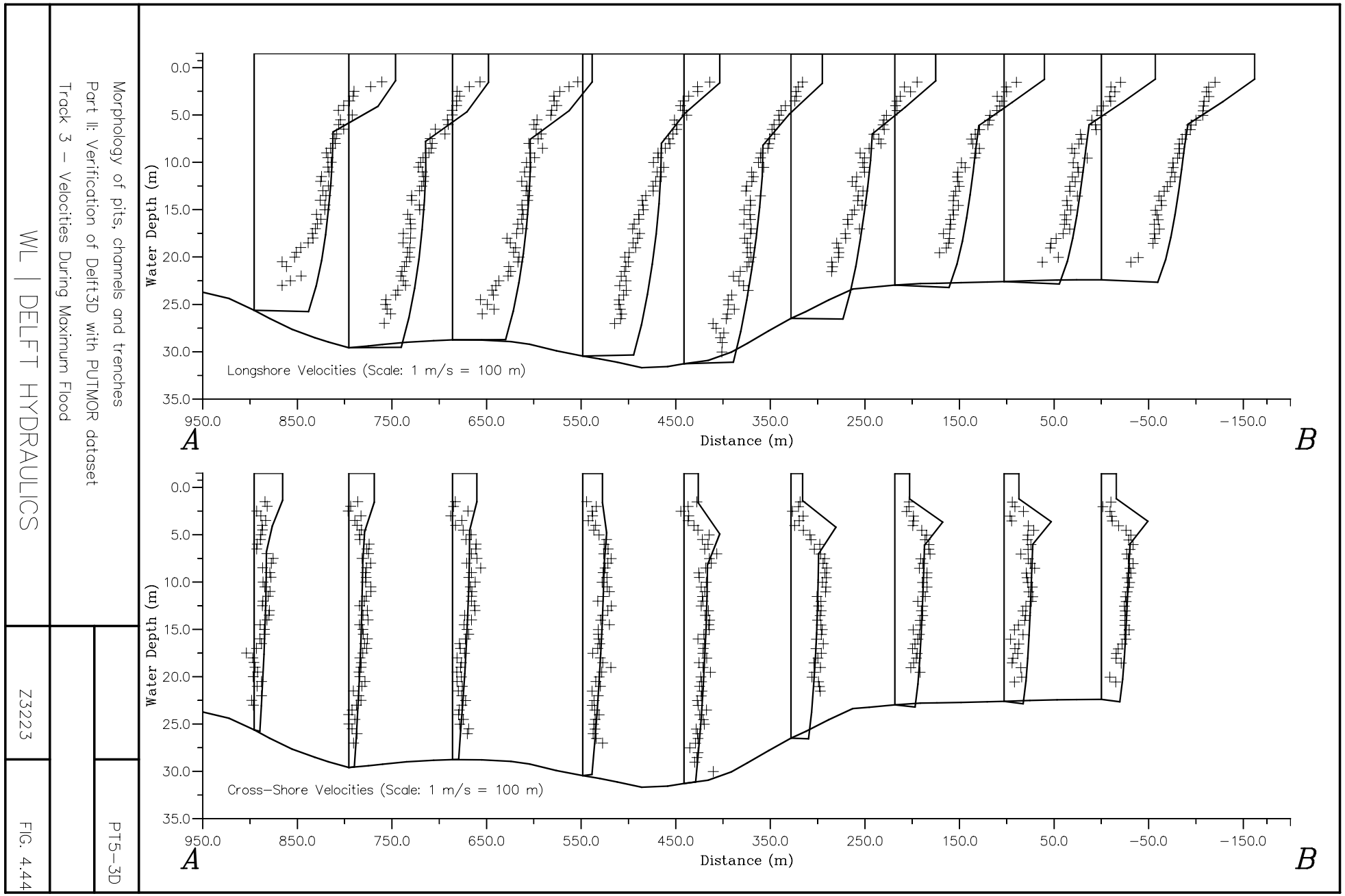

WL | DELFT HYDRAULICS

Morphology of pits, channels and trenches

Part II: Verification of Delft3D with PUTMOR dataset

Track 3 – Velocities During Maximum Flood

Z3223

PT5–3D

FIG. 4.44

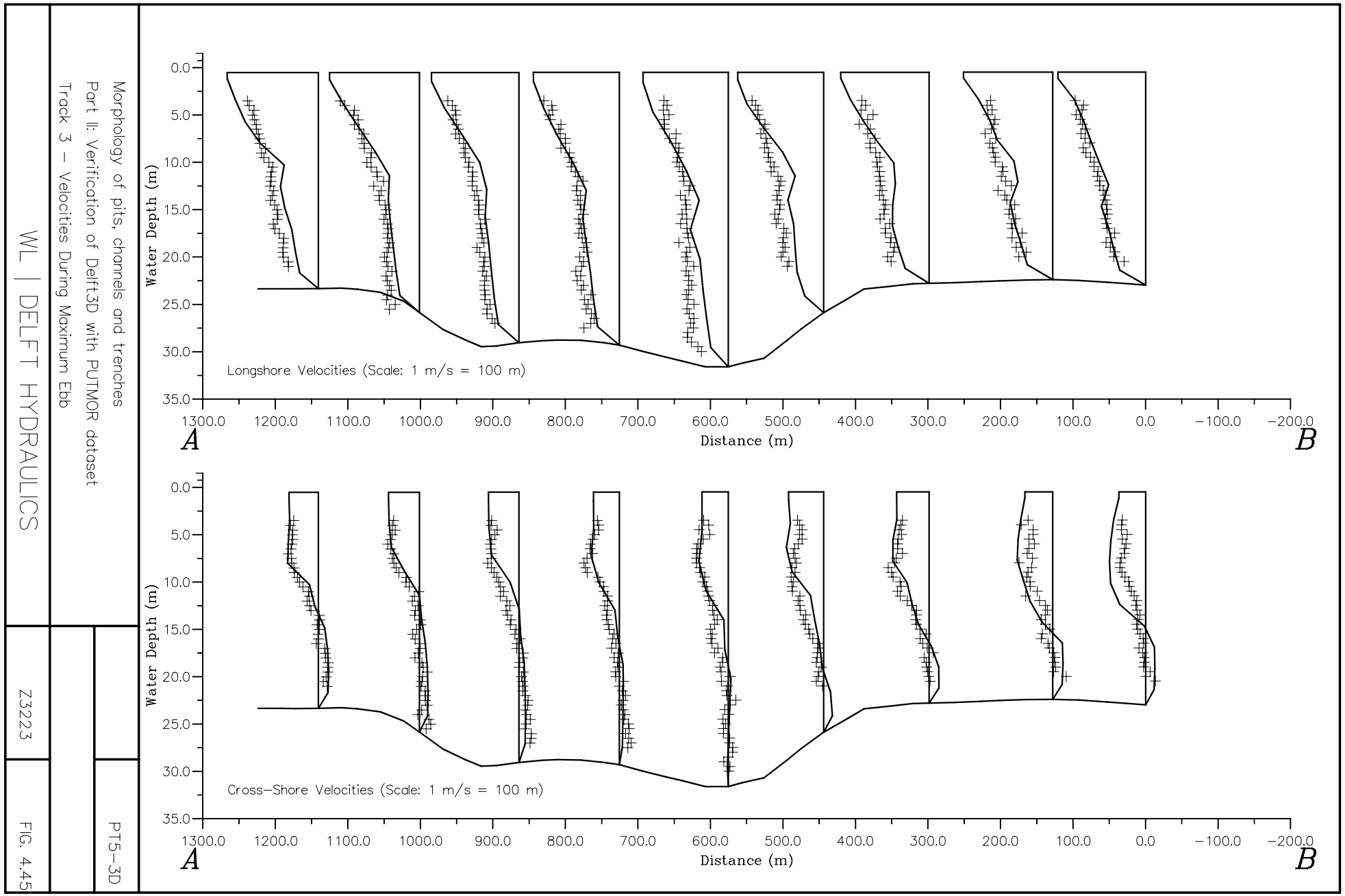

WL | DELFT HYDRAULICS

Morphology of pits, channels and trenches

Part II: Verification of Delft3D with PUTMOR dataset

Track 3 – Velocities During Maximum Ebb

Z3223

PT5–3D

FIG. 4.45

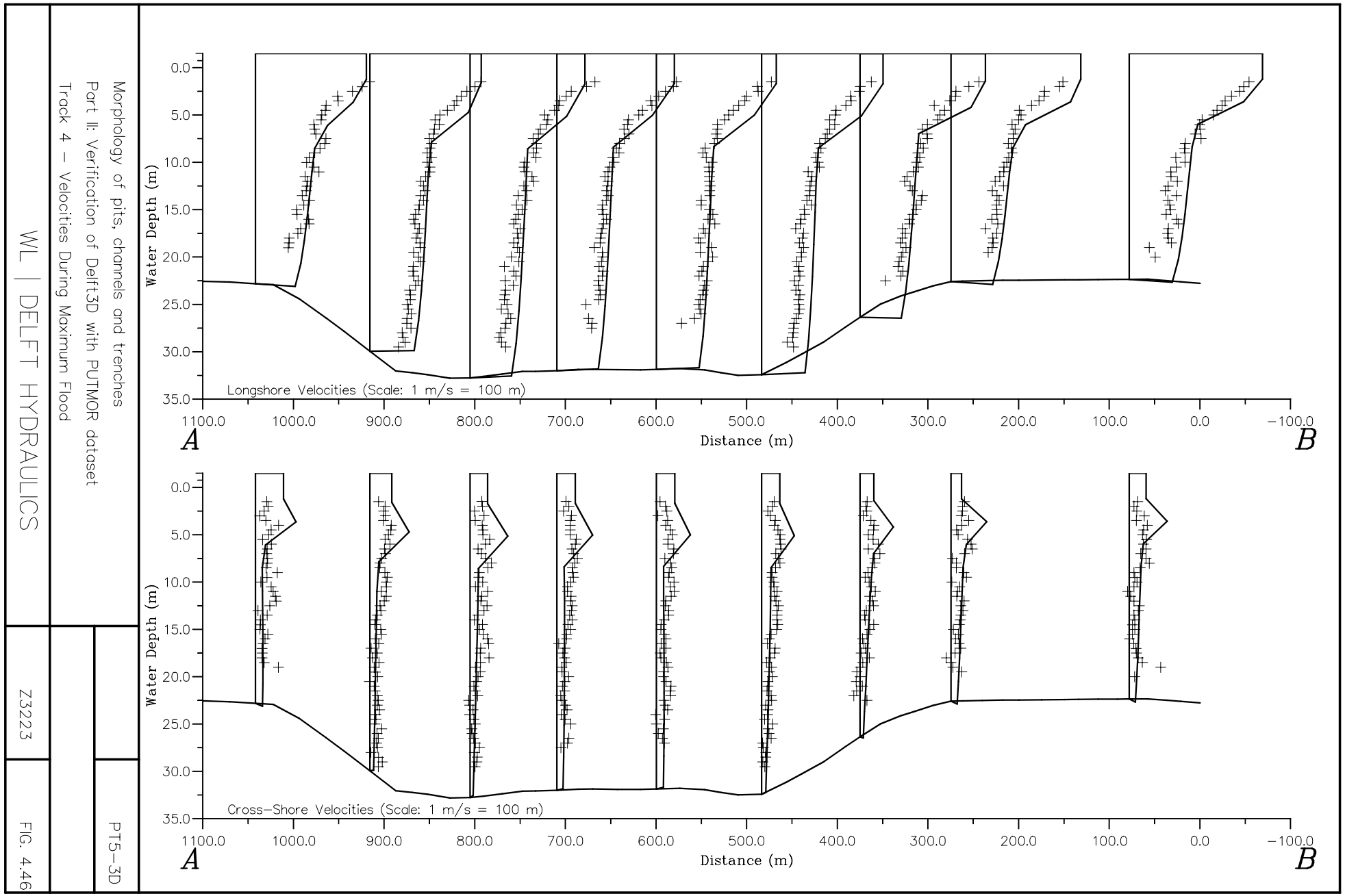

WL | DELFT HYDRAULICS

Morphology of pits, channels and trenches

Part II: Verification of Delft3D with PUTMOR dataset

Track 4 – Velocities During Maximum Flood

Z3223

PT5–3D

FIG. 4.46

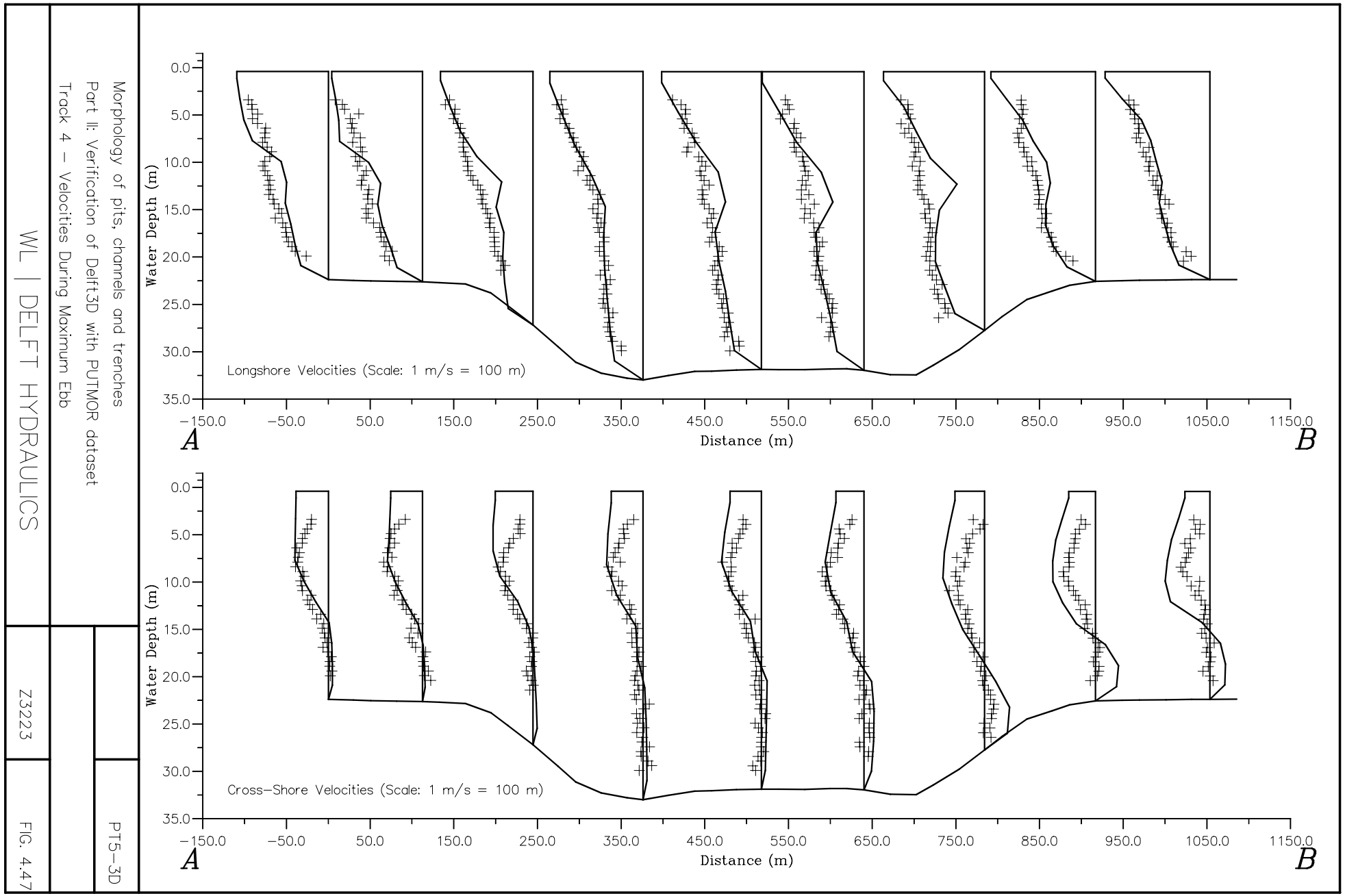

Morphology of pits, channels and trenches

Part II: Verification of Delft3D with PUTMOR dataset

Track 4 – Velocities During Maximum Ebb

WL | DELFT HYDRAULICS

Z3223

PT5–3D

FIG. 4.47

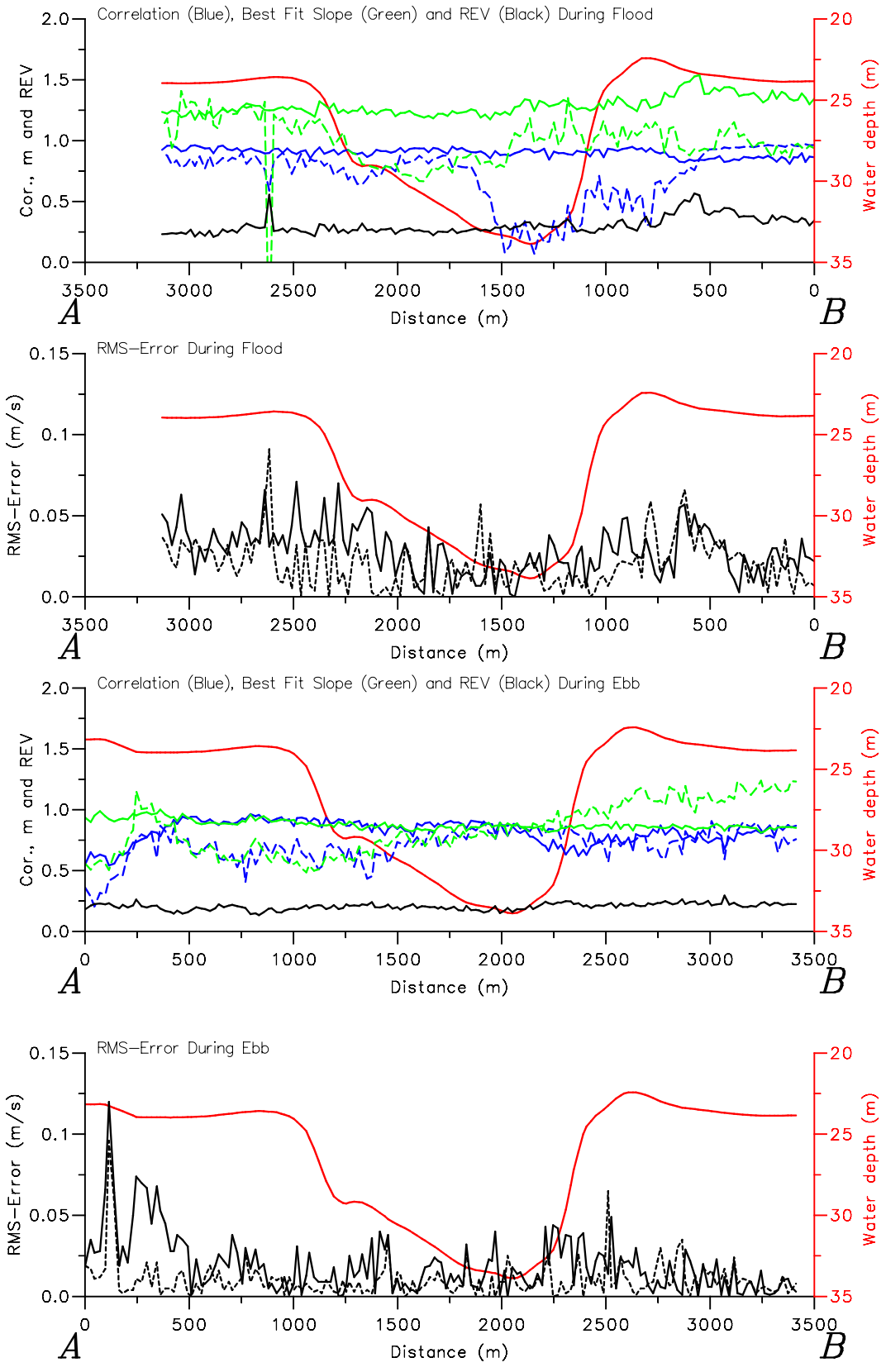

Morphology of pits, channels and trenches
Part II: Verification of Delft3D with PUTMOR dataset
Track 1 – Statistics (Longshore: Solid, Cross-Shore: Dashed)

PT5-3D

WL | DELFT HYDRAULICS

Z3223

FIG. 4.48

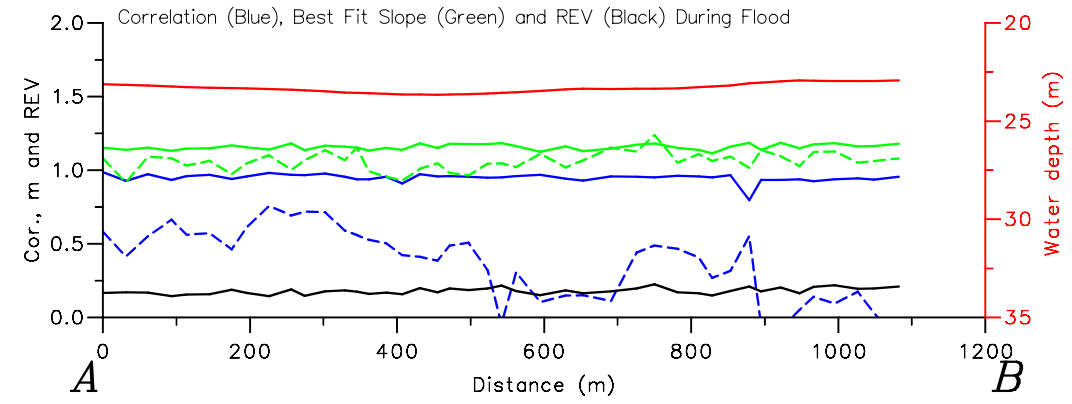

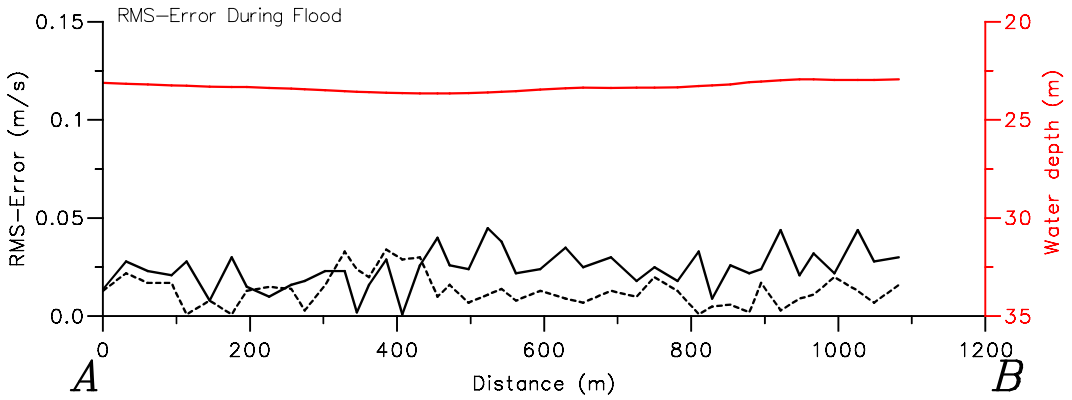

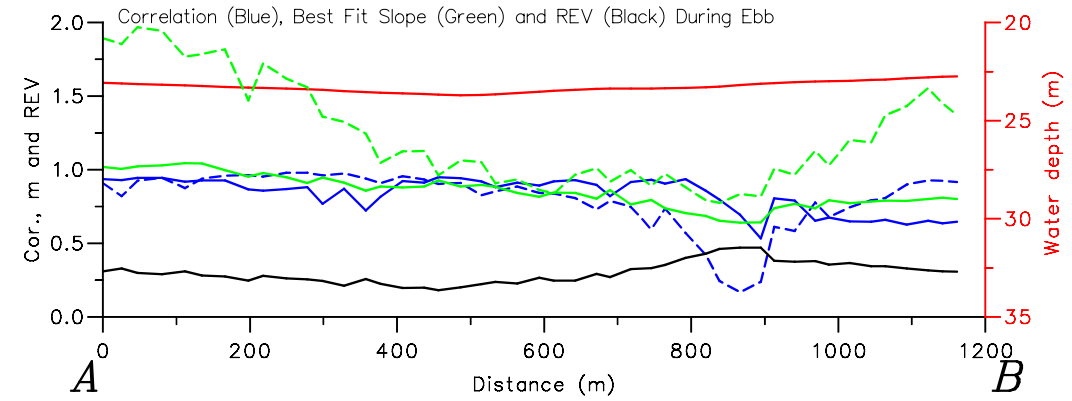

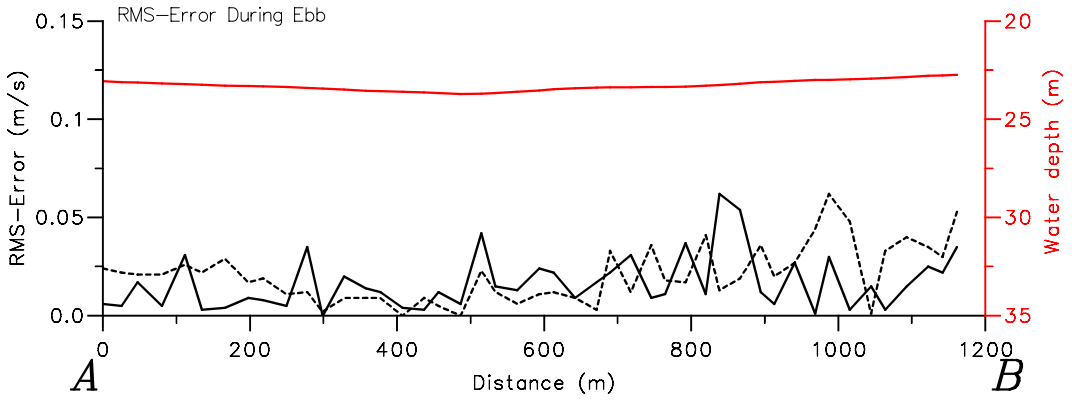

Blue: Correlation

Solid Black: Relative Error Vector

Solid Red: Bottom Profile

Green: Best Fit Slope

Solid lines: Longshore – Dashed Lines: Cross-Shore

Morphology of pits, channels and trenches Part II: Verification of Delft3D with PUTMOR dataset Track 2 – Statistics (Longshore: Solid, Cross-Shore: Dashed)		PT5-3D
WL | DELFT HYDRAULICS	Z3223	FIG. 4.49

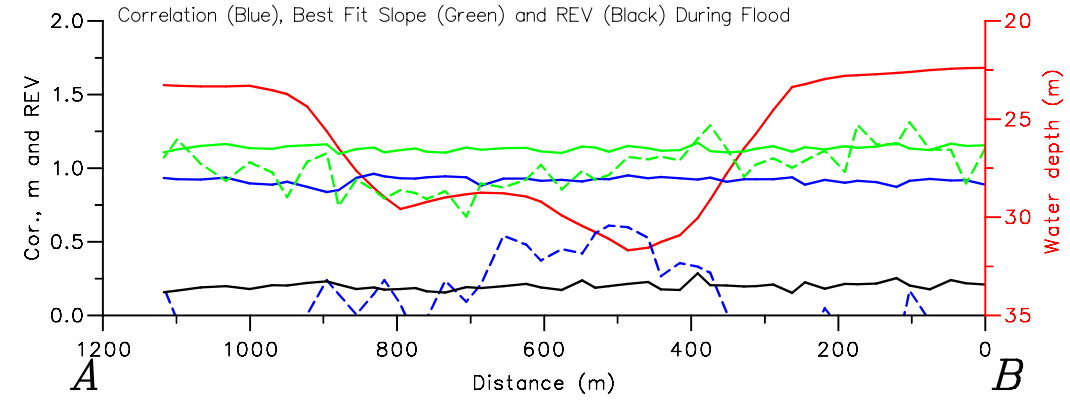

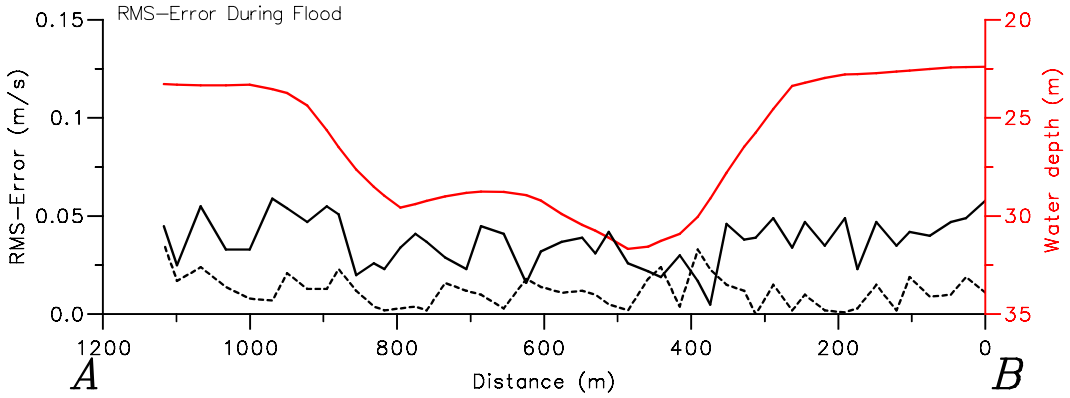

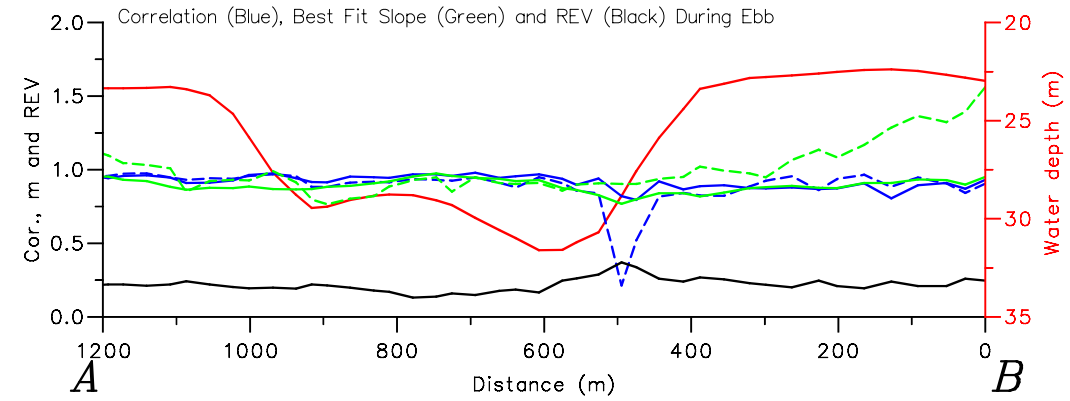

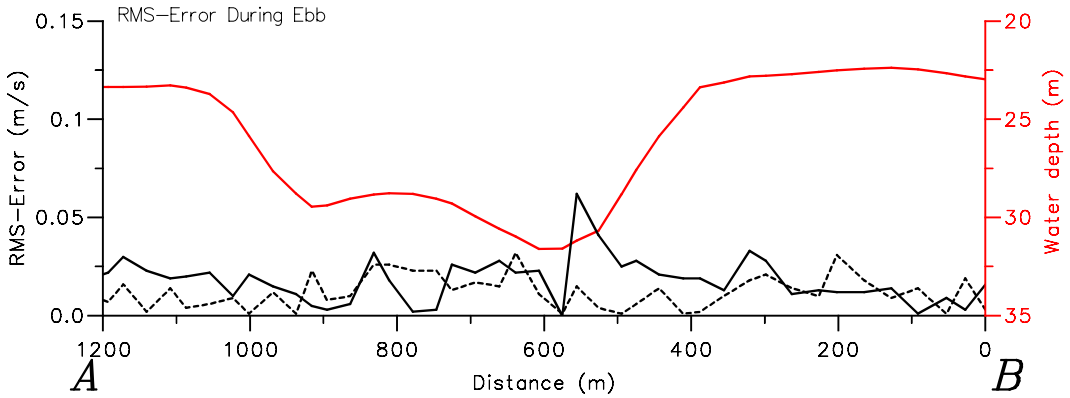

Blue: Correlation — Solid Black: Relative Error Vector

Solid Red: Bottom Profile — Green: Best Fit Slope

Solid lines: Longshore – Dashed Lines: Cross-Shore

Morphology of pits, channels and trenches Part II: Verification of Delft3D with PUTMOR dataset Track 3 – Statistics (Longshore: Solid, Cross-Shore: Dashed)		PT5-3D
WL | DELFT HYDRAULICS	Z3223	FIG. 4.50

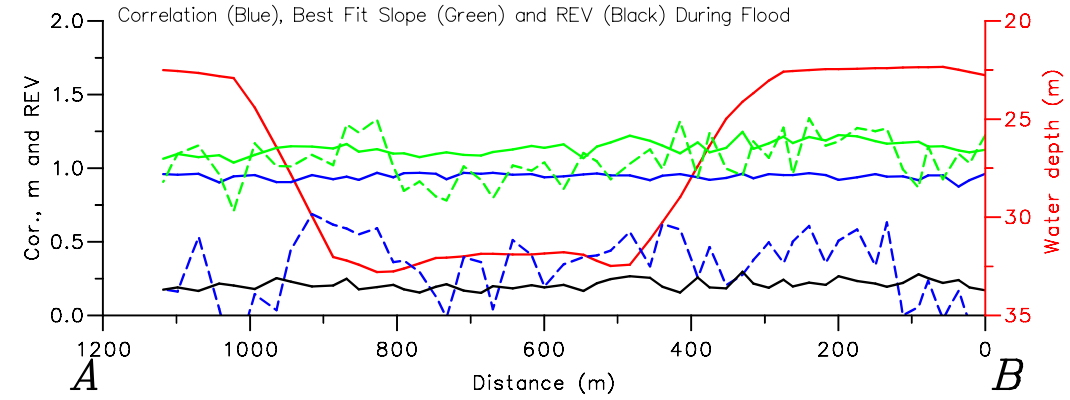

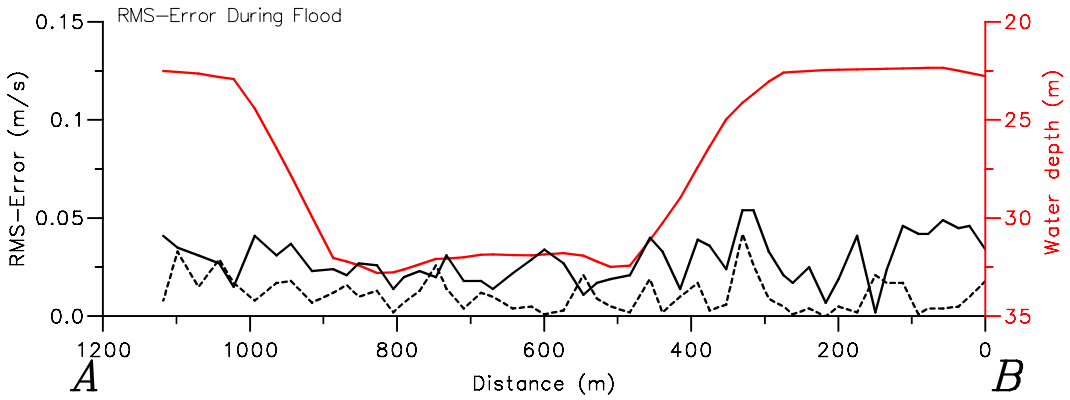

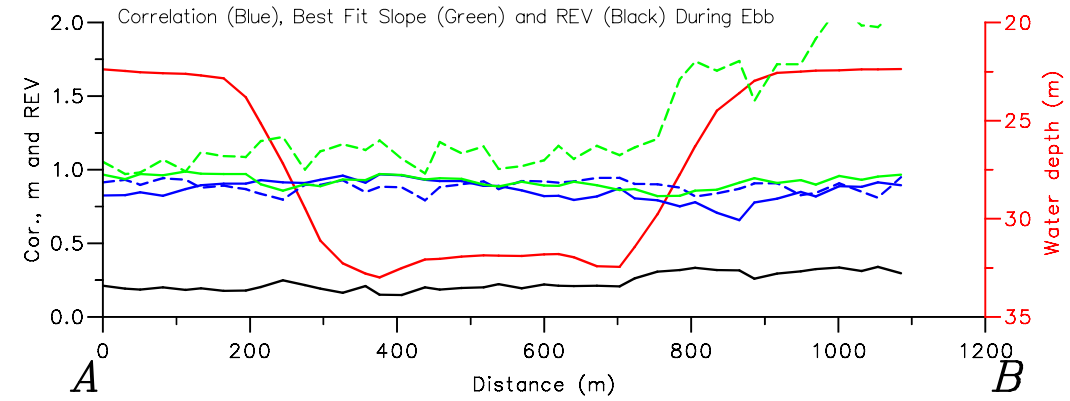

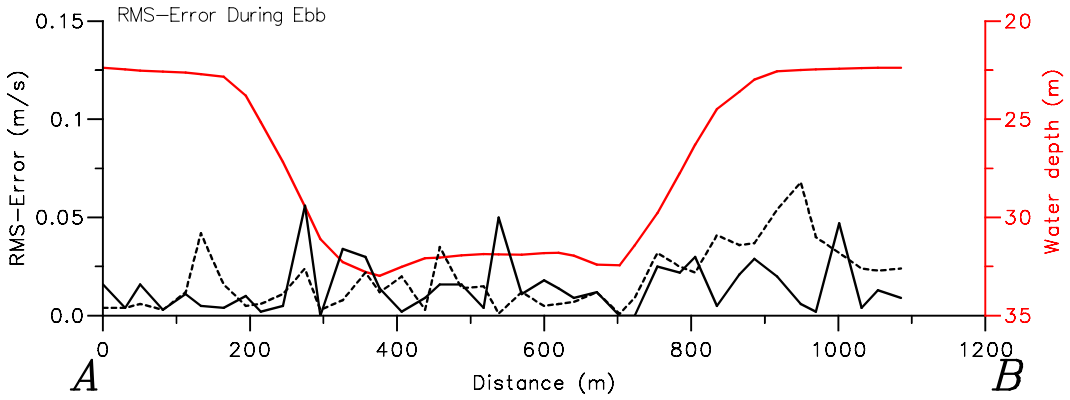

Blue: Correlation

Solid Red: Bottom Profile

Solid Black: Relative Error Vector

Green: Best Fit Slope

Solid lines: Longshore – Dashed Lines: Cross-Shore

Morphology of pits, channels and trenches Part II: Verification of Delft3D with PUTMOR dataset Track 4 – Statistics (Longshore: Solid, Cross-Shore: Dashed)		PT5-3D
WL | DELFT HYDRAULICS	Z3223	FIG. 4.51

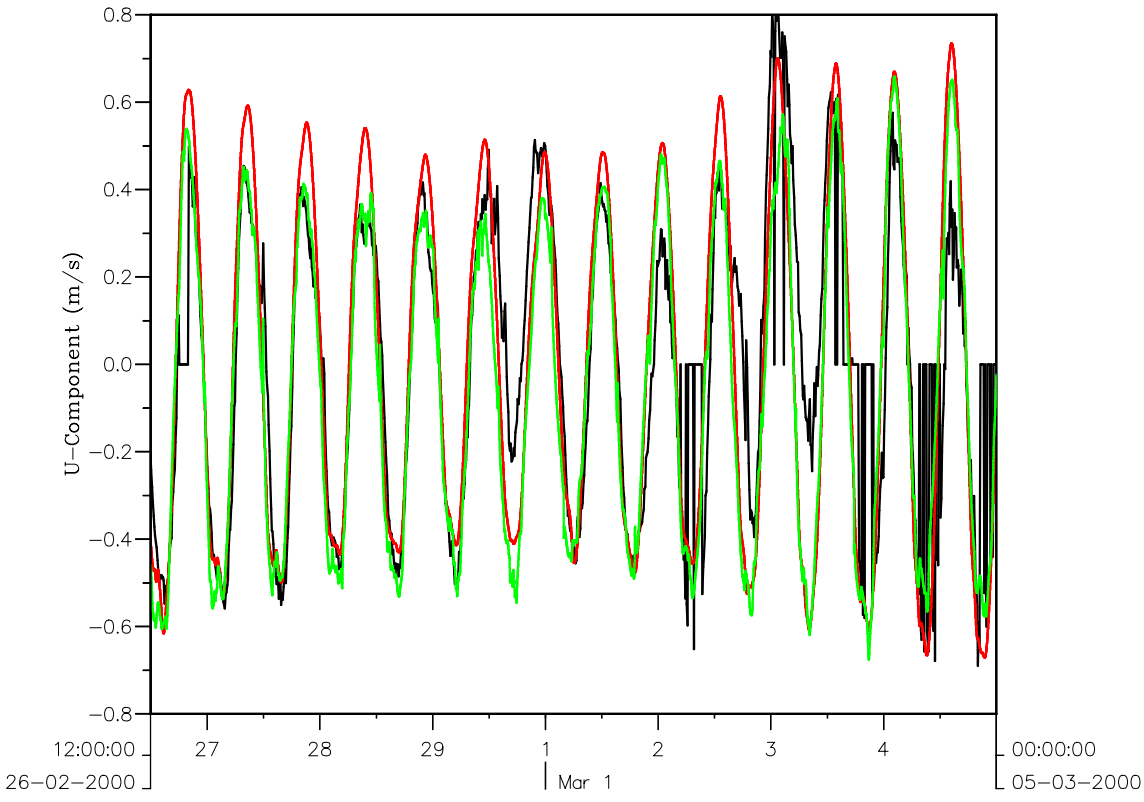

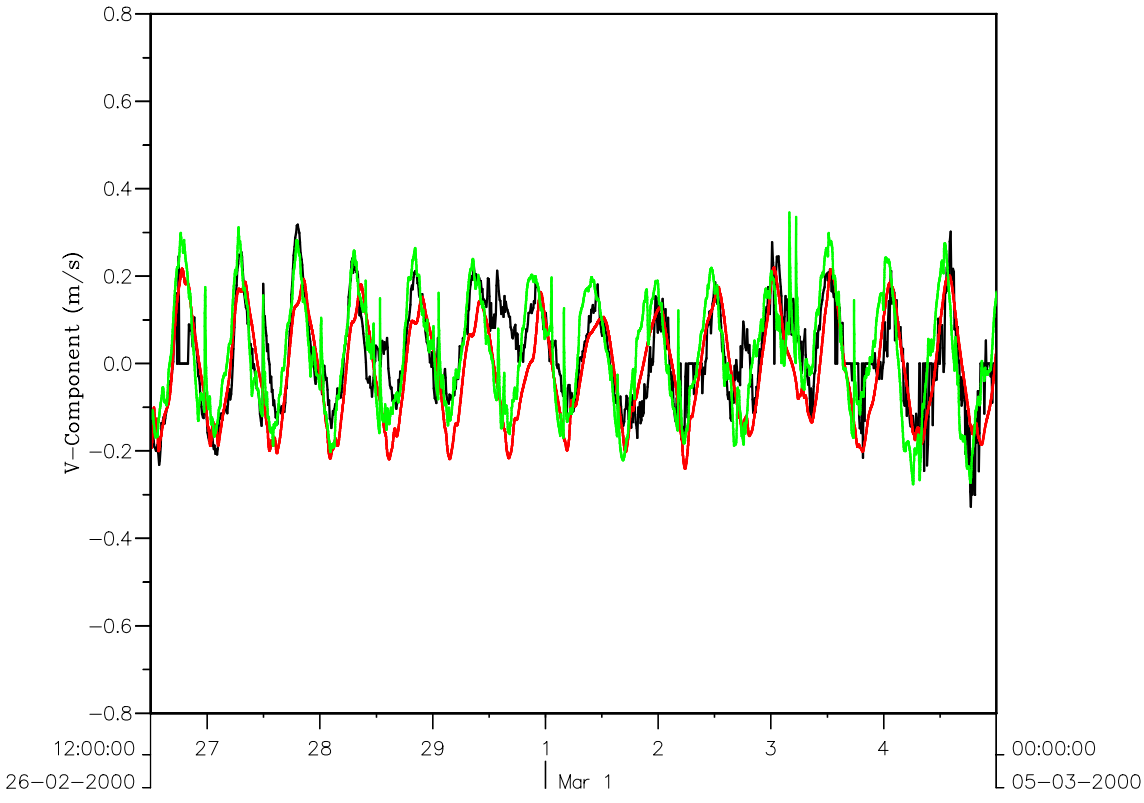

Morphology of pits, channels and trenches Part II: Verification of Delft3D with PUTMOR dataset Loc. A Depth−Averaged Currents (Black: meas., Red: 2DH, Green: 3D)		PT2 & PT2−3D
	26−02 to 05−03	
WL | DELFT HYDRAULICS	Z3223	Fig. 4.52

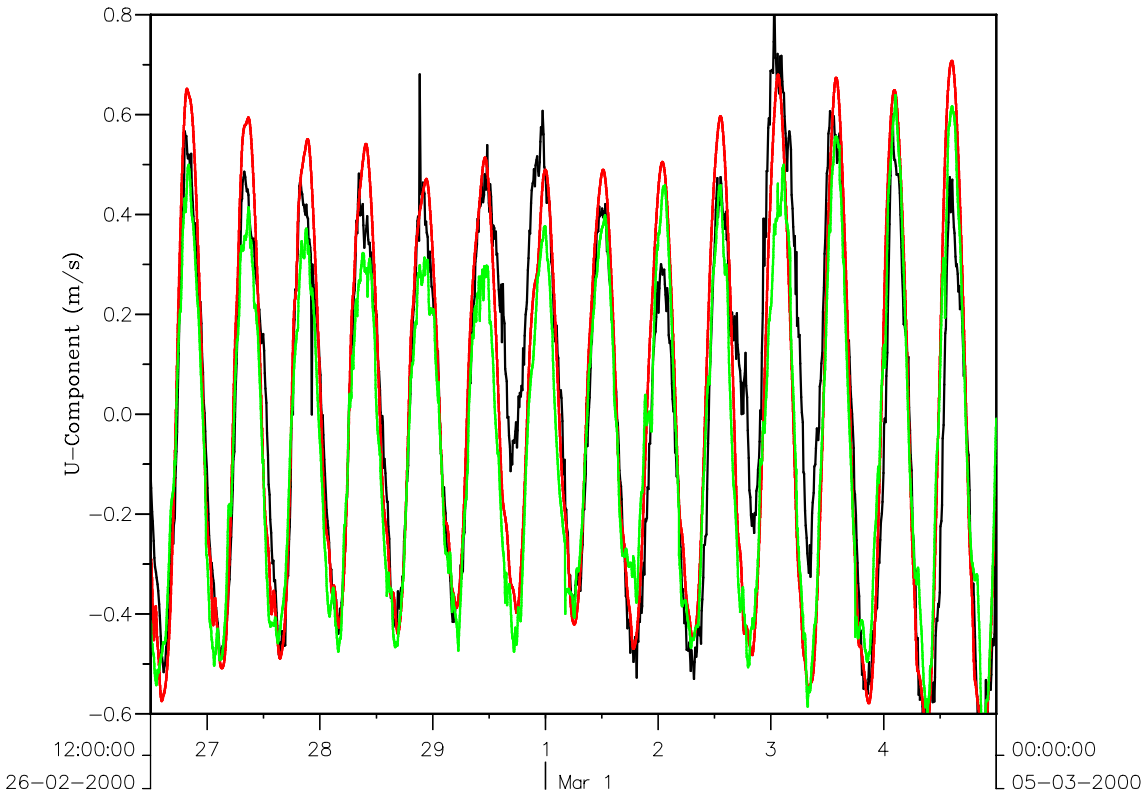

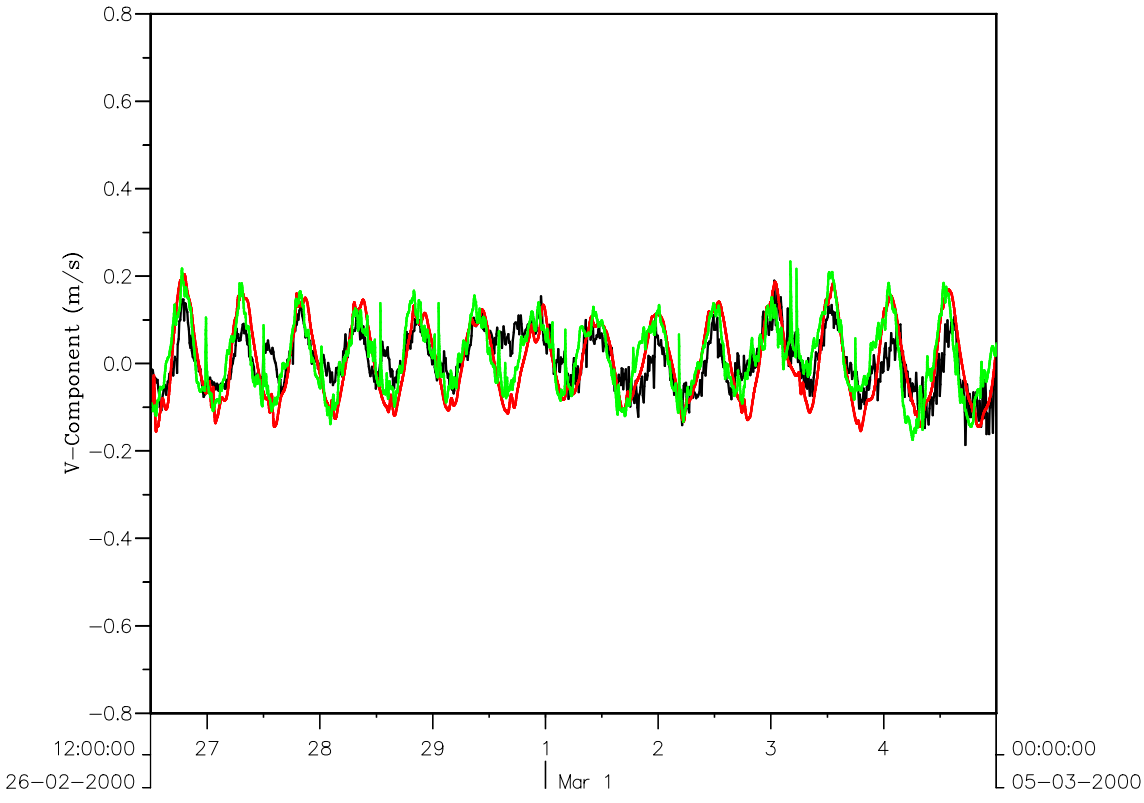

Morphology of pits, channels and trenches Part II: Verification of Delft3D with PUTMOR dataset Loc. M Depth−Averaged Currents (Black: meas., Red: 2DH, Green: 3D)		PT2 & PT2−3D
	26−02 to 05−03	
WL | DELFT HYDRAULICS	Z3223	Fig. 4.53

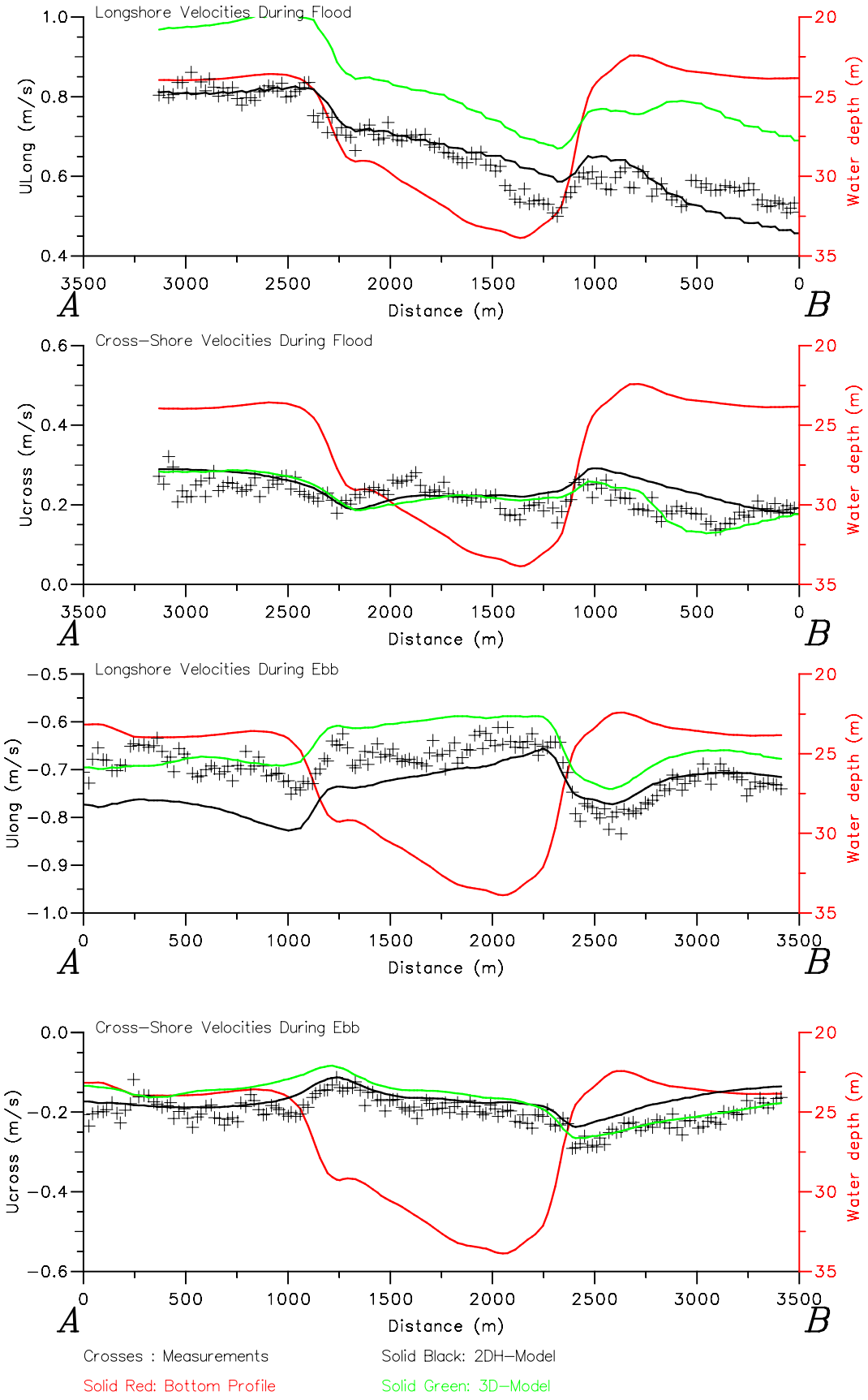

Morphology of pits, channels and trenches
Part II: Verification of Delft3D with PUTMOR dataset
Track 1 – Depth Averaged Velocities (From 2DH and 3D model)

PT5 & PT5–3D

WL | DELFT HYDRAULICS

Z3223

FIG. 4.54

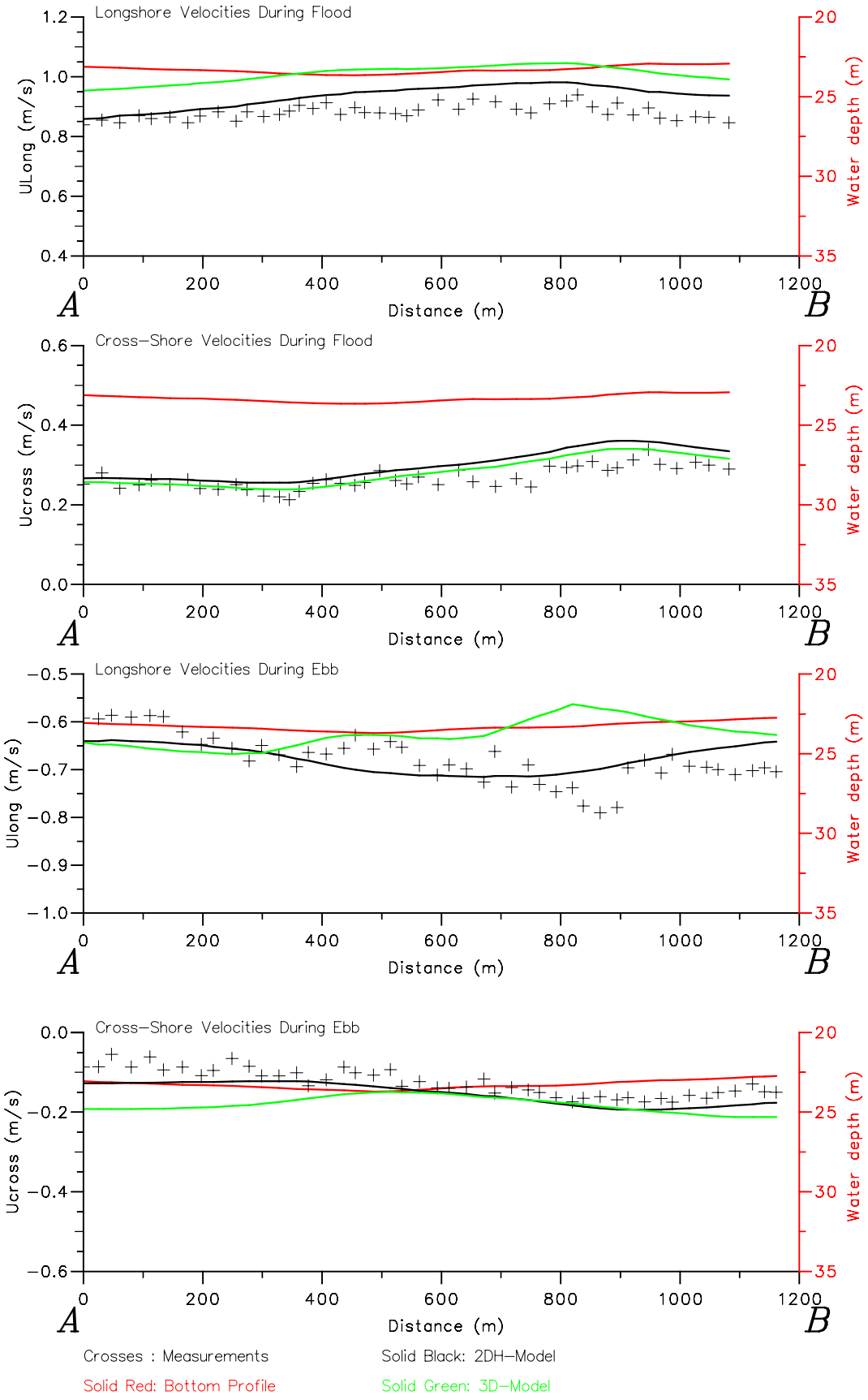

Morphology of pits, channels and trenches Part II: Verification of Delft3D with PUTMOR dataset Track 2 – Depth Averaged Velocities (From 2DH and 3D model)		PT5 & PT5–3D
WL | DELFT HYDRAULICS	Z3223	FIG. 4.55

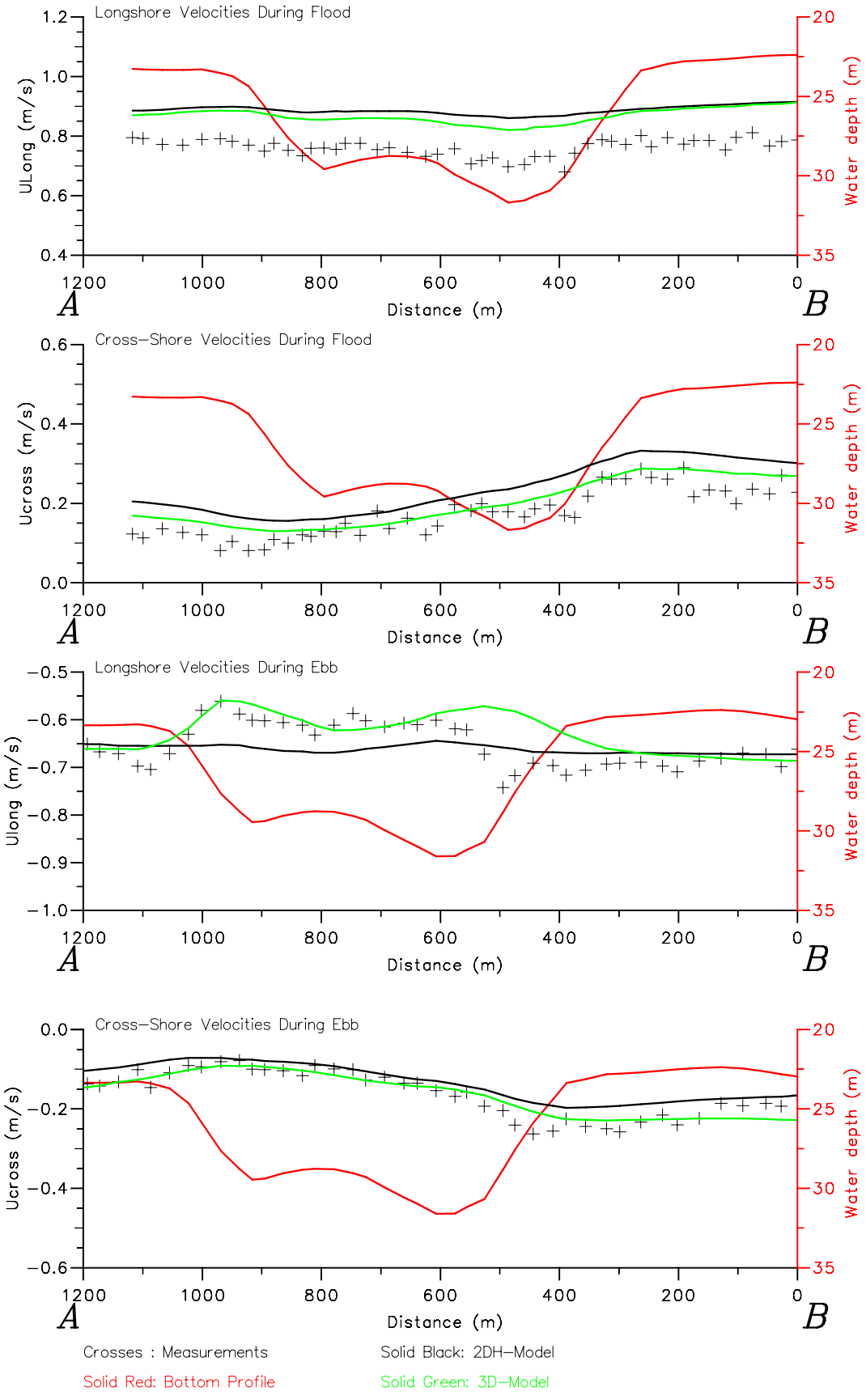

Morphology of pits, channels and trenches Part II: Verification of Delft3D with PUTMOR dataset Track 3 – Depth Averaged Velocities (From 2DH and 3D model)		PT5 & PT5–3D
WL | DELFT HYDRAULICS	Z3223	FIG. 4.56

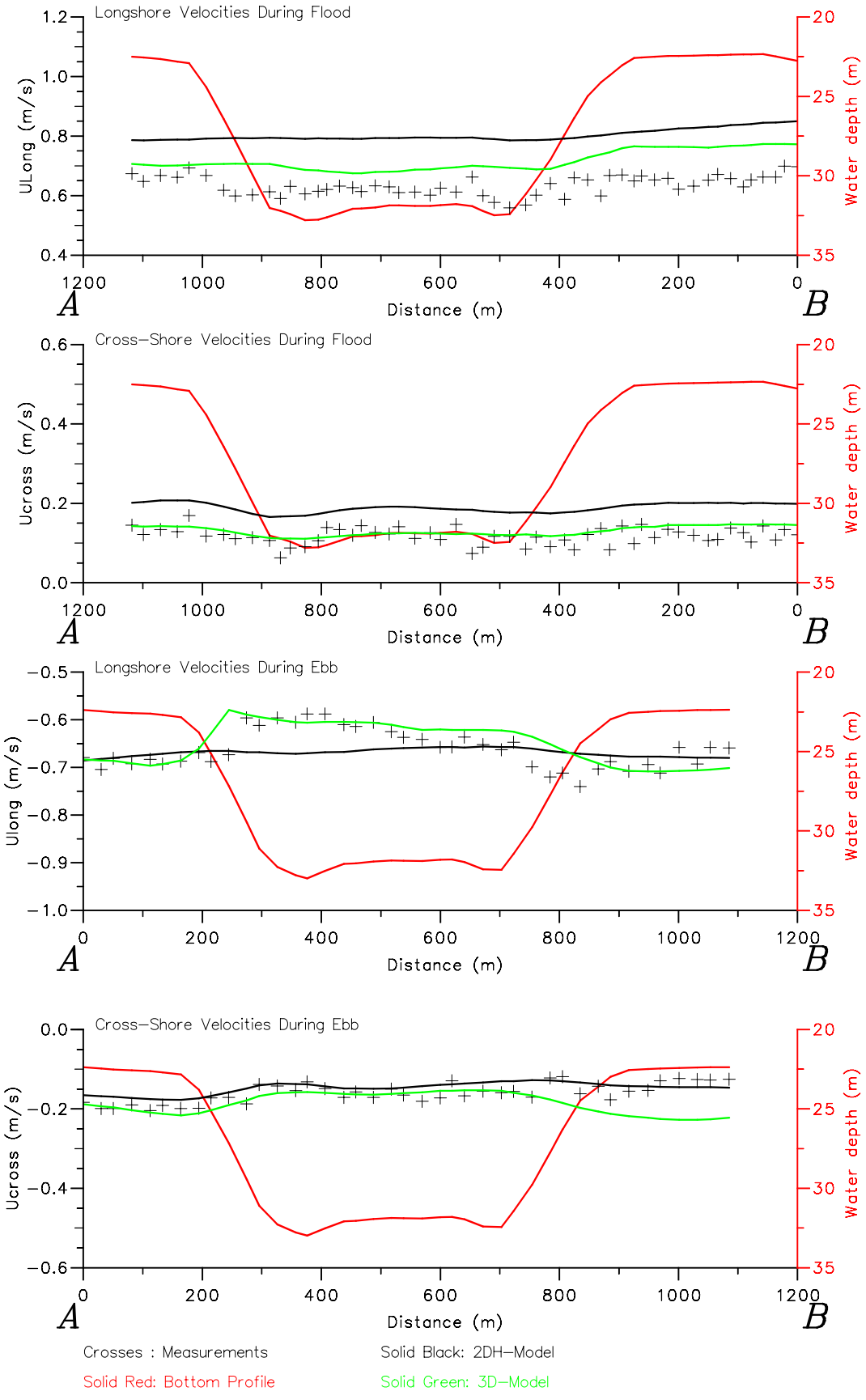

Morphology of pits, channels and trenches Part II: Verification of Delft3D with PUTMOR dataset Track 4 – Depth Averaged Velocities (From 2DH and 3D model)		PT5 & PT5–3D
WL | DELFT HYDRAULICS	Z3223	FIG. 4.57

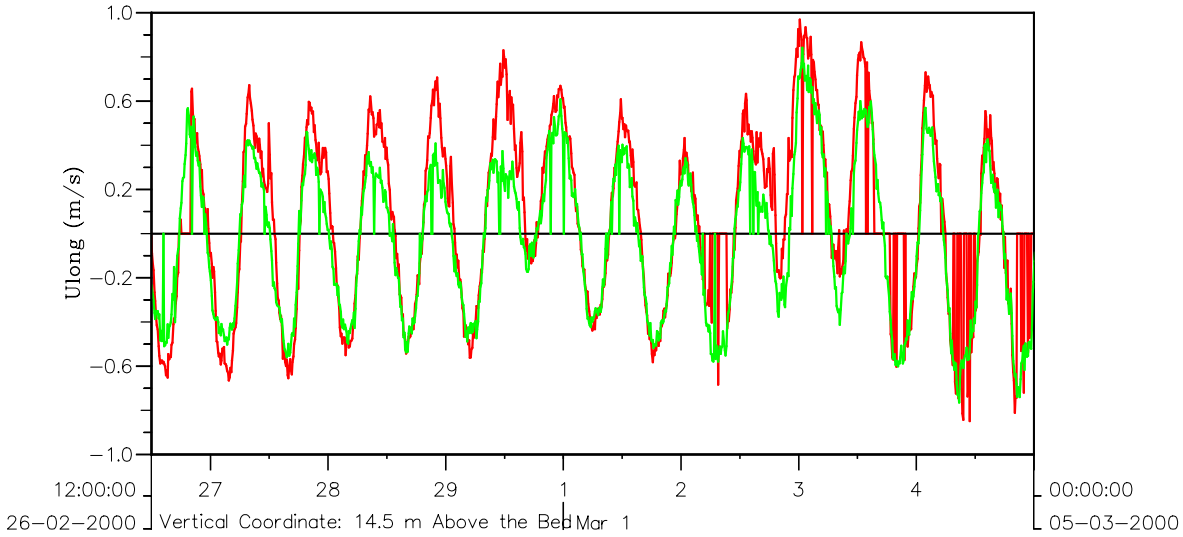

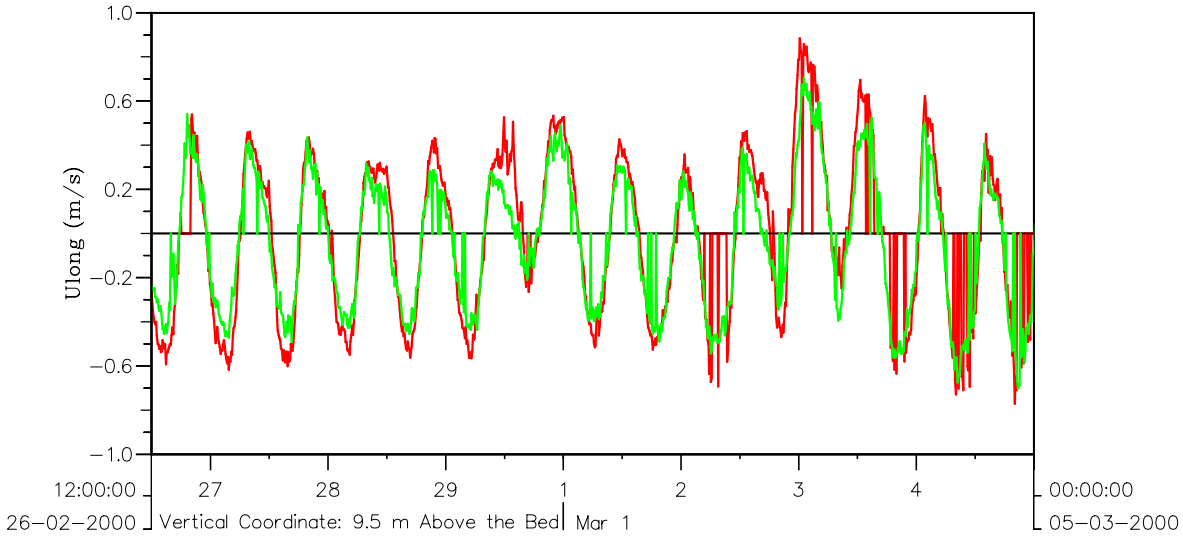

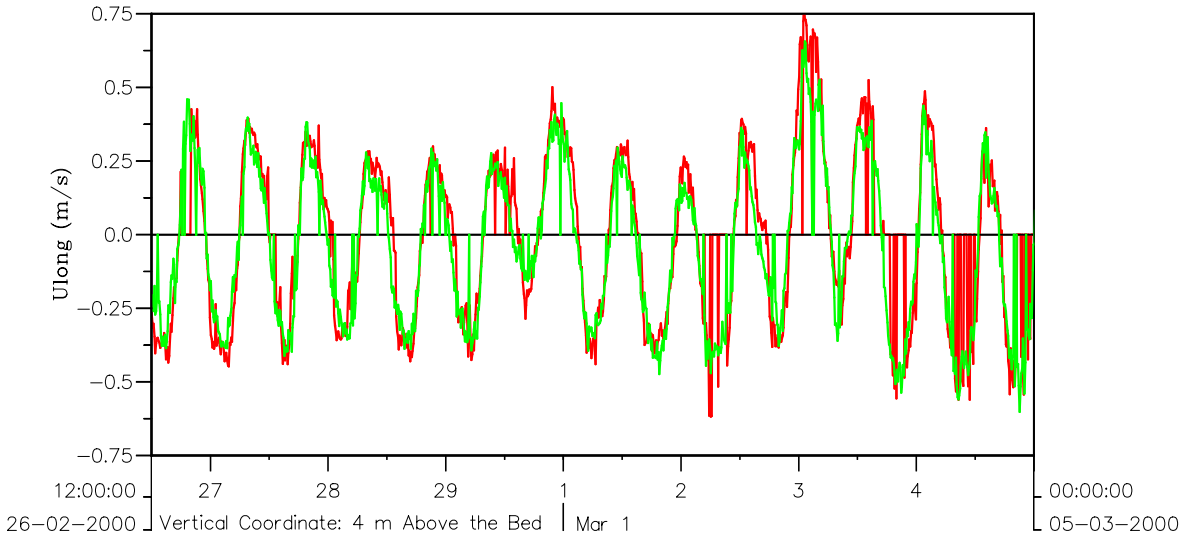

Morphology of pits, channels and trenches

Comparison of measured longshore velocities at Locations A and M

Red: Location A, Green: Location M

WL | DELFT HYDRAULICS

Z3223

FIG. 4.60

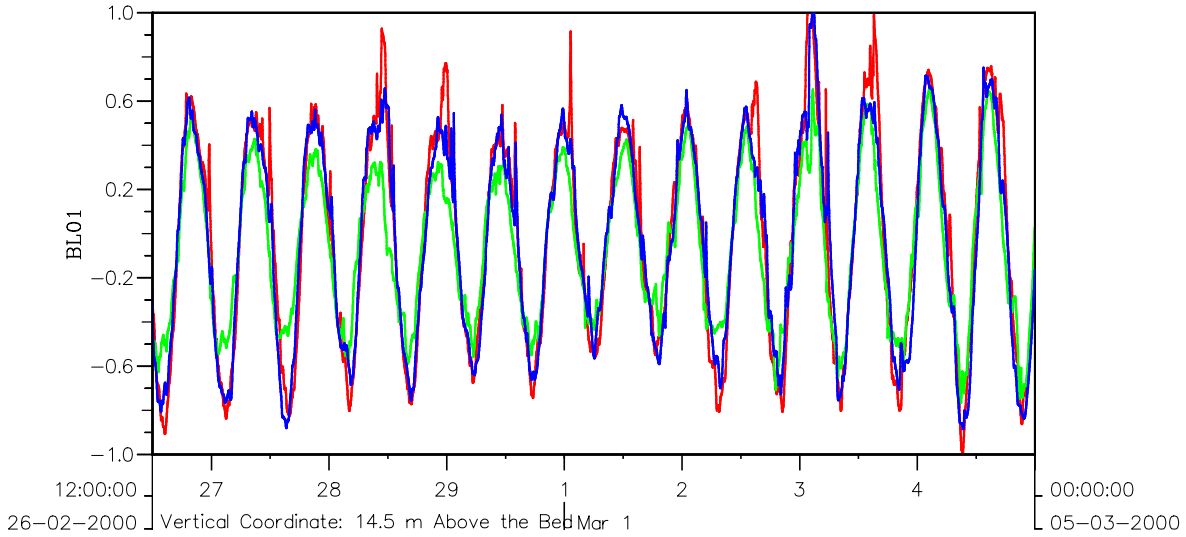

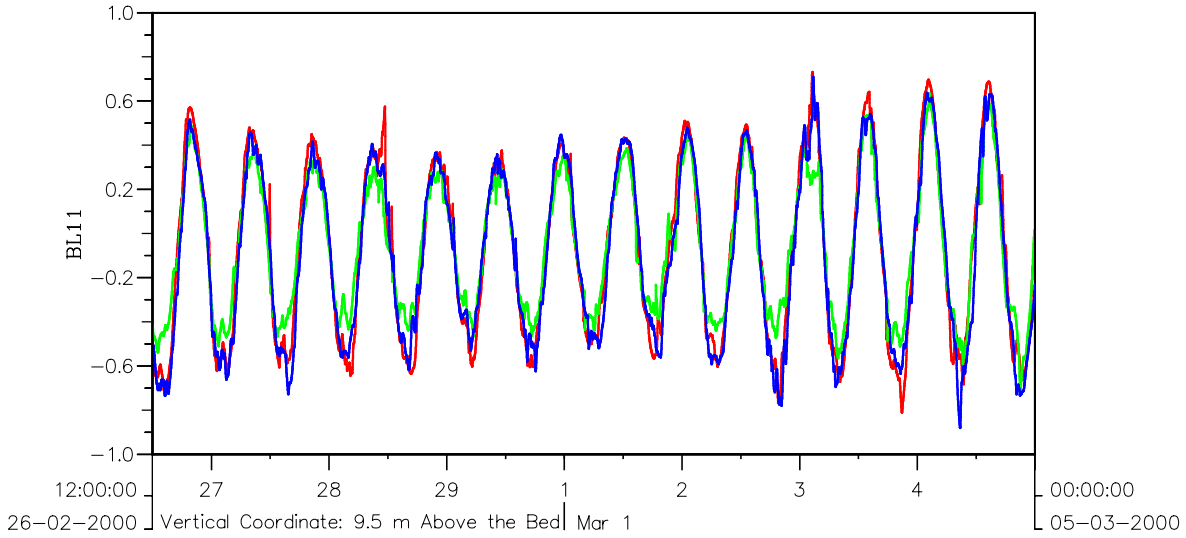

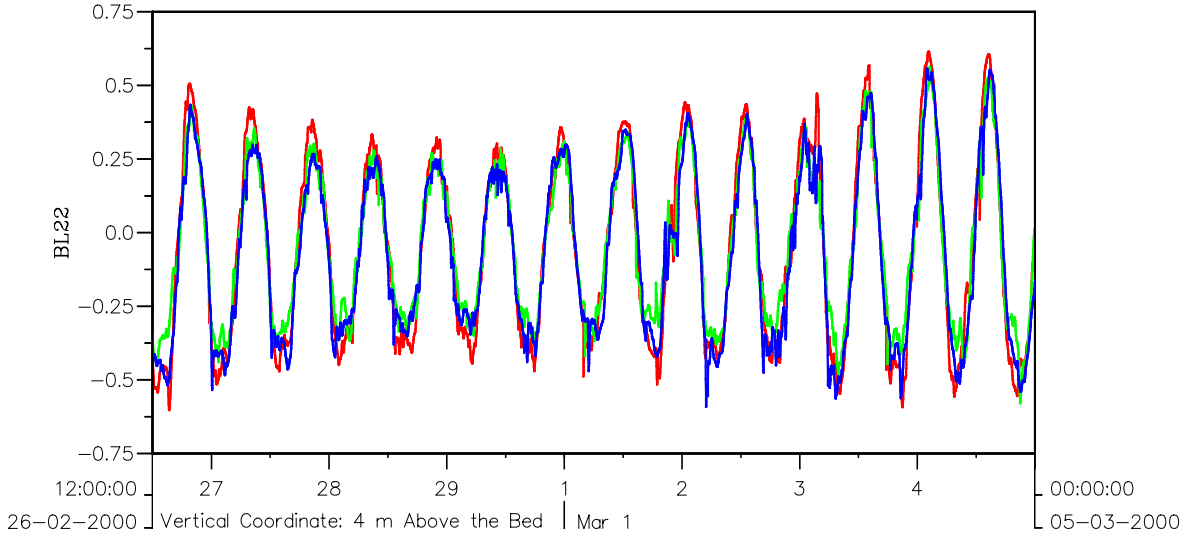

Morphology of pits, channels and trenches

Comparison of modelled longshore velocities at Locations A and M

Red: Location A, Green: Location M, Blue: Location B

WL | DELFT HYDRAULICS

Z3223

FIG. 4.61

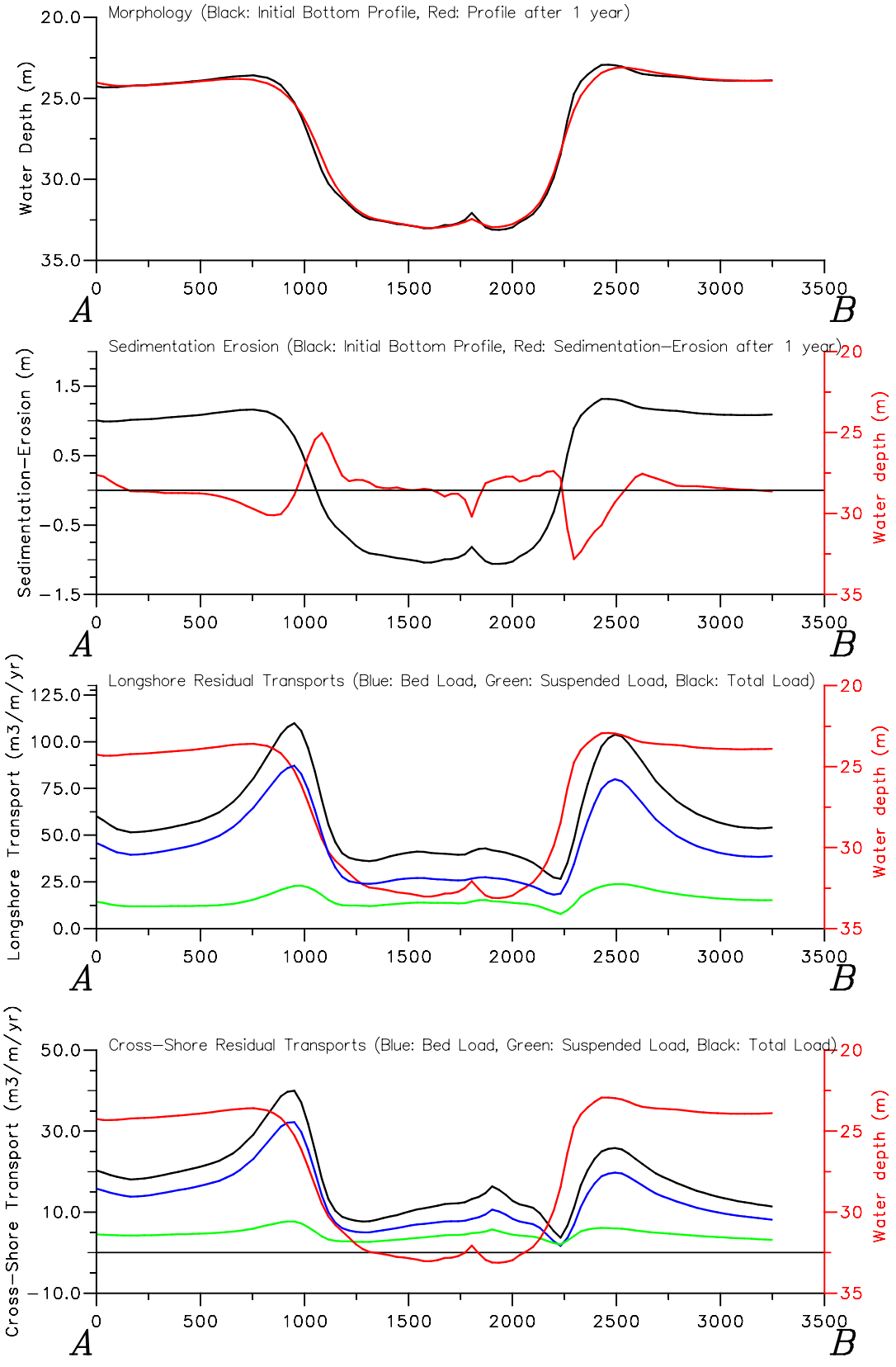

Morphology of pits, channels and trenches Part II: Verification of Delft3D with the PUTMOR Dataset Morphology and Residual Transports along "SUTRENCH–TRACK"		S01–2DH
WL | DELFT HYDRAULICS	Z3223	FIG. 4.63

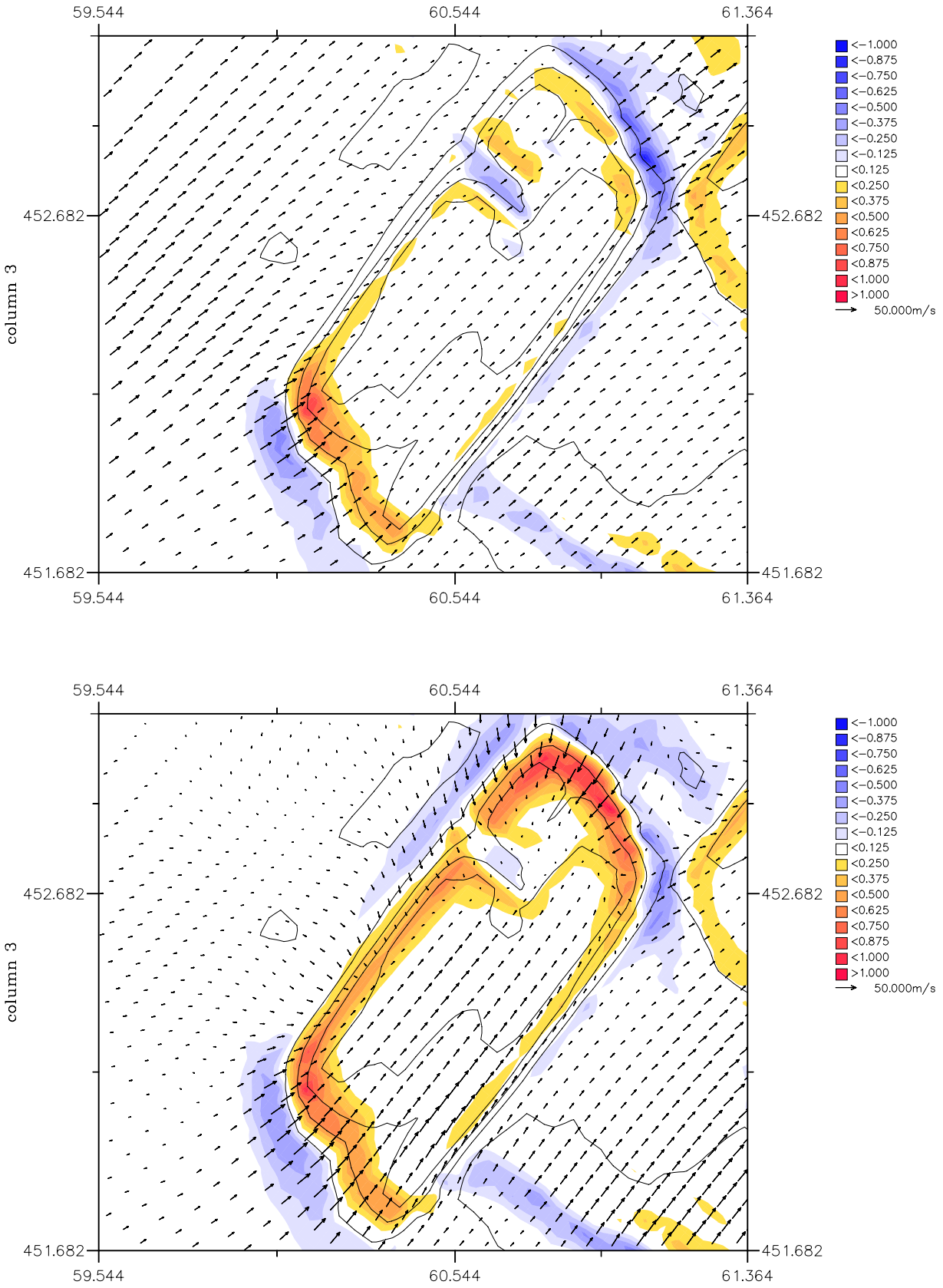

Morphology of pits, channels and trenches
Period I – Sedimentation Erosion and Residual Total Transports
2DH (top) and 3D (bottom)

PT2 & PT2–3D

WL | DELFT HYDRAULICS

Z3223

FIG. 4.64

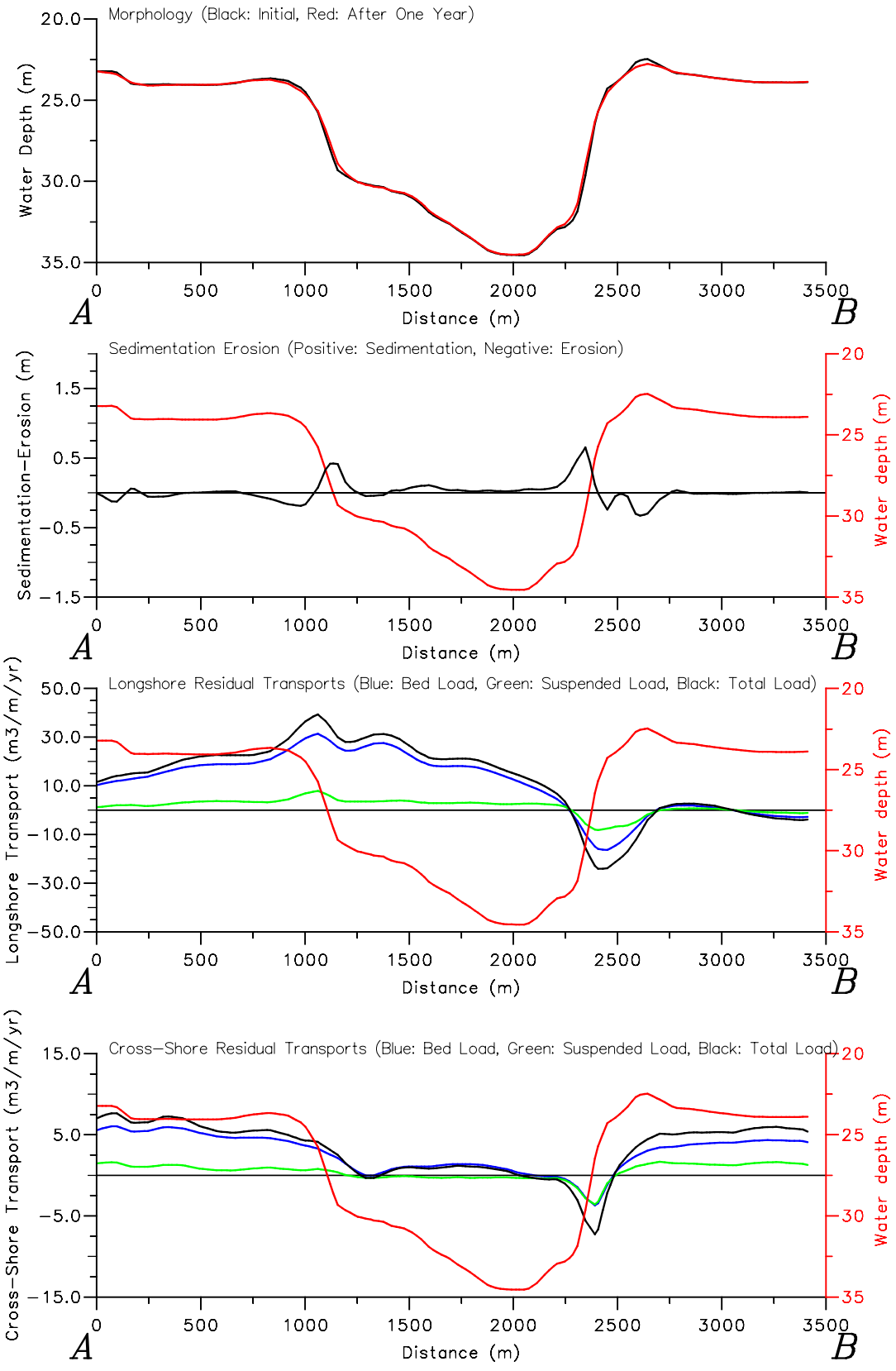

Morphology of pits, channels and trenches Part II: Verification of Delft3D with PUTMOR dataset Track 1 – Period I – 3D – Morphology and Residual Transports		pt2-3d
WL | DELFT HYDRAULICS	Z3223	FIG. 4.65

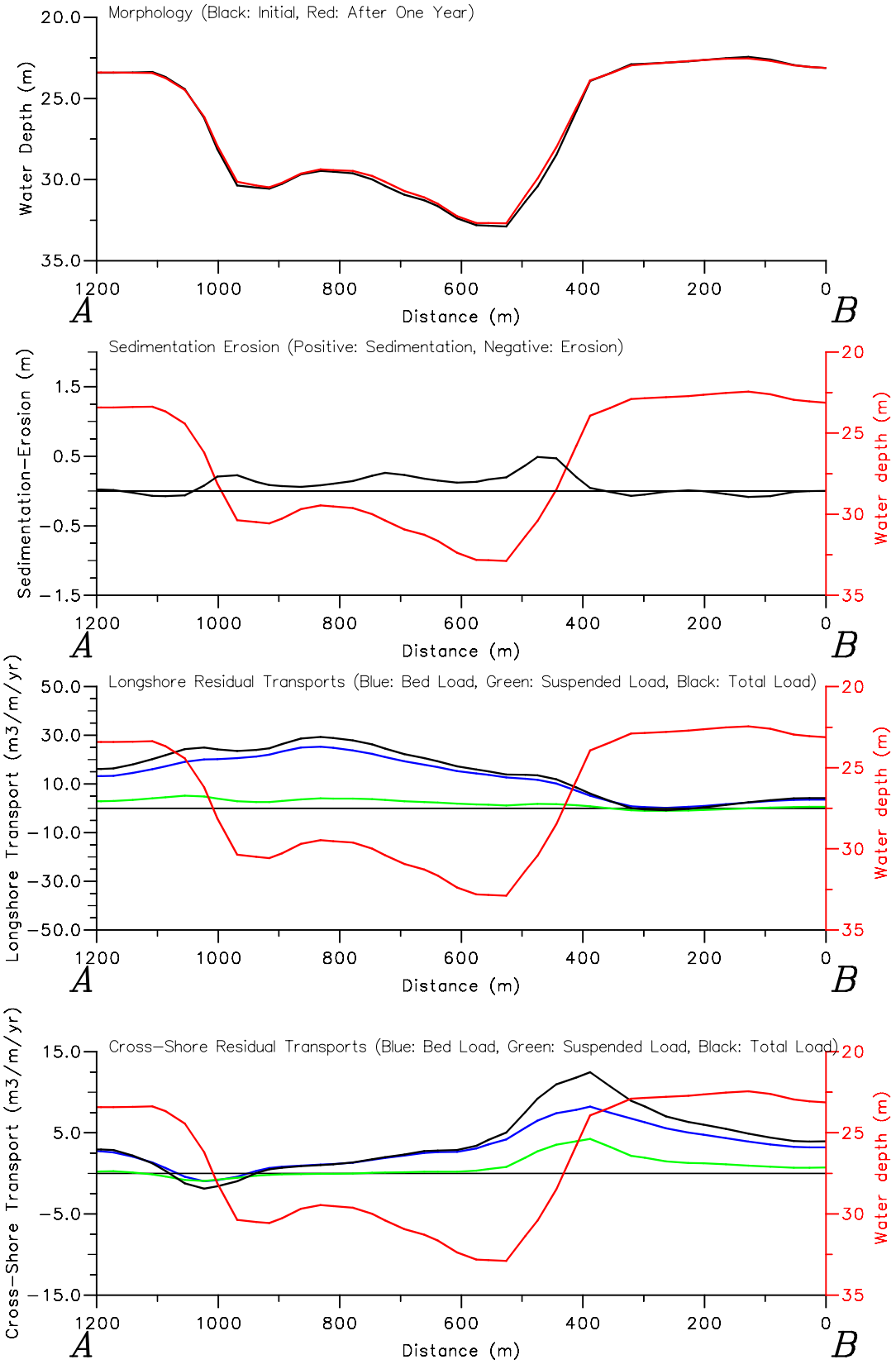

Morphology of pits, channels and trenches Part II: Verification of Delft3D with PUTMOR dataset Track 3 – Period I – 3D – Morphology and Residual Transports		pt2-3d
WL | DELFT HYDRAULICS	Z3223	FIG. 4.66

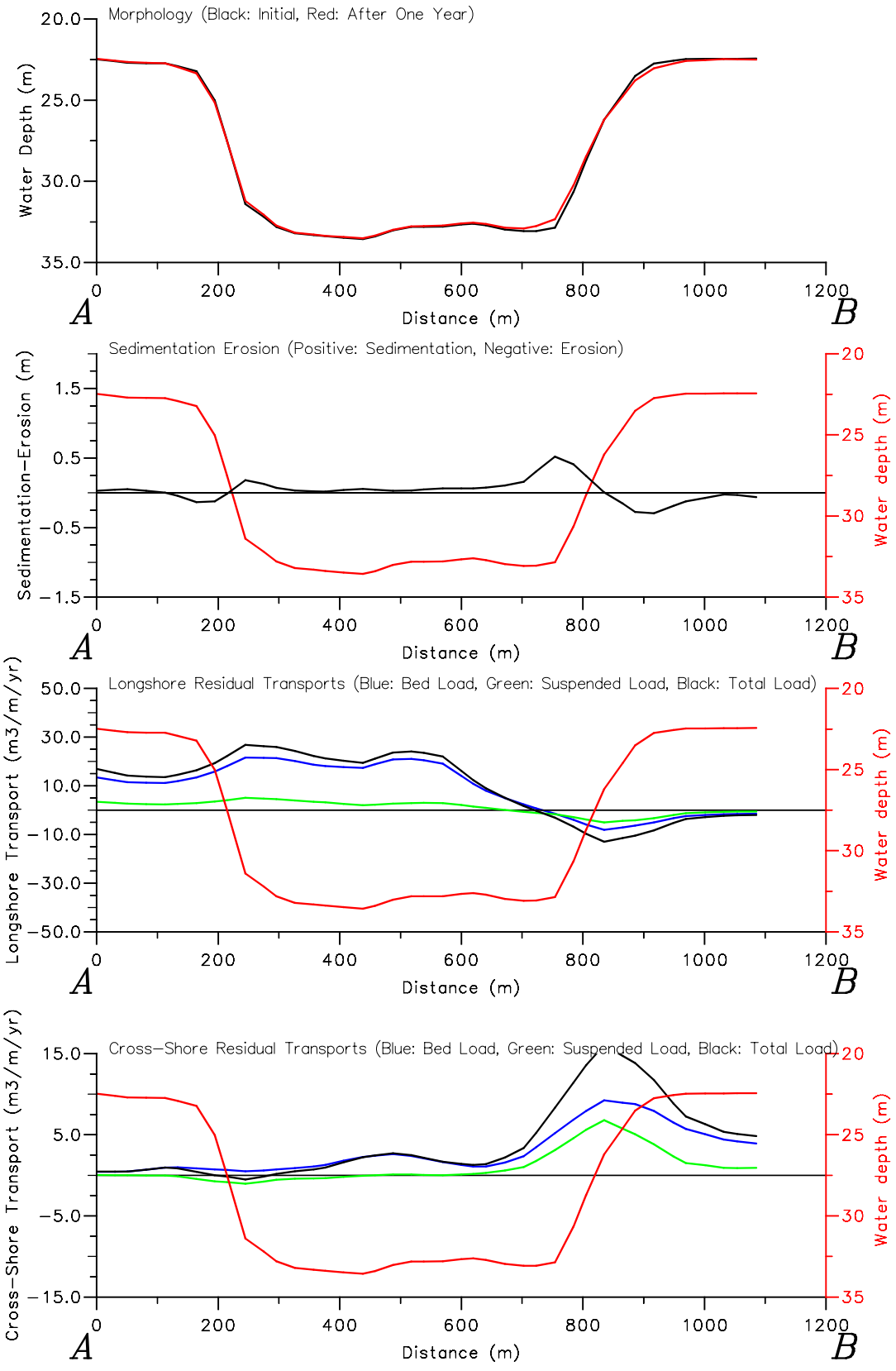

Morphology of pits, channels and trenches Part II: Verification of Delft3D with PUTMOR dataset Track 4 – Period I – 3D – Morphology and Residual Transports		pt2-3d
WL | DELFT HYDRAULICS	Z3223	FIG. 4.67

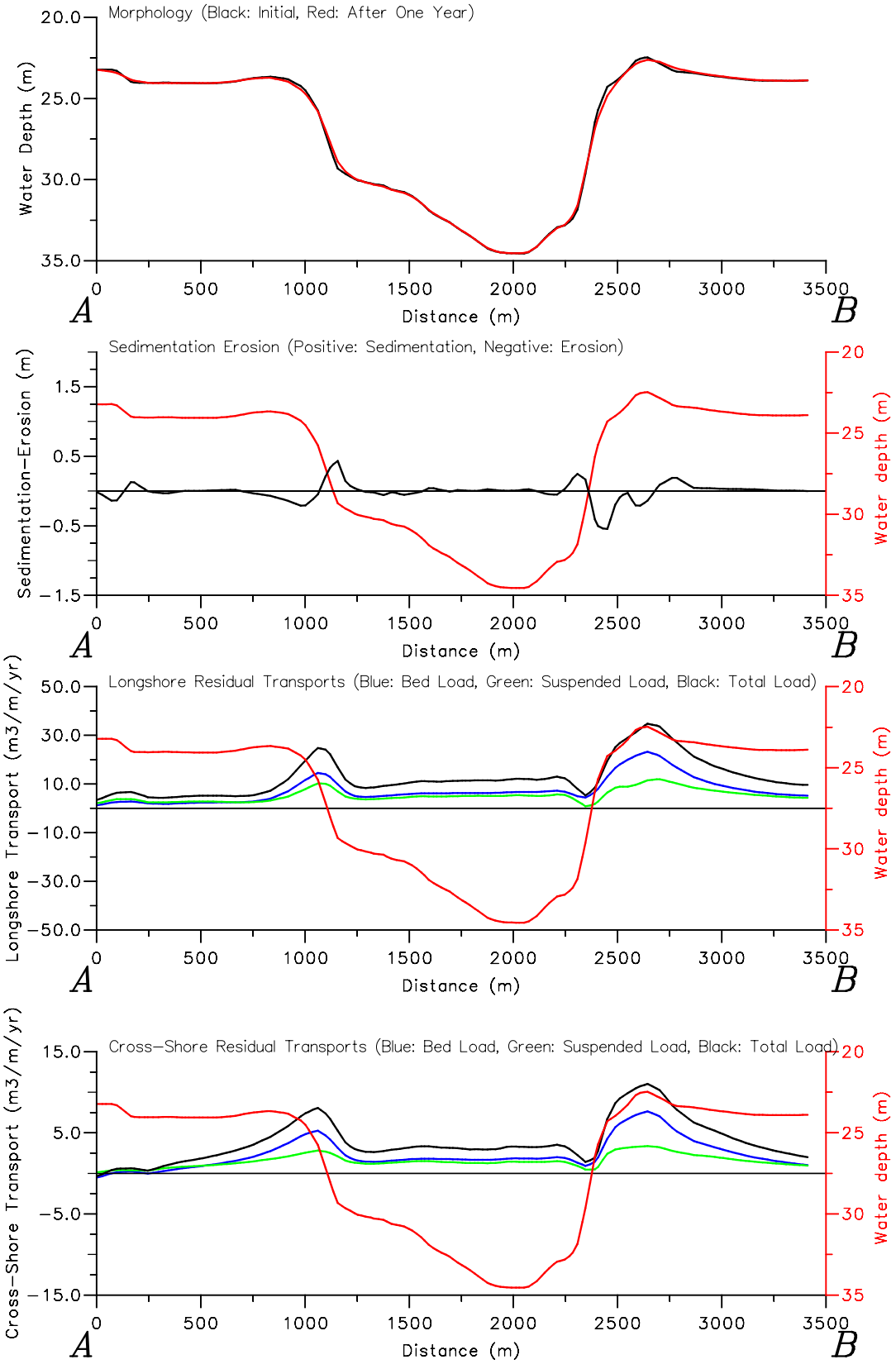

Morphology of pits, channels and trenches Part II: Verification of Delft3D with PUTMOR dataset Track 1 – Period I – 2DH – Morphology and Residual Transports		PT2-2DH
WL | DELFT HYDRAULICS	Z3223	FIG. 4.68

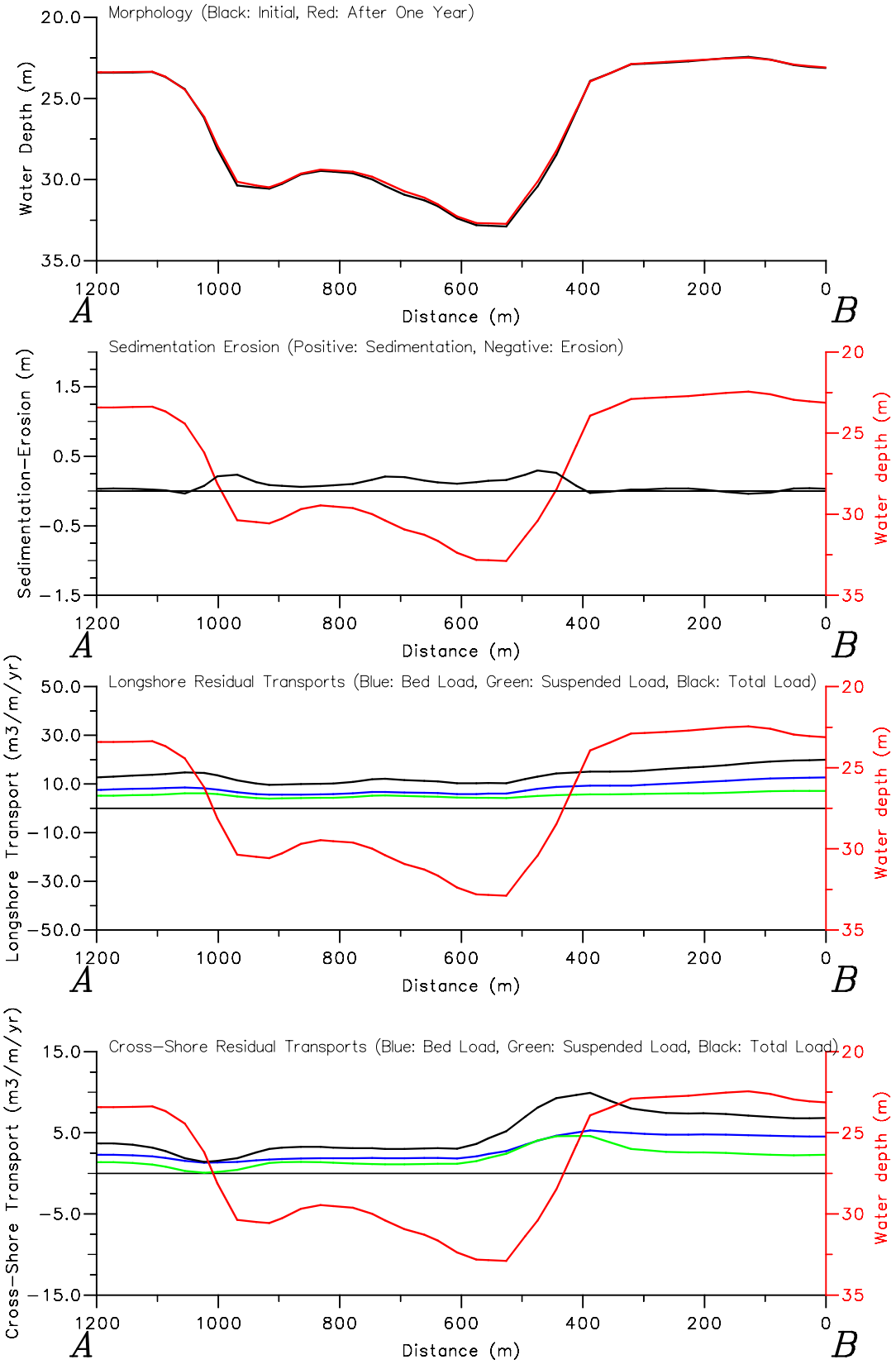

Morphology of pits, channels and trenches Part II: Verification of Delft3D with PUTMOR dataset Track 3 – Period I – 2DH – Morphology and Residual Transports		PT2-2DH
WL | DELFT HYDRAULICS	Z3223	FIG. 4.69

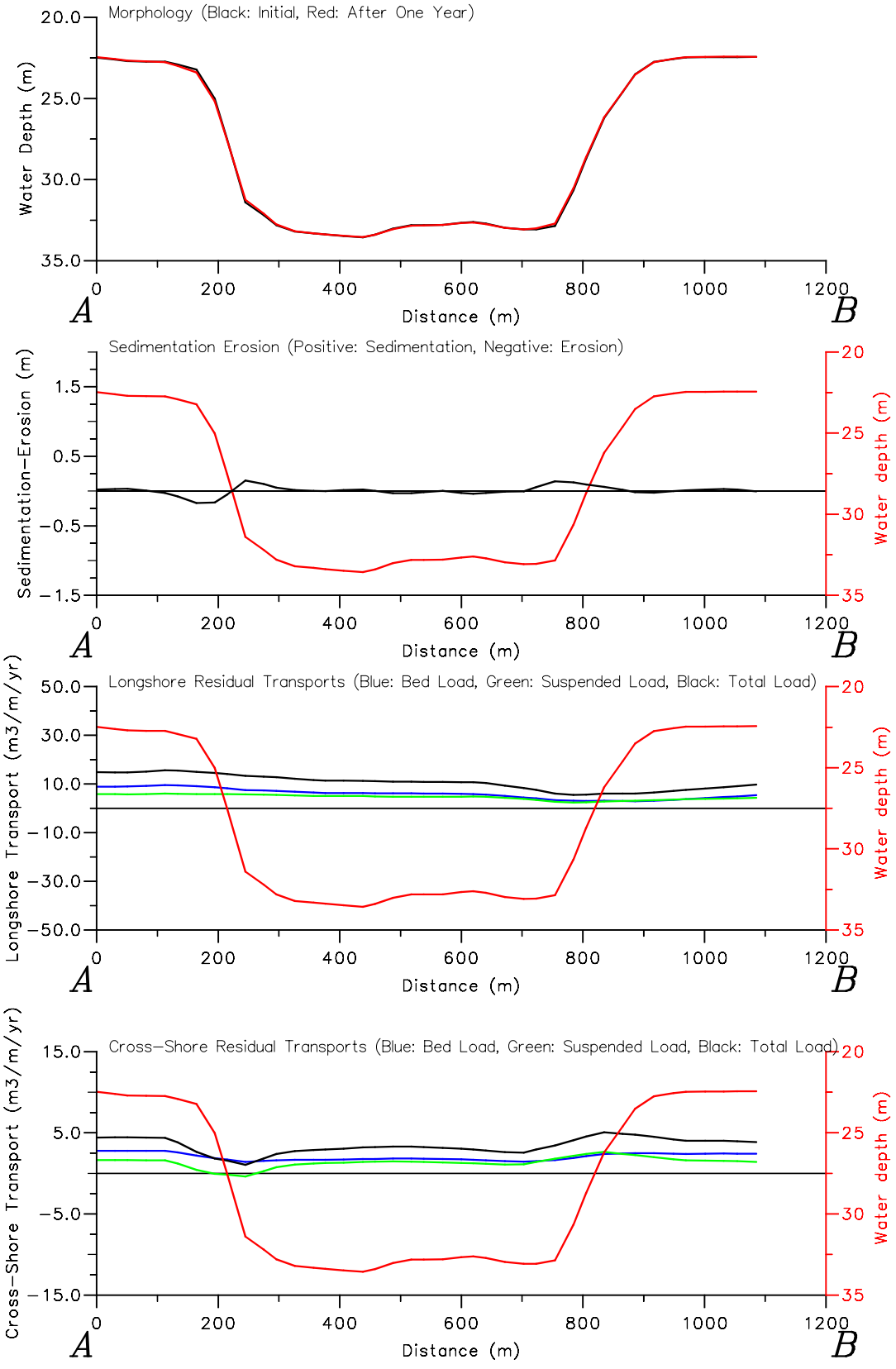

Morphology of pits, channels and trenches Part II: Verification of Delft3D with PUTMOR dataset Track 4 – Period I – 2DH – Morphology and Residual Transports		PT2-2DH
WL | DELFT HYDRAULICS	Z3223	FIG. 4.70

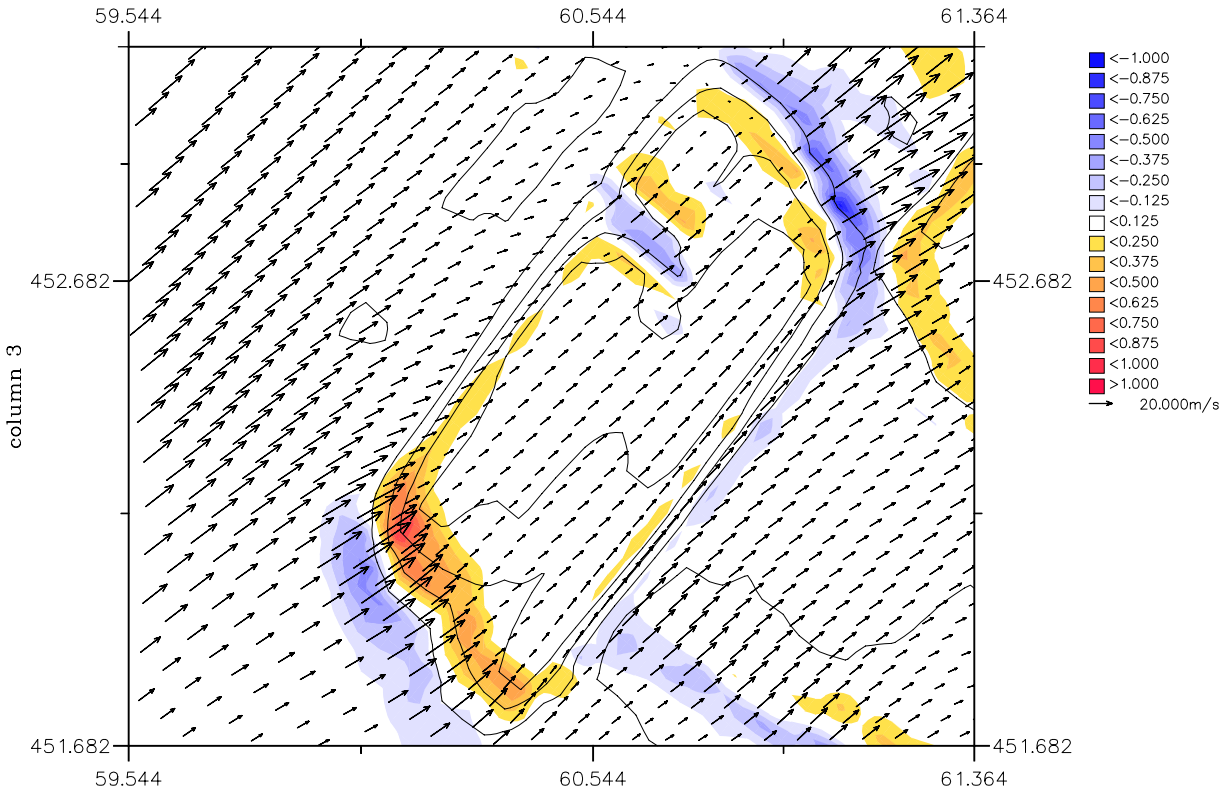

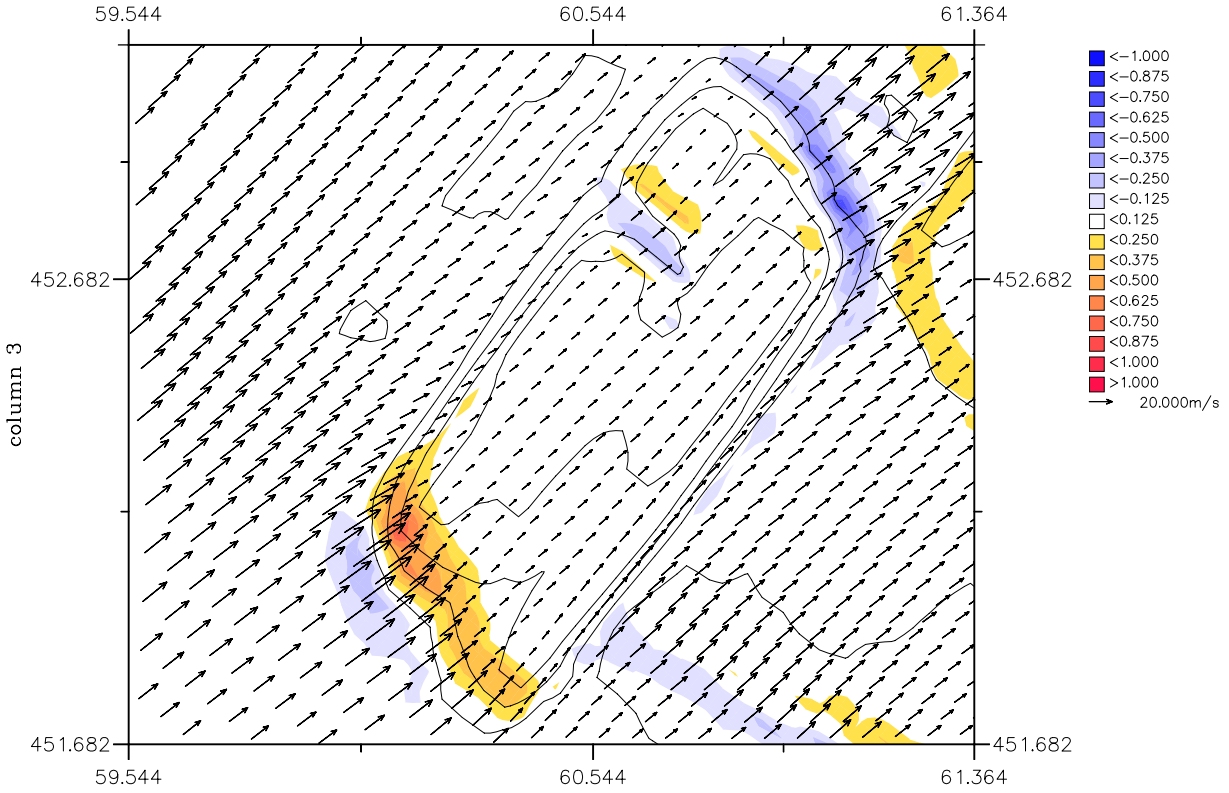

Morphology of pits, channels and trenches
Period I – Sedimentation Erosion and Residual Total Transports
2DH Simulations with waves (top) and without waves (bottom)

PT2 & PT2–NW

WL | DELFT HYDRAULICS

Z3223

FIG. 4.71

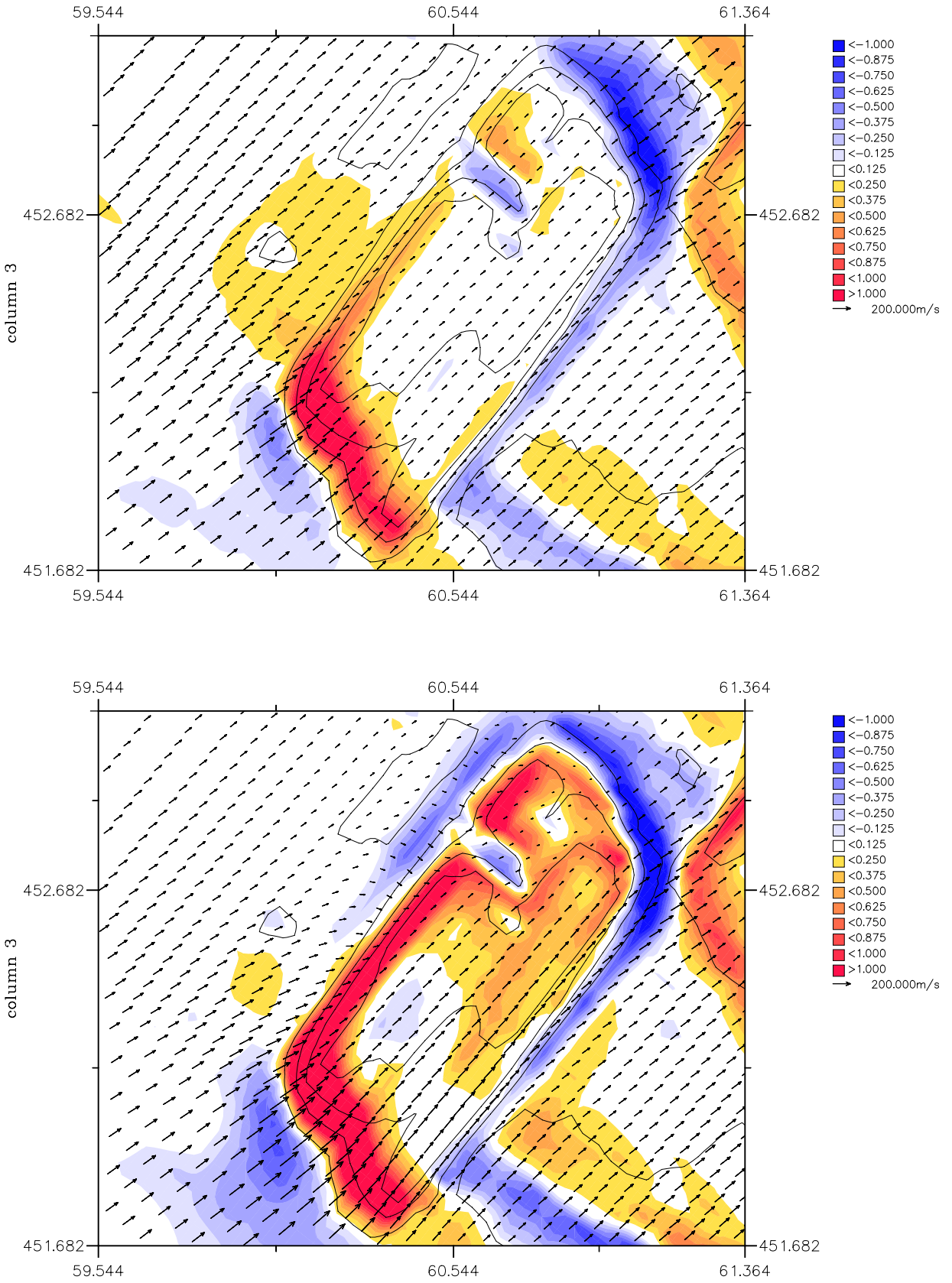

Morphology of pits, channels and trenches Period II – Sedimentation Erosion and Residual Total Transports 2DH (top) and 3D (bottom)		PT5 & PT5–3D
WL | DELFT HYDRAULICS	Z3223	FIG. 4.72

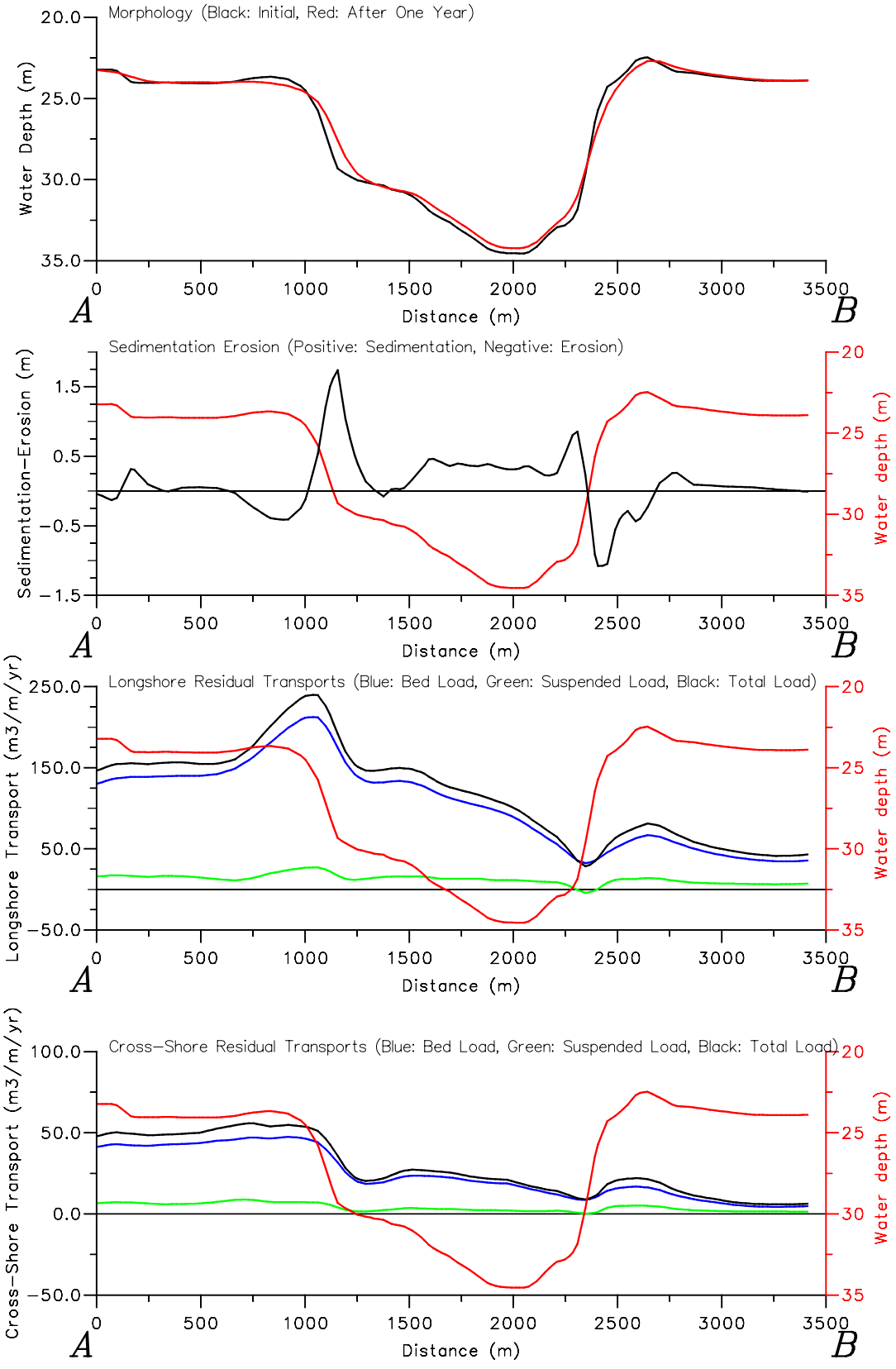

Morphology of pits, channels and trenches Part II: Verification of Delft3D with PUTMOR dataset Track 1 – Period II – 3D – Morphology and Residual Transports		PT5-3D
WL | DELFT HYDRAULICS	Z3223	FIG. 4.73

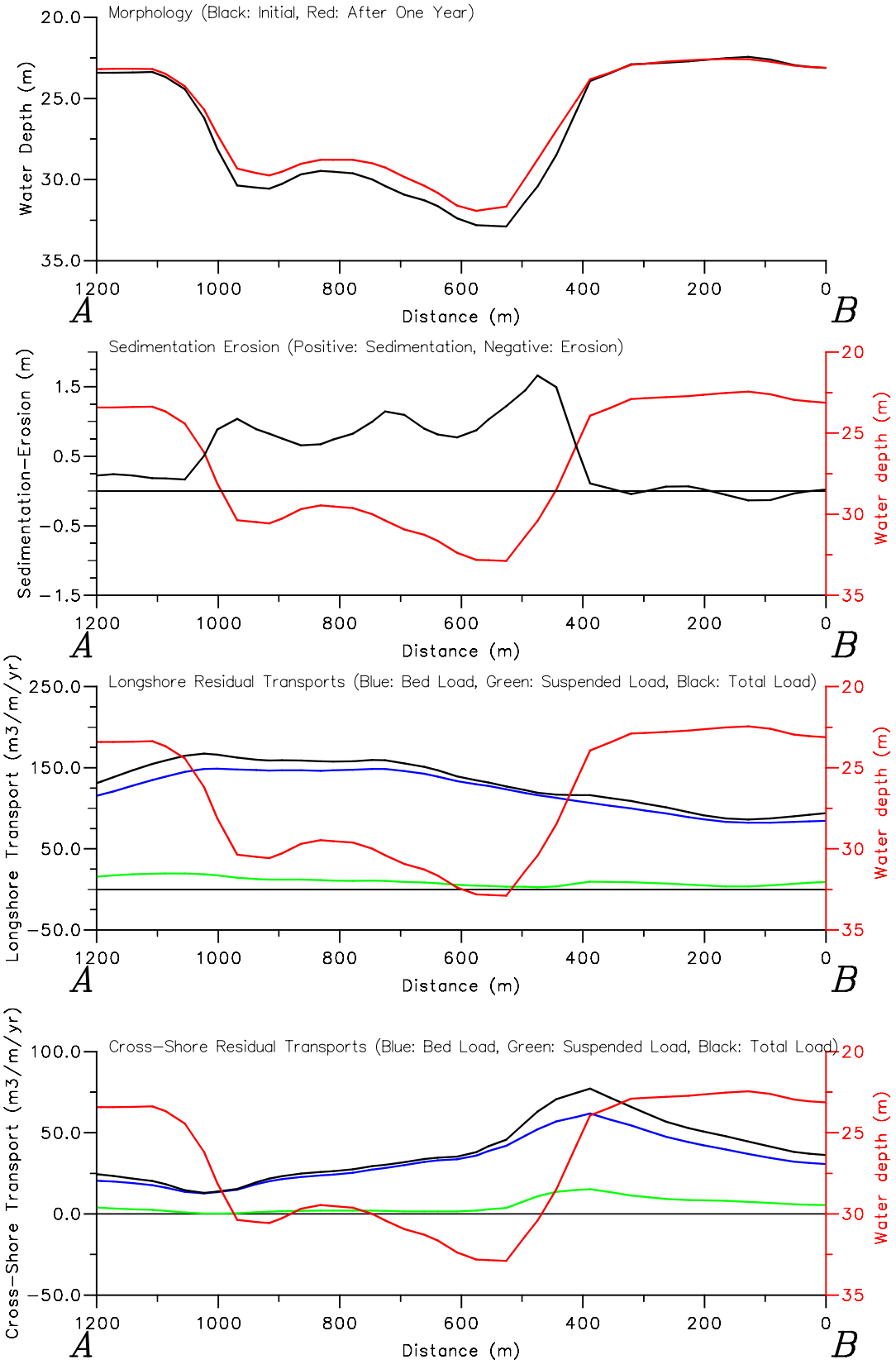

Morphology of pits, channels and trenches Part II: Verification of Delft3D with PUTMOR dataset Track 3 – Period II – 3D – Morphology and Residual Transports		PT5-3D
WL | DELFT HYDRAULICS	Z3223	FIG. 4.74

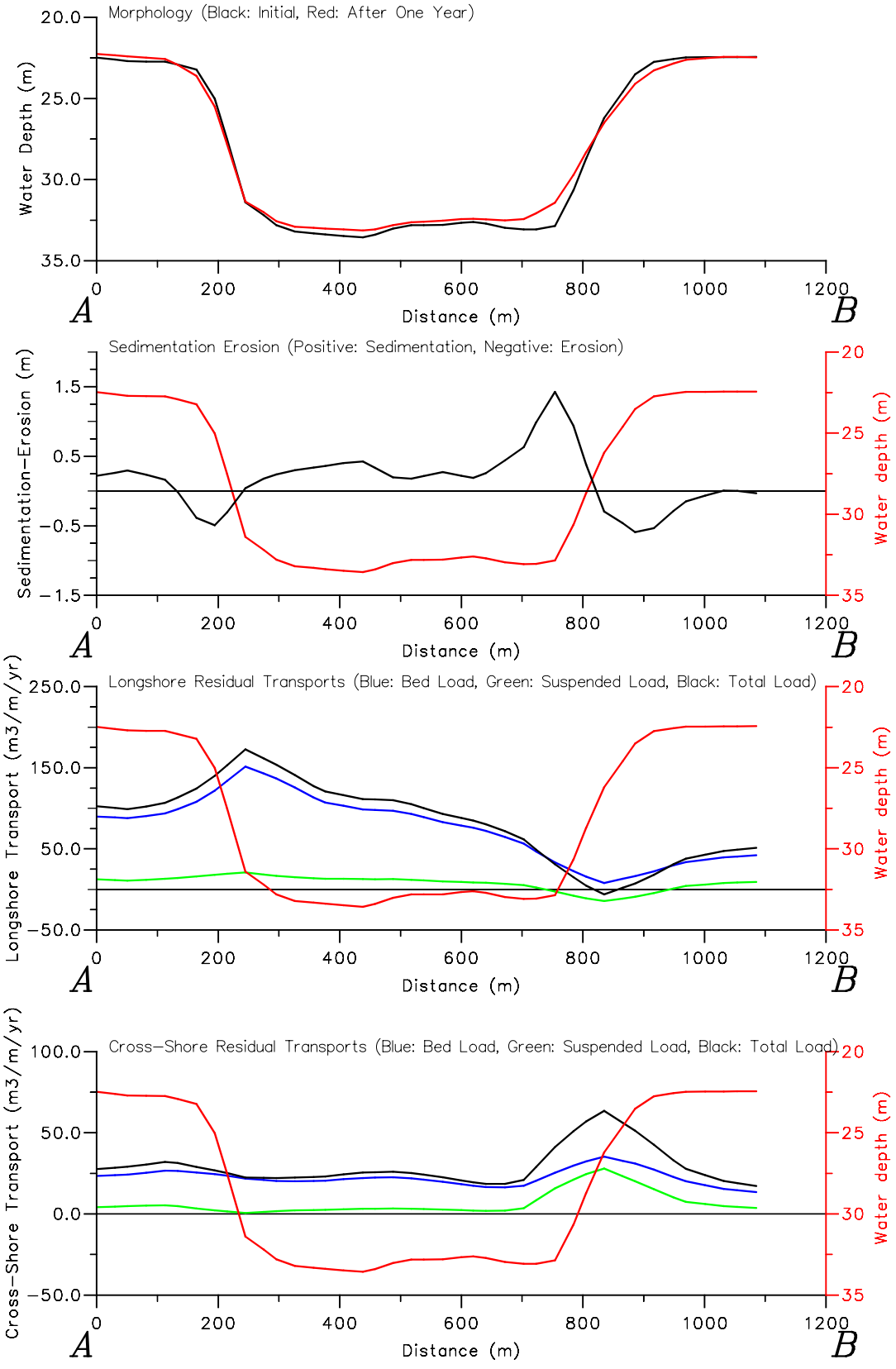

Morphology of pits, channels and trenches Part II: Verification of Delft3D with PUTMOR dataset Track 4 – Period II – 3D – Morphology and Residual Transports		PT5-3D
WL | DELFT HYDRAULICS	Z3223	FIG. 4.75

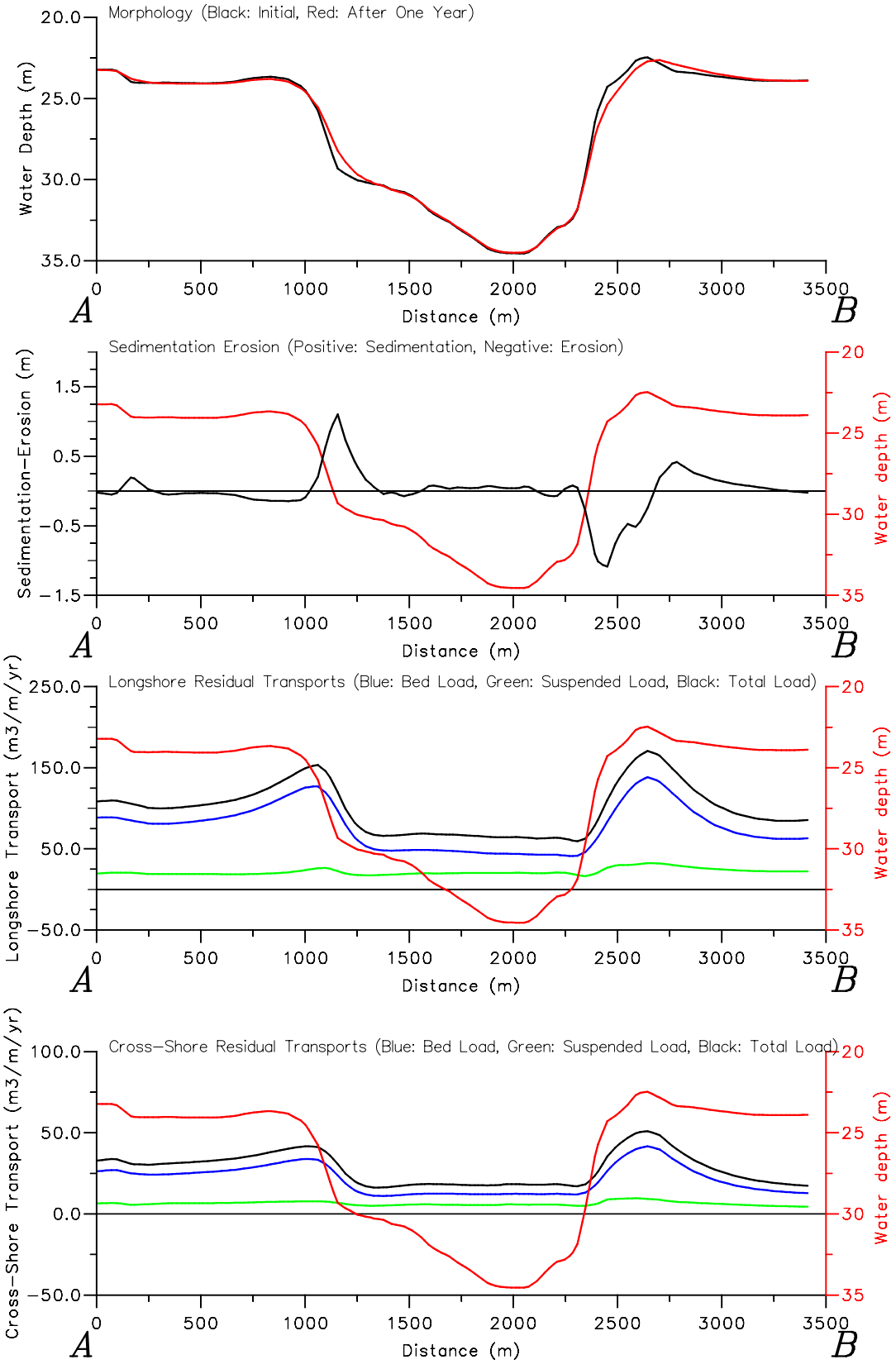

Morphology of pits, channels and trenches Part II: Verification of Delft3D with PUTMOR dataset Track 1 – Period II – 2DH – Morphology and Residual Transports		PT5-2DH
WL | DELFT HYDRAULICS	Z3223	FIG. 4.76

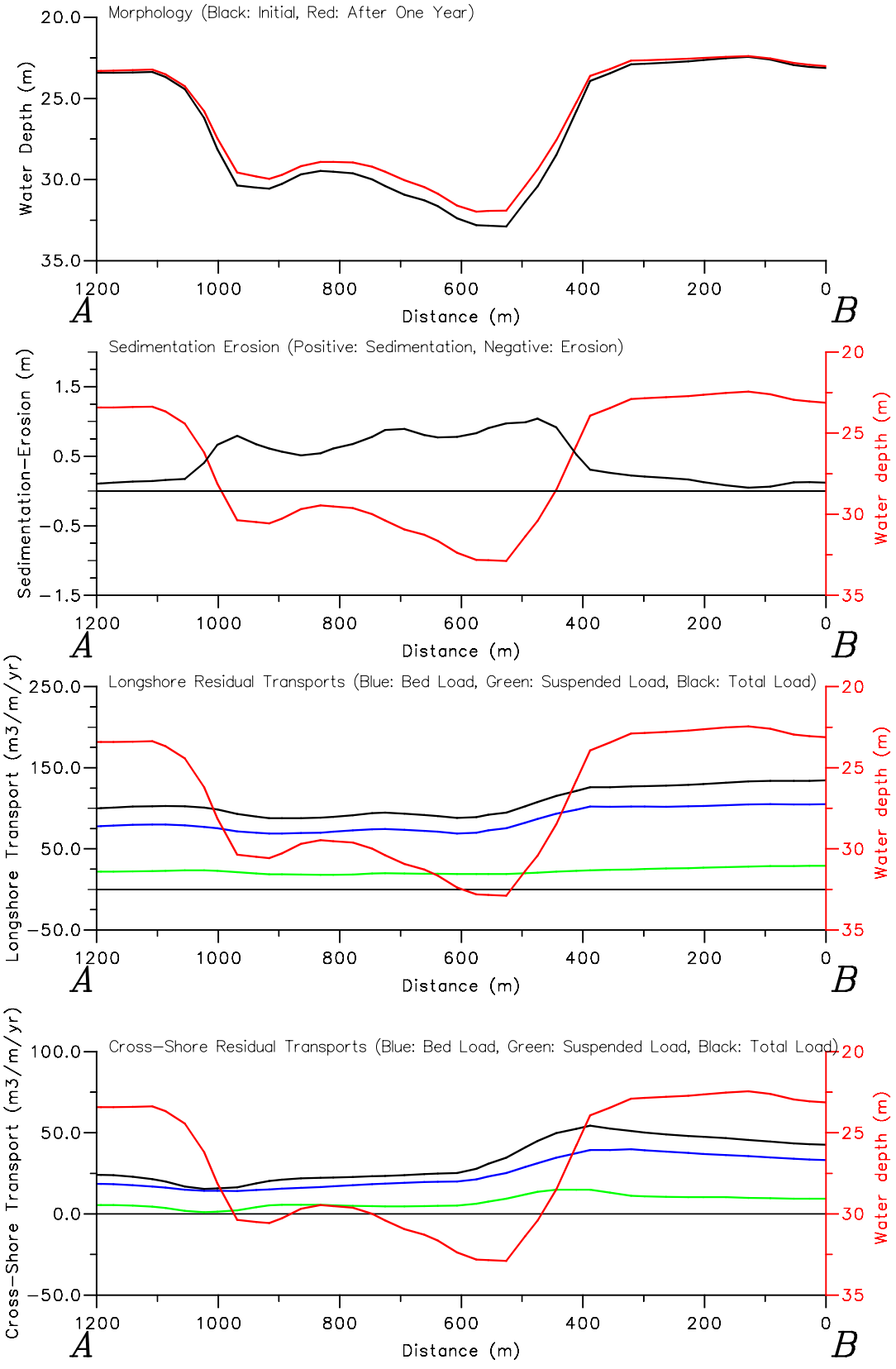

Morphology of pits, channels and trenches Part II: Verification of Delft3D with PUTMOR dataset Track 3 – Period II – 2DH – Morphology and Residual Transports		PT5-2DH
WL | DELFT HYDRAULICS	Z3223	FIG. 4.77

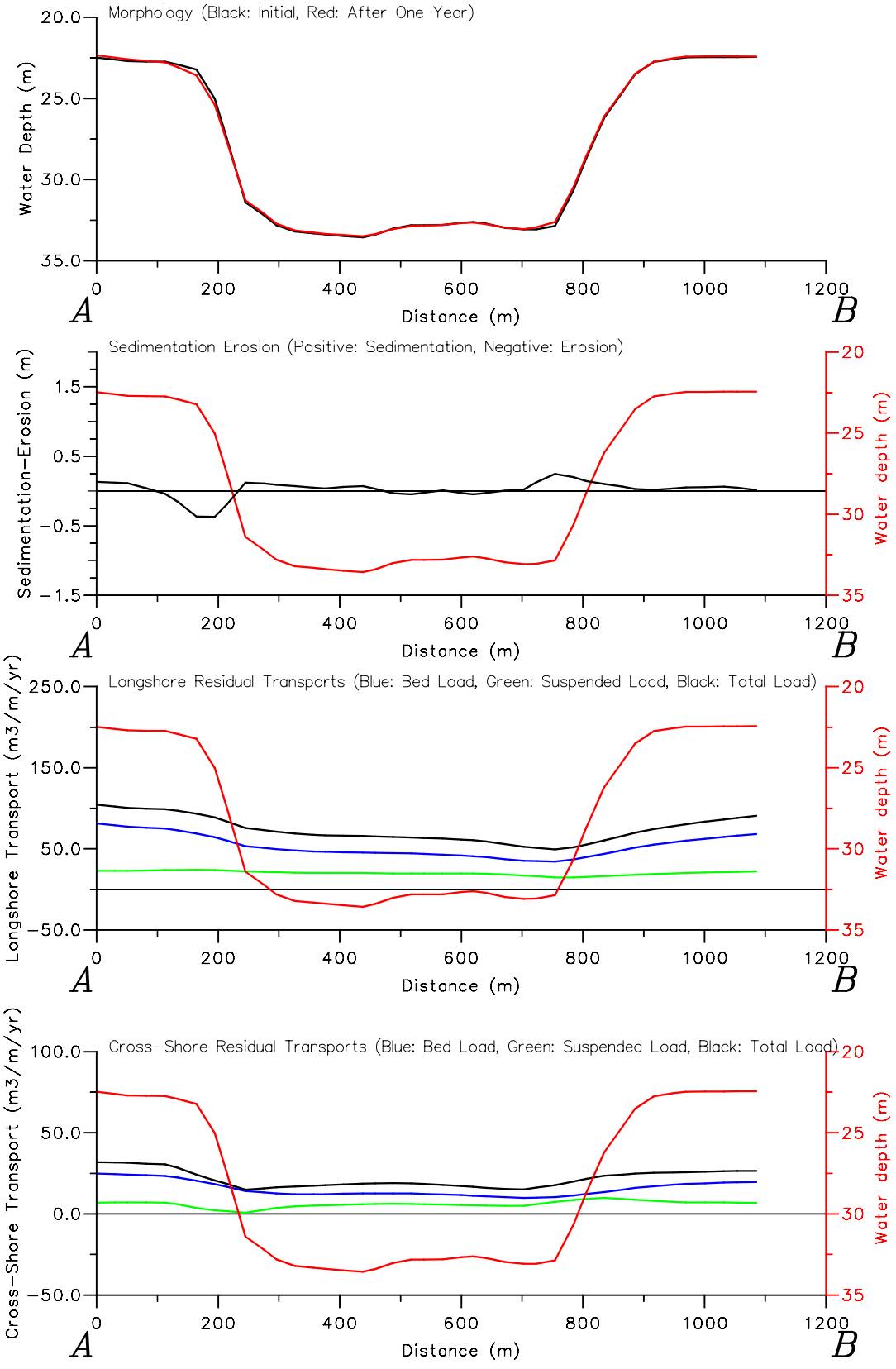

Morphology of pits, channels and trenches Part II: Verification of Delft3D with PUTMOR dataset Track 4 – Period II – 2DH – Morphology and Residual Transports		PT5-2DH
WL | DELFT HYDRAULICS	Z3223	FIG. 4.78

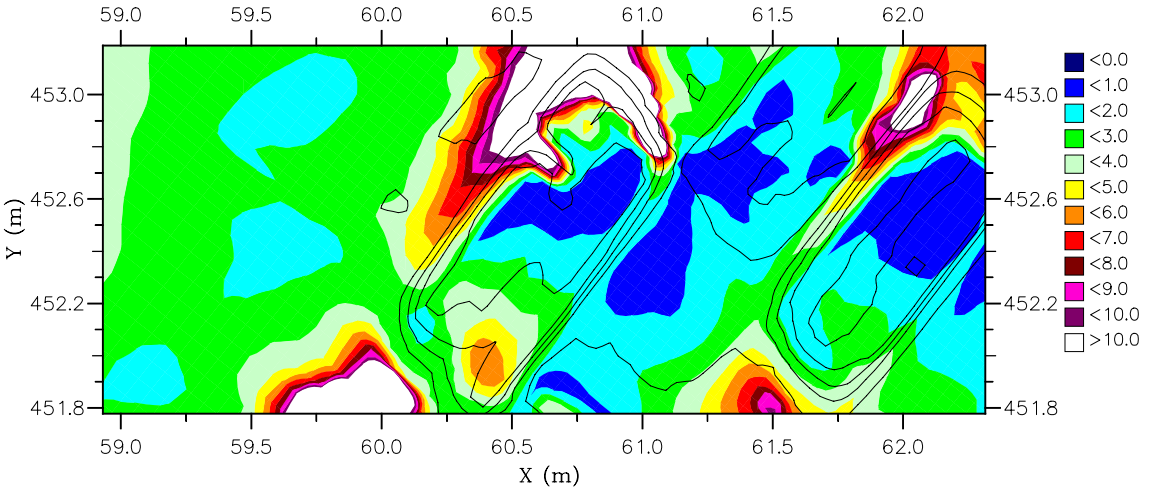

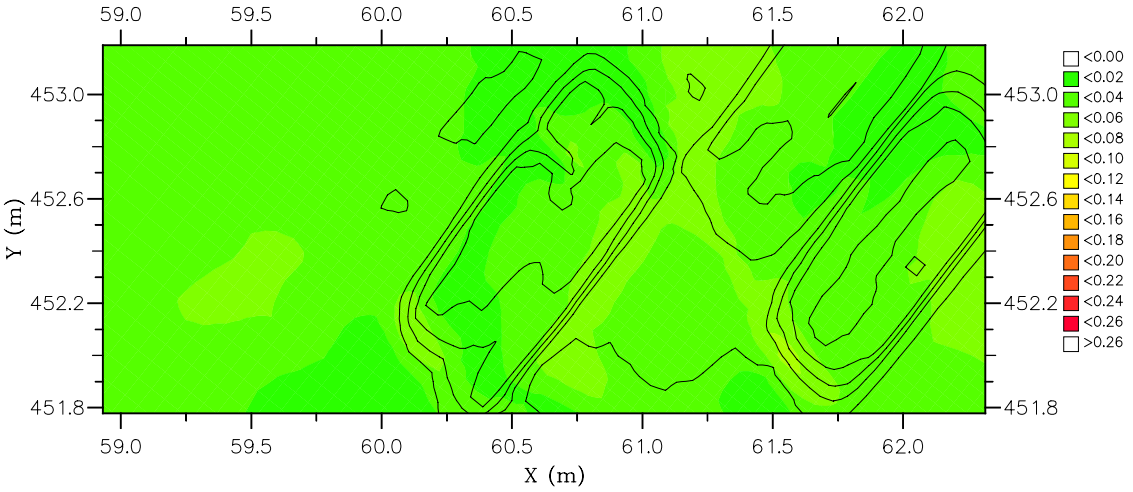

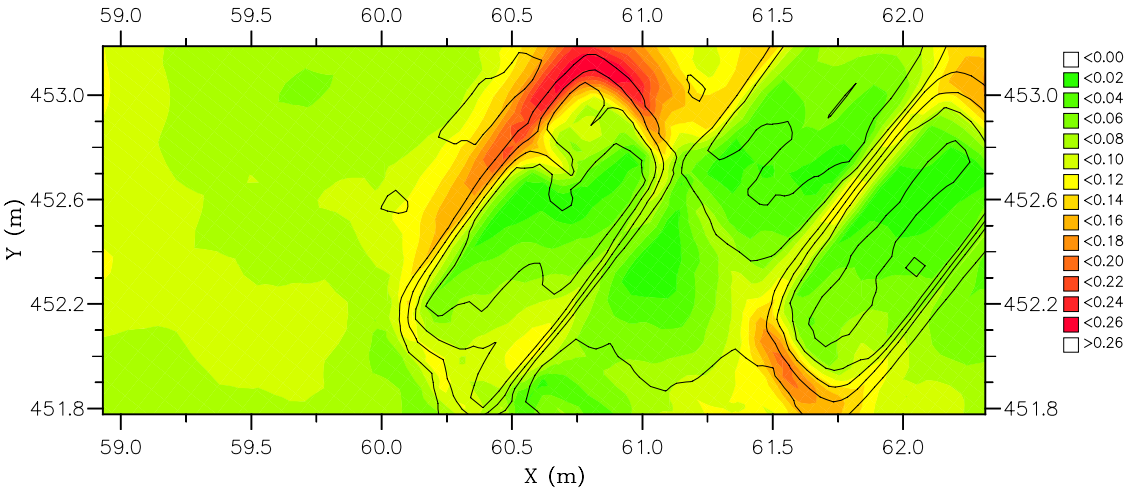

Morphology of pits, channels and trenches

Comparison of averaged bottom shear stress magnitudes for Period I

Top: ratio between 2DH and 3D, Middle: 2DH, Bottom: 3D

PT2

WL | DELFT HYDRAULICS

Fig. 4.79

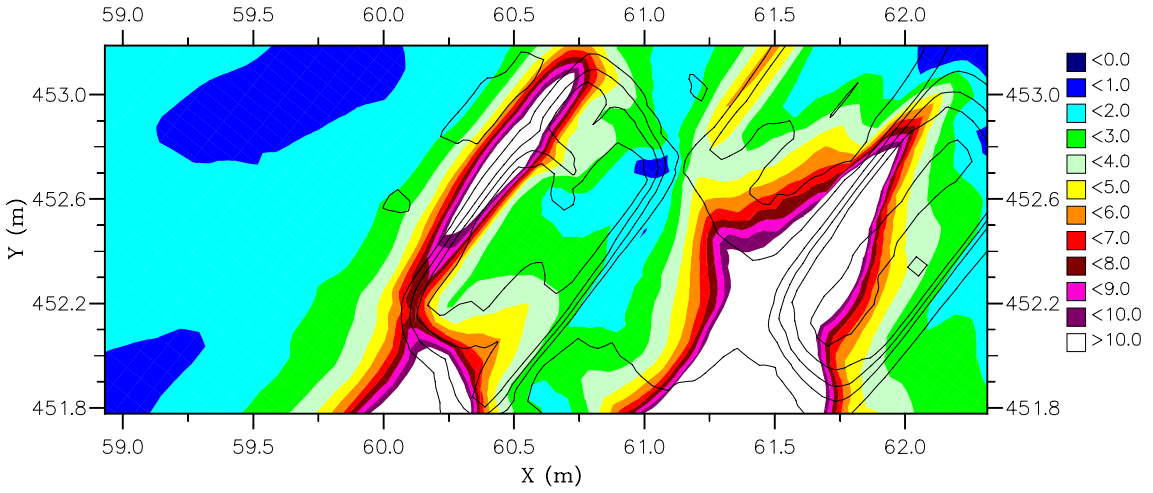

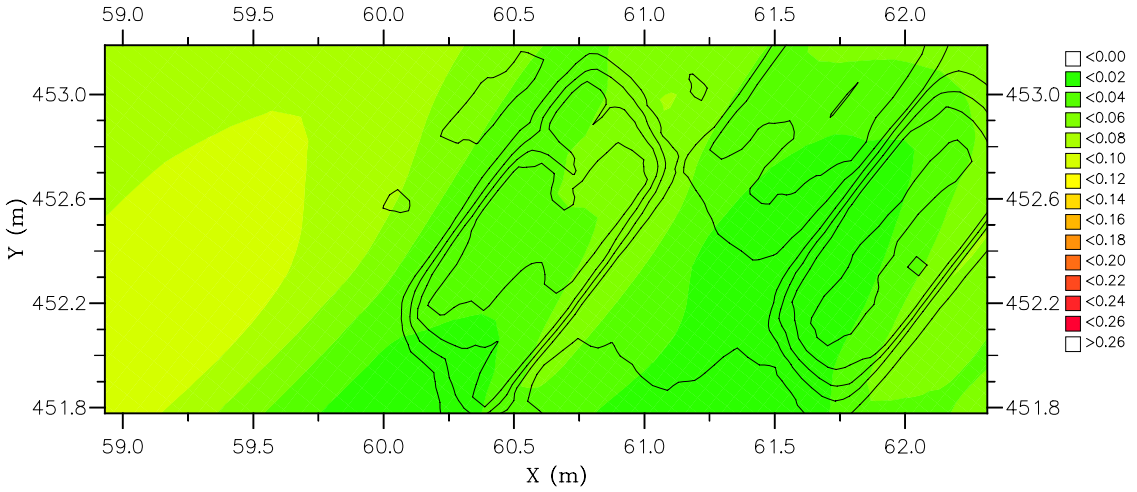

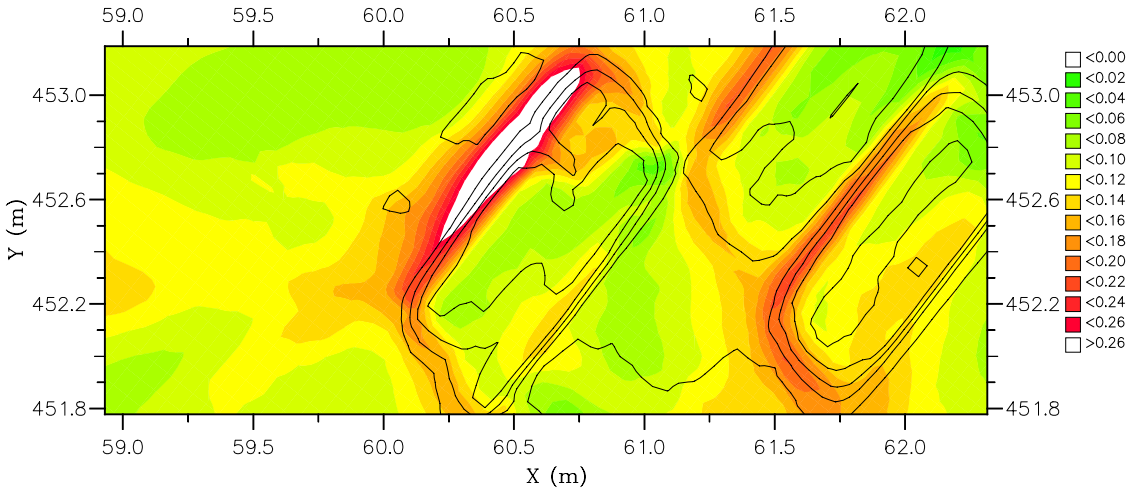

Morphology of pits, channels and trenches

Comparison of averaged bottom shear stress magnitudes for Period II

Top: ratio between 2DH and 3D, Middle: 2DH, Bottom: 3D

PT5

WL | DELFT HYDRAULICS

Fig. 4.80